Polymer/DNA Bio-conjugates via Grafting-from and Grafting-to

Thesis submitted for fulfilment of the degree of Doctor of Philosophy

Simon Jacques Michel Clark Bou

BSc (Extended Major Chemistry), BSc (Hons, First Class)

Flinders
UNIVERSITY

Adelaide South Australia

College of Science and Engineering

Supervised by **Professor Amanda V. Ellis** (College of Science and Engineering)

Co-supervised by **Professor Clare Lenehan** (College of Science and Engineering)

November 2017

Declaration

I certify that this thesis does not incorporate without acknowledgment any material previously submitted for a degree or diploma in any university; and that to the best of my knowledge and belief it does not contain any material previously published or written by another person except where due reference is made in the text.

Signed .....

Simon J.M.C. Bou

Dated November 2017

.

Acknowledgments

This thesis could not have been accomplished without the help, support and encouragement of many, many people. Firstly, I would like to thank my supervisor Professor Amanda Vera Ellis, your passion and drive in pursuit of scientific excellence has always inspired me to strive for more and hopefully achieve more. Thank you for all the advice, encouragement or criticism, as it has made me a better scientist, writer and communicator. I must thank my co supervisor Professor Clare Lenehan for all her support throughout this journey but especially for the last few months. A big thank you to all the members of the Ellis group, over the many years. A special thanks to Dr Chris Gibson for his help with AFM, Dr Ashley Connolly for his help with PCR and Dr Charlotte Williams at CSIRO for her help with GPC analysis. I would also like to thank the entire academic staff, and professional staff who helped to train me as a scientist in undergraduate and beyond. All of you have always been willing to aid whenever it was required and for this I am very grateful.

I am also very grateful for the scholarship opportunity I received from the National Institute for Materials Science (NIMS) and to my supervisor Dr Mitsuhiro Ebara who gave me the chance to study in Japan for six months. I must thank all the members of the Bio materials group who made me feel very welcome while I was there.

This journey could not have been possible without the support and understanding of my long-suffering family. Massive wholehearted thanks must go to my in-laws Angela and Roger Stuart. Without your support, it is unlikely that I would have ever attempted this journey and it is because of you both that I have been able to pursue my intellectual aspirations. I hope one day that I will be able to repay all the kindness you have shown me over the many years. I also must thank my Mum, you raised me to be respectful, kind and curious, even though you have been living in another country during this time, you have always believed in me and for that I am grateful. To my dad, even though you are no longer here, it's because of the example you set while I was growing up that inspired me to be the person you always thought I could be.

To my children Charlize and Mijan, I love you both very much and I thank you for your patience and understanding over these last few years.

Finally, to my wife Dianna, thank you for everything, your love and support has been amazing, your positivity and kindness throughout this time has got me through some difficult times. I don't know how I will ever repay you, but I will try.

Abstract

Polymer bio-conjugates can be prepared by the grafting-from, grafting-through and the grafting-to approach. Grafting-from involves the preparation of a bio-macro initiator, where a functional group attached to the bio-molecule is used to initiate the polymerisation of a monomer. The grafting-through approach, involves the preparation of bio-monomer that is polymerisable; and the grafting to approach is where the polymer is prepared separately with specific functionality that can be used to attach bio-molecules. This thesis investigated grafting-from and grafting-to as a method of making polymer bio-conjugates that have potential use in bio-medical applications.

Polymer bio-conjugates were initially prepared by the grafting-from approach. First *N*-hydroxyl succinimide/*N*-ethyl-*N'*-(3-dimethylaminopropyl)carbodiimide (NHS/EDC) coupling chemistry transformed the end groups of a trithiocarbonate reversible addition fragmentation chain transfer (RAFT) agent. Solution proton nuclear magnetic resonance (^{1}H NMR) spectroscopy and electrospray ionisation (ESI) mass spectrometry (MS) confirmed the synthesis of the RAFT ester agent. Amide coupling between an amine functionalised oligonucleotide and the synthesised activated ester RAFT agent yielded a bio-macro initiator agent. RAFT polymerisation of 2-hydroxyethyl acrylate (HEA) in solution, using the bio-macro agent under a range of reaction conditions was performed to grow p(HEA) from the oligonucleotide. The purification of the polymer bio-conjugates was found to be straight-forward, however, growth from the bio-macro agent was found to be slow and limited.

Polymer bio-conjugates were also prepared by the grafting-to approach. Five poly(*N*-isopropyl acrylamide)-*co*-hydroxymethlyacrylamide (pNIPAAm-*co*-HMAAm) copolymers were prepared by RAFT polymerisation. It was confirmed by ^{1}H NMR spectroscopy and attenuated total reflectance Fourier transform infrared (ATR-FTIR) spectroscopy that the feed ratio of the monomer in the copolymerisation was retained in the final polymer composition. The polydispersity (Đ) of between 1.3-1.6 for the pNIPAAm-*co*-HMAAm copolymers indicated that good control over molecular weight was achieved by RAFT polymerisation. The temperature response of the pNIPAAm-*co*-HMAAm copolymers was determined by measuring their lower critical solution temperatures (LCSTs). The results clearly showed that the LCSTs of the pNIPAAm-*co*-HMAAm copolymers could be controlled by the changing the ratio of HMAAm monomer in the pNIPAAm-*co*-HMAAm copolymer. It was proposed that the pNIPAAm-*co*-HMAAm copolymers form a domain at their LCST that is favourable for SYBR Green (SG) intercalation. The interaction between SG and pNIPAAm-*co*-HMAAm copolymers was measured by the monitoring the change in SG intensity when they were mixed together in solution. The SG fluorescence intensity for all synthesised pNIPAAm-*co*-HMAAm copolymers increased with polymer concentration. The initial increase in SG fluorescence intensity for the five pNIPAAm-*co*-

HMAAm copolymers occurred at the calculated LCSTs of the copolymers. The critical micelle concentration (CMC) of the pNIPAAm-*co*-HMAAm copolymers was determined by extrapolation from a graph of SG intensity versus polymer concentration. The CMC concentration of the pNIPAAm-*co*-HMAAm copolymers was found to increase as the HMAAm composition increased. Dynamic light scattering (DLS) measured the diameters of the pNIPAAm-*co*-HMAAm copolymer aggregates at different concentrations. The results indicated that aggregation was dependent on temperature, concentration and HMAAm content. The pNIPAAm-*co*-HMAAm copolymer aggregates sizes were also measured by atomic force microscopy (AFM). The results suggested that the copolymers with the increased HMAAm content wet the surface more readily. This was thought to be due to a greater amount of hydrophilic character as the HMAAm content is increased. It was proposed that the interaction between the polar head groups of the HMAAm copolymer will wet the surface of the mica more readily leading to greater spreading of the particle.

The hydroxyl functionality of the pNIPAAm-*co*-HMAAm copolymers were transformed by Steglich esterification to introduce a strained alkyne (SA) functionality dibenzylcyclooctyne-acid (DBCO). For the first time, the LCSTs of SA functionalised pNIPAAm-*co*-HMAAm copolymers were measured using a newly developed light scattering method. This was performed using a thermal cycler that can measure light scattering in real-time. This light scattering method can also measure the LCSTs at very low volumes and in high-throughput. Making this a very useful method of measuring polymer bio-conjugates, since they are often synthesised in limited quantities. In a grafting-to approach, DNA end functionalised with azides were coupled via click chemistry to pNIPAAm-*co*-HMAAm copolymers. The melt temperature of DNA was found to be impacted by its conjugation to pNIPAAm-*co*-HMAAm copolymers, which has potential implications for drug delivery applications.

NHS functionalised polyethylene glycol (PEG) copolymers were prepared by free radical polymerisation (FRP). The NHS-PEG copolymers were transformed into alkene functionalised PEG copolymers. ^{1}H NMR spectroscopy and ATR-FTIR spectroscopies confirmed the transformation. Cross-linked hydrogel disks were prepared by thiol-ene photo polymerisation of the alkene functionalised PEG copolymers. Increasing the cross-link density decreased the swelling profile of the hydrogel disk in water. At low cross-link density, a sustained release of a model drug was observed. When the cross-link density was increased the release, profile changed to burst release. The PEG copolymers thus display tuneable cross-link properties which could make them useful in drug delivery applications.

Table of Contents

List of Figures

List of Tables

List of Abbreviations and Symbols

AHA-CalB	Azide containing enzyme *Candida antarctica* type B lipase
ACVA	4'-azobis (4-cyanovaleric acid)
AFM	Atomic force microscopy
AIBN	Azobisisobutyronitrile
AA-NHS	Acrylic acid *N*-hydroxysuccinimide
APS	Ammonium persulfate
ATRP	Atom transfer radical polymerisation
ATR-FTIR	Attenuated Reflectance-Fourier Transform Infrared
BSA	Bovine serum albumin
bp	Base pairs
CCl_3	Chloroform
$CDCl_3$	Deuterated chloroform
CLP	Cross-linked PEG
CMC	Critical micelle concentration
CMT	Critical micelle temperature
CRNA's	Circulating microRNAs
CRP	Controlled radical polymerisation
CTA 1	bis(carboxymethyl)trithiocarbonate chain transfer agent
CTA 2	4-Cyano-4-(thiobenzoylthio) pentanoic acid
CPT	Camptothecin
CuAAC	Click" azide alkyne cycloaddition
DCC	Dicyclohexylcarbodiimde
DCM	Dichloromethane
DBCO	Dibenzocyclooctyne-acid
DIBAC	Aza-dibenzocyclooctyne
DIBO	Dibenzocyclootynols
DIFO	Difluorinated cyclooctyne
DMA	*N,N*-dimethylacrylamide
DMAP	Dimethylaminopyridine
DMF	Dimethyllformamide
DMSO-d6	Deuterated dimethylsulfoxide

DNA	Deoxyribonucleic acid
DOX	Doxorubicin
d-PAGE	Denaturing polyacrylamide gel electrophoresis
DTPO	Diphenyl, (2,4,6-trimethylbenzoyl) phosphine oxide
DLS	Dynamic light scattering
DVB	Divinylbenzene
EDC	*N*-ethyl-*N'*-(3-dimethylaminopropyl)carbodiimide
EGDA	Ethylene glycol diacrylate
ESI-MS	Electrospray ionisation mass spectrometry
EO	Ethylene oxide
EPR	Enhanced permeation effects
FOL	Folate
FRP	Free radical polymerisation
ICPN	Interconnected crystalline polymer network
GPC	Gel permeation chromatography
HA	Hydroxyapatite
HEA	2-Hydroxyethyl acrylate
HEMA	2-Hydroxymethyl methacrylate
^{1}H NMR	Proton nuclear magnetic resonance
LAM's	Less activated monomers
LCST	Lower critical solution temperature
MALDI-TOF	Matrix assisted laser desorption time of flight
MAM's	More activated monomers
mPEGA	methyl(polyethyleneglycol)methacrylate
MMA	Methyl methacrylate
M_n	Number average molecular weight
MW	Molecular weight
M_w	Weighted average
MW	Molecular weight
NAS	*N*-acryloxysuccinimide
NGS	Next generation sequencing
NHS	*N*-hydroxyl succinimide
NHS-PEG	NHS functionalised polyethylene glycol
NIPAAm	Nisopropylacryamide

NMP	Nitroxide mediated polymerisation
nM	Nanomolar
Ns	Packing parameter
PAGE	Polyacrylamide gel electrophoresis
PCR	Polymerase chain reaction
Đ	Polydispersity index
PDP	4-pyrrolidinpyridine
PDMS	Polydimethylsiloxane
PEG	Polyethylene glycol
PEO	Poly(ethylene) oxide
PEO-MI	PEO based macro-initiator
PEO-MM	PEO macro monomer
p(mPEGA-*co*-AA-NHS)	Poly(methyl(polyethyleneglycol)methacrylate-*co*-acrylic acid-*N*-hydroxy succinimide)
poly(mPEGA-co-AA-allylamine)	Poly(methyl(polyethyleneglycol)methacrylate-*co*-acrylic acid-Allylamine
pNIPAAm-co-HMAAm	poly*N*-isopropyl-*co*-hydroxymethylacrylamide
pH	
PLGA	Poly(*D*, *L*-lactide-*co*-glycolide)
pNIPAAmn	Poly *N*-isopropylacryamide
POEGMA	Poly[oligo(ethylene glycol)monomethyl ether methacrylate]
ppm	Parts per million
qPCR	Quantitative polymerase chain reaction
RAFT	Reversible addition-fragmentation chain transfer
R-ssDNA	23 mer ssDNA bio-conjugated RAFT agent
ROP	Ring open polymerisation
SA	Strained alkyne
SEC	Size exclusion chromatography
SEM	Scanning electron microscope
SNA	Spherical nucleic acid
SPAAC	Strain promoted azide alkyne reaction
ss-DNA	Single stranded DNA
SYBR GREEN	SG
TAE	Tris acetate EDTA

TEM	Transmission electron microscopy
TEMED	*N,N,N'*,-tetramethylethylene-diamine
TR-PCR	Temperature responsive PCR bioconjugates
TBE	Tris borate EDTA
UV-Vis	Ultra violet-visible spectrophotometry
W_d	Dry weight
W_s	Swollen weight

Chapter 1. Introduction and Literature Review

Synopsis

Bio-molecules conjugated to polymers have been synthesised for their therapeutic or diagnostic applications. This chapter presents a review of some of the chemical methods used in the coupling of polymers to bio-molecules, as well as the history of their use and the progress that has recently occurred. It also highlights the synthesis, design and impact PEG and pNIPAAm have had in developing polymer bio-conjugates for the bio-medical field and why these polymers have been so successful. Finally, this chapter examines the structural characteristics of DNA, its chemical synthesis, amplification and why DNA polymer bio-conjugates remain important to bio-medical applications.

1 Chapter 1. Introduction

1.1 Overview

Polymer bio-conjugates are simply polymers that are attached to bio-molecules via some sort of chemical linkage. It was bio-medical and pharmaceutical applications that drove the early research into the field of polymer bio-conjugates [1]. There are numerous polymer and bio-molecule combinations possible, as the library of synthetic polymers or biomolecules is extensive. Choosing the type of polymer can depend on the application. For example, when developing polymer bio-conjugates for bio-medical applications polyethylene glycol (PEG) is commonly chosen due to its bio-compatibility properties (discussed further in Chapter 1, Section 1.5-1.6). Selecting the method of polymerisation is also important when designing new polymer bio-conjugates (discussed further in Chapter 1, Section 1.3-1.4). While the number of polymer bio-conjugates appears to be endlessly diverse, the synthesis of these polymer bio-conjugates is achieved through a few main strategies. Grafting-to (Figure 1.1 a), grafting-from (Figure 1.1 b) and grafting-through (Figure1.1 c) are the three main approaches used in producing polymer bio-conjugates [2].

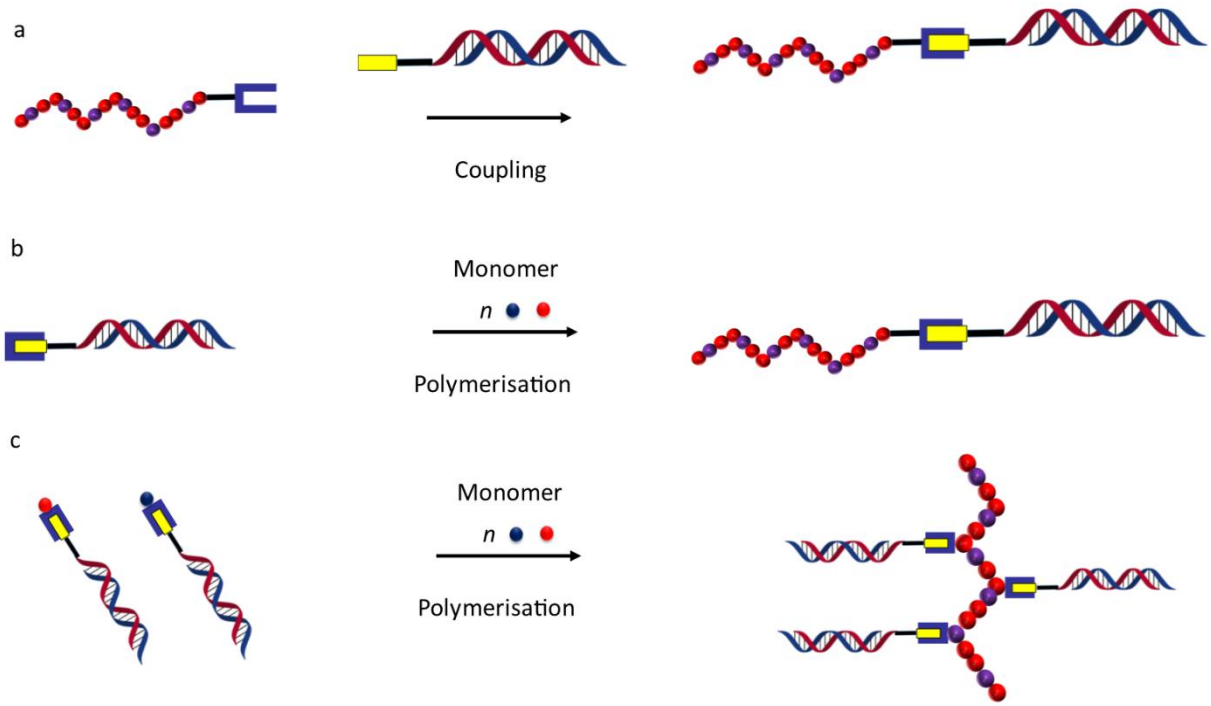

Figure 1.1. a), Grafting-to: a pre-formed polymer (red/blue chain) that is functionalised (blue rectangle) is conjugated via the bio-molecules functionalised group (yellow group), b) Grafting-from: the bio-macro-initiator (blue group) initiates polymerisation of n monomers (red dot and blue dot) and c) Grafting-through: the bio-molecule contains a polymerisable group (red dot and blue dot) and can be polymerised with other n monomers to produce a polymeric chain that has bio-molecules attached. Adapted from [2].

Grafting-to is performed when a pre-formed polymer (red/blue chain, Figure 1.1 a that is functionalised (blue rectangle) is conjugated via the bio-molecules functionalised group (yellow group, Figure 1.1 a, when grafting-from, an initiator is chemically attached to the bio-molecule to produce a bio-macro initiator. The bio-macro-initiator (blue group, Figure 1.1 b initiates polymerisation of n monomers (red dot and blue dot, Figure 1.1 b. Grafting-through is performed when a bio-molecule contains a polymerisable group (red dot and blue dot, Figure 1.1 c and can be polymerised with other n monomers to produce a polymeric chain that has bio-molecules attached.

1.1.1 Grafting-to

Grafting-to has been widely adopted due to its simplicity. This method can involve coupling bio-molecules to polymers using chemical techniques that target specific functional groups found in bio-molecules [3-8]. Grafting-to allows for the independent preparation of polymers not limited by the choice of solvent, temperature, radical concentration and other synthetic conditions that may affect the other methods of preparing polymer bio-conjugates [9]. The purification, and conjugation efficiency of polymer bio-conjugates produced by the grafting-to method are some of the reasons that other methods of producing polymer bio-conjugates have been pursued [10].

Early strategies of coupling PEG to proteins focused on the common functional groups (amines and/ or thiol (or sulfhydryl) groups present in proteins. The amine functionality is very common in proteins and so coupling strategies were developed to target this functional group. A key milestone for polymer bio-conjugates occurred when Abuchowski *et al.* [11] covalently attached activated cyanuric chloride functionalised PEG by a substitution reaction with the primary amine of bovine serum albumin (BSA). The group found that when their PEG-protein conjugate was introduced into the bloodstream of a rabbit, it did not elicit an immune response. Because there was no significant immune response, the PEG-protein conjugate was shown to have longer circulation times in the rabbit's bloodstream. The preparation of PEG-protein conjugates by Abuchowski *et al.* [11] now commonly known as PEGylation, opened a new field of research into polymer bio-conjugates for therapeutic use. Another early example of a polymer bio-conjugate strategy that targeted the amine functionality involved the alkylation of the amino group and used aldehyde functionalised PEG. The reaction proceeds via a Schiff base that is reduced *in-situ* to yield a stable secondary amine linkage [12]. A much more common approach to PEGylation that is still in use, involves the acylation of amine functionalised proteins with activated esters PEG polymers. This reaction proceeds under near physiological conditions and produces stable amide linkages (discussed further in Chapter 1, Section 1.2.1) [13].

While the amine functional group in polymer protein conjugation still receives widespread attention, one of the drawbacks of grafting polymers to proteins with this functional group is the non-specific attachment that can occur due to the number of amine groups available [14]. Other, more recent methods of polymer protein

conjugation, target the less common cysteine groups found in proteins. PEG, functionalised with disulphide groups or maleimide groups made conjugation to proteins more selective. This is because the thiol functionality in cysteine groups reacts more selectively with disulphide or maleimide groups. Also, since cysteine groups can now be genetically engineered into proteins through the replacement of a non-essential amino acid, the site of polymer attachment can be better directed [15]. However, some side reactions can still occur; disulphide functionalised PEG can react with reducing agents and maleimide functionalised PEG can react with amines resulting in undesirable non-specific reactions [14].

The desire for site specific polymer bio-conjugation methods that are kinetically fast and selective to specific functional groups present in bio-molecules led to the development of bio-orthogonal reactions. Highly efficient site-specific conjugation using bio-orthogonal chemistry utilises functional groups not found in bio-molecules (discussed further in Chapter 1, Section 1.2.3-1.2.6)) In this thesis polymer bio-conjugates were prepared through the grafting-to process using carbodiimide chemistry (discussed in Chapter 1, Section 1.2.1 and Chapter 3, Section 3.2) and bio-orthogonal chemistry (discussed in Chapter 1, Section 1.2.3 and Chapter 5, Section 5.4).

1.1.2 Grafting-from

The grafting-from method involves the attachment of an initiating agent to a bio-molecule (bio-macro initiator), polymer is then grown from the bio-molecule during the polymerisation of a monomer [16-18]. An advantage of the grafting-from method is that directly growing polymer from the bio-molecule can lead to an improvement in conjugation efficiency [19]. It is for this reason grafting-from was then explored in this thesis, details in Chapter 3.

1.1.3 Grafting-through

When a bio-molecule is functionalised with a polymerisable group it then becomes a bio-macro monomer [20]. The polymerisation of this bio-macro monomer is known as grafting-through [20]. This strategy was not explored here as the focus involved relatively large bio-molecules and steric hindrance during polymerisation of the bio-macro monomer is reported to be problematic [21].

1.2 Carbodiimide Coupling

1.2.1 Coupling Chemistry: Carbodiimide and Steglich Esterification

Carbodiimide coupling chemistry in this thesis provided a bio-macro initiator from which polymer bio-conjugates were produced via the grafting-from method. The following section describes the mechanism of carbodiimide reactions and how the fabricated polymer bio-conjugates can be used in bio-medical applications.

The formation of an amide or ester bond in organic chemistry that results from the coupling of a carboxylic acid with an amine or an alcohol moiety, respectively, is a commonly utilised reaction in organic chemistry [22, 23]. This chemistry has also been applied in the bio-conjugation of bio-molecules to polymers, nanoparticles and surfaces [24-26]. In general, most methods of coupling these moieties operate in a way that activates the carboxylic acid through dehydration. Carbodiimide coupling, is one such example that is commonly used. The carboxylic acid molecule can be activated by a coupling reagent such as *N*-ethyl-*N'*-(3-dimethylaminopropyl)carbodiimide (EDC) [27]. In Scheme 1.1, the reaction between a carboxylic acid group (molecule 1, Scheme 1.1) and EDC is shown. First intramolecular cyclisation and deprotonation of the acid by the base EDC results in the formation of the carboxylate anion. This is followed by nucleophilic attack at the delta positive carbon on the EDC molecule followed by ring opening to produce the *O*-acylisourea activated ester (molecule 2, Figure 1.2) [28]. The activated ester can then react with a nucleophile (R-X, Scheme 1.1) at the delta positive carbon to produce an amide, ester or thioester product (molecule 3, Scheme 1.1) [29]. The formation of the desired compound is also accompanied by the formation of a urea product (molecule 4, Scheme 1.1) [29]. If there is an excess of molecule 1, nucleophilic attack by the carboxylate ion leads to the formation of the carboxylic acid anhydride (molecule 5, Scheme 1.1) and this can also result in the formation of the desired product (molecule 3, Scheme 1.1) and regeneration of the carboxylic acid starting material [30]. There is also a competing undesirable reaction, the rearrangement of *O*-acylisourea active ester (molecule 2, Scheme 1.1) to the *N*-acylurea by-product (molecule 6, Scheme 1.1) which can form due to the presence of water [30].

The conditions developed by Steglich *et al.* [31] overcame the formation of the undesired by-product (molecule 6, Scheme 1.1) when they introduced dimethylaminopyridine (DMAP) as a catalyst. The fast reaction between DMAP and the *O*-acylisourea (molecule 2, Scheme 1.1) results in the formation of an acyl pyridinium species that cannot form the undesired by-product through the rearrangement mechanism [31]. The acyl pyridinium can then react with the desired nucleophile to form the desired product (amide, ester or thioester) [31].

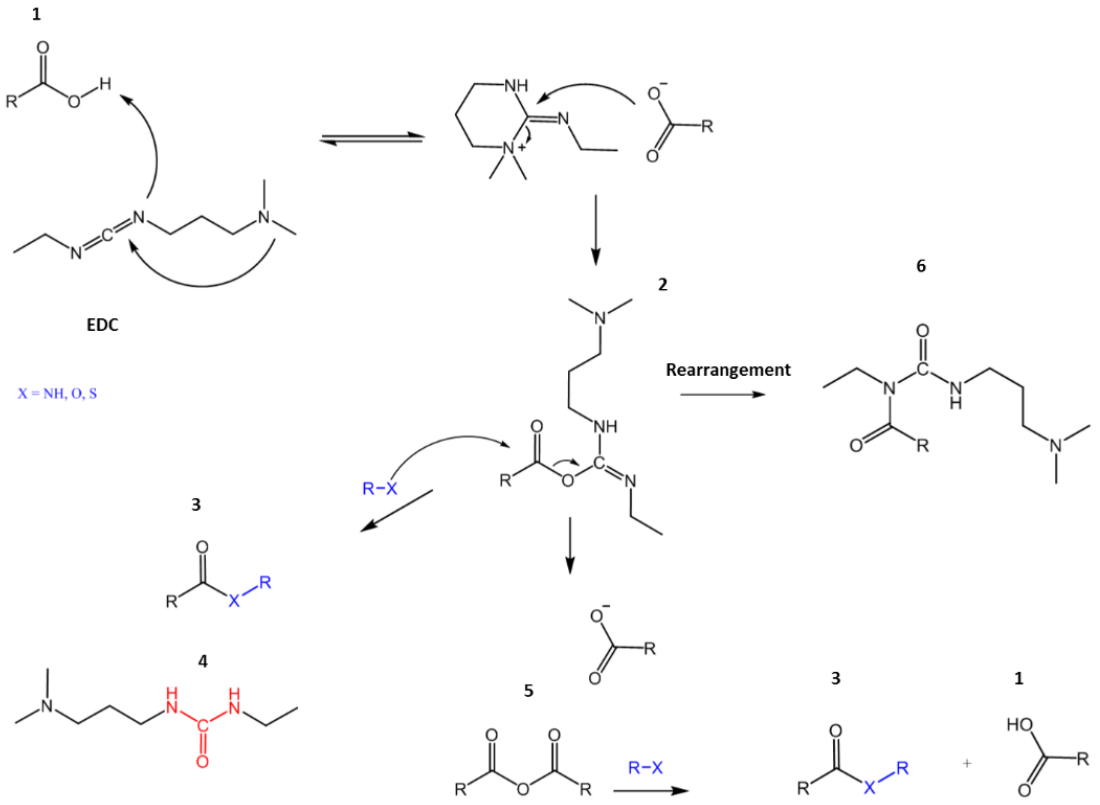

Scheme 1.1. Mechanism of carbodiimide coupling using EDC [28, 30].

1.2.2 Bio-medical Applications of Carbodiimide Coupling

There are numerous examples in the literature where bio-medical application studies have utilised carbodiimide coupling, including those involved in the synthesis of polymer bio-conjugates for immunoassay applications, the design of drug carriers or those used in the surface attachment of bio-molecules in microarray applications [21, 32-35]. Hoffman *et al.* [5] pioneered the use of EDC and *N*-hydroxyl succinimide (NHS) as a method of immobilising bio-molecules to polymers for therapeutics. The group prepared a monomer conjugated bio-molecule using NHS/EDC chemistry and then grafted it to pre-irradiated cellulose where the trapped radicals reacted with the monomer conjugated bio-molecule thus immobilising the bio-molecule to a substrate [5]. The introduction of the NHS moiety in carbodiimide coupling imparted greater stability when performing amide coupling, or in preparing active ester substrates that could be post functionalised with amine nucleophiles [29, 36]. The NHS moiety reacts with carboxyl compounds to give the more stable amino acyl ester, which can then be isolated or reacted *in situ* with amine nucleophiles [37]. Photo cross-linked PEG/acrylic acid networks prepared by Hubbell *et al.* [38] had their carboxylic acid functional group activated by NHS groups to then successfully attach peptides. The amount of peptide attached to these systems was controlled by the amount of acrylic acid incorporated into the polymer network [38]. The group also demonstrated that cell adhesion to a polymeric substrate could be controlled by the peptide that was attached to the polymer network [38].

Nanoparticles prepared by Choi *et al.* [39] for bone targeted drug delivery applications used carbodiimide chemistry to attach bio-molecules. The group chose to make nanoparticles as drug delivery vehicles because studies have shown that the hydrodynamic volume and molecular weight is decreased relative to linear counterparts; and this is thought to be important for their circulation, uptake and accumulation in organs [40-42]. The targeting molecule, alendronate was conjugated to synthesised poly(*D*, *L*-lactide-*co*-glycolide) (PLGA). Alendronate was reported to have a strong affinity for hydroxyapatite (HA), which is found in bone and teeth [43]. The conjugation of alendronate was achieved by first activating the carboxylic acid of the synthesised PLGA polymer with EDC/NHS chemistry to produce an activated ester polymer [39]. Alendronate contains a primary amine functionality and will therefore react with active esters [43]. Post functionalisation with alendronate resulted in a stable amide bond between the alendronate and the PLGA polymer [39]. The nanoparticles were prepared by the dialysis method which involved mixing the alendronate conjugated PLGA polymer with synthesised monomethoxy PEG (mPEG)-*co*-poly(*D*, *L*-lactide-*co*-glycolide block copolymers [39]. Their study revealed that the hydrophilic block length (mPEG) did not appear to affect the size of the nanoparticles that formed and that the release of a drug (estrogen) was not influenced by increasing the hydrophilic block length [39]. Changing the block length however, was found to affect the ability of alendronate to target HA [39]. The nanoparticle system prepared by Choi *et al.* [39] using the dialysis method showed limited capabilities in controlling the release of a target drug, which is a common problem for self-assembly drug delivery systems [44, 45].

The controlled release of drugs from drug delivery systems can be achieved through a degradable covalent attachment or by cross-linking the polymeric system [45]. Sang *et al.* [46] demonstrated sustained release and increased cellular uptake by combining free doxorubicin (DOX) with DOX conjugated to PEG to form nano-aggregates 200 nm in size. The group used dicyclohexylcarbodiimde (DCC) DCC/NHS chemistry to covalently attach the DOX molecules and targeting folate (FOL) molecules to the α and ω terminal end of a PEG chain [46]. Their approach saw 40 % decrease in human tumour volumes of xenograft nude mice over 23 days when compared to the free DOX control; which they attribute to enhanced permeation effects (EPR) and the targeting effects of the covalent attached FOL receptor [46].

When choosing a strategy to couple bio-molecules to polymers it is prudent to consider a reaction that does not interfere with the bio-molecule, is unreactive to any undesirable groups that may be present and produces a stable covalent bond. While carbodiimide reactions and NHS groups are a useful strategy for bio-conjugation and was used in the grafting-from strategy in this thesis; it remains a reaction that is not regiospecific and can react with other nucleophilles present in a biological system. Bio-orthogonal reactions are non-reactive to undesirable groups and so were employed in this thesis for the bio-conjugation of DNA to synthesised polymers using the grafting-to method. The following section examines the mechanism of bio-orthogonal reactions and why this has become an important tool in designing polymer bio-conjugates for bio-medical applications.

1.2.3 Staudinger Ligation

For a reaction between functional groups to classify as being bio-orthogonal, it must not interfere or interact with a biological system [47]. The terms of reference for such reactions stipulate that a reaction between functional groups must result in a stable covalent linkage [47]. Since the concentration of the reactants is likely to be quite low, the reaction must have fast kinetics and the reaction must occur at physiologically relevant temperatures and pH [47]. Interest in the classic Staudinger reduction reaction came from researchers looking for small molecules not present in the biological system, which because of their selective reactivity, would not interfere with or interact with the many number of functional groups present in the biological system [48]. The azide, due to its absence from the biological system, kinetic stability and preference for soft electrophiles (like phosphines) made it an ideal candidate for ligating bio-molecules with reporter labels [48].

The Staudinger ligation of azides and phosphines sparked a new era in bio-orthogonal chemistry, the classic Staudinger reduction of azides was modified through the addition of an ester group at the ortho position on one of the aryl rings of the triphenylphosphine reagent [47, 48]. The ester group offered a new pathway of reactivity in which the nucleophilic nitrogen atom reacted with this electrophilic trap to form an intermediate, which, upon hydrolysis, yielded a stable amide-linked product [48, 49]. This modification overcame the hydrolysis removal of the covalent linkage formed during the classic Staudinger reduction reaction [48, 50-52]. The Staudinger ligation reaction was shown to be nontoxic and effective at ligating bio-molecules via a bio-orthogonal chemical reaction, however, the triphenylphosphine oxide group remained covalently attached to the two groups that were coupled together [53-55]. The emergence of the traceless Staudinger ligation overcame this initial deficit by attaching the phosphine reagent to a cleavable linker. The hydrolysis step in the traceless Staudinger ligation removed the interfering phosphine oxide group, now, only an amide bond linked the two groups together [56].

The immobilisation of proteins on a PEG derivatised glass slide reported by Soellner *et al.* [57] utilised the traceless Staudinger ligation reaction. scheme 1 of Scheme 1.2, shows the mechanism by which a stable amide bond is formed through the reaction between a phosphinothioester reagent and an acyl functionalised azide [57]. Scheme 2 of Scheme 1.2, illustrates the traceless Staudinger ligation method of covalently attaching proteins to a glass slide [57]. Firstly, an amine derivatised glass slide is reacted with NHS terminated PEG; this is followed by nucleophilic removal of the terminal NHS group and addition of the phosphine reagent [57]. A terminal azide group attached to the protein via lysine or PEG is then ligated via the traceless Staudinger reaction to yield site specific covalent immobilisation of proteins [57].

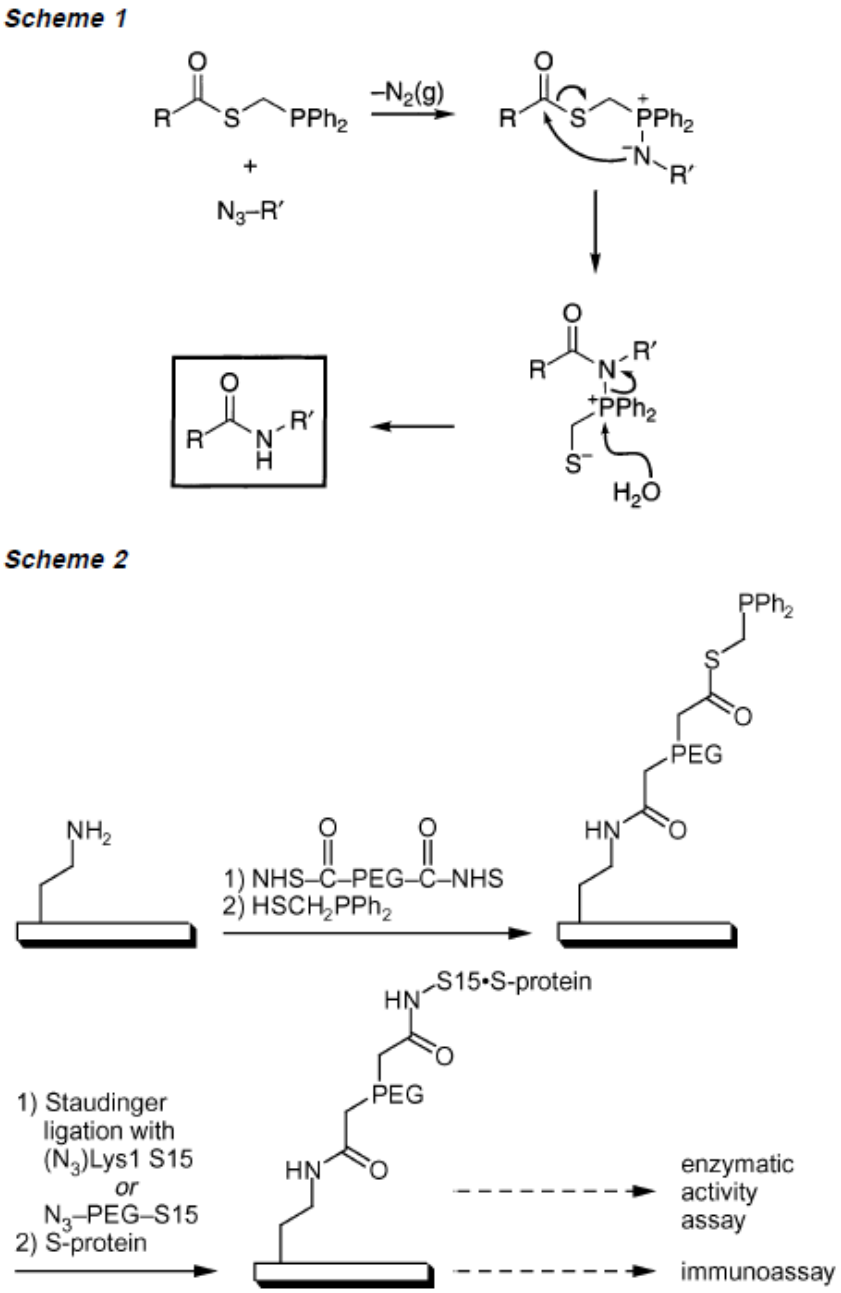

Scheme 1.2. Scheme 1: Traceless Staudinger reaction mechanism. Scheme 2: Amine derivatised glass slide treated with NHS functionalised PEG followed by protein immobilisation using traceless Staudinger reaction. Adapted from [57].

The group found that compared to randomly attached peptides (shown by amide coupling experiments), site selective attachment led to increased protein activity [57]. This was theorised to be due to the random attachment of proteins using amide coupling chemistry [57]. Since this chemistry is non-selective, amino groups, important for protein function are also reactive to the amide coupling methodology [57]. The subsequent loss of these groups in the random attachment methods is why the Staudinger ligation reaction is thought to be a more effective technique for attaching proteins to a surface [57].

While the Staudinger ligation is an effective method of coupling two groups together, there are problems with the phosphine reagent being oxidised in biological systems and the kinetics of the reaction (typically second order rate constant of 0.0020 M^{-1} s^{-1}) necessitated high concentrations of the phosphine reagent. This in turn led to problems with fluorescence imaging applications since the high concentrations resulted in a high background signal [58]. Mechanistic modifications of the phosphine reagent showed that the nucleophilic attack (phosphine) on the azide is the rate limiting step [49]. Efforts were then made to increase the rate but the modifications to the phosphine reagent led to reduced stability [47]. The Staudinger ligation is still widely used in bio-conjugation applications but the slow kinetics of this reaction remains unsolved [55].

1.2.4 Copper Catalysed Azide Alkyne 1,3 Dipolar Cycloaddition Click Reaction

Another bio-orthogonal reaction emerged in the early 2000's that again was a modified version of a classic reaction that of the standard Huisgen 1,3 dipolar cycloaddition reaction between azides and conventional alkynes. This reaction had slow kinetics at low temperatures and normal pressure and was typically performed at conditions unsuitable for biological applications [59, 60]. Sharpless and Meldal [59, 60] introduced the copper(I) catalysed "click" azide alkyne cycloaddition (CuAAC) reaction which had faster kinetics than the Staudinger ligation and was seven orders of magnitude faster than the classic Huisgen reaction. The reaction can be performed at room temperature, at a range of pH's and is considered bioorthogonal [59, 60]. The CuAAC reaction has been embraced by organic synthesis, polymer chemistry and materials chemistry [61-64]. The only drawback of the CuAAC reaction in bio-conjugation applications is copper toxicity to living systems [65-67]. A detailed study on copper based catalysts and ligands led to Finn *et al.* [68, 69] demonstrating the utility of the CuAAC reaction in bio-conjugation applications. The group coupled carbohydrates, proteins and polymers to bio-macromolecules using the bathophenanthroline ligand they found from their detailed study [68, 69]. Their inexpensive ligands were found to accelerate the reaction of azides and terminal alkynes [68, 69]. This meant that only low concentrations of copper were needed and by sequestering copper the ligands reduced protein or polynucleotide interaction [68]. The major drawback of this reaction however, was the need for inert oxygen free conditions.

1.2.5 Strain Promoted Azide Alkyne 1,3 Dipolar Cycloaddition Click Reaction

In this thesis, the strain promoted azide alkyne reaction (SPAAC) was used to conjugate azide DNA to poly(*N*-isopropyl acrylamide)-*co*-hydroxymethlyacrylamide (pNIPAAm-*co*-HMAAm) copolymers (Chapter 5). The following section examines the mechanism of this reaction and the bio-medical applications of click reactions. The "Click" like reaction involving azides and strained alkynes developed by Bertozzi *et al.* [70] for *in vivo* applications sought to overcome the one drawback of the CuAAC reaction, its toxicity to living cells due to the use of a copper catalyst. The SPAAC eliminated the need for copper catalysts and because it also utilises the important azide molecule, it is easily integrated into existing methodologies [70]. Interest in the reaction of strained alkynes and azides originated from the report by Wittig and Krebs [71], where they described in 1961 the "explosive like" reaction of neat cyclooctyne with phenyl azide to form a triazole product. The dipole distortion energy (18.1 kcal/mol) of the azide is the largest contributor to overcoming the activation energy barrier in 1,3 dipolar cycloaddition reactions with linear alkynes [72, 73]. It was theorised that the massive bond angle deformation of the acetylene group in cyclooctyne to 163^{O} accounts for nearly 18 kcal/mol of ring strain and that this is responsible for lowering the activation energy that is required to distort the 1,3 dipole (azide) and dipolariphile (alkyne) to the required transition state geometry [74, 75]. Initially, the first generation cyclooctynes conjugated to biotin probes, termed OCT, had limited solubility and slow kinetics, this led to mechanistic modifications of the cyclooctyne through the addition of an electron withdrawing fluorine atom [76]. The addition of a second fluorine atom to the cyclooctyne structure produced difluorinated cyclooctyne (DIFO), which resulted in an order of magnitude improvement over the kinetics of the OCT reaction with azides [76]. Boons *et al.* [77] were also working with cyclooctynes for cell labelling studies at the same time as Bertozzi *et al.* [76]. They synthesised dibenzocyclootynols (DIBO) molecules which displayed similar kinetic reactivity with azides to that which was already shown by DIFO [77]. They subsequently used the synthesised DIBO group to label glycoproteins in living cells [77]. Another group inspired by the DIBO molecule developed by Boons *et al.* [77] improved the kinetics by an order of magnitude over DIBO by introducing an amide bond to the DIBO scaffold [78]. Their version of the strained alkyne aza-dibenzocyclooctyne (DIBAC), was reported to have a rate constant of k= 0.31 M^{-1} s^{-1} [78]. DIBO was subsequently used by the group for the PEGylation of an azide containing enzyme *Candida antarctica* type B lipase (AHA-CalB) [78].

1.2.6 Click Reactions and their Applications

Bio-conjugation through click chemistry can involve the labelling of bio-molecules such as proteins, glycans, lipids and nucleic acids for *in vitro* or *in vivo* applications [58, 70, 79, 80]. The click reactions have also been exploited when conjugating bio-molecules to surfaces for use in microarray applications and when conjugating bio-molecules to polymers for drug delivery applications [81, 82]. The chemical modification of DNA using "click" chemistry has been explored ever since these valuable techniques were first developed. In

a study by Carrel *et al.* [83] the utility of the CuAAC reaction was demonstrated when the group used alkyne modified triphosphates instead of conventional triphosphates in a polymerase chain reaction (PCR) reaction (discussed in Section 1.7) to produce PCR products with different alkyne densities. Azide functionalised sugars and azide functionalised fluorescent labels were then conjugated to the alkyne functionalised PCR products via the CuAAC reaction [83]. The enzymatic incorporation of alkyne groups through PCR using these modified nucleotides followed by the simple, fast and efficient click reaction with azide functionalised labels resulted in a much greater labelling capacity [83]. For bio-orthogonal reactions involving click reactions the azide chemical reporters (Figure 1.2, blue circle) are in general, incorporated into the target bio-molecule, and the probe molecule or label must in general contain the alkyne moiety. Both the chemical reporter and probe must not interact with other molecules present in the system (Figure 1.2, grey shapes) [65].

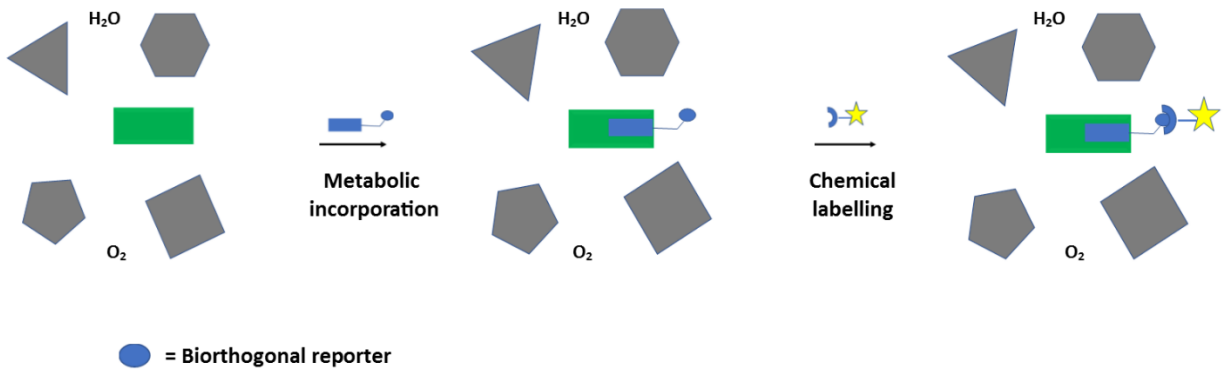

Figure 1.2. Scheme depicting the bio-orthogonal reporter strategy. Adapted from [65].

For *in vivo* and *in vitro* applications, azides are commonly incorporated into bio-molecules like proteins, glycans and lipids because of their small size and lack of reactivity with nucleophiles found within the biological system [48, 84, 85]. Azide incorporation into DNA has been performed enzymatically and chemically [86, 87]. Chemically synthesised azide functionalised DNA by the phosphoramidite method (discussed later in, Section 1.7) is generally post modified to contain azide functionality since the trivalent phosphorus used in this method reacts (Staudinger reaction) with azide groups [88]. Studies have shown however, that it is possible to chemically synthesise azide functionalised DNA by the phosphoramidite method using a H-phosphonate monomer in a mixed method coupling system [87].

To best use polymer bio-conjugates for both *in vitro* and *in vivo* applications. This thesis has utilised azide functionalised DNA's (chemical reporters) and strained alkyne functionalised polymers (capture probe). The aim was to prepare polymer bio-conjugates which could be used in the separation, enrichment and detection of dilute biomarkers, or as novel targeted drug delivery vehicles. It is important that when optimising a polymer bio-conjugate, the design of the capture probe (polymer) is tailored towards its application. Reversible addition-fragmentation chain transfer (RAFT) polymerisation is a useful tool for designing new

polymer bio-conjugates. RAFT polymerisation was investigated in this thesis for the design of new polymer bio-conjugates, the following section examines the mechanism of RAFT, the importance of matching the RAFT agent to the monomer and the post modification advantages of RAFT.

1.3 Reversible Addition Fragmentation Chain Transfer (RAFT) Polymerisation

Since the introduction of the process of controlled radical polymerisation (CRP), it is now possible to produce a wide range of polymer architectures from linear to star shaped [89, 90]. This has also resulted in an increase in the synthetic number and variety of block copolymers produced [89]. The RAFT method of polymerisation is one of the most widely used CRP processes, also known as a member of the reversible deactivation radical polymerisation processes. In theory chain transfer reactions have similar kinetics to RAFT, however the stability of the intermediate is an important facet of RAFT polymerisation. RAFT has produced many examples of novel temperature responsive copolymers and block copolymers useful for bio-medical applications [91, 92]. The flexibility of the RAFT process to different solvents and reaction conditions make it an ideal choice when considering a pathway to synthesise new polymers architectures [93]. Until the introduction of a universal RAFT agent occurred, it remained problematic to block polymerise monomers like vinyl acetate and styrene [94]. Vinyl acetate belongs to a monomer class termed less activated monomers (LAM's) while the styrene monomer belongs to class of monomers termed more activated monomers (MAM's) [94]. In general, one type of RAFT agent is best suited to LAM's (e.g., dithiocarbamates) and the other is best suited to MAM's (e.g., dithiobenzoate) [94]. The recent introduction of pH switchable RAFT agents means that it is now possible to synthesise well controlled block copolymers of MAM's and LAM's by RAFT polymerisation; however, the range of monomers and degree of control does not yet match that which is available through choosing a more tailored RAFT agent [95]. RAFT, due to its versatility is capable of molecular weight (MW) control when polymerising monomers like acrylamide derivatives, acrylate derivatives and methacrylate monomers [96, 97]. These monomers are successfully polymerised by RAFT by careful selection of the appropriate RAFT agent [98].

1.3.1 RAFT Mechanism

The conventional mechanism generally accepted for the RAFT is illustrated in Figure 1.5 [99]. The first step involves radicals being produced from an external source, the most common source of radicals are produced via the thermal decomposition of azobisisobutyronitrile (AIBN) [100]. Other initiator sources have been reported in the literature; these methods include photo initiation and laser irradiation [101, 102]. However, the most widely used method in RAFT polymerisation involves an initiator source that degrades thermally to give radicals. The decomposition of the thermal initiator source (Scheme 1.3, step 1) produces radicals which then go on to react with the monomer to produce oligomeric radicals [101]. These monomer radicals then react preferentially with the RAFT agent (Scheme 1.3, step 2) due to the reactive thiocarbonyl group [99].

This is an important step, as any reaction with further monomer would lead to short, dead chain length polymer, resulting in a broadening of molecular weight and an increase in the polydispersity index (Đ) [99]. The crucial control mechanism of RAFT is the reversible chain transfer process (Scheme 1.3, step 2). This is where the RAFT adduct radical can fragment back to the original RAFT agent or an oligomeric radical, (Scheme 1.3, poly RAFT agent) and a reinitiating R radical [100].

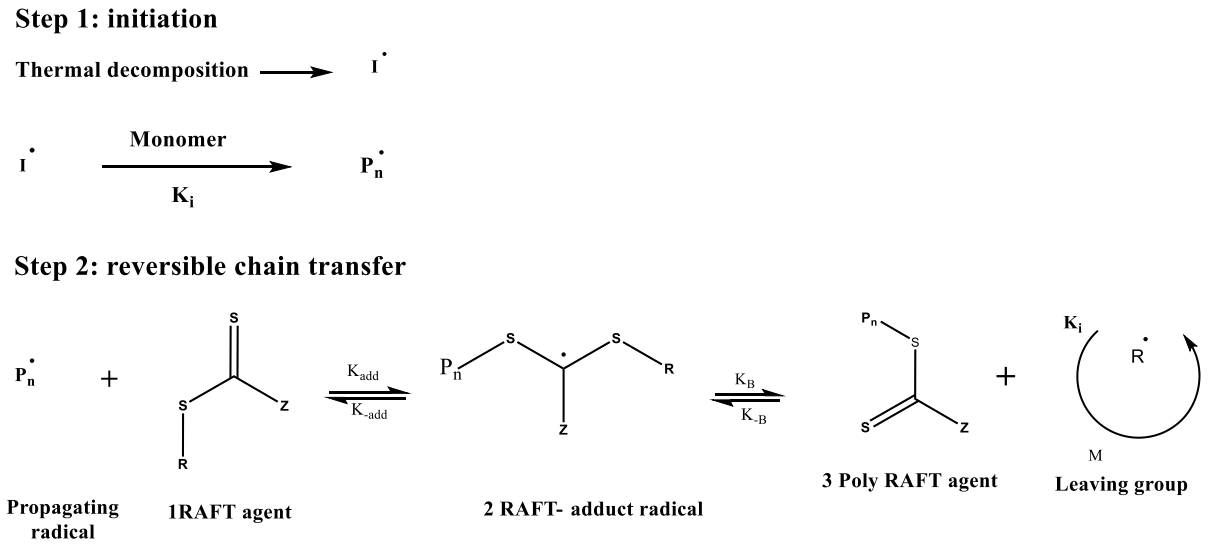

Scheme 1.3. Synthetic scheme for initiation, reversible chain transfer and reinitiating of RAFT polymerisation [103].

In Scheme 1.3, step 3 the R radical produced in step 2 can go on to react with more monomer and reinitiate the process. In Scheme 1.4, step 4 there is a rapid exchange between the propagating radicals and the RAFT adduct radical. It is this step that reduces the number of growing radical chains and therefore limits the termination reactions [100]. The resulting RAFT equilibrium shown in Scheme 1.4, step 4 does not directly influence the rate of polymerisation; instead it participates in the reduction and the narrowing of the molar mass distribution [100]. Finally, the reaction can be terminated via combination or disproportionation, although this is expected to be limited due to the RAFT mechanism (Scheme 1.4, step 5) [103]. The synthetic design of a RAFT agent is a crucial element that influences its ability to control the polymerisation of a chosen monomer system [103].

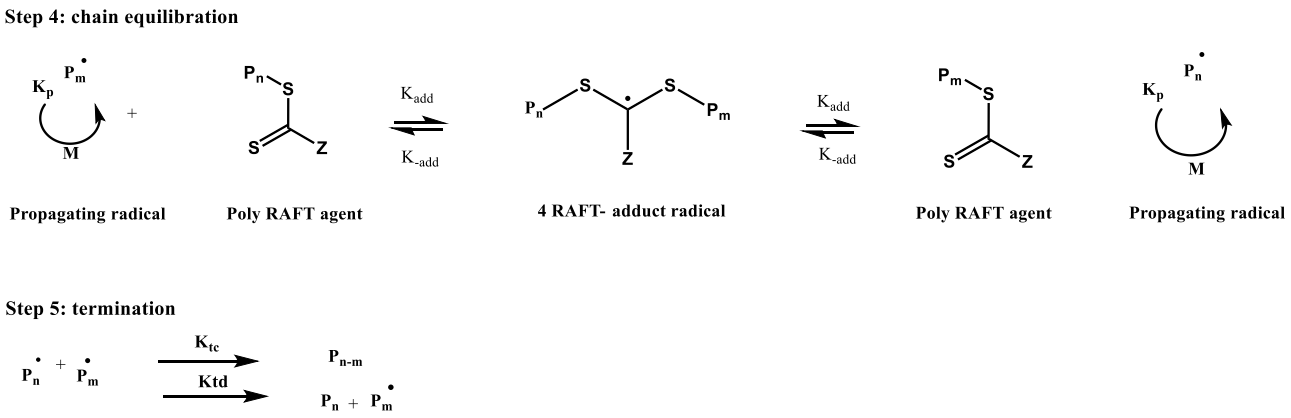

Scheme 1.4. Synthetic scheme for chain equilibration and termination for RAFT polymerisation [103].

1.3.2 RAFT Design: Role of the R Group and Z Group

For the RAFT mechanism to be effective, the structure of the RAFT agent is vital [100, 103]. Thang *et al.* [100, 103] have published comprehensive research in the design of RAFT agents; they indicate that the structure and role of the R and Z group (Figure 1.3) is critical to the RAFT mechanism.

The R group functionality needs to act both as a good leaving group and as a species which reinitiates the polymerisation [103]. If the R group does not fragment preferentially to the oligomeric radical then control over the polymerisation will be lost, resulting in dead chain polymer and poor control over Đ [103]. Studies performed by Chong *et al.* [104] into RAFT polymerisation of methyl methacrylate (MMA) have shown that the structure of R plays a more critical role with some polymers. They found that the steric bulk of the R group and the stability of the newly formed radical determine the partition coefficient and the reinitiating of the system [104]. When the R group was cumyl or cyanoisopropyl the steric bulk and electrophilic nature of these groups afforded better leaving group capacity and improved the capacity to reinitiate the polymerisation process [104].

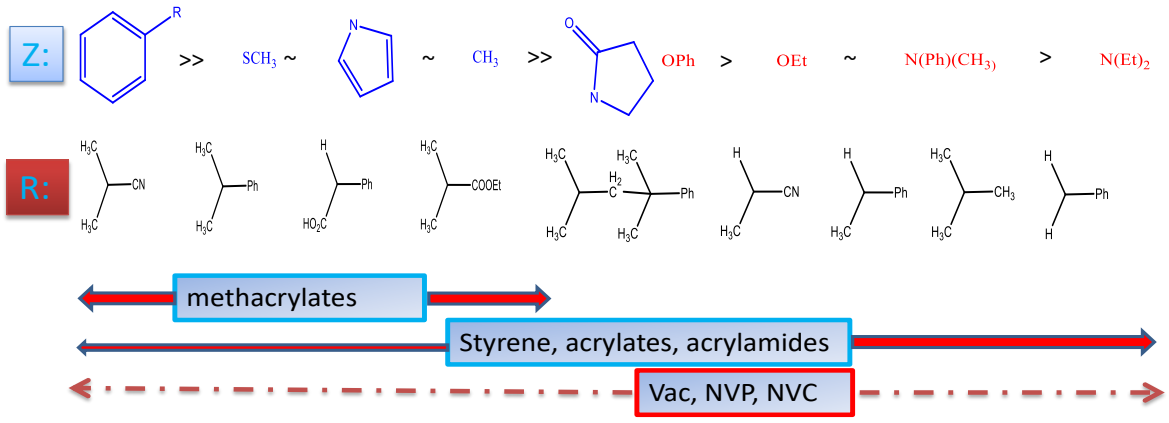

Figure 1.3. Guidelines for selection of RAFT agents for various polymerisations. Adapted from [105].

A strategy often used in the design of RAFT agents is to have an R group such that it has structural similarity to the monomer being polymerised [106]. By having an R group that has similar electronic and structural properties, the ability for the leaving radical to reinitiate the polymer is increased [106]. Roshan *et al.* [99] have shown experimentally that control over the polymerisation of styrene with dithioesters, (Z = alkyl or aryl) trithiocarbonates (Z = SR'), and dithiocarbamates (Z = NR'R") can be achieved. However, their studies also revealed that the attached nitrogen group on the Z group of the RAFT agent will interfere and prevent control, if the lone pair of electrons are able to conjugate to the thiocarbonyl bond [99]. It is therefore important when designing a RAFT agent for styrene polymerisations that the lone pair of electrons from the Z group are unable to conjugate through the thiocarbonyl bond [107]. Conjugation through the thiocarbonyl group by the lone pair of electrons is known to lead to slower rates of addition at the sulphur bond. An example of such a RAFT agent includes dithiocarbamate derivatives derived from pyrrole and imidazole [108]. The aromatic Z group of the dithiocarbamate RAFT agent prevents the nitrogen from conjugating with the thiocarbonyl group and thus prevents the reduction in the double bond character of the thiocarbonyl group [107]. Instead the aromatic group conjugates to the lone pair electrons on the nitrogen group leading to an increase in the chain transfer rate [107]. Thus, pyrrole and imidazole based RAFT agents, because of their design, have been shown to exhibit good control over the polymerisation of styrene [99].

1.3.3 Acrylamide /Methacrylamide Monomers

The choice of monomers used in RAFT polymerisation includes nearly all monomers used in conventional FRP [99]. The large range of monomers available for RAFT polymerisation affords the polymer chemist greater choice and design flexibility that subsequently leads to an increase in the diversity of polymers that can be synthesised [109, 110]. In this thesis, RAFT polymerisation of methacrylamide, acrylamide, and acrylate monomers was conducted, and a review of the literature was performed to establish the most appropriate RAFT agent to use when polymerising these monomers. Methacrylamide monomers are best controlled using dithiobenzoates [111]. Steric effects of the R and $R^{\bullet}$ radical substituent investigated by Thang *et al.* [111] have shown that bulky substituents slow down the rate of addition to the carbon disulphide bond. Therefore, the Z substituent needs to be sufficiently stabilising to enhance addition to the carbon disulphide bond [111]. *N,N*-dimethylacrylamide (DMA) and NIPAAm have been polymerised by RAFT using dithiobenzoate as the RAFT agent [111]. The plot of M_n versus conversion (Figure 1.4) shows a straight line, indicating that control over molecular weight was achieved [111]. Figure 1.4 also shows the plot of (M_n) and the weighted average (M_w) M_w/M_n versus conversion obtained from the RAFT polymerisation of NIPAAm in 1,4 dioxane at 60 ^{O}C [111]. The plot shows pNIPAAm polymer conversions measured below 80% had Đ below 1.2 indicating that the dithiobenzoate agent maintained good control over the polymerisation [111]. Other RAFT agents have also been tested for their effectiveness at polymerising acrylamide monomers such as aliphatic dithioesters, trithiocarbonates, and aromatic dithiocarbamates [99, 111, 112]. The results obtained showed that controlled polymeric architectures were achievable due to reasonably well controlled Đ [112]. There are

however, recent reports in the literature that highlight trithiocarbonate degradation when polymerising *N*-phenyl methacrylamides [113].

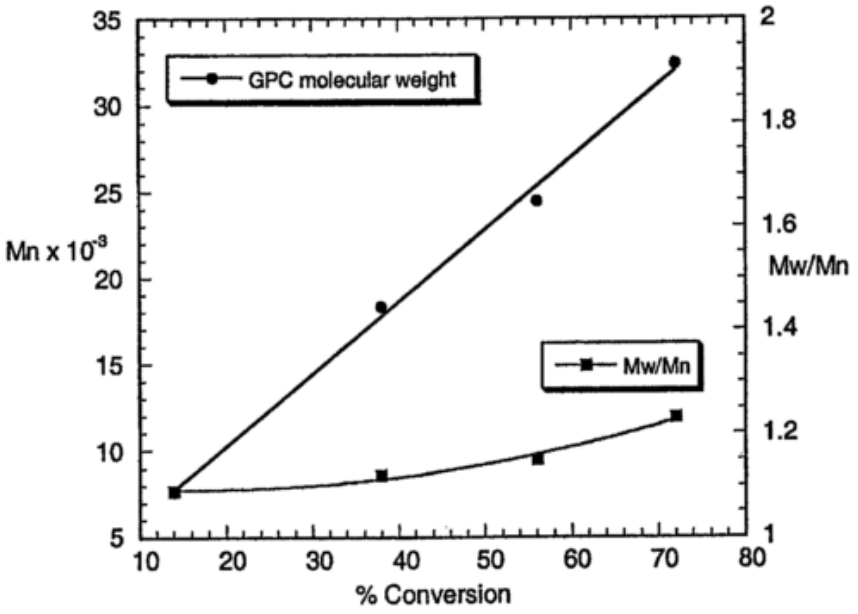

Figure 1.4. Change in molecular weight and Đ with conversion for the polymerisation of NIPAAm using the RAFT agent (dithiobenzoate). Adapted from [111].

1.3.4 Acrylates

In this thesis, the 2-hydroxyethyl acrylate (HEA) monomer was polymerised by a synthesised bio-macro RAFT agent. A trithiocarbonate RAFT agent was chosen as it was thought that this could facilitate the preparation of a tri-block copolymer. The CRP of acrylate monomers provides control of molecular weight by limiting the termination reaction or chain transfer reactions [114]. Living polymerisations such as nitroxide mediated polymerisation (NMP) and atom transfer radical polymerisation (ATRP) are an extension of the CRP process and enable the preparation of block, graft or end functionalised polymers [115]. Monomers such as HEA and 2-hydroxy methyl methacrylate (HEMA) have been polymerised by CRP methods [116, 117]. The controlled polymerisation of monomers such as HEA and HEMA have substantial commercial interest due to their use in fields such as bio-medical coatings, bio-materials, drug delivery and tissue engineering [118-121].

Coca *et al.* [117] first reported the homopolymerisation of HEA by ATRP in the late 1990's. The group performed the successful polymerisation of HEA in organic and aqueous solvents which resulted in pHEA polymers with relatively high molecular weights that went to high conversions and exhibited low Đ [117]. FRP of acrylates typically produce reactive radicals with low steric bulk [111]. Therefore, an appropriate RAFT agent to control the polymerisation of acrylates should be suited to reactive, low steric bulk, propagating radicals [111]. Control over the polymerisations of acrylates has been demonstrated by a wide range of Z

groups, with only the dithiocarbamates performing poorly [104]. Symmetrical trithiocarbonates have been shown to be effective RAFT agents in the polymerisation of acrylate monomers [122]. They have also been used in the literature to produce polystyrene-*b*-poly(*n*-butyl acrylate)-*b*-polystyrene ABA triblock copolymers in two steps [123]. The leaving group capability of the trithiocarbonate can also be used as a method of controlling where the location of the trithiocarbonate moiety is on the polymer chain [124]. Symmetric trithiocarbonates will be in the centre of the polymer chain whereas trithiocarbonates that have leaving groups with differing reactivity's will result in trithiocarbonates at the terminus end of the polymer chain [123]. Recently, Steinhauer *et al.* [125] synthesised well defined, low Đ, pHEA-*co*-2-methoxyethyl acrylate copolymers via RAFT polymerisation using a symmetric trithiocarbonate agent. The resulting polymers displayed temperature responsive properties over a broad range of temperatures (0-60 ^{O}C) [125]. The temperature response of pHEA-*co*-2-methoxyethyl acrylate copolymers was controlled by increasing the composition of pHEA in the copolymers produced [125].

1.3.5 End Group Modification

A further advantage of using RAFT in the design of novel polymer architectures is the ease by which the thiocarbonyl end group can be transformed post polymerisation [126, 127]. There are many synthetic techniques to modify the thiocarbonyl group described in the literature, they include, aminolysis (nucleophilic), radical catalysed reduction, radical addition fragmentation and thermolysis [126, 128-130]. The aminolysis reaction converts the thiocarbonyl group to a thiol group, this reaction is often used in the literature to prepare bio-functionalised polymers and block copolymers via di sulphide reactions or click chemistry and can be used as a method of attaching drug molecules or fluorescent molecules [131-134]. Often the end groups are easily transformed by simple chemistry to facilitate the coupling of homopolymer blocks. RAFT groups with carboxylic acid end groups can easily be transformed by carbodiimide reactions to impart end group functionality that is useful for coupling reactions [135].

The post modification of polymers synthesised by RAFT using thiol functionalised groups can occur via transformation of the thiocarbonyl group, RAFT end group or through the reaction with substituents on the polymer backbone [127, 136-138]. Recently, end group functionalised poly[oligo(ethylene glycol)monomethyl ether methacrylate] (POEGMA) was synthesised by RAFT polymerisation [139]. Activated ester end groups and aminolysis of the thiocarbonyl group were used to modify the end group functionality of the POEGMA polymer [139]. The effects on the lower critical solution temperature (LCST) due to end group exchange, were systematically studied; where it was then established that hydrophobic end groups lowered the LCST, and charged end groups increased the LCST [139].

Thiol-ene reactions are also a promising strategy for the modification of RAFT polymers, the next section will examine the mechanism of the thiol-ene reaction and its use in the modification of RAFT polymers.

1.4 Thiol-ene "Click"

The term "click chemistry" was reintroduced by Sharpless *et al.* [61] who borrowed the term from the copper-catalysed Huisgen 1,3-dipolar cycloaddition of azides and alkynes [61, 140-143]. This was based on its original definition which said that a "click reaction" must possess a very high thermodynamic driving force, be stereospecific and side products must be limited and inert [61]. The two-step click process, shown in Scheme 1.5, involves the radical addition of mercaptans (RSH) across a vinyl double bond and meets the requirements of "click chemistry" through its quantitative yields and regioselectivity (anti-Markovnikov) [62].

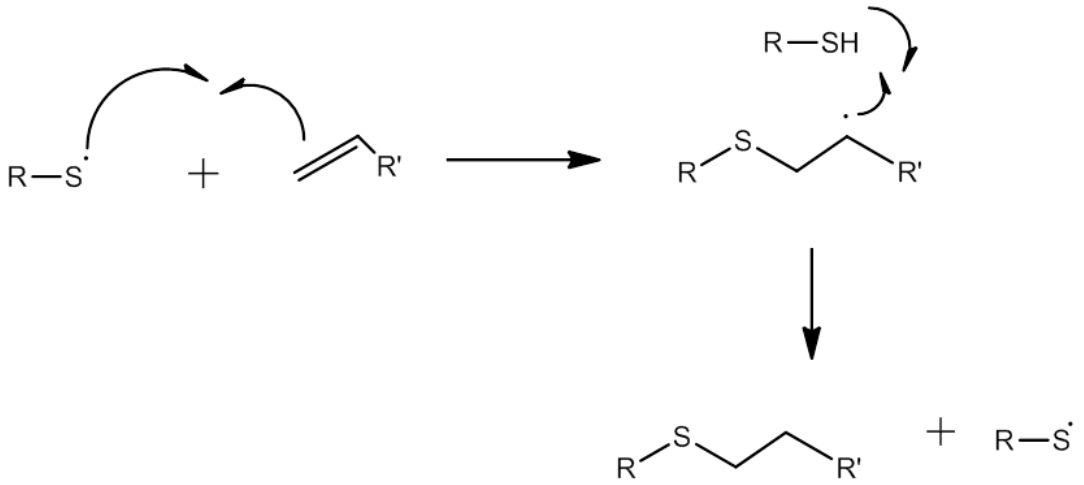

Scheme 1.5. Mechanism - anti-Markovnikov addition [62].

RAFT as a method of designing new polymer architectures will without doubt play a crucial role in the future advances in polymer synthesis. There are however, some other strategies of designing new polymer architectures that could compliment the RAFT method [142]. These strategies often use click chemistry as a powerful way of linking linear, branched or dendritic polymer structures to form new sophisticated polymer architectures [62, 142]. Stimuli responsive polymers (explained later in Section 1.6) such as pNIPAAm have also been synthesised using RAFT agents [144, 145]. This approach has proved useful in introducing branched polymer structures that modify the LCST of the resulting polymer and is a useful method of conjugating bio-molecules [144, 145]. Nucleophilic thiol-ene reactions were used by Yu *et al.* [146] to modify the thiol carbonyl end group of RAFT polymerised pNIPAAm polymers. The end groups of the pNIPAAm homopolymers were functionalised with allyl or alkyne groups, which were then further modified using radical thiol-ene/thiol-yne reactions [146]. Hydrophobic and hydrophilic groups were added to the end of pNIPAAm polymers via the radical thiol-ene/thiol-yne reactions [146]. The LCST of the end functionalised pNIPAAm polymers increased when hydrophilic groups were attached and decreased when hydrophobic groups were attached [146]. Hawker *et al.* [147] recently demonstrated how the thiol-ene click reaction was an efficient orthogonal strategy that enables allyl functionalisation of RAFT or ATRP prepared linear polymers throughout the polymer backbone or at the chain end. The group also end functionalised linear PEG with allyl bromide

and then proceeded to react the allyl polymers with thiol moieties via thiol-ene click chemistry using photochemical or thermal initiators [147]. The photochemical initiators were found to increase yields and reduce reaction times [147]. The group thus prepared a catalogue of end functionalised or backbone functionalised linear polymers that combined the benefits of the CRP process and the orthogonal thiol-ene click reaction [147]. Greater hydrogel stability can be achieved through the photo polymerisation of thiol and alkene functionalised monomers and if desired, bio-molecules can be incorporated into these hydrogels with minimal effect on bio-activity [148]. PEG, due to its bio-compatibility and resistance to protein adsorption is often used to prepare hydrogel networks [148]. PEG can also be easily functionalised with thiol and alkene groups [148]. RAFT polymerisation used in conjunction with thiol-ene click is shown in the literature to be useful way to prepare well defined polymers. In this thesis, photo cross-linking was used as way to cross-link PEG, photo polymerisation was used to prepare hydrogel disks.

1.4.1 Thiol-ene "Click" Hydrogels and Thiol-ene Photo Polymerisation

In this thesis PEG copolymers with activated ester functionality (Chapter 6) were transformed into alkene functionalised copolymers which were then cross-linked to form hydrogels disks. The following section looks at the mechanism of thiol-ene photo polymerisation.

Thiol-ene polymerisation which occurs via the "click chemistry" reaction mechanism, shown in Scheme 1.6, has been accepted for nearly one hundred years. In step 1 a radical is formed from a UV sensitive initiator and then hydrogen abstraction from a thiol monomer occurs (step 2). The resulting thiyl radical can then propagate or terminate [149, 150]. In step 3 and 4 the classic chain transfer propagation steps are observed, which gives rise to the step growth thiol-ene polymerisation [149].

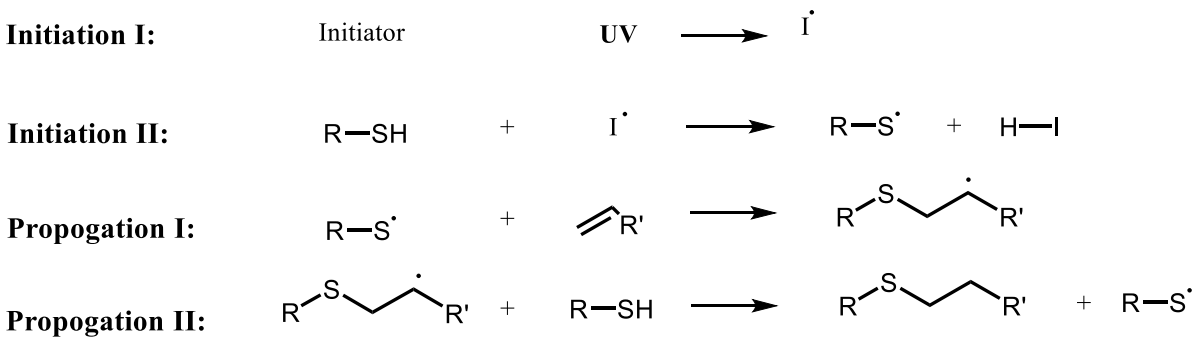

Scheme 1.6. General mechanism for thiol-ene polymerisation process [151].

Thiol-ene photo polymerisation has emerged as a convenient method to prepare branched polymers or hydrogels by cross-linking allyl or ene functionalised linear or branched structures using a multi-functional thiol crosslink monomer [152-156]. Since PEG is the most common polymer used in bio-medical applications, this thesis investigated its use in the development of polymer bio-conjugates.

1.5 Bio-compatible Polymers

1.5.1 Poly(ethylene) oxide (PEO) and Poly(ethylene glycol) (PEG) Polymers Background

The following section examines how PEG has been synthesised and used in bio-medical applications and how it has been combined with thiol-ene click chemistry to prepare polymer hydrogels for drug delivery. The use of poly(ethylene) oxide (PEO), polypropylene oxide (PPO) and PEG polymers in bio-medical research is ubiquitous due to their excellent water solubility, bio-compatibility, non-toxicity and low protein adsorption properties [157, 158]. Block copolymers comprised of PEG-*b*-PPO-*b*-PEG known as Pluronics were commercialised in the 1960's for the controlled release of pharmaceutical reagents [159]. The mechanism of drug release depends on their reversible temperature dependant phase transition from sol to gel at low and high temperatures [160]. However, these block copolymers were not bio-degradable and instability issues that arise from the weak hydrophobic interactions during the gel state have led to further research to overcome these issues [160, 161]. Polyester blocks have been introduced to aid bio-degradability and star polymers have been investigated to influence the sol to gel stability [161-163]. PEG polymers when chemically cross-linked through irradiation formed PEG hydrogels sheets that are still used today as wound dressings [164]. The number of applications for PEO/PEG polymers is vast, ranging from lubricants, emulsifiers and non-ionic surfactants to skin creams, drug delivery vehicles and peptide therapeutics [165-169]. PEO and PEG polymers, are commonly synthesised by the base/acid initiated ring open polymerisation (ROP) of ethylene oxide (EO) [170]. The most common method of synthesis of PEO/PEG is via the anionic polymerisation of EO, a base catalysed technique, which uses alcohols or water as the nucleophile that then reacts with the high ring strain of the epoxide monomer (Scheme 1.7) [170].

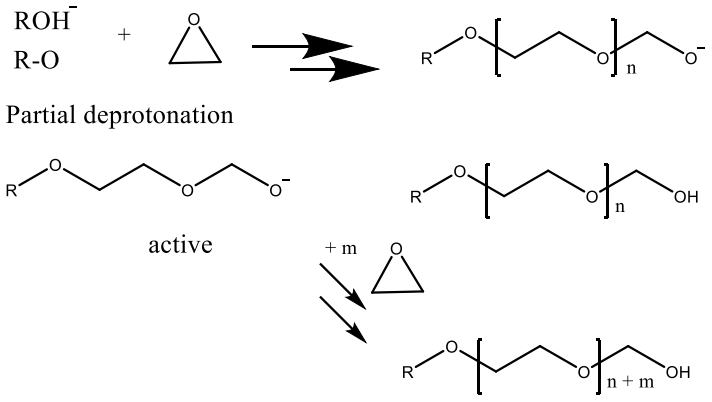

Scheme 1.7. Synthetic scheme for the anionic living polymerisation of ethylene oxide. Adapted from [170].

Scheme 1.7 illustrates the anionic living polymerisation of EO via nucleophilic attack on the epoxide monomer from the partially deprotonated alcohol leading to chain growth through degenerative chain transfer which has both an active (alkoxide) and dormant (hydroxyl terminated) component [170, 171]. When the polymer produced by anionic polymerisation has a MW greater than 30,000 g/mol it is generally named PEO, below this MW, it is known as PEG [166, 172]. Historically synthesis of PEO/PEG polymers has produced linear

polymers or end functionalised polymers. Recently, the copolymerisation of EO with some co-monomers has been done to develop multifunctional and branched PEO/PEG polymers as new dendritic polymers that increase drug loading capacity in drug delivery applications [173, 174].

There are however a limited number of monomers that can be synthesised through anionic polymerisation and so alternative strategies have been sought. Some of the other methods to synthesise hyperbranched or dendritic PEG polymers include, CRP and FRP of methacrylate PEG monomers, click couplings of prefabricated linear chains and polycondensation reactions [175-177]. In this thesis PEG copolymers were synthesised by FRP and pNIPAAm copolymers were synthesised by RAFT polymerisation. Thiol-ene reactions can be used to couple polymers, cross-link and attach bio-molecules. The next section examines how the techniques used in this thesis have been used in the literature to prepare hyperbranched and cross-linked polymers.

1.5.2 Hyperbranched PEG Polymers via Free Radical and Controlled Radical Polymerisation

Polymerisation by CRP techniques such as NMP, ATRP, and RAFT allow for greater control over molecular weight, polydispersity and the resulting polymer structure [99, 178, 179]. There are few studies in the literature where NMP has been used to polymerise methacrylated PEG, since NMP has been historically unable to control methacrylate polymerisations [179]. Recently, Chenal *et al.* [180] synthesised comb-shaped polymethacrylates with PEG side chains by NMP. The group could control the polymerisation by using a small amount of acrylonitrile monomer and a second generation nitroxide structure [180]. ATRP and RAFT polymerisation of PEG methacrylates in the literature are more common due to their ability to control methacrylate polymerisations under a greater range of reaction conditions [181]. Li *et al.* [182] performed a useful study into the advantages/disadvantages of synthesising star polymers either by CRP or FRP. An amphiphilic star shaped polymer was synthesised by FRP using a methyl methacrylate PEO macro monomer (PEO-MM) and by ATRP using a PEO based macro-initiator (PEO-MI) [182]. Their strategy was to use the more efficient “arm first” approach, where the linear polymer arms are linked together using divinylbenzene (DVB) or ethylene glycol diacrylate (EGDA) as the cross-linker molecule [182].

Figure 1.5 shows the synthetic scheme for the synthesis of the star polymers, i) the initiator, cross-linker and PEO-MM were dissolved in CH_2Cl_2 to form an organic phase (FRP), ii) catalysts $CuBR_2$/Bis(2-pyridylmethyl) octadecylamine ($CuBr_2$/BPMODA for ATRP) and polyethylene oxide macro initiator (PEO-MI) or polyethylene oxide macro monomer (PEO-MM) were dissolved in CH_2Cl_2 to form an organic phase, iii) *in situ* micellisation was performed through addition of water to the mixture followed by organic evaporation (FRP and ATRP) [182]. Both FRP and ATRP yielded uniform amphiphilic star polymers, which was confirmed by dynamic light scattering (DLS) measurements [182]. The star polymers synthesised by ATRP were found to be more uniform in structure whereas the optimised synthesis of star polymers by FRP achieved greater yields [182].

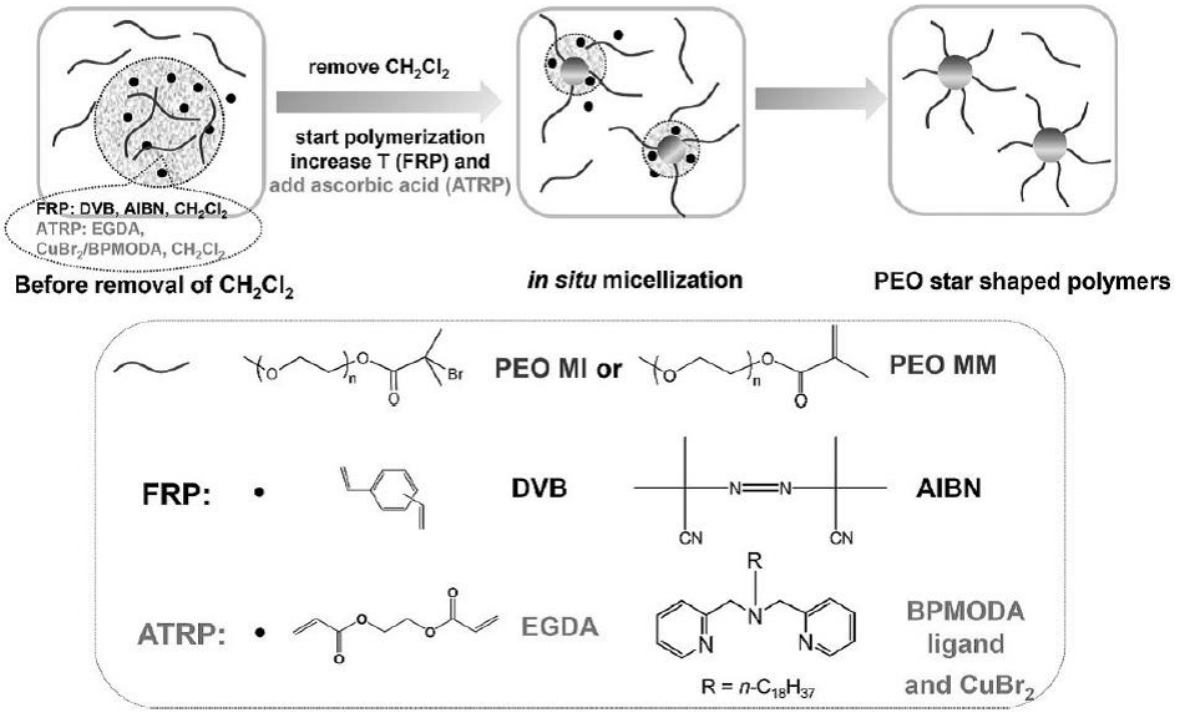

Figure 1.5. Synthetic scheme for the synthesis of star polymers. Adapted from [182].

1.5.3 Hyperbranched PEG Polymers via Thiol-ene Coupling "Click" Reactions

The reaction between an alkene and a thiol has been understood for over a century, but has gained renewed popularity of late due to its utility in the preparation of hyperbranched polymers that was recently highlighted by Hawker *et al.* [183]. Recently, Syrett *et al.* [184] fabricated branched star polymers first through RAFT polymerisation of poly(ethylene glycol) methacrylate (poly(PEGA)) to make the arms and then trialled a number of non-degradable and degradable cross-linkers (ethylene glycol dimethacrylate, disulphide dimethacrylate and a ketal dimethacrylate) to optimise the synthesis of the star polymers. The RAFT dithiocarbamate Z end groups (Figure 1.6, red dot)) were retained after the synthesis of the PEG arms and were converted to thiols via aminolysis after the cross-linker step [184]. The cross-linked star polymers with thiol groups were then reacted with fluorescein acrylate utilising the thiol click reaction to create tagged star polymers [184].

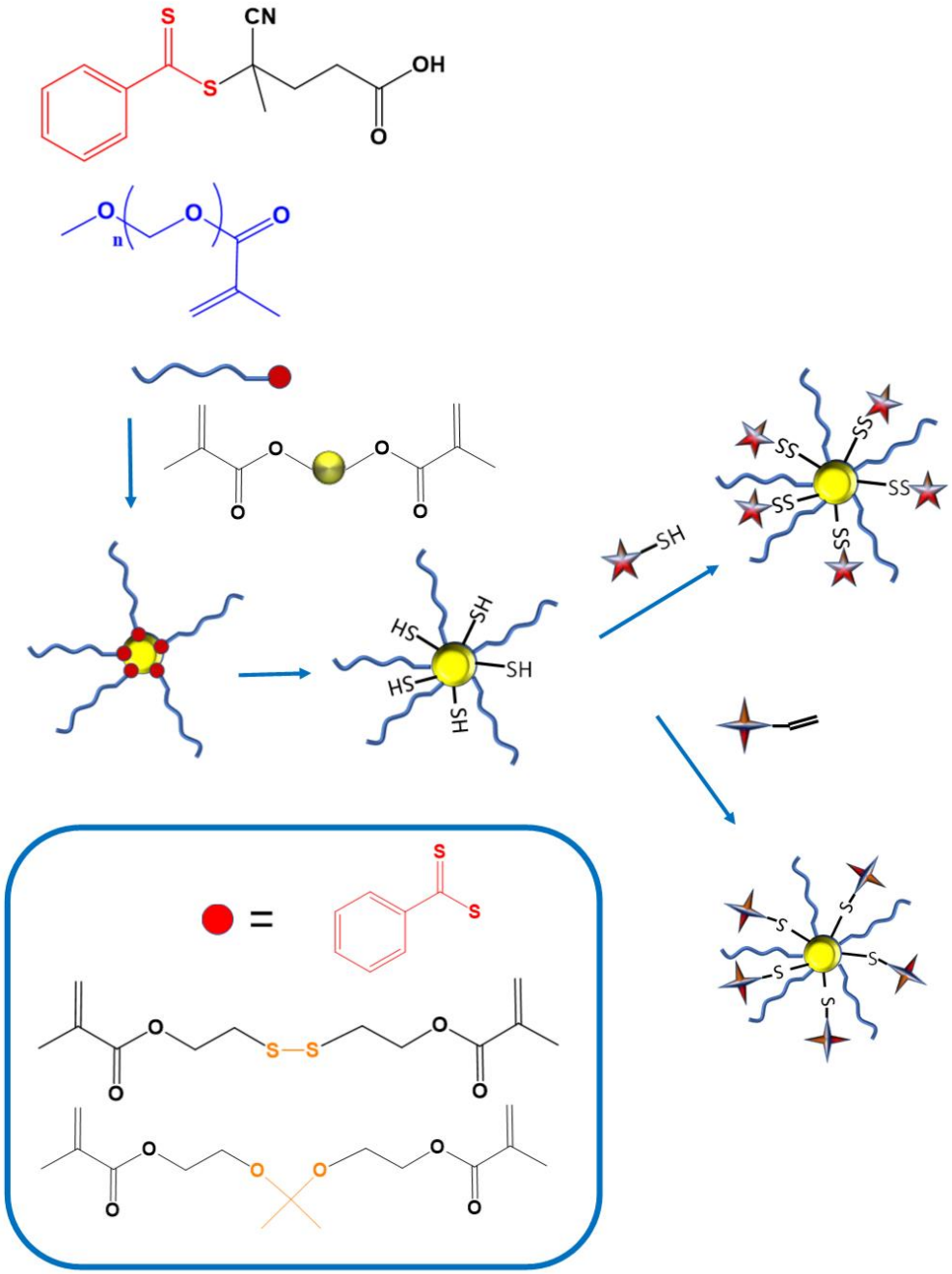

Figure 1.6. Synthetic scheme for the synthesis of PEG cross-linked star polymers. Adapted from [184].

1.5.4 Hydrogels via Thiol-ene Coupling "Click" Reactions

PEG hydrogels from PEG polymers were explored and commercialised as wound dressings and drug delivery vehicles in early studies that used irradiation cross-linking and cross-linkers between isocyanate and hydroxyl groups [166, 185]. Control over the cross-link density is a key feature in the design of covalently linked hydrogels as this can influence the controlled release of drugs or therapeutics incorporated in to the hydrogel. Kinetically fast click reactions like the thiol-ene reaction are also under investigation as a method to cross-link PEG hydrogels since they proceed under benign reaction conditions [186]. The click reaction

between the thiol and alkene functional group can be base catalysed which results in a thiol Michael type reaction or they can be initiated by light and a radical initiator [151, 187].

PEG hydrogels were synthesised by Kennedy *et al.* [188] through *in situ* gelation from highly branched alkene functionalised PEG polymers and a thiol functionalised hyaluronic acid cross-linker. The gelation mechanism occurred through thiol-ene coupling reactions which initially resulted in rapid network swelling, however after 48hr the hydrogel network remained stable [188]. An alternative method of making PEG hydrogels performed by Salinas *et al.* [189] that does not use the "arm first" approach was to copolymerise acrylate PEG polymers with thiol functionalised peptides to form PEG-peptide hydrogels networks. Photo polymerisation of the two moieties results in two competing reactions where the step growth thiol-acrylate reaction competes with the acrylate homopolymerisation [189]. Optimisation of the ratios of acrylate PEG and thiol peptides was required to enhance peptide integration into the PEG hydrogel, steric effects and hydrogen bonding due to the peptide sequence were also shown to affect the reactivity of the thiol group during the polymerisation [189]. While PEG polymer bio-conjugates have dominated the landscape in bio-medical fields that involve drug delivery applications, a particular stimuli responsive polymer, pNIPAAm has been the major player in the research area of protein capture and analysis [190]. The temperature response of pNIPAAm has been extensively investigated and the number of proposed applications remains significant [190]. The following section examines more closely pNIPAAm and its use in bio-medical applications.

1.6 Stimuli Responsive Polymers

1.6.1 Poly(*N*-isopropyl acrylamide) (pNIPAAm) Polymers Background

In this thesis pNIPAAm copolymers were synthesised to possess different solution temperatures, and the temperature driven self-assembly of these copolymers into micelles was investigated (Chapter 4, Section 4.4). The following section looks at the synthesis of pNIPAAm and copolymers of pNIPAAm and the many different applications of these stimuli response materials. PNIPAAm is perhaps the most studied member of a class of stimuli responsive polymers that respond sensitively to a stimulus [190]. The continued popularity of pNIPAAm within the bio-medical research community is due to the sharp phase transition in aqueous solution that occurs for pNIPAAm at the bio-medically relevant temperature of around 32 ^{O}C [190]. The phase separation of pNIPAAm in water is spontaneously driven by a gain in entropy as water is dehydrated from the isopropyl amide group functionality at a critical temperature and through hydrophobic effects that result from polymer-polymer interactions [191, 192]. This critical temperature, is known as the LCST and can be increased or decreased through the copolymerisation of pNIPAAm with hydrophilic or hydrophobic co-monomers [193, 194].

1.6.2 PNIPAAm Polymers Synthesis

Synthesis of pNIPAAm before the introduction of controlled radical polymerisations like RAFT or ATRP was

predominately performed by FRP in an organic solvent using radical initiators such as AIBN [191]. The MW and Đ of pNIPAAm was controlled through the careful selection of solvent and external chain transfer agents, however the goal of producing low Đ pNIPAAm remained difficult [191]. The redox polymerisation of pNIPAAm using ammonium persulfate (APS) initiator and *N,N,N'*,-tetramethylethylene-diamine (TEMED) as the accelerator is often polymerised in a buffered solution to mediate the Đ [195]. The literature has also shown that control over the MW of pNIPAAm using redox systems can be governed by the metabisulphite radical concentration [196]. While redox polymerisation of NIPAAm is a very useful method of producing cross-linked hydrogels, its application in designing novel polymer architectures is reflected by the limited number of recent publications [197]. This may be due to the poor Đ control, redox polymerisation has over NIPAAm polymers and the limited reaction conditions that can be employed in this type of polymerisation [196]. Since the early 2000's pNIPAAm and pNIPAAm copolymers have been synthesised by both RAFT and ATRP under a range of different solvent/initiator conditions [198-201]. Controlled radical polymerisation methods have enabled researchers to produce pNIPAAm polymers with low Đ, controlled molecular weights and various polymer architectures [202, 203].

1.6.3 PNIPAAm Polymer Applications

Researchers in the bio-medical field have repeatedly sought to exploit pNIPAAm's temperature response in aqueous solution [204]. Some of the proposed bio-medical applications of pNIPAAm include smart surfaces, smart drug delivery systems, smart hydrogels and smart diagnostic assays [205-208]. The term "smart" is often used in literature to describe polymers which exhibit sharp physical or chemical responses to stimulus. PNIPAAm is a smart temperature responsive polymer that can be grafted onto a surface to produce smart surfaces that become hydrophobic above their LCST and change to hydrophilic when temperature is reduced below their LCST [209].

Reversibly switchable pNIPAAm grafted surface have been used by Okano *et al.* [210] to grow myocardial cells that will adhere to hydrophobic pNIPAAm grafted surfaces through adhesive proteins via hydrophobic-hydrophobic interactions [210]. When the system is cooled below the LCST of pNIPAAm, cells spontaneously release from the surface, eliminating the need for enzymatic digestion of the adhesive proteins [210]. To promote the growth of bovine aortic endothelial cells Ebara *et al.* [211] grafted a pNIPAAm copolymer to a polystyrene surface via electron beam irradiation. The pNIPAAm copolymer contained carboxyl groups that were then used to immobilise cell adhesive peptides using carbodiimide chemistry [211]. In order to fabricate complex three-dimensional (3D) structures from cells attached to polymeric surfaces, researchers have looked at stacking cell sheets that have been removed from a pNIPAAm grafted surface [212]. This layered approach avoids the need for scaffolds and because the tissues are only comprised of cells, they have a much higher cell density [212]. Expansion of the pNIPAAm surface method of growing cells to a scaffold based capture and release system, was recently highlighted by Kim *et al.* [213]. The group prepared pNIPAAm

copolymers which contained a UV reactive benzophenone group (Figure 1.7b), the pNIPAAm copolymers were then electrospun into nanofibers (Figure 1.7 a, b) and cross-linked through UV exposure [213]. Through manipulation of temperature above and below the LCST of pNIPAAm, the group demonstrated the capture, proliferation and subsequent release of cells using the pNIPAAm cross-linked nanofibers (Figure 1.7 a) [213].

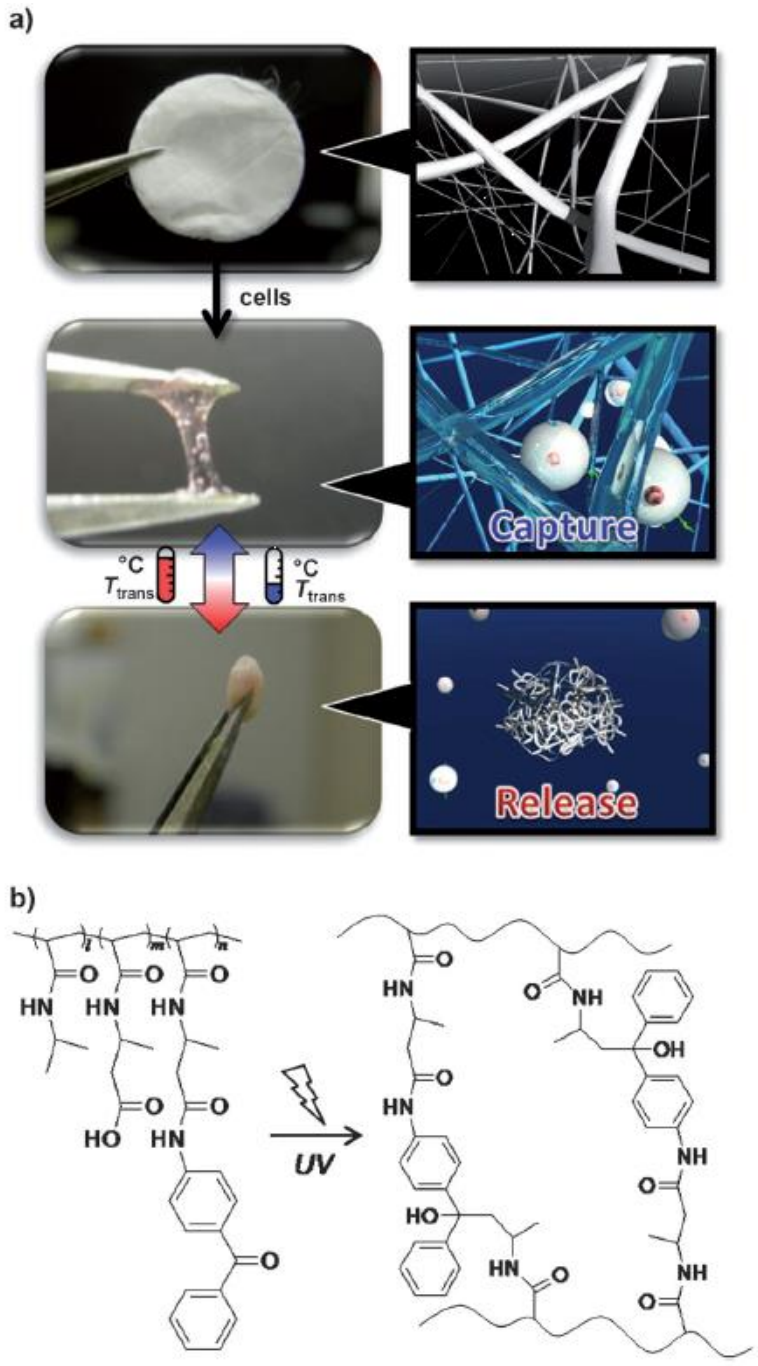

Figure 1.7. a) Scheme demonstrating the reversible swelling properties of cross-linked pNIPAAm nanofibers and, b) synthetic scheme for the synthesis of UV cross-linked pNIPAAm copolymer. Adapted from [213].

Smart drug delivery systems based upon pNIPAAm polymeric micelles have been heavily investigated for their potential as a controlled drug release system [214]. The micellular-based drug delivery systems often use pNIPAAm block copolymers where the pNIPAAm block can form either the core or the corona of the

polymeric micelle [214]. If the pNIPAAm block copolymer is synthesised to include a hydrophilic block, then, when in a solution at temperatures above the LCST, pNIPAAm forms the hydrophobic core of the micelle [215]. Hydrophobic drugs encapsulated into the hydrophobic core above the LCST can be dynamically released when the temperature drops below the LCST of pNIPAAm [215]. Alternatively, pNIPAAm can form the corona of the polymeric micelle when it is combined with a hydrophobic block [216]. Below the LCST of pNIPAAm, the hydrophobic block forms micelles in aqueous solutions and the hydrophobic drug is solubilised into the hydrophobic core [217, 218]. Heating above the LCST of pNIPAAm shrinks the pNIPAAm corona releasing the drugs from the polymeric micelle core [217]. Triblock and diblock temperature responsive copolymers of NIPAAm and DMA prepared by aqueous RAFT polymerisation by Convertine *et al.* [91] showed reversible micelle formation in response to a change in temperature. Figure 1.8 shows the micelle structure that formed at the critical micelle temperature (CMT) [91]. In this study, the synthesised ABA triblock copolymer was comprised of NIPAAm as the hydrophobic (core) B block and DMA was the hydrophilic (corona) A block [91]. At the LCST pNIPAAm chains were dehydrated and they formed aggregated micelles (Figure 1.8) [91]. Convertine *et al.* [91] showed by light scattering studies and by ^{1}H NMR spectroscopy that the block length of NIPAAm influenced the formation of micelles and that the micelles increased in size with increasing NIPAAm block length.

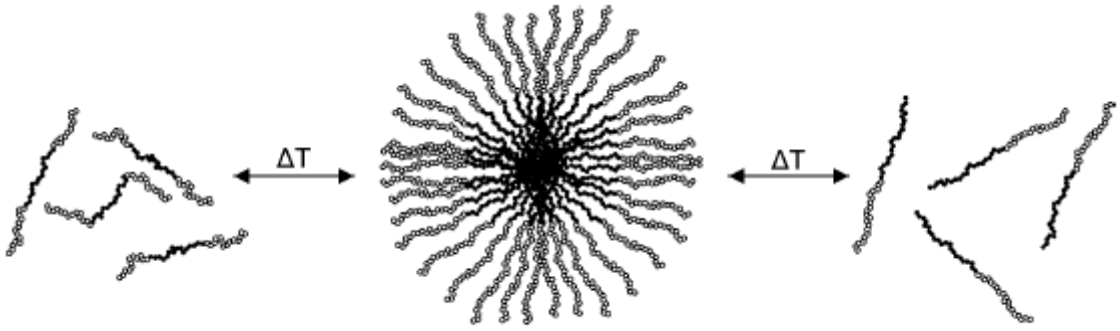

Figure 1.8. Scheme representing the reversible formation of micelles above and below the LCST of a tri block copolymer (pDMA-*b*-pNIPAAm-*b*-pDMA). Adapted from [91].

It has been previously reported by Chen *et al.* [219] that non cross-linked systems in drug delivery applications fail to deliver the full drug cargo due their target to instability of the system. Targeted, cross-linked, degradable polymers allow for controlled release at a target site, but it has also been theorised that stimuli release could play an important role in drug delivery applications. A recent paper by Zhang *et al.* [220] reported the synthesis of temperature tuneable, swellable micelles composed of a double hydrophilic block copolymer. The group used a RAFT PEO macro initiator to copolymerise temperature responsive pNIPAAm monomer and *N*-acryloxysuccinimide (NAS) monomer to yield poly(ethylene oxide)-*b*-poly(*N*-isopropylacrylamide-*co*-*N*-acryloxysuccinimide), PEO-*b*-p(NIPAAm-*co*-NAS)) [220]. The NAS functionality was used for the core cross linking of the polymeric micelles that formed in solution, cystamine was used to cross-

link the micelles as the amine functionality will react with the NAS group [221]. Through the addition of a reducing agent it was also demonstrated that the cross-linking could be reversible by cleavage of the disulphide linker, making these systems potentially useful for drug delivery and diagnostic applications [221].

A clever example of a triple stimuli response cross-linked micellular system that was recently developed for drug release applications by Klaikherd *et al.* [222] was achieved through their selection of stimuli response polymers and their engineering techniques. They could embed three different types of stimuli release mechanisms into their synthesised micellular system by combining a temperature responsive hydrophilic pNIPAAm polymer, an acid sensitive hydrophobic tetrahydropyran functionalised HEMA polymer and a cleavable di sulphide linker that bridged the two polymers [222]. Figure 1.9 shows the mechanism by which the self-assembled micelles of the block copolymer pNIPAAm-*co*-HEMA can disassemble in response to changes in temperature, pH and due to the copolymers redox sensitivity [222]. The group demonstrated the controlled release of Nile red, a hydrophobic guest molecule by altering the pH and simultaneously cleaving the redox sensitive linker by the addition of the reducing agent glutathione [222]. This study performed by Klaikherd *et al.* [222] highlighted how cross-linked micellular systems could be disassembled.

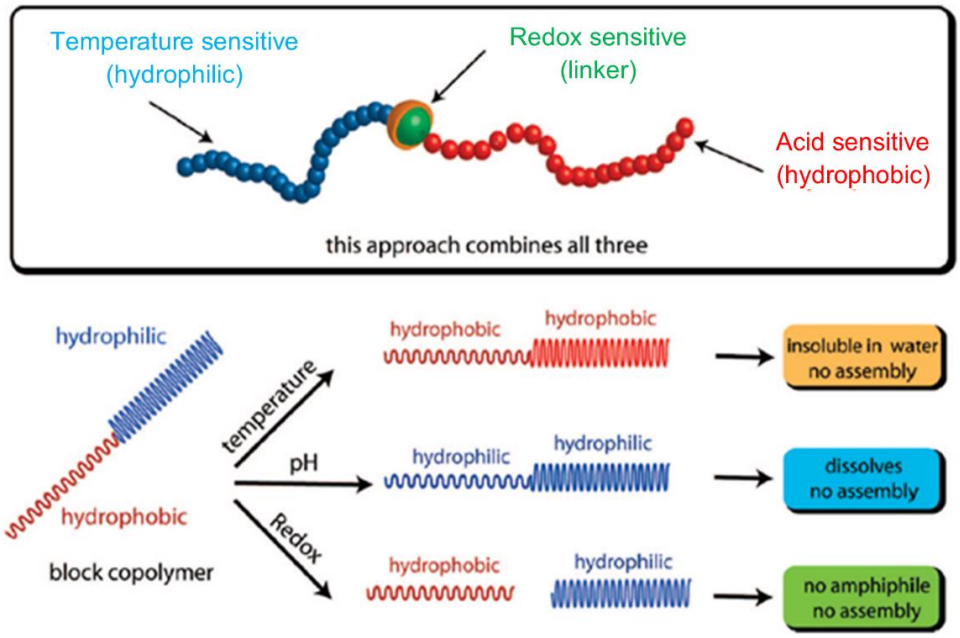

Figure 1.9. Scheme representing triple stimuli (pH, temperature and light) responsive amphiphilic block copolymer. Adapted from [222].

In this thesis, DNA has been conjugated to pNIPAAm. How this conjugation affected the LCST of pNIPAAm and DNA melt curves was investigated in Chapter 5, Section 5.7. Research, recently reported by Mirkin *et al.* [223] showed how the melt temperature of DNA could be influenced when conjugated to polymeric micelles. The group fabricated temperature responsive spherical nucleic acid (SNA) micelles from Pluoronic F127 (PEO-PPO-PEO) and amphiphilic DNA. The subsequent hybridisation of complimentary SNA micelles revealed a

significant change in the melt temperature when compared to their linear counterpart [223]. The increased stability of the SNA micelles makes them a potential candidate for therapeutic delivery applications [223]. PNIPAAm has also been grafted with single stranded DNA (ss-*DNA*) by Ooi *et al.* [224]. The group showed that the pNIPAAm conjugated DNA self-assembled into colloidal particles above the LCST; with pNIPAAm forming the core of the particles and DNA forming the coronal outer layer [224]. Kim *et al.* [225] have fabricated dual responsive DNA block copolymers with pNIPAAm being the temperature responsive block and DNA acting as the hydrophilic responsive block. Figure 1.10 shows schematically how the DNA-*b*-pNIPAAm-*b*-poly(methylacrylate) (PMA) (DNA-*b*-pNIPAAm-*b*-PMA) block copolymer reversibly changes shape depending on temperature and the introduction of complimentary DNA [225]. When the block copolymers were in solution below the LCST of pNIPAAm the micelles are arranged in a spherical shape, when the temperature of the solution was increased above the LCST of pNIPAAm, the micelle transformed to a cylindrical shape (Figure 1.10) [225]. When complimentary DNA was introduced to the solution, still above the LCST of pNIPAAm, the micelle shape changed back to spherical again (Figure 1.10) [225]. Using DLS and transmission electron microscopy (TEM), the group showed that the temperature induced micelle to cylinder and cylinder to micelle transitions were much faster than DNA induced cylinder to micelle transitions [225]. Polymeric micelles can also be chemically or physically cross-linked to form smart hydrogel systems [226].

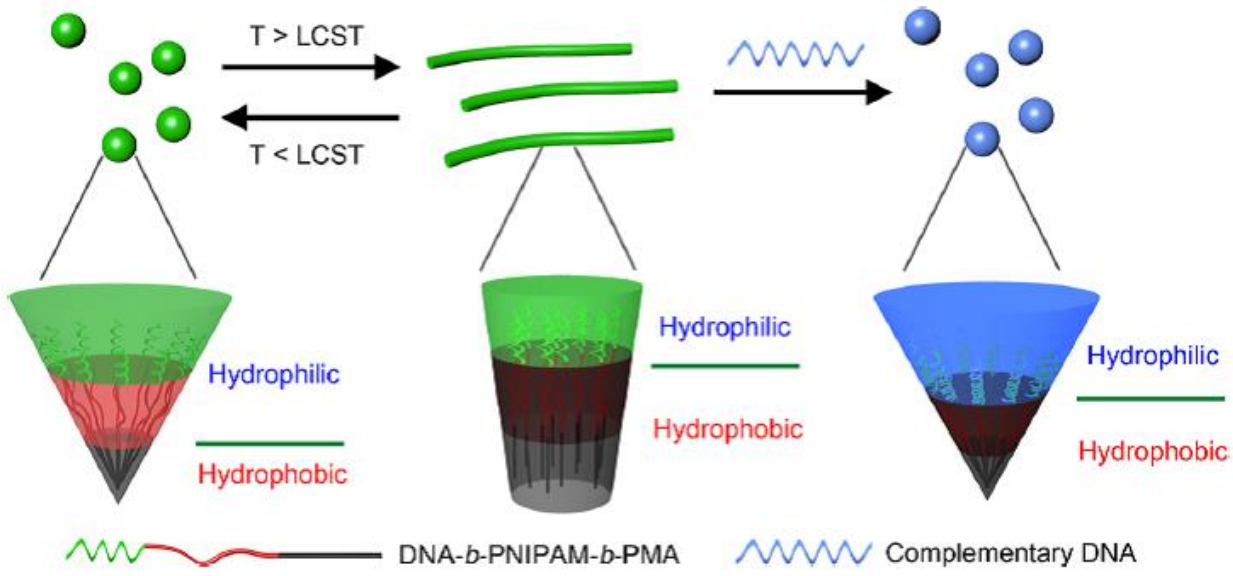

Figure 1.10. Scheme illustrating how a synthesised dual responsive DNA-*b*-pNIPAAm-*b*-PMA copolymer undergoes a change in micelle shape due to a temperature response (pNIPAAm) and a recognition response (complimentary DNA). Adapted from [225].

Hoffman *et al.* [197] pioneered the use of pNIPAAm smart hydrogels as a means of entrapping and releasing cells, drugs and enzymes. Smart hydrogels can be synthesised through cross-linking smart polymers like pNIPAAm, these hydrogels are ideal systems for the controlled release of encapsulated drugs or therapeutics [190]. These smart hydrogels will collapse and swell depending upon the solution temperature [190].

The stimuli response of pNIPAAm therefore, offers a facile method of controlling the release of an encapsulated drug. These smart hydrogels can be injected or implanted into the body, and instead of the drug release being controlled by degradation and diffusion; release of the drug can be controlled through temperature using hyperthermia treatment which stimulates the collapse of the cross-linked gel [227-230].

One of the earliest uses of cross-linked pNIPAAm hydrogels was in the diagnostics field when Hoffman *et al.* [231] conjugated a monoclonal antibody to pNIPAAm and used the polymer-antibody conjugate as an antigen bio-separation tool. Thus, they developed a simple and sensitive way of concentrating an antibody signal that could then be used in an immunoassay application [231]. Initially, the conjugation of proteins to the polymer backbone was random, however, site specific conjugation has been performed more recently to maintain or control the protein active site [232, 233]. Since the introduction of CRP methods such as RAFT and ATRP, it has become much easier to prepare well defined, site specific, polymer-protein conjugates [234-236]. More recently, these smart polymer-protein conjugates are being developed for clinical applications through their integration with microfluidic devices and magnetic or gold nanoparticles [237-239]. Affinity precipitation of streptavidin through the complimentary hybridisation of polymer conjugated oligonucleotides and polymer conjugated streptavidin presented by Fong *et al.* [240] highlighted how the unique recognition properties of DNA could be used to selectively separate targets from complex mixtures. While the diagnostic tools used to detect protein biomarkers in the laboratory are well advanced, a low cost, diagnostic platform for clinical applications remains a challenge [241]. Recently, circulating microRNAs (CRNA's) have emerged as new biomarkers for detecting cancer and just like the detection of protein biomarkers, there exists laboratory based methods of detecting CRNA's such as Northern blotting, qPCR, microarray technologies and next generation sequencing (NGS) [242]. Point-of-care methods for detecting CRNA's are also being developed to offer low cost alternatives when laboratory based detection is unavailable or too expensive [136, 243-247]. Perhaps a key sticking point in the development of sensitive point of care devices is the enrichment, and separation of dilute biomarkers [248]. It is here pNIPAAm may have a key role to play as it has previously shown its utility in the enrichment and separation of dilute protein biomarkers [249].

1.7 DNA Structure

In this thesis, synthetic DNA and synthetic DNA prepared by the PCR process were conjugated to synthesised polymers (see Chapter 4 and 5). The following section examines DNA structure, synthesis of synthetic DNA, PCR and how DNA polymer bio-conjugates have been important in the development of gene sequencing. It has been 60 years since Watson and Crick published in Nature their ground-breaking research into the molecular structure of deoxyribose nucleic acid (DNA) [250]. In the paper Watson and Crick explained the hydrogen bonding of the nucleotide bases that gave DNA its anti-parallel double-helical backbone [250]. Further they went on to hint at the possibility of the importance of DNA and its genetic potential [250]. The Human genome project completed in 2003, nearly fifty years after the first paper by Watson and Crick, was

a collaborative effort to map the human genome and to develop a deeper understanding of the field of genetics [251]. The biological importance of DNA is without question; however other scientific fields such as nanotechnology, medicine and biotechnology are looking to exploit the structural properties of DNA, for many different applications [251]. DNA engineers have come to view DNA essentially as a polymer, the DNA structure (Fig. 1.18) is made up of “monomers” called nucleotides [252]. Each of the nucleotides has a phosphate group and a sugar group (deoxyribose) [252]. The monomers (nucleotides) are connected via phosphodiester bonds; there are four different monomers, adenine (A), thymine (T), guanine (G) and cytosine (C) [252]. These monomers differ only by their nitrogenous bases [252]. Figure 1.11 is an example of the commonly observed Watson-Crick structure of DNA where adenine forms a pair with thymine and guanine pairs with cytosine. Thus by observing the base pair rules a double helix structure is observed [253]. The 5' and 3' notations of Figure 1.11 refer to the end group functionality of the single stranded DNA (ss-DNA). The end group can either be a phosphate group attached to the sugar backbone at carbon number 5, denoted as the 5' end, or it can be a hydroxyl group attached at the number 3 carbon of the sugar group, denoted as the 3' end. Two complimentary ss-DNA will thus hybridise to form a double helix structure, with the 5' and 3' ends running in an anti-parallel direction, this is driven by the Watson and Crick base pairing rules, which arise from the non-covalent forces, that drives the self-assembly of double stranded DNA (dsDNA) [252, 253].

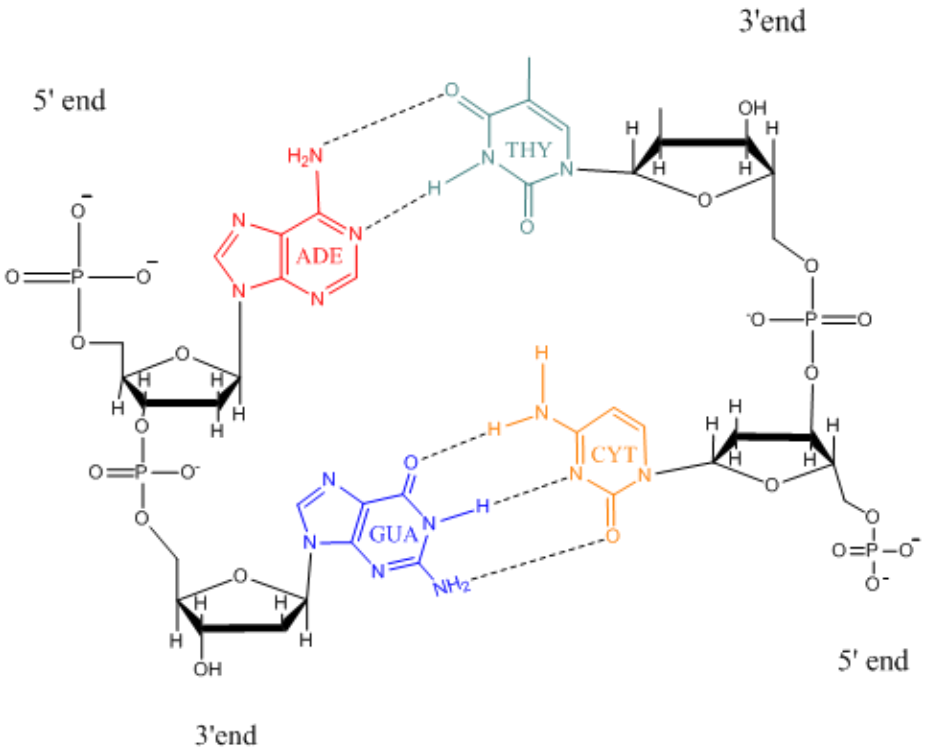

Figure 1.11. The Watson–Crick base-paring rules mean that adenine (A) pairs with thymine (T) and guanine (G) pairs with cytosine (C).

Biological/biochemical research involving gene sequencing and recombinant DNA placed a greater demand for faster and more efficient methods to produce synthetic analogues of DNA known as oligonucleotides. In

this thesis amine and azide end group functionalised oligonucleotides synthesised by the phosphoramidite process were conjugated to synthesised polymers using their end group functionality. The following section has a brief examination of oligonucleotides synthesis by the phosphoramidite process, as well as oligonucleotides application in DNA microarrays.

1.7.1 Background: Oligonucleotide Synthesis and Labelling

The preparation of synthetic oligonucleotides has come a long way since the 1970's when the chemical synthesis of a 21-base paired DNA duplex required many years to complete [254, 255]. Synthesis of DNA via the phosphoramidite approach (Scheme 1.8,), developed in the early 1980's and has been primarily adopted over other approaches such as the phosphate triester and H-phosphonate methods due to shorter reaction times and high yields [256-258]. Synthesis by the phosphoramidite (Scheme 1.8) method involves i) removal of dimethoxytrityl (DMTO) group from **3** to yield **4** with a protic acid (CH_2Cl_2). ii) Condensation of **5a-d** where x = chloro (**5a)**, tetrazolyl, (**5b)**, *N, N*-dimethylamino, (**5c)**, *N,N*-diisopropylamino (**5d);** R_1 = methyl or *B*-cyanoethyl) with **4** to yield **6**. Step (iii) the capping reaction with acetic anhydride and *N,N*-dimethylamino pyridine which acylates any **4 (**unreacted DNA) to **7.** Oxidation (step iv), converts the intermediate phosphite triester (**6**) to the phosphate triester (**8**) [259].

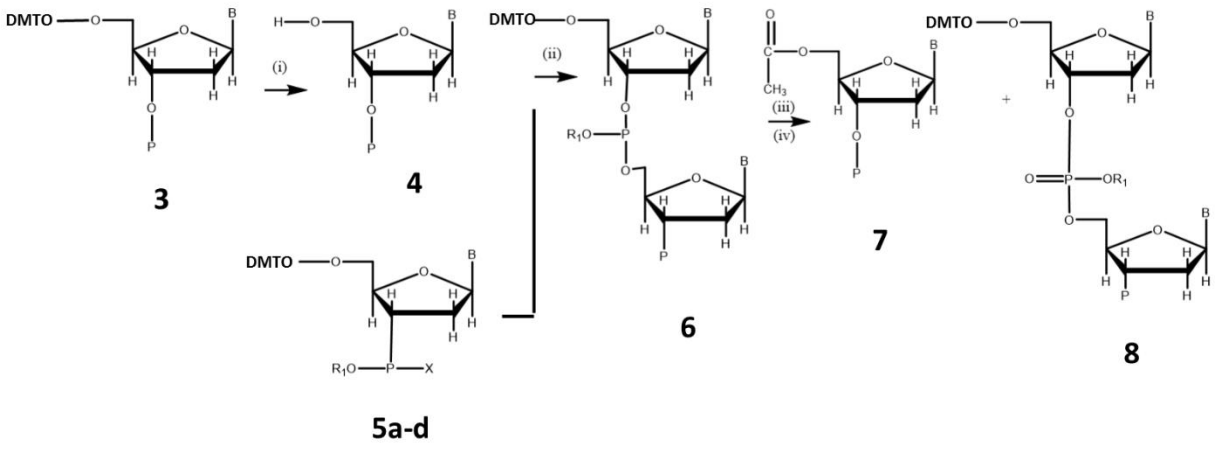

Scheme 1.8. Synthesis of DNA by the phosphoramidite method x = chloro, (**5a**), tetrazolyl, (**5b**), N,N-dimethylamino, (**5c**), N,N-diisopropylamino and (**5d**); R1 = methyl or B-cyanoethyl. Adapted from [259].

During the final stage of an automated DNA synthesis an *N*-protected amino alkyl phosphoramidite can be coupled at the 5' terminus end [260]. The amino functionality at the 5' end can then be manually coupled to fluorescent labels or other moiety's which contain activated groups that react with the amino functionality [260]. The fluorescent labels that are covalently attached to oligonucleotides have generally been performed using activated groups like NHS esters or isothiocyanates [261]. The synthesis of DNA and its analogues has now progressed to a level where 100 or more nucleotides can be coupled together in a fast and efficient manner that overcomes previous limitations encountered in the study of biological systems [259]. Synthetic

challenges that still need to be overcome include large scale synthesis of oligonucleotides and further derivatisation of the oligonucleotides [262].

1.7.2 Microarray Applications for Oligonucleotides

Gene profiling took a giant leap forward when the DNA microarray emerged, and the molecular biology practice of Southern hybridisation turned instead to high density (from thousands to millions) oligonucleotide probes on a solid support [263, 264]. The probes were designed to hybridise to targets that were fluorescently labelled; fluorescence measurements then quantified the binding events, enabling gene profiling at an unprecedented rate [265]. Glass supports are often used to attach oligonucleotides due to ease of functionalisation, high transparency and low fluorescence properties [266]. Oligonucleotides have been attached to glass surfaces at the 5' or 3' through amide linkages thiol/disulphide exchange and isothioocyanate linkages [267-270]. The density of probes attached by conventional microarrays prepared by photolithographic techniques are still limited by miniaturisation issues [271]. Random microarrays offer greater packing density since the location of the probes is not fixed on a surface [271]. The technology developed by Gunderson *et al.* [271] interrogates hybridisation events of dye labelled probes complimentary to probes immobilised on a bead. An algorithm was used to establish the identity of each bead through hybridisation reactions [271]. Tens of thousands of arrays, each with 1520 sequences were identified with a median error rate of less than 1×10^{-4} per bead [271]. DNA microarrays paved the way for a new generation of sequencing technologies that at its core still depends on dye labelled nucleotides that are directly synthesised from solid supports or are amplified from these supports by polymerase chain reaction (PCR) [272]. PCR using a thermostable polymerase which emerged in the 1980's, amplified target DNA, making it possible to up-scale the synthesis of DNA [273]. In this thesis, azide functionalised primers were used in a PCR process to make PCR products that were then coupled to strained alkyne functionalised pNIPAAm polymers (Chapter 5). The following section examines the PCR process and its application in gene sequencing and biomarker detection.

1.7.3 Background: Polymerase Chain Reaction (PCR)

PCR enables amplification of any target DNA that may have been isolated from living tissues or synthesised by DNA synthetic methods [273, 274]. PCR is a rapid, efficient and selective method to amplify target DNA [275, 276]. Oligonucleotide primers are designed to target specific regions of interest and are added in large excess along with deoxyribonucleotide triphosphates in an appropriate buffer [277, 278]. Double stranded DNA is first denatured (Figure 1.12, top) to allow the primers to anneal [277]. The denaturing step of DNA step is generally performed for 1 min at 94 ^{O}C. Figure 1.12 shows how primers are designed to locate on denatured DNA to ensure that newly synthesised strands are complimentary to each other [277, 279]. After the first heating, annealing and extension cycle the original DNA and complimentary copies of the target sequence are generated [277]. The primer annealing step proceeds at a temperature that is found

experimentally, typically 1 min at 55–65 ^{O}C. Repeat cycles (Figure 1.12) amplify the original DNA and the complimentary copies exponentially, where the number of copies generated proceeds at 2^n where n is the number of cycles [277].

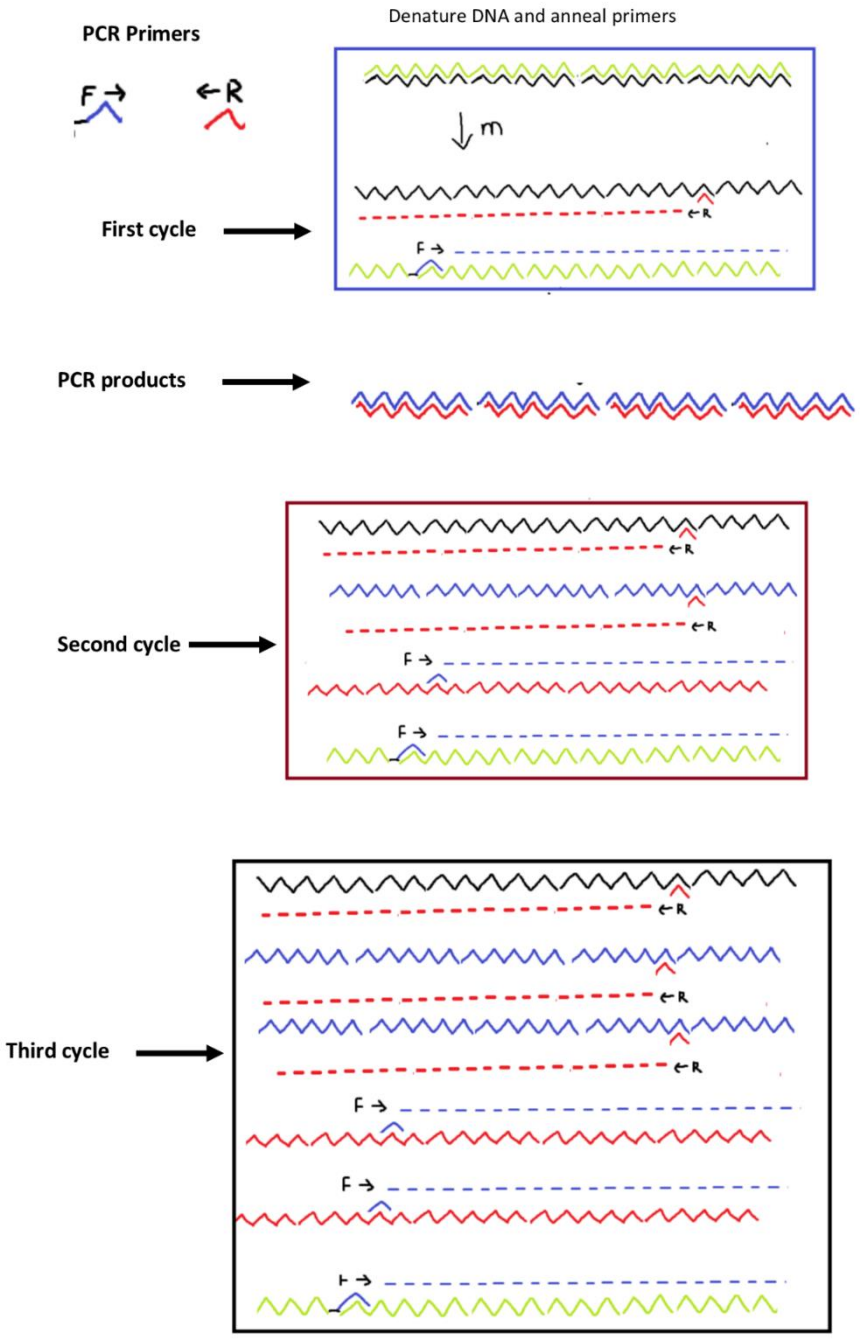

Figure 1.12. Polymerase chain reaction (PCR) amplification scheme. (i) Denature DNA and anneal primers, (ii) Extend with DNA polymerase, (iii) Repeat (i) and (ii) many times to achieve exponential accumulation. Adapted from [277].

1.7.4 Laboratory Based Applications of the Polymerase Chain Reaction (PCR)

Recently, Leamon *et al.* [280] combined NHS activated beads with amine functionalised DNA primers with hexaethylene glycol spacers and then performed solution phase and solid phase PCR amplification. The solid

phase PCR amplification of immobilised probes demonstrated a parallel processing method capable of sequencing whole genomes at a reduced cost [280-282]. Multiplex quantitative polymerase chain reaction (qPCR) uses probe based assays for the detection and quantitation of gene expression in real time [283]. Each probe is uniquely fluorescently labelled and the signal from each dye is used for quantification either in a tube or microtiter well [283-285].

1.7.5 Point of Care Applications of the Polymerase Chain Reaction (PCR) and Capture/Purification of DNA

In this thesis, stimuli responsive nanoparticle capture probes were developed (Chapter 4 and 5). Combining synthesised DNA conjugated pNIPAAm copolymers and synthesised PEG copolymers (Chapter 6) via thiol-ene click may have potential use in micro total analysis systems designed for the detection of miRNA biomarkers. The following section examines how stimuli response polymers and photocurable PEG have been used in point-of-care gene sequencing and biomarker detection. Gene sequencing, profiling and synthesis using sophisticated technology and equipment has advanced at an astonishing pace, however the current systems are geared towards expensive laboratory's that are not amenable to point of care diagnostics [286]. Micro total analysis systems (μTAS) using qPCR have emerged as a potential solution to medium through put personal gene sequencing [286]. Key challenges such as DNA purification from real samples or high-speed PCR still need to be overcome for sequencing to be realised using μTAS at the point-of-care [286, 287]. DNA capture and purification from real samples performed on microfluidic systems before PCR amplification and detection, largely involves their adsorption to silica substrates such as, silica beads or silica magnetic beads [288-290]. Known inhibitors of the PCR process such as chaotropic salts and organic solvents are often used to desorb captured DNA from the silica substrates [291].

Cao *et al.* [292] reported that by coating silica beads with a pH responsive chitosan it removed the need for organic solvents or chaotropic salts when desorbing DNA. Instead altering the pH of the system was used as the mechanism of DNA capture and release [292]. Acrylamide-oligonucleotide conjugates with single base differences were separated through affinity to an acrylamide coated capillary electrophoresis column [293]. The single base detection system is useful for gene mutation studies and is well suited for microfabrication applications [293, 294]. Polymers which respond to a specific stimulus such as pH, temperature, light or an electric field have been extensively researched for their use in bio-medical applications [234]. Hoffman *et al.* [238, 239, 295] have published extensive work on the use of microfluidic devices that use antigen conjugated temperature responsive polymers like pNIPAAm to capture/purify protein biomarkers for immunoassays applications.

However, there are very few publications that have used pNIPAAm for the separation, enrichment and early detection of DNA biomarkers. Recently, Maeda *et al.* [296] demonstrated that microRNAs (miRNAs) an emerging important early diagnostic cancer biomarker, can be detected using biotinylated capture probes.

Jung *et al.* [297] recently used photocurable PEG to make microparticle capture probes to perform qPCR amplification and detection of miRNAs. Their approach uses lithographic and microfabrication techniques that allow for easy workflow analysis; making it a novel platform that has potential use in point-of-care genetic profiling of disease makers [297].

1.8 Motivation

This project was directed towards developing temperature responsive, bio-compatible bio-conjugated polymers that could be adapted for drug delivery, tissue engineering and affinity applications. Stimuli response polymers and bio-compatible polymers (PEG) were investigated in this thesis. Two approaches to synthesising polymer bio-conjugates were pursued. Firstly, the grafting-from method was chosen to prepare polymer bio-conjugates since it has been theorised to be an efficient method of conjugating bio-molecules to polymers. The second strategy, grafting-to, allows for the independent preparation of polymers with subsequent bio-conjugation. RAFT polymerisation was used to prepare stimuli response copolymers with different solution properties. Post polymerisation modification of the copolymers was pursued by grafting DNA to the copolymer using bio-orthogonal chemistry. Bio-compatible PEG copolymers were synthesised by FRP with different degrees of functionality. These PEG copolymers were designed to be reactive to amine groups and thiol groups, which made them a versatile platform that was easy to transform using different nucleophiles.This thesis consists of an experimental chapter (Chapter 2) and a series of results chapters (Chapters 3-6) and a concluding chapter (Chapter 7). In Chapter 2, the experimental details and methods used in the synthesis of polymer and polymer bio-conjugates are outlined. The methods and instruments used to characterise the polymers and polymer bio-conjugates produced in this thesis are also covered. Chapter 3 discusses polymer bio-conjugates prepared by the grafting-from strategy. The chapter focuses on the synthesis and characterisation of a bio-macro RAFT agent and RAFT polymerisations using the bio-macro RAFT agent. The following chapters discuss the preparation of stimuli response polymers, hydrogels and the bio-conjugation techniques used in the grafting-to strategy. Chapter 4 discusses the synthesis and characterisation of a range of stimuli responsive copolymers prepared by RAFT polymerisation. A detailed study of the copolymers solution properties was undertaken. These studies included the calculation of the CMC and the LCST of the copolymers. Further investigation by DLS and AFM revealed the size of the polymeric micelles at the CMC and LCST. Chapter 5 follows on from Chapter 4, where the stimuli responsive copolymers prepared in Chapter 4 were used in the grafting-to strategy to couple DNA to the copolymers. This chapter investigated changes in the solution properties of the stimuli responsive copolymers and the changes to the melt temperature of DNA using a novel light scattering method. In Chapter 6, PEG copolymers were prepared. These PEG copolymers were cross-linked to produce hydrogel disks with different cross-link density. The cross-link density of the hydrogel disks was examined by their swelling in water and through the release profile of a model drug.

1.9 References

1. Klibanov, A.M., *Enzyme stabilization by immobilization.* Analytical Biochemistry, 1979. **93**: p. 1-25.
2. Cobo, I., et al., *Smart hybrid materials by conjugation of responsive polymers to biomacromolecules.* Nature Materials, 2015. **14**(2): p. 143-159.
3. Devouge, S., C. Salvagnini, and J. Marchand-Brynaert, *A practical molecular clip for immobilization of receptors and biomolecules on devices' surface: Synthesis, grafting protocol and analytical assay.* Bioorganic & Medicinal Chemistry Letters, 2005. **15**(13): p. 3252-3256.
4. Cosnier, S. and A. Lepellec, *Poly(pyrrole–biotin): a new polymer for biomolecule grafting on electrode surfaces.* Electrochimica Acta, 1999. **44**(11): p. 1833-1836.
5. Dong, L.C. and A.S. Hoffman, *A new method for immobilization of biomolecules using preirradiation grafting at low temperature.* International Journal of Radiation Applications and Instrumentation. Part C. Radiation Physics and Chemistry, 1986. **28**(2): p. 177-182.
6. Tang, S.C., et al., *UV-Induced Grafting Processes with In Situ Formed Photomask for Micropatterning of Two-Component Biomolecules.* Langmuir, 2010. **26**(12): p. 9905-9910.
7. Li, C., et al., *Creating "Living" Polymer Surfaces to Pattern Biomolecules and Cells on Common Plastics.* Biomacromolecules, 2013. **14**(5): p. 1278-1286.
8. Custódio, C.A., et al., *Immobilization of fibronectin in chitosan substrates improves cell adhesion and proliferation.* Journal of Tissue Engineering and Regenerative Medicine, 2010. **4**(4): p. 316-323.
9. Broyer, R.M., G.N. Grover, and H.D. Maynard, *Emerging synthetic approaches for protein-polymer conjugations.* Chemical Communications, 2011. **47**(8): p. 2212-2226.
10. Bulmus, V., *RAFT polymerization mediated bioconjugation strategies.* Polymer Chemistry, 2011. **2**(7): p. 1463-1472.
11. Abuchowski, A., et al., *Alteration of immunological properties of bovine serum albumin by covalent attachment of polyethylene glycol.* Journal of Biological Chemistry, 1977. **252**(11): p. 3578-3581.
12. Kinstler, O.B., et al., *Characterization and Stability of N-terminally PEGylated rhG-CSF.* Pharmaceutical Research, 1996. **13**(7): p. 996-1002.
13. Zalipsky, S., *Synthesis of an end-group functionalized polyethylene glycol-lipid conjugate for preparation of polymer-grafted liposomes.* Bioconjugate Chemistry, 1993. **4**(4): p. 296-299.
14. Roberts, M.J., M.D. Bentley, and J.M. Harris, *Chemistry for peptide and protein PEGylation.* Advanced Drug Delivery Reviews, 2012. **64**: p. 116-127.
15. Goodson, R.J. and N.V. Katre, *Site-directed pegylation of recombinant interleukin-2 at its glycosylation site.* Bio/technology (Nature Publishing Company), 1990. **8**(4): p. 343-346.
16. Li, H., et al., *Block copolymer conjugates prepared by sequentially grafting from proteinsvia*

RAFT. Polymer Chemistry, 2011. **2**(7): p. 1531-1535.

17. De, P., et al., *Temperature-Regulated Activity of Responsive Polymer−Protein Conjugates Prepared by Grafting-from via RAFT Polymerization.* Journal of the American Chemical Society, 2008. **130**(34): p. 11288-11289.
18. Averick, S., et al., *ATRP under Biologically Relevant Conditions: Grafting from a Protein.* ACS Macro Letters, 2012. **1**(1): p. 6-10.
19. Heredia, K.L. and H.D. Maynard, *Synthesis of protein-polymer conjugates.* Organic & Biomolecular Chemistry, 2007. **5**(1): p. 45-53.
20. Coulembier, O., et al., *Synthesis of Amphiphilic Poly((R,S)-β-malic acid)-graft-poly(ε-caprolactone): "Grafting From" and "Grafting Through" Approaches.* Macromolecules, 2005. **38**(8): p. 3141-3150.
21. Auditore-Hargreaves, K., et al., *Phase-separation immunoassays.* Clinical Chemistry, 1987. **33**(9): p. 1509-1516.
22. Anderson, G.W., J.E. Zimmerman, and F.M. Callahan, *The use of esters of N-hydroxysuccinimide in peptide synthesis.* Journal of the American Chemical Society, 1964. **86**(9): p. 1839-1842.
23. Hassner, A. and V. Alexanian, *Direct room temperature esterification of carboxylic acids.* Tetrahedron Letters, 1978. **19**(46): p. 4475-4478.
24. Desai, M.C. and L.M. Stephens Stramiello, *Polymer bound EDC (P-EDC): A convenient reagent for formation of an amide bond.* Tetrahedron Letters, 1993. **34**(48): p. 7685-7688.
25. Ranjan, R. and W.J. Brittain, *Combination of Living Radical Polymerization and Click Chemistry for Surface Modification.* Macromolecules, 2007. **40**(17): p. 6217-6223.
26. Yu, W.W., et al., *Water-soluble quantum dots for biomedical applications.* Biochemical and Biophysical Research Communications, 2006. **348**(3): p. 781-786.
27. Haslam, E., *Recent developments in methods for the esterification and protection of the carboxyl group.* Tetrahedron, 1980. **36**(17): p. 2409-2433.
28. Williams, A. and I.T. Ibrahim, *A new mechanism involving cyclic tautomers for the reaction with nucleophiles of the water-soluble peptide coupling reagent 1-ethyl-3-(3'-(dimethylamino) propyl) carbodiimide (EDC).* Journal of the American Chemical Society, 1981. **103**(24): p. 7090-7095.
29. Sehgal, D. and I.K. Vijay, *A Method for the High Efficiency of Water-Soluble Carbodiimide-Mediated Amidation.* Analytical Biochemistry, 1994. **218**(1): p. 87-91.
30. Tsakos, M., et al., *Ester coupling reactions - an enduring challenge in the chemical synthesis of bioactive natural products.* Natural Product Reports, 2015. **32**(4): p. 605-632.
31. Neises, B. and W. Steglich, *Simple method for the esterification of carboxylic acids.* Angewandte Chemie International Edition in English, 1978. **17**(7): p. 522-524.
32. Patri, A.K., I.J. Majoros, and J.R. Baker Jr, *Dendritic polymer macromolecular carriers for drug delivery.* Current Opinion in Chemical Biology, 2002. **6**(4): p. 466-471.

33. Castillo, J.J., et al., *Monitoring the functionalization of single-walled carbon nanotubes with chitosan and folic acid by two-dimensional diffusion-ordered NMR spectroscopy.* Carbon, 2012. **50**(8): p. 2691-2697.
34. Gutmann, O., et al., *Fast and reliable protein microarray production by a new drop-in-drop technique.* Lab on a Chip, 2005. **5**(6): p. 675-681.
35. Gong, P. and D.W. Grainger, *Comparison of DNA immobilization efficiency on new and regenerated commercial amine-reactive polymer microarray surfaces.* Surface Science, 2004. **570**(1–2): p. 67-77.
36. Fischer, M.J.E., *Amine Coupling Through EDC/NHS: A Practical Approach*, in *Surface Plasmon Resonance: Methods and Protocols*, N.J. Mol and M.J.E. Fischer, Editors. 2010, Humana Press: Totowa, NJ. p. 55-73.
37. Millan, K.M. and S.R. Mikkelsen, *Sequence-selective biosensor for DNA based on electroactive hybridization indicators.* Analytical Chemistry, 1993. **65**(17): p. 2317-2323.
38. Drumheller, P.D. and J.A. Hubbell, *Polymer Networks with Grafted Cell Adhesion Peptides for Highly Biospecific Cell Adhesive Substrates.* Analytical Biochemistry, 1994. **222**(2): p. 380-388.
39. Choi, S.-W. and J.-H. Kim, *Design of surface-modified poly(d,l-lactide-co-glycolide) nanoparticles for targeted drug delivery to bone.* Journal of Controlled Release, 2007. **122**(1): p. 24-30.
40. Duncan, R., *The dawning era of polymer therapeutics.* Nature Reviews Drug Discovery, 2003. **2**(5): p. 347-360.
41. Kopeček, J., et al., *HPMA copolymer–anticancer drug conjugates: design, activity, and mechanism of action.* European Journal of Pharmaceutics and Biopharmaceutics, 2000. **50**(1): p. 61-81.
42. Seymour, L.W., et al., *Effect of molecular weight (Mw) of N-(2-hydroxypropyl)methacrylamide copolymers on body distribution and rate of excretion after subcutaneous, intraperitoneal, and intravenous administration to rats.* Journal of Biomedical Materials Research, 1987. **21**(11): p. 1341-1358.
43. Wang, D., et al., *Synthesis and Evaluation of Water-Soluble Polymeric Bone-Targeted Drug Delivery Systems.* Bioconjugate Chemistry, 2003. **14**(5): p. 853-859.
44. Haag, R., *Supramolecular Drug-Delivery Systems Based on Polymeric Core–Shell Architectures.* Angewandte Chemie International Edition, 2004. **43**(3): p. 278-282.
45. Kopeček, J. and R. Duncan, *Targetable polymeric prodrugs.* Journal of Controlled Release, 1987. **6**(1): p. 315-327.
46. Yoo, H.S. and T.G. Park, *Folate-receptor-targeted delivery of doxorubicin nano-aggregates stabilized by doxorubicin–PEG–folate conjugate.* Journal of Controlled Release, 2004. **100**(2): p. 247-256.
47. Sletten, E.M. and C.R. Bertozzi, *From Mechanism to Mouse: A Tale of Two Bioorthogonal*

Reactions. Accounts of Chemical Research, 2011. **44**(9): p. 666-676.

48. Saxon, E. and C.R. Bertozzi, *Cell Surface Engineering by a Modified Staudinger Reaction.* Science, 2000. **287**: p. 2007.
49. Lin, F.L., et al., *Mechanistic Investigation of the Staudinger Ligation.* Journal of the American Chemical Society, 2005. **127**(8): p. 2686-2695.
50. Staudinger, H. and J. Meyer, *Über neue organische Phosphorverbindungen III. Phosphinmethylenderivate und Phosphinimine.* Helvetica Chimica Acta, 1919. **2**(1): p. 635-646.
51. Leffler, J.E. and R.D. Temple, *Staudinger reaction between triarylphosphines and azides. Mechanism.* Journal of the American Chemical Society, 1967. **89**(20): p. 5235-5246.
52. Gololobov, Y.G., I.N. Zhmurova, and L.F. Kasukhin, *Sixty years of staudinger reaction.* Tetrahedron, 1981. **37**(3): p. 437-472.
53. Lemieux, G.A., C.L. de Graffenried, and C.R. Bertozzi, *A Fluorogenic Dye Activated by the Staudinger Ligation.* Journal of the American Chemical Society, 2003. **125**(16): p. 4708-4709.
54. Nilsson, B.L., L.L. Kiessling, and R.T. Raines, *Staudinger Ligation: A Peptide from a Thioester and Azide.* Organic Letters, 2000. **2**(13): p. 1939-1941.
55. Schilling, C.I., et al., *Bioconjugation viaazide-Staudinger ligation: an overview.* Chemical Society Reviews, 2011. **40**(9): p. 4840-4871.
56. Saxon, E., J.I. Armstrong, and C.R. Bertozzi, *A "Traceless" Staudinger Ligation for the Chemoselective Synthesis of Amide Bonds.* Organic Letters, 2000. **2**(14): p. 2141-2143.
57. Soellner, M.B., et al., *Site-Specific Protein Immobilization by Staudinger Ligation.* Journal of the American Chemical Society, 2003. **125**(39): p. 11790-11791.
58. Chang, P.V., et al., *Imaging Cell Surface Glycans with Bioorthogonal Chemical Reporters.* Journal of the American Chemical Society, 2007. **129**(27): p. 8400-8401.
59. Rostovtsev, V.V., et al., *A stepwise huisgen cycloaddition process: copper (I)-catalyzed regioselective "ligation" of azides and terminal alkynes.* Angewandte Chemie, 2002. **114**(14): p. 2708-2711.
60. Tornøe, C.W., C. Christensen, and M. Meldal, *Peptidotriazoles on Solid Phase: [1,2,3]-Triazoles by Regiospecific Copper(I)-Catalyzed 1,3-Dipolar Cycloadditions of Terminal Alkynes to Azides.* The Journal of Organic Chemistry, 2002. **67**(9): p. 3057-3064.
61. Kolb, H.C., M.G. Finn, and K.B. Sharpless, *Click Chemistry: Diverse Chemical Function from a Few Good Reactions.* Angewandte Chemie International Edition in English, 2001. **40**(11): p. 2004-2021.
62. Dondoni, A., *The Emergence of Thiol–Ene Coupling as a Click Process for Materials and Bioorganic Chemistry.* Angewandte Chemie International Edition, 2008. **47**(47): p. 8995-8997.
63. Sumerlin, B.S., et al., *Highly Efficient "Click" Functionalization of Poly(3-azidopropyl methacrylate) Prepared by ATRP.* Macromolecules, 2005. **38**(18): p. 7540-7545.

64. Moses, J.E. and A.D. Moorhouse, *The growing applications of click chemistry.* Chemical Society Reviews, 2007. **36**(8): p. 1249-1262.
65. Prescher, J.A. and C.R. Bertozzi, *Chemistry in living systems.* Nature Chemical Biology, 2005. **1**(1): p. 13-21.
66. Wolbers, F., et al., *Viability study of HL60 cells in contact with commonly used microchip materials.* ELECTROPHORESIS, 2006. **27**(24): p. 5073-5080.
67. Kennedy, D.C., et al., *Cellular Consequences of Copper Complexes Used To Catalyze Bioorthogonal Click Reactions.* Journal of the American Chemical Society, 2011. **133**(44): p. 17993-18001.
68. Gupta, S.S., et al., *Accelerated Bioorthogonal Conjugation: A Practical Method for the Ligation of Diverse Functional Molecules to a Polyvalent Virus Scaffold.* Bioconjugate Chemistry, 2005. **16**(6): p. 1572-1579.
69. Lewis, W.G., et al., *Discovery and Characterization of Catalysts for Azide−Alkyne Cycloaddition by Fluorescence Quenching.* Journal of the American Chemical Society, 2004. **126**(30): p. 9152-9153.
70. Agard, N.J., J.A. Prescher, and C.R. Bertozzi, *A Strain-Promoted [3 + 2] Azide−Alkyne Cycloaddition for Covalent Modification of Biomolecules in Living Systems.* Journal of the American Chemical Society, 2004. **126**(46): p. 15046-15047.
71. Wittig, G. and A. Krebs, *Zur Existenz niedergliedriger Cycloalkine, I.* Chemische Berichte, 1961. **94**(12): p. 3260-3275.
72. Ess, D.H. and K.N. Houk, *Theory of 1,3-Dipolar Cycloadditions: Distortion/Interaction and Frontier Molecular Orbital Models.* Journal of the American Chemical Society, 2008. **130**(31): p. 10187-10198.
73. Meldal, M. and C.W. Tornøe, *Cu-Catalyzed Azide−Alkyne Cycloaddition.* Chemical Reviews, 2008. **108**(8): p. 2952-3015.
74. Meier, H., H. Petersen, and H. Kolshorn, *Die Ringspannung von Cycloalkinen und ihre spektroskopischen Auswirkungen.* Chemische Berichte, 1980. **113**(7): p. 2398-2409.
75. Ess, D.H., G.O. Jones, and K.N. Houk, *Transition States of Strain-Promoted Metal-Free Click Chemistry: 1,3-Dipolar Cycloadditions of Phenyl Azide and Cyclooctynes.* Organic Letters, 2008. **10**(8): p. 1633-1636.
76. Codelli, J.A., et al., *Second-Generation Difluorinated Cyclooctynes for Copper-Free Click Chemistry.* Journal of the American Chemical Society, 2008. **130**(34): p. 11486-11493.
77. Ning, X., et al., *Visualizing Metabolically Labeled Glycoconjugates of Living Cells by Copper-Free and Fast Huisgen Cycloadditions.* Angewandte Chemie International Edition, 2008. **47**(12): p. 2253-2255.
78. Debets, M.F., et al., *Aza-dibenzocyclooctynes for fast and efficient enzyme PEGylation via copper-free (3+2) cycloaddition.* Chemical Communications, 2010. **46**(1): p. 97-99.
79. Laughlin, S.T., et al., *In Vivo Imaging of Membrane-Associated Glycans in Developing*

Zebrafish. Science, 2008. **320**(5876): p. 664-667.

80. Beatty, K.E., et al., *Fluorescence Visualization of Newly Synthesized Proteins in Mammalian Cells.* Angewandte Chemie, 2006. **118**(44): p. 7524-7527.
81. Sun, X.-L., et al., *Carbohydrate and Protein Immobilization onto Solid Surfaces by Sequential Diels−Alder and Azide−Alkyne Cycloadditions.* Bioconjugate Chemistry, 2006. **17**(1): p. 52-57.
82. Lutz, J.-F., H.G. Börner, and K. Weichenhan, *Combining ATRP and "Click" Chemistry: a Promising Platform toward Functional Biocompatible Polymers and Polymer Bioconjugates.* Macromolecules, 2006. **39**(19): p. 6376-6383.
83. Gierlich, J., et al., *Click Chemistry as a Reliable Method for the High-Density Postsynthetic Functionalization of Alkyne-Modified DNA.* Organic Letters, 2006. **8**(17): p. 3639-3642.
84. Link, A.J. and D.A. Tirrell, *Cell Surface Labeling of Escherichia coli via Copper(I)-Catalyzed [3+2] Cycloaddition.* Journal of the American Chemical Society, 2003. **125**(37): p. 11164-11165.
85. Kho, Y., et al., *A tagging-via-substrate technology for detection and proteomics of farnesylated proteins.* Proceedings of the National Academy of Sciences of the United States of America, 2004. **101**(34): p. 12479-12484.
86. Evans, R.K., J.D. Johnson, and B.E. Haley, *5-Azido-2'-deoxyuridine 5'-triphosphate: a photoaffinity-labeling reagent and tool for the enzymatic synthesis of photoactive DNA.* Proceedings of the National Academy of Sciences, 1986. **83**(15): p. 5382-5386.
87. Kiviniemi, A., P. Virta, and H. Lönnberg, *Utilization of Intrachain 4'-C-Azidomethylthymidine for Preparation of Oligodeoxyribonucleotide Conjugates by Click Chemistry in Solution and on a Solid Support.* Bioconjugate Chemistry, 2008. **19**(8): p. 1726-1734.
88. Sylvers, L.A. and J. Wower, *Nucleic acid-incorporated azidonucleotides: Probes for studying the interaction of RNA or DNA with proteins and other nucleic acids.* Bioconjugate Chemistry, 1993. **4**(6): p. 411-418.
89. Perrier, S. and P. Takolpuckdee, *Macromolecular design via reversible addition–fragmentation chain transfer (RAFT)/xanthates (MADIX) polymerization.* Journal of Polymer Science Part A: Polymer Chemistry, 2005. **43**(22): p. 5347-5393.
90. Mayadunne, R.T.A., et al., *Living Free Radical Polymerization with Reversible Addition−Fragmentation Chain Transfer (RAFT Polymerization): Approaches to Star Polymers.* Macromolecules, 2003. **36**(5): p. 1505-1513.
91. Convertine, A.J., et al., *Direct Synthesis of Thermally Responsive DMA/NIPAM Diblock and DMA/NIPAM/DMA Triblock Copolymers via Aqueous, Room Temperature RAFT Polymerization.* Macromolecules, 2006. **39**(5): p. 1724-1730.
92. Poon, C.K., et al., *Preparation of Inert Polystyrene Latex Particles as MicroRNA Delivery Vectors by Surfactant-Free RAFT Emulsion Polymerization.* Biomacromolecules, 2016. **17**(3): p. 965-973.

93. Sogabe, A., J.D. Flores, and C.L. McCormick, *Reversible Addition−Fragmentation Chain Transfer (RAFT) Polymerization in an Inverse Microemulsion: Partitioning of Chain Transfer Agent (CTA) and Its Effects on Polymer Molecular Weight§.* Macromolecules, 2010. **43**(16): p. 6599-6607.
94. Quemener, D., et al., *RAFT and click chemistry: A versatile approach to well-defined block copolymers.* Chemical Communications, 2006(48): p. 5051-5053.
95. Keddie, D.J., et al., *Switchable Reversible Addition–Fragmentation Chain Transfer (RAFT) Polymerization in Aqueous Solution, N,N-Dimethylacrylamide.* Macromolecules, 2011. **44**(17): p. 6738-6745.
96. de Lambert, B., et al., *Poly(N-tert-butyl acrylamide-b-N-acryloylmorpholine) amphiphilic block copolymers via RAFT polymerization: Synthesis, purification and characterization.* Polymer, 2007. **48**(2): p. 437-447.
97. Segui, F., X.P. Qiu, and F.M. Winnik, *An efficient synthesis of telechelic poly (N-isopropylacrylamides) and its application to the preparation of α, ω-dicholesteryl and α, ω-dipyrenyl polymers.* Journal of Polymer Science Part A: Polymer Chemistry, 2008. **46**(1): p. 314-326.
98. Vasilieva, Y.A., et al., *Direct controlled polymerization of a cationic methacrylamido monomer in aqueous media via the RAFT process.* Macromolecules, 2004. **37**(8): p. 2728-2737.
99. Mayadunne, R.T.A., et al., *Living Radical Polymerization with Reversible Addition−Fragmentation Chain Transfer (RAFT Polymerization) Using Dithiocarbamates as Chain Transfer Agents.* Macromolecules, 1999. **32**(21): p. 6977-6980.
100. Chiefari, J., et al., *Living Free-Radical Polymerization by Reversible Addition−Fragmentation Chain Transfer: The RAFT Process.* Macromolecules, 1998. **31**(16): p. 5559-5562.
101. Quinn, J.F., et al., *Reversible addition-fragmentation chain transfer polymerization initiated with ultraviolet radiation.* Macromolecules, 2002. **35**(20): p. 7620-7627.
102. Lu, L., N. Yang, and Y. Cai, *Well-controlled reversible addition–fragmentation chain transfer radical polymerisation under ultraviolet radiation at ambient temperature.* Chemical communications, 2005(42): p. 5287-5288.
103. Keddie, D.J., et al., *RAFT Agent Design and Synthesis.* Macromolecules, 2012. **45**(13): p. 5321-5342.
104. Chong, Y.K., et al., *Thiocarbonylthio Compounds [SC(Ph)S−R] in Free Radical Polymerization with Reversible Addition-Fragmentation Chain Transfer (RAFT Polymerization). Role of the Free-Radical Leaving Group (R).* Macromolecules, 2003. **36**(7): p. 2256-2272.
105. Moad, G., E. Rizzardo, and S.H. Thang, *Living Radical Polymerization by the RAFT Process.* Australian Journal of Chemistry, 2005. **58**(6): p. 379-410.
106. Boyer, C., et al., *Bioapplications of RAFT Polymerization.* Chemical Reviews, 2009. **109**(11):

p. 5402-5436.

107. Chiefari, J., et al., *Thiocarbonylthio Compounds (SC(Z)S−R) in Free Radical Polymerization with Reversible Addition-Fragmentation Chain Transfer (RAFT Polymerization). Effect of the Activating Group Z.* Macromolecules, 2003. **36**(7): p. 2273-2283.
108. Thang, S.H., et al., *A novel synthesis of functional dithioesters, dithiocarbamates, xanthates and trithiocarbonates.* Tetrahedron Letters, 1999. **40**(12): p. 2435-2438.
109. Dehn, S., et al., *Altering Peptide Fibrillization by Polymer Conjugation.* Biomacromolecules, 2012. **13**(9): p. 2739-2747.
110. Johnson, R.P., J.V. John, and I. Kim, *Recent developments in polymer–block–polypeptide and protein–polymer bioconjugate hybrid materials.* European Polymer Journal, (0).
111. Rizzardo, E., et al. *Synthesis of defined polymers by reversible addition-fragmentation chain transfer: the RAFT process*. ACS Publications.
112. Lowe, A.B., M. Torres, and R. Wang, *A doubly responsive AB diblock copolymer: RAFT synthesis and aqueous solution properties of poly (N-isopropylacrylamide-block-4-vinylbenzoic acid).* Journal of Polymer Science Part A: Polymer Chemistry, 2007. **45**(24): p. 5864-5871.
113. Abel, B.A. and C.L. McCormick, *Mechanistic Insights into Temperature-Dependent Trithiocarbonate Chain-End Degradation during the RAFT Polymerization of N-Arylmethacrylamides.* Macromolecules, 2016. **49**(2): p. 465-474.
114. Gao, H. and K. Matyjaszewski, *Synthesis of functional polymers with controlled architecture by CRP of monomers in the presence of cross-linkers: From stars to gels.* Progress in Polymer Science, 2009. **34**(4): p. 317-350.
115. Matyjaszewski, K. and J. Xia, *Atom Transfer Radical Polymerization.* Chemical Reviews, 2001. **101**(9): p. 2921-2990.
116. Samsonova, O., et al., *Low Molecular Weight pDMAEMA-block-pHEMA Block-Copolymers Synthesized via RAFT-Polymerization: Potential Non-Viral Gene Delivery Agents?* Polymers, 2011. **3**(2): p. 693-718.
117. Coca, S., et al., *Polymerization of acrylates by atom transfer radical polymerization. Homopolymerization of 2-hydroxyethyl acrylate.* Journal of Polymer Science Part A: Polymer Chemistry, 1998. **36**(9): p. 1417-1424.
118. *2-Hydroxyethyl Methacrylate (HEMA): Chemical Properties and Applications in Biomedical Fields.* Journal of Macromolecular Science, Part C, 1992. **32**(1): p. 1-34.
119. Sekula-Neuner, S., et al., *Phospholipid arrays on porous polymer coatings generated by micro-contact spotting.* Beilstein Journal of Nanotechnology, 2017. **8**: p. 715-722.
120. Rojo, L., et al., *Designing dapsone polymer conjugates for controlled drug delivery.* Acta Biomaterialia, 2015. **27**: p. 32-41.
121. Guntari, S.N., et al., *Low-Fouling, Biospecific Films Prepared by the Continuous Assembly of Polymers.* Biomacromolecules, 2013. **14**(8): p. 2477-2483.

122. Lima, V., et al., *Synthesis and characterization of telechelic polymethacrylates via RAFT polymerization.* Journal of Polymer Science Part A: Polymer Chemistry, 2005. **43**(5): p. 959-973.
123. Mayadunne, R.T., et al., *Living polymers by the use of trithiocarbonates as reversible addition-fragmentation chain transfer (RAFT) agents: ABA triblock copolymers by radical polymerization in two steps.* Macromolecules, 2000. **33**(2): p. 243-245.
124. Motokucho, S., A. Sudo, and T. Endo, *Polymer having a trithiocarbonate moiety in the main chain: Application to reversible addition–fragmentation chain transfer controlled thermal and photoinduced monomer insertion polymerizations.* Journal of Polymer Science Part A: Polymer Chemistry, 2006. **44**(21): p. 6324-6331.
125. Steinhauer, W., et al., *Copolymerization of 2-Hydroxyethyl Acrylate and 2-Methoxyethyl Acrylate via RAFT: Kinetics and Thermoresponsive Properties.* Macromolecules, 2010. **43**(17): p. 7041-7047.
126. Moad, G., E. Rizzardo, and S.H. Thang, *End-functional polymers, thiocarbonylthio group removal/transformation and reversible addition–fragmentation–chain transfer (RAFT) polymerization.* Polymer International, 2011. **60**(1): p. 9-25.
127. Spruell, J.M., et al., *Facile postpolymerization end-modification of RAFT polymers.* Journal of Polymer Science Part A: Polymer Chemistry, 2009. **47**(2): p. 346-356.
128. Harrisson, S., *Radical-Catalyzed Oxidation of Thiols by Trithiocarbonate and Dithioester RAFT Agents: Implications for the Preparation of Polymers with Terminal Thiol Functionality.* Macromolecules, 2009. **42**(4): p. 897-898.
129. Chong, B., et al., *Thermolysis of RAFT-Synthesized Poly(Methyl Methacrylate).* Australian Journal of Chemistry, 2006. **59**(10): p. 755-762.
130. Roth, P.J., et al., *Synthesis of Reactive Telechelic Polymers Based on Pentafluorophenyl Esters.* Macromolecules, 2008. **41**(22): p. 8513-8519.
131. Zhuang, Y., et al., *Facile fabrication of redox-responsive thiol-containing drug delivery system via RAFT polymerization.* Biomacromolecules, 2014. **15**(4): p. 1408-1418.
132. Goldmann, A.S., et al., *Surface Modification of Poly (divinylbenzene) Microspheres via Thiol− Ene Chemistry and Alkyne− Azide Click Reactions.* Macromolecules, 2009. **42**(11): p. 3707-3714.
133. Boyer, C., V. Bulmus, and T.P. Davis, *Efficient Usage of Thiocarbonates for Both the Production and the Biofunctionalization of Polymers.* Macromolecular Rapid Communications, 2009. **30**(7): p. 493-497.
134. York, A.W., et al., *Facile Synthetic Procedure for ω, Primary Amine Functionalization Directly in Water for Subsequent Fluorescent Labeling and Potential Bioconjugation of RAFT-Synthesized (Co)Polymers†.* Biomacromolecules, 2007. **8**(8): p. 2337-2341.
135. Perrier, S., et al., *Versatile Chain Transfer Agents for Reversible Addition Fragmentation Chain Transfer (RAFT) Polymerization to Synthesize Functional Polymeric Architectures.*

Macromolecules, 2004. **37**(8): p. 2709-2717.

136. Mousavi, M.Z., et al., *Urinary micro-RNA biomarker detection using capped gold nanoslit SPR in a microfluidic chip.* Analyst, 2015. **140**(12): p. 4097-4104.
137. Boyer, C., et al., *Well-Defined Protein−Polymer Conjugates via in Situ RAFT Polymerization.* Journal of the American Chemical Society, 2007. **129**(22): p. 7145-7154.
138. Zhu, M.-Q., et al., *Thermosensitive Gold Nanoparticles.* Journal of the American Chemical Society, 2004. **126**(9): p. 2656-2657.
139. Mark, D., et al., *Microfluidic lab-on-a-chip platforms: requirements, characteristics and applications.* Chemical Society Reviews, 2010. **39**(3): p. 1153-82.
140. Gress, A., A. Volkel, and H. Schlaad, *Thio-click modification of poly [2-(3-butenyl)-2-oxazoline].* Macromolecules, 2007. **40**(22): p. 7928-7933.
141. Hoyle, C.E., T.Y. Lee, and T. Roper, *Thiol-enes: Chemistry of the past with promise for the future.* Journal. Polymer. Science. Part A: Polymer. Chemistry, 2004. **42**(21): p. 5301-5338.
142. Binder, W.H. and R. Sachsenhofer, *'Click' Chemistry in Polymer and Materials Science.* Macromolecules. Rapid Communications, 2007. **28**(1): p. 15-54.
143. Lutz, J.F. and G. Nanotechnology for Life Science Research, *1,3-dipolar cycloadditions of azides and alkynes: a universal ligation tool in polymer and materials science.* Angewandte Chemie International Edition in English, 2007. **46**(7): p. 1018-25.
144. Vogt, A.P. and B.S. Sumerlin, *Tuning the temperature response of branched poly (N-isopropylacrylamide) prepared by RAFT polymerization.* Macromolecules, 2008. **41**(20): p. 7368-7373.
145. De, P., S.R. Gondi, and B.S. Sumerlin, *Folate-conjugated thermoresponsive block copolymers: highly efficient conjugation and solution self-assembly.* Biomacromolecules, 2008. **9**(3): p. 1064-1070.
146. Yu, B., et al., *Sequential thiol-ene/thiol-ene and thiol-ene/thiol-yne reactions as a route to well-defined mono and bis end-functionalized poly (N-isopropylacrylamide).* Journal of Polymer Science Part A: Polymer Chemistry, 2009. **47**(14): p. 3544-3557.
147. Campos, L.M., et al., *Development of Thermal and Photochemical Strategies for Thiol−Ene Click Polymer Functionalization.* Macromolecules, 2008. **41**(19): p. 7063-7070.
148. McCall, J.D. and K.S. Anseth, *Thiol–ene photopolymerizations provide a facile method to encapsulate proteins and maintain their bioactivity.* Biomacromolecules, 2012. **13**(8): p. 2410-2417.
149. Cramer, N.B. and C.N. Bowman, *Kinetics of thiol-ene and thiol-acrylate photopolymerizations with real-time fourier transform infrared.* Journal of. Polymer. Science. Part A: Polymer. Chemistry, 2001. **39**(19): p. 3311-3319.
150. Kharasch, M.S., E.M. May, and F.R. Mayo, *The Peroxide Effect in the Addition of Reagents to Unsaturated Compounds. Xviii. The Addition and Substitution of Bisulfite*.* The Journal of

Organic Chemistry, 1938. **03**(2): p. 175-192.

151. Cramer, N.B., et al., *Mechanism and Modeling of a Thiol−Ene Photopolymerization.* Macromolecules, 2003. **36**(12): p. 4631-4636.
152. Kharkar, P.M., et al., *Thiol–ene click hydrogels for therapeutic delivery.* ACS Biomaterials Science & Engineering, 2016. **2**(2): p. 165-179.
153. Kade, M.J., D.J. Burke, and C.J. Hawker, *The power of thiol-ene chemistry.* Journal of Polymer Science Part A: Polymer Chemistry, 2010. **48**(4): p. 743-750.
154. Fairbanks, B.D., et al., *Thiol− Yne photopolymerizations: novel mechanism, kinetics, and step-growth formation of highly cross-linked networks.* Macromolecules, 2008. **42**(1): p. 211-217.
155. Barbey, R., et al., *Polymer Brushes via Surface-Initiated Controlled Radical Polymerization: Synthesis, Characterization, Properties, and Applications.* Chemical Reviews, 2009. **109**(11): p. 5437-5527.
156. Durham, O.Z., H.R. Norton, and D.A. Shipp, *Functional polymer particles via thiol-ene and thiol-yne suspension "click" polymerization.* RSC Advances, 2015. **5**(82): p. 66757-66766.
157. Kjellander, R. and E. Florin, *Water structure and changes in thermal stability of the system poly(ethylene oxide)-water.* Journal of the Chemical Society, Faraday Transactions 1: Physical Chemistry in Condensed Phases, 1981. **77**(9): p. 2053-2077.
158. Zalipsky, S. and J.M. Harris, *Introduction to Chemistry and Biological Applications of Poly(ethylene glycol)*, in *Poly(ethylene glycol)*. 1997, American Chemical Society. p. 1-13.
159. Buwalda, S.J., et al., *Hydrogels in a historical perspective: From simple networks to smart materials.* Journal of Controlled Release, 2014. **190**: p. 254-273.
160. Barz, M., et al., *Overcoming the PEG-addiction: well-defined alternatives to PEG, from structure-property relationships to better defined therapeutics.* Polymer Chemistry, 2011. **2**(9): p. 1900-1918.
161. Li, S., et al., *Hydrolytic and enzymatic degradations of physically crosslinked hydrogels prepared from PLA/PEO/PLA triblock copolymers.* Journal of Materials Science: Materials in Medicine, 2002. **13**(1): p. 81-86.
162. Cerritelli, S., et al., *Aggregation Behavior of Poly(ethylene glycol-bl-propylene sulfide) Di- and Triblock Copolymers in Aqueous Solution.* Langmuir, 2009. **25**(19): p. 11328-11335.
163. Velthoen, I.W., et al., *Thermo-responsive hydrogels based on highly branched poly(ethylene glycol)–poly(l-lactide) copolymers.* Reactive and Functional Polymers, 2011. **71**(3): p. 245-253.
164. Mandy, S.H., *A New Primary Wound Dressing Made of Polyethylene Oxide Gel.* The Journal of Dermatologic Surgery and Oncology, 1983. **9**(2): p. 153-155.
165. Caliceti, P. and F.M. Veronese, *Pharmacokinetic and biodistribution properties of poly(ethylene glycol)–protein conjugates.* Advanced Drug Delivery Reviews, 2003. **55**(10): p. 1261-1277.

166. King, P.A. and J.A. Ward, *Radiation chemistry of aqueous poly(ethylene oxide) solutions. I.* Journal of Polymer Science Part A-1: Polymer Chemistry, 1970. **8**(1): p. 253-262.
167. Veronese, F.M. and G. Pasut, *PEGylation, successful approach to drug delivery.* Drug discovery today, 2005. **10**(21): p. 1451-1458.
168. Hillery, A.M. and A.T. Florence, *The effect of adsorbed poloxamer 188 and 407 surfactants on the intestinal uptake of 60-nm polystyrene particles after oral administration in the rat.* International journal of pharmaceutics, 1996. **132**(1-2): p. 123-130.
169. Alexandridis, P. and J.F. Holzwarth, *Differential scanning calorimetry investigation of the effect of salts on aqueous solution properties of an amphiphilic block copolymer (Poloxamer).* Langmuir, 1997. **13**(23): p. 6074-6082.
170. Herzberger, J., et al., *Polymerization of Ethylene Oxide, Propylene Oxide, and Other Alkylene Oxides: Synthesis, Novel Polymer Architectures, and Bioconjugation.* Chemical Reviews, 2016. **116**(4): p. 2170-2243.
171. Berlinova, I., I. Panayotov, and C.B. Tsvetanov, *Influence of the polyether chain on the dissociation of "living" polymers obtained in the anionic polymerization of ethylene oxide.* European Polymer Journal, 1977. **13**(10): p. 757-760.
172. Bailey, F.J., *Poly (ethylene oxide)*. 1976: Academic Press.
173. Feng, X.-S., et al., *Toward an easy access to dendrimer-like poly (ethylene oxide) s.* Journal of the American Chemical Society, 2005. **127**(31): p. 10956-10966.
174. Feng, X., et al., *Fast access to dendrimer-like poly (ethylene oxide) s through anionic ring-opening polymerization of ethylene oxide and use of nonprotected glycidol as branching agent.* Macromolecules, 2009. **42**(19): p. 7292-7298.
175. Huh, K.M. and Y.H. Bae, *Synthesis and characterization of poly (ethylene glycol)/poly (L-lactic acid) alternating multiblock copolymers.* Polymer, 1999. **40**(22): p. 6147-6155.
176. Deng, G., D. Ma, and Z. Xu, *Synthesis of ABC-type miktoarm star polymers by "click" chemistry, ATRP and ROP.* European polymer journal, 2007. **43**(4): p. 1179-1187.
177. Lutz, J.-F. and A. Hoth, *Preparation of Ideal PEG Analogues with a Tunable Thermosensitivity by Controlled Radical Copolymerization of 2-(2-Methoxyethoxy)ethyl Methacrylate and Oligo(ethylene glycol) Methacrylate.* Macromolecules, 2005. **39**(2): p. 893-896.
178. Wang, J.-S. and K. Matyjaszewski, *Controlled/"living" radical polymerization. atom transfer radical polymerization in the presence of transition-metal complexes.* Journal of the American Chemical Society, 1995. **117**(20): p. 5614-5615.
179. Nicolas, J., et al., *Nitroxide-mediated polymerization.* Progress in Polymer Science, 2013. **38**(1): p. 63-235.
180. Chenal, M., et al., *Facile synthesis of innocuous comb-shaped polymethacrylates with PEG side chains by nitroxide-mediated radical polymerization in hydroalcoholic solutions.* Macromolecules, 2010. **43**(22): p. 9291-9303.

181. Chu, D.S.H., et al., *Application of Living Free Radical Polymerization for Nucleic Acid Delivery.* Accounts of Chemical Research, 2012. **45**(7): p. 1089-1099.
182. Li, W. and K. Matyjaszewski, *Uniform PEO star polymers synthesized in water via free radical polymerization or atom transfer radical polymerization.* Macromolecular rapid communications, 2011. **32**(1): p. 74-81.
183. Killops, K.L., L.M. Campos, and C.J. Hawker, *Robust, efficient, and orthogonal synthesis of dendrimers via thiol-ene "click" chemistry.* Journal of the American Chemical Society, 2008. **130**(15): p. 5062-5064.
184. Syrett, J.A., et al., *Functional, star polymeric molecular carriers, built from biodegradable microgel/nanogel cores.* Chemical Communications, 2011. **47**(5): p. 1449-1451.
185. McNeill, M. and N. Graham, *Vaginal pessaries from crystalline/rubbery hydrogels for the delivery of prostaglandin E2.* Journal of Controlled Release, 1984. **1**(2): p. 99-117.
186. Arslan, M., et al., *Fabrication of poly (ethylene glycol)-based cyclodextrin containing hydrogels via thiol-ene click reaction.* European Polymer Journal, 2015. **62**: p. 426-434.
187. O'Shea, T.M., et al., *Synthesis and Characterization of a Library of In-Situ Curing, Nonswelling Ethoxylated Polyol Thiol-ene Hydrogels for Tailorable Macromolecule Delivery.* Advanced Materials, 2015. **27**(1): p. 65-72.
188. Kennedy, R., et al., *In situ formed hybrid hydrogels from PEG based multifunctional hyperbranched copolymers: a RAFT approach.* Polymer Chemistry, 2014. **5**(6): p. 1838-1842.
189. Salinas, C.N., et al., *Chondrogenic differentiation potential of human mesenchymal stem cells photoencapsulated within poly (ethylene glycol)–arginine-glycine-aspartic acid-serine thiol-methacrylate mixed-mode networks.* Tissue engineering, 2007. **13**(5): p. 1025-1034.
190. Hoffman, A.S., *Stimuli-responsive polymers: Biomedical applications and challenges for clinical translation.* Advanced Drug Delivery Reviews, 2013. **65**(1): p. 10-16.
191. Schild, H.G., *Poly(N-isopropylacrylamide): experiment, theory and application.* Progress in Polymer Science, 1992. **17**(2): p. 163-249.
192. Heskins, M. and J.E. Guillet, *Solution Properties of Poly(N-isopropylacrylamide).* Journal of Macromolecular Science: Part A - Chemistry, 1968. **2**(8): p. 1441-1455.
193. Schild, H.G. and D.A. Tirrell, *Microcalorimetric detection of lower critical solution temperatures in aqueous polymer solutions.* The Journal of Physical Chemistry, 1990. **94**(10): p. 4352-4356.
194. Schilli, C.M., et al., *A New Double-Responsive Block Copolymer Synthesized via RAFT Polymerization: Poly(N-isopropylacrylamide)-block-poly(acrylic acid).* Macromolecules, 2004. **37**(21): p. 7861-7866.
195. Wooten, W., R. Blanton, and H. Coover, *Effect of pH on homopolymerization of N-isopropylacrylamide.* Journal of Polymer Science, 1957. **25**(111): p. 403-412.

196. Bokias, G., A. Durand, and D. Hourdet, *Molar mass control of poly(N-isopropylacrylamide) and poly(acrylic acid) in aqueous polymerizations initiated by redox initiators based on persulfates.* Macromolecular Chemistry and Physics, 1998. **199**(7): p. 1387-1392.
197. Hoffman, A.S., A. Afrassiabi, and L.C. Dong, *Thermally reversible hydrogels: II. Delivery and selective removal of substances from aqueous solutions.* Journal of Controlled Release, 1986. **4**(3): p. 213-222.
198. Ganachaud, F., et al., *Molecular Weight Characterization of Poly(N-isopropylacrylamide) Prepared by Living Free-Radical Polymerization.* Macromolecules, 2000. **33**(18): p. 6738-6745.
199. Masci, G., L. Giacomelli, and V. Crescenzi, *Atom Transfer Radical Polymerization of N-Isopropylacrylamide.* Macromolecular Rapid Communications, 2004. **25**(4): p. 559-564.
200. Ye, J. and R. Narain, *Water-assisted atom transfer radical polymerization of N-isopropylacrylamide: nature of solvent and temperature.* The Journal of Physical Chemistry B, 2008. **113**(3): p. 676-681.
201. Bai, W., et al., *A Very Useful Redox Initiator for Aqueous RAFT Polymerization of N-Isopropylacrylamide and Acrylamide at Room Temperature.* Macromolecular Rapid Communications, 2008. **29**(7): p. 562-566.
202. Shivapooja, P., et al., *ARGET–ATRP Synthesis and Characterization of PNIPAAm Brushes for Quantitative Cell Detachment Studies.* Biointerphases, 2012. **7**(1): p. 32.
203. Audouin, F. and A. Heise, *Surface-initiated RAFT polymerization of NIPAM from monolithic macroporous polyHIPE.* European Polymer Journal, 2013. **49**(5): p. 1073-1079.
204. Cole, M.A., et al., *Stimuli-responsive interfaces and systems for the control of protein–surface and cell–surface interactions.* Biomaterials, 2009. **30**(9): p. 1827-1850.
205. Liu, G., et al., *Hairy Polyelectrolyte Brushes-Grafted Thermosensitive Microgels as Artificial Synovial Fluid for Simultaneous Biomimetic Lubrication and Arthritis Treatment.* ACS Applied Materials & Interfaces, 2014. **6**(22): p. 20452-20463.
206. Mura, S., J. Nicolas, and P. Couvreur, *Stimuli-responsive nanocarriers for drug delivery.* Nature Materials, 2013. **12**(11): p. 991-1003.
207. Satarkar, N.S. and J.Z. Hilt, *Magnetic hydrogel nanocomposites for remote controlled pulsatile drug release.* Journal of Controlled Release, 2008. **130**(3): p. 246-251.
208. Kim, J., S. Nayak, and L.A. Lyon, *Bioresponsive Hydrogel Microlenses.* Journal of the American Chemical Society, 2005. **127**(26): p. 9588-9592.
209. Zhao, T., et al., *Inhibition of protein adsorption and cell adhesion on PNIPAAm-grafted polyurethane surface: Effect of graft molecular weight.* Colloids and Surfaces B: Biointerfaces, 2011. **85**(1): p. 26-31.
210. Shimizu, T., et al., *Cell sheet engineering for myocardial tissue reconstruction.* Biomaterials, 2003. **24**(13): p. 2309-2316.
211. Ebara, M., et al., *Immobilization of cell-adhesive peptides to temperature-responsive*

surfaces facilitates both serum-free cell adhesion and noninvasive cell harvest. Tissue Engineering, 2004. **10**(7-8): p. 1125-1135.

212. Haraguchi, Y., et al., *Fabrication of functional three-dimensional tissues by stacking cell sheets in vitro.* Nature. Protocols, 2012. **7**(5): p. 850-858.
213. Kim, Y.-J., M. Ebara, and T. Aoyagi, *A Smart Nanofiber Web That Captures and Releases Cells.* Angewandte Chemie International Edition, 2012. **51**(42): p. 10537-10541.
214. Liu, R., M. Fraylich, and B.R. Saunders, *Thermoresponsive copolymers: from fundamental studies to applications.* Colloid and Polymer Science, 2009. **287**(6): p. 627-643.
215. Topp, M., et al., *Thermosensitive micelle-forming block copolymers of poly (ethylene glycol) and poly (N-isopropylacrylamide).* Macromolecules, 1997. **30**: p. 8518-8520.
216. Kujawa, P., F. Tanaka, and F.M. Winnik, *Temperature-Dependent Properties of Telechelic Hydrophobically Modified Poly(N-isopropylacrylamides) in Water: Evidence from Light Scattering and Fluorescence Spectroscopy for the Formation of Stable Mesoglobules at Elevated Temperatures.* Macromolecules, 2006. **39**(8): p. 3048-3055.
217. Wei, H., et al., *Self-assembled, thermosensitive micelles of a star block copolymer based on PMMA and PNIPAAm for controlled drug delivery.* Biomaterials, 2007. **28**(1): p. 99-107.
218. Adelsberger, J., et al., *Thermoresponsive PS-b-PNIPAM-b-PS Micelles: Aggregation Behavior, Segmental Dynamics, and Thermal Response.* Macromolecules, 2010. **43**(5): p. 2490-2501.
219. Chen, H., et al., *Release of hydrophobic molecules from polymer micelles into cell membranes revealed by Förster resonance energy transfer imaging.* Proceedings of the National Academy of Sciences, 2008. **105**(18): p. 6596-6601.
220. Zhang, J., et al., *Facile Fabrication of Reversible Core Cross-Linked Micelles Possessing Thermosensitive Swellability.* Macromolecules, 2007. **40**(25): p. 9125-9132.
221. Zhang, L., et al., *Shell-Cross-Linked Micelles Containing Cationic Polymers Synthesized via the RAFT Process: Toward a More Biocompatible Gene Delivery System.* Biomacromolecules, 2007. **8**(9): p. 2890-2901.
222. Klaikherd, A., C. Nagamani, and S. Thayumanavan, *Multi-Stimuli Sensitive Amphiphilic Block Copolymer Assemblies.* Journal of the American Chemical Society, 2009. **131**(13): p. 4830-4838.
223. Banga, R.J., et al., *Cross-Linked Micellar Spherical Nucleic Acids from Thermoresponsive Templates.* Journal of the American Chemical Society, 2017. **139**(12): p. 4278-4281.
224. Ooi, W.-Y., et al., *Structural characterization of nanoparticles from thermoresponsive poly(N-isopropylacrylamide)-DNA conjugate.* Journal of Colloid and Interface Science, 2012. **374**(1): p. 315-320.
225. Kim, C.-J., X. Hu, and S.-J. Park, *Multimodal Shape Transformation of Dual-Responsive DNA Block Copolymers.* Journal of the American Chemical Society, 2016. **138**(45): p. 14941-14947.

226. Li, Y., B.S. Lokitz, and C.L. McCormick, *Thermally Responsive Vesicles and Their Structural "Locking" through Polyelectrolyte Complex Formation.* Angewandte Chemie International Edition, 2006. **45**(35): p. 5792-5795.
227. Bendtsen, S.T. and M. Wei, *Synthesis and characterization of a novel injectable alginate-collagen-hydroxyapatite hydrogel for bone tissue regeneration.* Journal of Materials Chemistry B, 2015. **3**(15): p. 3081-3090.
228. Jeong, B., Y.H. Bae, and S.W. Kim, *Drug release from biodegradable injectable thermosensitive hydrogel of PEG–PLGA–PEG triblock copolymers.* Journal of Controlled Release, 2000. **63**(1–2): p. 155-163.
229. Zhang, J., et al., *The targeted behavior of thermally responsive nanohydrogel evaluated by NIR system in mouse model.* Journal of Controlled Release, 2008. **131**(1): p. 34-40.
230. Timko, B.P., et al., *Near-infrared–actuated devices for remotely controlled drug delivery.* Proceedings of the National Academy of Sciences, 2014. **111**(4): p. 1349-1354.
231. Monji, N. and A.S. Hoffman, *A novel immunoassay system and bioseparation process based on thermal phase separating polymers.* Applied Biochemistry and Biotechnology, 1987. **14**(2): p. 107-120.
232. Dehn, S., et al., *Synthetic Strategies for the Design of Peptide/Polymer Conjugates.* Polymer Reviews, 2011. **51**(2): p. 214-234.
233. Ding, Z., et al., *Temperature Control of Biotin Binding and Release with A Streptavidin-Poly(N-isopropylacrylamide) Site-Specific Conjugate.* Bioconjugate Chemistry, 1999. **10**(3): p. 395-400.
234. Heredia, K.L., et al., *In Situ Preparation of Protein−"Smart" Polymer Conjugates with Retention of Bioactivity.* Journal of the American Chemical Society, 2005. **127**(48): p. 16955-16960.
235. Heredia, K.L., et al., *Synthesis of Heterotelechelic Polymers for Conjugation of Two Different Proteins.* Macromolecules, 2009. **42**(7): p. 2360-2367.
236. Lele, B.S., et al., *Synthesis of Uniform Protein−Polymer Conjugates.* Biomacromolecules, 2005. **6**(6): p. 3380-3387.
237. Nash, M.A., et al., *Mixed stimuli-responsive magnetic and gold nanoparticle system for rapid purification, enrichment, and detection of biomarkers.* Bioconjugate chemistry, 2010. **21**(12): p. 2197-2204.
238. Ebara, M., et al., *A Photoinduced Nanoparticle Separation in Microchannels via pH-Sensitive Surface Traps.* Langmuir, 2013. **29**(18): p. 5388-5393.
239. Ebara, M., et al., *Smart Bioconjugates*, in *Smart Biomaterials*. 2014, Springer Japan. p. 237-284.
240. Fong, R.B., et al., *Thermoprecipitation of Streptavidin via Oligonucleotide-Mediated Self-Assembly with Poly(N-isopropylacrylamide).* Bioconjugate Chemistry, 1999. **10**(5): p. 720-725.

241. Sanjay, S.T., et al., *Biomarker detection for disease diagnosis using cost-effective microfluidic platforms.* Analyst, 2015. **140**(21): p. 7062-7081.
242. Liu, J., et al., *Next generation sequencing for profiling expression of miRNAs: technical progress and applications in drug development.* Journal of biomedical science and engineering, 2011. **4**(10): p. 666-676.
243. Wang, J., et al., *Direct Quantification of MicroRNA at Low Picomolar Level in Sera of Glioma Patients Using a Competitive Hybridization Followed by Amplified Voltammetric Detection.* Analytical Chemistry, 2012. **84**(15): p. 6400-6406.
244. Tu, Y., et al., *Fluorescence quenching of gold nanoparticles integrating with a conformation-switched hairpin oligonucleotide probe for microRNA detection.* Chemical Communications, 2012. **48**(87): p. 10718-10720.
245. Sun, Y., et al., *Rapid and direct microRNA quantification by an enzymatic luminescence assay.* Analytical Biochemistry, 2012. **429**(1): p. 11-17.
246. Bartosik, M., et al., *Magnetic bead-based hybridization assay for electrochemical detection of microRNA.* Analytica Chimica Acta, 2014. **813**: p. 35-40.
247. Baker, M.B., G. Bao, and C.D. Searles, *In vitro quantification of specific microRNA using molecular beacons.* Nucleic Acids Research, 2012. **40**(2): p. e13-e13.
248. Kishikawa, T., et al., *Circulating RNAs as new biomarkers for detecting pancreatic cancer.* World Journal of Gastroenterology : WJG, 2015. **21**(28): p. 8527-8540.
249. Lai, J.J., et al., *Dynamic bioprocessing and microfluidic transport control with smart magnetic nanoparticles in laminar-flow devices.* Lab on a chip, 2009. **9**(14): p. 1997-2002.
250. Watson, J.D. and F.H. Crick, *Molecular structure of nucleic acids.* Nature, 1953. **171**(4356): p. 737-738.
251. Seeman, N.C., *At the Crossroads of Chemistry, Biology, and Materials: Structural DNA Nanotechnology.* Chemistry & Biology, 2003. **10**(12): p. 1151-1159.
252. Roh, Y.H., et al., *Engineering DNA-based functional materials.* Chemical Society Reviews, 2011. **40**(12): p. 5730-5744.
253. Seeman, N.C., *DNA engineering and its application to nanotechnology.* Trends in Biotechnology, 1999. **17**(11): p. 437-443.
254. Yansura, D., D. Goeddel, and M. Caruthers, *Studies on gene control regions. 2. Enzymatic joining of chemically synthesized lactose operator deoxyribonucleic acid segments.* Biochemistry, 1977. **16**(9): p. 1772-1780.
255. Matteucci, M.D. and M. Caruthers, *Synthesis of deoxyoligonucleotides on a polymer support.* Journal of the American Chemical Society, 1981. **103**(11): p. 3185-3191.
256. Caruthers, M.H., *Synthesis of Oligonucleotides and Oligonucleotide Analogues*, in *Oligodeoxynucleotides: Antisense Inhibitors of Gene Expression*, J.S. Cohen, Editor. 1989, Macmillan Education UK: London. p. 7-24.
257. Garegg, P.J., et al., *Nucleoside H-phosphonates. III. Chemical synthesis of*

oligodeoxyribonucleotides by the hydrogenphosphonate approach. Tetrahedron Letters, 1986. **27**(34): p. 4051-4054.

258. Itakura, K., J.J. Rossi, and R.B. Wallace, *Synthesis and use of synthetic oligonucleotides.* Annual review of biochemistry, 1984. **53**(1): p. 323-356.
259. Caruthers, M.H., *Chemical synthesis of DNA and DNA analogs.* Accounts of chemical research, 1991. **24**(9): p. 278-284.
260. Davies, M.J., A. Shah, and I.J. Bruce, *Synthesis of fluorescently labelled oligonucleotides and nucleic acids.* Chemical Society Reviews, 2000. **29**(2): p. 97-107.
261. Proudnikov, D. and A. Mirzabekov, *Chemical methods of DNA and RNA fluorescent labeling.* Nucleic acids research, 1996. **24**(22): p. 4535-4542.
262. Kosuri, S. and G.M. Church, *Large-scale de novo DNA synthesis: technologies and applications.* Nature methods, 2014. **11**(5): p. 499-507.
263. Southern, E., et al., *Arrays of complementary oligonucleotides for analysing the hybridisation behaviour of nucleic acids.* Nucleic Acids Research, 1994. **22**(8): p. 1368-1373.
264. Southern, E., K. Mir, and M. Shchepinov, *Molecular interactions on microarrays.* Nature genetics, 1999. **21**: p. 5-9.
265. Lipshutz, R.J., et al., *High density synthetic oligonucleotide arrays.* Nature genetics, 1999. **21**: p. 20-24.
266. Shi, L., R.G. Perkins, and W. Tong, *The current status of DNA microarrays*, in *Microarrays*. 2009, Springer. p. 3-24.
267. Beattie, W.G., et al., *Hybridization of DNA targets to glass-tethered oligonucleotide probes.* Molecular biotechnology, 1995. **4**(3): p. 213-225.
268. Maskos, U. and E.M. Southern, *Oligonucleotide hybridisations on glass supports: a novel linker for oligonucleotide synthesis and hybridisation properties of oligonucleotides synthesised in situ.* Nucleic acids research, 1992. **20**(7): p. 1679-1684.
269. Rogers, Y.-H., et al., *Immobilization of oligonucleotides onto a glass support via disulfide bonds: a method for preparation of DNA microarrays.* Analytical biochemistry, 1999. **266**(1): p. 23-30.
270. Guo, Z., et al., *Direct fluorescence analysis of genetic polymorphisms by hybridization with oligonucleotide arrays on glass supports.* Nucleic acids research, 1994. **22**(24): p. 5456-5465.
271. Gunderson, K.L., et al., *Decoding randomly ordered DNA arrays.* Genome research, 2004. **14**(5): p. 870-877.
272. Metzker, M.L., *Sequencing technologies—the next generation.* Nature reviews genetics, 2010. **11**(1): p. 31-46.
273. Saiki, R., et al., *Primer-directed enzymatic amplification of DNA with a thermostable DNA polymerase.* Science, 1988. **239**(4839): p. 487-491.
274. von Beroldingen, C.H., et al., *Applications of PCR to the Analysis of Biological Evidence*, in

PCR Technology: Principles and Applications for DNA Amplification, H.A. Erlich, Editor. 1989, Palgrave Macmillan UK: London. p. 209-223.

275. Coleman, W.B. and G.J. Tsongalis, *The Polymerase Chain Reaction*, in *Molecular Diagnostics: For the Clinical Laboratorian*, W.B. Coleman and G.J. Tsongalis, Editors. 2005, Humana Press: Totowa, NJ. p. 47-55.
276. Navidi, W. and N. Arnheim, *Using PCR in preimplantation genetic disease diagnosis.* Human reproduction, 1991. **6**(6): p. 836-849.
277. Gibbs, R.A., *DNA amplification by the polymerase chain reaction.* Analytical Chemistry (Washington), 1990. **62**(13): p. 1202-1214.
278. Lee, C.C. and C.T. Caskey, *cDNA cloning using degenerate primers.* PCR protocols: A guide to methods and applications, 1990: p. 46-53.
279. White, T.J., N. Arnheim, and H.A. Erlich, *The polymerase chain reaction.* Trends in genetics, 1989. **5**: p. 185-189.
280. Leamon, J.H., et al., *A massively parallel PicoTiterPlate™ based platform for discrete picoliter-scale polymerase chain reactions.* Electrophoresis, 2003. **24**(21): p. 3769-3777.
281. Margulies, M., et al., *Genome sequencing in microfabricated high-density picolitre reactors.* Nature, 2005. **437**(7057): p. 376-380.
282. Shendure, J. and H. Ji, *Next-generation DNA sequencing.* Nature biotechnology, 2008. **26**(10): p. 1135-1145.
283. Hawkins, S.F. and P.C. Guest, *Multiplex Analyses Using Real-Time Quantitative PCR.* Multiplex Biomarker Techniques: Methods and Applications, 2017: p. 125-133.
284. Burkart-Waco, D., et al., *Next-Generation Sequencing for Targeted Discovery of Rare Mutations in Rice*, in *Biotechnologies for Plant Mutation Breeding*. 2017, Springer. p. 323-340.
285. Kolacsek, O., et al., *Ct shift: A novel and accurate real-time PCR quantification model for direct comparison of different nucleic acid sequences and its application for transposon quantifications.* Gene, 2017. **598**: p. 43-49.
286. Liu, P. and R.A. Mathies, *Integrated microfluidic systems for high-performance genetic analysis.* Trends in biotechnology, 2009. **27**(10): p. 572-581.
287. Burroughs, N. and E. Karteris, *10 Ultra-High-Speed PCR.* PCR Technology: Current Innovations, 2013: p. 143.
288. Duarte, G.R., et al., *Characterization of dynamic solid phase DNA extraction from blood with magnetically controlled silica beads.* Analyst, 2010. **135**(3): p. 531-537.
289. Breadmore, M.C., et al., *Microchip-based purification of DNA from biological samples.* Analytical chemistry, 2003. **75**(8): p. 1880-1886.
290. Tian, H., A.F. Hühmer, and J.P. Landers, *Evaluation of silica resins for direct and efficient extraction of DNA from complex biological matrices in a miniaturized format.* Analytical biochemistry, 2000. **283**(2): p. 175-191.

291. Hagan, K.A., et al., *Chitosan-coated silica as a solid phase for RNA purification in a microfluidic device.* Analytical chemistry, 2009. **81**(13): p. 5249-5256.
292. Cao, W., et al., *Chitosan as a polymer for pH-induced DNA capture in a totally aqueous system.* Analytical chemistry, 2006. **78**(20): p. 7222-7228.
293. Anada, T., et al., *The separation of oligodeoxynucleotides having a single-base difference by affinity capillary electrophoresis using oligodeoxynucleotide-polyacrylamide conjugate.* Electrophoresis, 2002. **23**(14): p. 2267-2273.
294. Kanayama, N., et al., *RAFT-generated polyacrylamide-DNA block copolymers for single-nucleotide polymorphism genotyping by affinity capillary electrophoresis.* Biomacromolecules, 2009. **10**(4): p. 805-813.
295. Ebara, M., et al., *Surface modification of microfluidic channels by UV-mediated graft polymerization of non-fouling and 'smart' polymers.* Radiation Physics and Chemistry, 2007. **76**(8–9): p. 1409-1413.
296. HASEGAWA, K., et al., *Specificity of MicroRNA Detection on a Power-free Microfluidic Chip with Laminar Flow-assisted Dendritic Amplification.* Analytical Sciences, 2017. **33**(2): p. 171-177.
297. Jung, S., et al., *Extensible Multiplex Real-time PCR of MicroRNA Using Microparticles.* Scientific reports, 2016. **6**.

2 Chapter 2. Experimental

Synopsis

This Chapter outlines the materials and methods used in this thesis. Included are all the relevant experimental details such as polymer synthesis, bio-conjugation, sample preparation as well as characterisation and instrumental techniques.

2.1 Materials

2.1.1 Reagents for Bio-Macro Agent Synthesis and Polymer Synthesis

Table 2.1. Reagents for bio-macro agent synthesis and polymer synthesis.

Name	**Manufacturer**	**Additional INFO**
Acetonitrile (ACN)	Sigma Aldrich, Australia	Distilled over calcium hydride before use
Acrylic acid-*N*-hydroxy succinimide (AA-NHS)	Sigma Aldrich, Australia	Used as purchased
Azobisisobutyronitrile (AIBN)	Sigma Aldrich, Australia	Recrystalised from methanol
4'-azobis (4-cyanovaleric acid) (ACVA)	Sigma Aldrich, Australia	Used as purchased
Basic alumina	Sigma Aldrich, Australia	Used as purchased
Bis(carboxymethyl) trithiocarbonate	Sigma Aldrich, Australia	Used as purchased
Cellu.SepT1 regenerated cellulose tubular membranes MWCO 3500 Da	Fisher Biotec	Used as purchased
4-Cyano-4-(thiobenzoylthio)pentanoic acid (CTA)	Sigma Aldrich, Australia	Used as purchased
1-ethyl-3-(dimethylaminopropyl) carbodiimide hydrochloride (EDC)	Sigma Aldrich, Australia	Used as purchased
Dibenzocyclooctyne-acid	Sigma Aldrich, Australia	Used as purchased
Dichloromethane (analytical grade	Sigma Aldrich, Australia	Used as purchased
1.4 dioxane (Analytical grade)	Sigma Aldrich, Australia	Used as purchased

Name	Manufacturer	Additional INFO
2-hydroxyethylacrylate (HEA, 98%)	Sigma Aldrich, Australia	Purified using an inhibitor remover column to remove methyl hydroquinone inhibitor
N-hydroxysuccinimide acid (NHS)	Sigma Aldrich, Australia	Used as purchased
N,*N*-dimethylformamide (DMF) (Analytical grade)	Sigma Aldrich, Australia	Used as purchased
N-isopropylacrylamide (NIPAAm; Aldrich 97%)	Sigma Aldrich, Australia	Used as purchased
N-(hydroxymethyl)acrylamide	Chem Supply	Used as purchased
4-pyrrolidinopyridine (PDP)	Sigma Aldrich, Australia	Used as purchased
Poly(ethylene glycol) methyl ether methacrylate (mPEGA)	Sigma Aldrich, Australia	Purified using an inhibitor remover column to remove methyl hydroquinone inhibitor. MW 480 g/mol, aprox 9 repeating units of PEG
Tetrahydrofuran (THF) (Analytical grade)	Sigma Aldrich, Australia	Distilled before use.

2.1.2 Chemicals

Table 2.2. Chemicals used in this study.

Name	Manufacturer	Additional INFO
Acrylamide	Sigma Aldrich, Australia	Used as purchased
Acetic acid	Sigma Aldrich, Australia	Used as purchased
Acetone (Analytical grade)	Sigma Aldrich, Australia	Used as purchased
Ammonium persulfate (APS)	Sigma Aldrich, Australia	Used as purchased
2,2-Bis[[(mercaptoacetyl)oxy]methyl]-1,3-propanediyl bis(mercaptoacetate)	Sigma Aldrich, Australia	Used as purchased
Calcium hydride	Sigma Aldrich, Australia	Used as purchased

Name	Manufacturer	Additional INFO
Chloroform (Analytical grade)	Sigma Aldrich, Australia	Used as purchased
Chloroform, deuterated (CDCl3) with tetramethyl silane (TMS)	Sigma Aldrich, Australia	Used as purchased
Dimethyl sulfoxide, deuterated (d6-DMSO)	Sigma Aldrich, Australia	Used as purchased
Deuterium oxide (D_2O)	Sigma Aldrich, Australia	Used as purchased
2,2-dimethoxy-2-phenylacetophenone	Sigma Aldrich, Australia	Used as purchased
EDTA	Sigma Aldrich, Australia	Used as purchased
Ethyl acetate (Analytical grade)	Sigma Aldrich, Australia	Used as purchased
Formamide	Sigma Aldrich, Australia	Used as purchased
Hexane (Analytical grade)	Sigma Aldrich, Australia	Used as purchased
Tris borate EDTA buffer 10 X	Sigma Aldrich, Australia	Used as purchased
Urea (Analytical standard)	Sigma Aldrich, Australia	Used as purchased
N,*N*,*N*',*N*'-Tetramethylethylenediamine (TEMED)	Sigma Aldrich, Australia	Used as purchased
Potassium phosphate dibasic mono basic	Sigma Aldrich, Australia	Used as purchased
Mineral oil	Sigma Aldrich, Australia	Used as purchased
Milli-Q water	N/A	Prepared by filtering through resin membrane filters to a resistivity of 18.3 MΩ cm
1,3,5-triallyl-1,3,5-triazine-2,4,6(1H,3H,5H)-trione	Sigma Aldrich, Australia	Used as purchased

2.1.3 DNA Samples

Single-stranded DNA (ss-DNA) purchased from Integrated DNA Technologies. DNA templates and oligonucleotide PCR primers (Table 2.3) were also purchased from Integrated DNA Technologies and the Oligonucleotides were diluted in 0.05% Tween 20 then stored at -20°C.

Table 2.3. DNA samples used in this thesis.

Base	Code	Sequence	Tm (^{O}C)	Mw (g/mol)
23	AMEL-R-REVCOMP-NH_2	5'NH_2-C6-AGC-TTC-CCA-GTT-TAA-GCT-CTG-AT-3'	56.2	71687
50/1350	50bp-DNA ladder	DNA Ladder (PAGE)	N/A	
10/60	Oligostandards	DNA Ladder (Agarose)	N/A	
20	Azide-Fwd Primer 2	5’(Azide)CAGTACCACTCGCGTTCAGA-3’	56.8	6380.3
20	VP1-Fwd Primer 2	5’CAGTACCACTCGCGTTCAGA-3’	56.8	6062
17	5620 Rev Primer	5’TCGTCCTTGTCTGTCCA-3’	52.7	5236.5
17	5620 Rev Primer	5’ (Alkyne)TCGTCCTTGTCTGTCCA-3’	52.7	5236.5
63	VP1 Target	5’CAGTACCACTCGCGTTCAGA-gtccaccatagagaacttcctgtgt-TGGACAGACAAGGACGA-3’		

2.2 Grafting-from Strategy

2.2.1 Synthesis of *N*-hydroxyl Succinimide Trithiocarbonate Chain Transfer Agent (RAFT NHS Ester)

N-hydroxy succinimide (NHS) (0.5 g, 4.3 X 10^{-3} mol), *N-(*3-dimethylaminopropyl)-*N'*-ethylcarbodiimide hydrochloride (EDC) (0.1g, 5.2 X 10^{-3} mol) and 4-pyrrolidinopyridine (0.074 g, 5.0 X 10^{-4} mol) were added to a (25 mL) solution of 60/40 dichloromethane/dioxane. The solution was then stirred under nitrogen. The mixture was then added drop wise over 1 h under nitrogen to a stirred, cooled (3 ^{O}C) solution of 60/40 dioxane/DCM (25 mL) containing the bis(carboxymethyl)trithiocarbonate chain transfer agent (0.5 g, 2 X 10^{-3} mol). After 1 h, the reaction was brought to room temperature and a yellow oil was observed in the reaction vessel. The solution was decanted off and the yellow so-called RAFT NHS ester product was extracted and purified by a water wash (50 mL x 2) and acid wash (5% acetic acid x 2) and then dried with anhydrous Na_2SO_4. The solution was filtered and then the product (0.21 g, 25%) was dried under vacuum. The RAFT NHS ester agent was characterised by ^{1}H NMR spectroscopy and ESI mass spectrometry (see Chapter 3, Section 3.2).

2.2.2 Preparation of Stock Solutions of DNA and RAFT Ester Agent

Stock solutions between 5-25 µg/µL of amine functionalised ss-DNA were prepared by adding 40-180 µL of Miili-Q water to 1 mg of ss-DNA. The RAFT ester agent 200 µg/µL stock solution was prepared by adding 40 mg of RAFT ester agent to 200 µL of DMF. Reaction stock solutions between 1-15 µg/µL were prepared by dilution of the 200 µg/µL stock solutions

2.2.3 Bio-conjugation of the RAFT NHS Ester Agent to an Amine Terminated Oligonucleotide

RAFT NHS ester agent (1 µg, 2.3 X 10^{-9} mol) was added to 5 µL of DMF and 1 µL of potassium phosphate buffer (1.0 M, PH 7.6) and 4 µL (2.3 X 10^{-9} mol) of 5'NH_2-C6-AGC-TTC-CCA-GTT-TAA-GCT-CTG-AT-3' in a 1.5 mL centrifuge tube. Mineral oil (100 µL) was added to the centrifuge tube to prevent evaporation. The reaction was placed on a thermo-mixer shaking at 350 rpm overnight at 30 ^{O}C. The centrifuge tube was removed from the thermo-mixer and the mineral oil was sucked off the top by vacuum. Cold 2% $NaClO_4$ in acetone (1 mL) was added to the tube and then placed in the freezer for 30 min. After the allotted time, the tube containing the now so-called RAFT bio-macro agent was then centrifuged for 30 min at 14000 rpm. A pellet was observed at the bottom of the tube, and the solution was removed via suction. The crude RAFT bio-macro agent was then washed with acetone (1 mL) and centrifuged using an Eppendorf micro spin centrifuge for 10 min at 14000 rpm. The solution was removed via suction and then dried for 5 min at 45 ^{O}C and 14000 rpm. The solution was then resuspended in deionised water (50 µL) and stored in the freezer. The RAFT bio-macro agent product was characterised using MALDI-TOF mass spectrometry (see Chapter 3, Section 3.2) and PAGE (see Chapter 3, Section 3.2).

2.2.4 Polymerisation of 2-Hydroxyethyl Acrylate (HEA) using the RAFT Bio-macro Agent.

The RAFT bio-macro agent (50 µL, 2.3 nmol) solution was purged with nitrogen and then injected into a septum sealed vial with a stir bar containing a solution of deionised water (200 µL), AIBN (0.5 nmol) and 2-hydroxyethyl acrylate (8 µmol). The vial was heated to 40 ^{O}C and the polymerisation was stopped after 1, 2, 3, 4 and 7 days by opening the vial to air and precipitating the polymer in cold 2% $NaClO_4$ in acetone solution (4000 µL) which was then placed in the freezer for 30 min. After the allotted time, the so-called p(HEA)-ssDNA bio-conjugate was centrifuged for 30 min at 4000 rpm (Eppendorf micro spin centrifuge). The p(HEA)-ssDNA bio-conjugate product was washed with acetone and centrifuged for 30 min and then dried for 50 min at 50 ^{O}C, the polymer bioconjugate product was then lyophilised overnight under vacuum at -50 ^{O}C using Labconco Freeze-drier. The p(HEA)-ssDNA bio-conjugate product was characterised by MALDI-TOF mass spectrometry, PAGE, ATR-FTIR spectroscopy and UV-Vis spectroscopy (see Chapter 3, Section 3.4).

2.2.5 Polymerisation of 2-Hydroxyethyl Acrylate (HEA) using the RAFT Bio-macro Agent (Lower Concentration of Monomer).

The RAFT bio-macro agent (200 µL, 44 nmol) solution was purged with nitrogen and then injected into a septum sealed vial with a stirrer bar containing a solution of deionised water (200 µL), AIBN (0.5 nmol) and HEA (0.3 µmol). The vial was heated to 60 ^{O}C and the polymerisation was stopped after 1 day by opening the vial to air and precipitating the polymer in cold 2% $NaClO_4$ in acetone solution (4000 µL) which was then placed in the freezer for 30 min. After the allotted time, the so-called p(HEA)-ssDNA bio-conjugate product was then centrifuged for 30 min at 4000 rpm. The p(HEA)-ssDNA bio-conjugate product was washed with acetone and centrifuged for 30 min and then dried for 50 min at 50 ^{O}C. The polymer bio-conjugate was then lyophilised overnight under vacuum at -50 ^{O}C. The p(HEA)-ssDNA bio-conjugate product was characterised by MALDI-TOF mass spectrometry (see Chapter 3 Section 3.5).

2.2.6 Polymerisation of 2-Hydroxyethyl Acrylate (HEA) using the RAFT Bio-macro Agent (Stepwise Addition)

The RAFT bio-macro agent (200 µL, 44 nmol) solution was purged with nitrogen and then injected into a septum sealed vial with a stirrer bar containing a solution of deionised water (200 µL), AIBN (0.5 nmol) and 2-hydroxyethyl acrylate (0.3 µmol). The vial was heated to 60 ^{O}C, after 24 h 100 µL of the solution was extracted and then 100 µL of deionised water, AIBN (0.5 nmol) and (0.3 µmol) was added to the reaction vial and polymerisation was continued. The polymerisation was stopped after 24 h and 48 h by opening the vial to air and precipitating the polymer in cold of 2% $NaClO_4$ in acetone solution (4000 µL) which was then placed in the freezer for 30 min. After the allotted time, the so-called p(HEA)-ssDNA bio-conjugate product was then centrifuged for 30 min at 4000 rpm. The p(HEA)-ssDNA bio-conjugate product was washed with acetone and centrifuged for 30 min and then dried for 50 min at 50 ^{O}C. The polymer was then lyophilised overnight under vacuum at -50 ^{O}C. The p(HEA)-ssDNA bio-conjugate product was characterised by MALDI-TOF mass

spectrometry and PAGE (see, Chapter 3, Section 3.6).

2.3 Grafting-to Strategy

2.3.1 RAFT Polymerisation PNIPAAm-*co*-HMAAm (2.5, 5, 7.5, 10, 12.5 mol %)

The pNIPAAm-*co*-HMAAm copolymers were synthesised by RAFT polymerisation. An example of a typical synthesis for 2.5 mol % pNIPAAm-*co*-HMAAm was as follows; NIPAAm (1 g, 9 mmol), and HMAAm (0.025 g, 0.2 mmol), and 4-cyano-4-(thiobenzoylthio) pentanoic acid (CTA 2) (6.75 mg, 0.02 mmol) were dissolved in a reaction vial with dioxane (5.9 mL), sealed and deoxygenated for 15 min with nitrogen. Separately, a stock solution of 4'-azobis (4-cyanovaleric acid) (ACVA) (27.5 mg) was prepared in dioxane (1 mL). After deoxgenation 0.1 mL (0.0098 mmol) was injected into the reaction vial, and then placed in an oil bath while stirring at 70 ^{O}C for 24 h. The resulting copolymer (0.5 g, yield 52 %, calculated gravimetrically) was dialysed first with ethanol (3 days) then with water (3 days) at room temperature. Water was then removed by freeze-drying to give a white powder. This synthesis was repeated for 5, 7.5, 10 and 12.5 mol % HMAAm, hereafter defined as 0H, 2.5H, 5H, 7.5H, 10H and 12.5H. The HMAAm content was estimated by ^{1}H NMR and ATR-FTIR spectroscopies and the molecular weights (M_n) and the polydispersity indices (Đ) were measured by GPC (see Chapter 4, Section 4.2)

2.3.2 EDC coupling DBCO-Acid: PNIPAAm-*co*-HMAAm-*co*-SA (2.5, 5, 7.5, 10, 12.5 mol %)

PNIPAAm-*co*-HMAAm-*co*-SA was prepared by Steglich esterification. A typical procedure for esterification of pNIPAAm-*co*-HMAAm (10H) was as follows; DBCO (10 mg $3x10^{-9}$ mol) was dissolved in DCM and then stirred on ice. In a separate vial p(NIPAAm-*co*-HMAAm) (60 mg, $3x10^{-5}$ mol) was dissolved in a 60/40 solution of DCM/dioxane (10 mL) and stirred. EDC (23 mg, 0.118 mmol) and 4-pyrrolidinpyridine (PDP) (8.7 mg, 0.059 mmol) was added to the pNIPAAm-*co*-HMAAm solution. Then the pNIPAAm-*co*-HMAAm solution was added drop wise into the DBCO solution while stirring for 1 h. The reaction was then brought to room temperature for 1 h while stirring. After evaporating the solvent, the oily product (pNIPAAm-*co*-HMAAm-*co*-SA) was re-dissolved in THF and precipitated in diethyl ether (100 mL). The solution was then centrifuged at 3000 rpm for 10 min and the ether was decanted off. The remaining oil was dissolved in a small volume of Milli-Q water and then dialysed with ethanol (3 days) and then water (3 days). Water was then removed by freeze drying to give a white powder (0.01 g, 16 %). This synthesis was repeated for, 2.5H, 5H, 7.5H, and 12.5H, to yield hereafter defined as the 2.5S, 5S, 7.5S, 10S and 12.5S pNIPAAm-*co*-HMAAm-*co*-SA copolymers. The DBCO content was investigated by ^{1}H NMR and ATR-FTIR spectroscopies (see Chapter 5, Section 5.2).

2.3.3 PCR to Prepare Azide Functionalised Double Stranded 63 bp PCR Product.

PCR reactions (20 µL) contained 0.5 mM of the forward and reverse primers (Table 2.3) 0.01M tris HCl, 5 mM KCl, 0.5 mM dNTPs, 1 unit of GoTaq DNA polymerase (Promega) and 200 nM of DNA target (Table 2.3). Reactions were denatured at 95 ^{O}C for 1 min, 50 ^{O}C for 1 min and 72 ^{O}C for 1 min for 37 cycles.

2.3.4 Agarose Gel Electrophoresis

PCR product (5 uL) was mixed with DNA loading buffer and electrophoresed through a 5% agarose gel in 1xTAE buffer (40 mM Tris-acetate, 1 mM EDTA, pH 8.3). DNA was stained for 10 min in ethidium bromide (1 mg/mL in Milli-Q water) then photographed with UV illumination using an EZ gel doc system (Promega) and analysed using Geldoc Software Image Lab 5.2.1(see Chapter 5, Section 5.5- 5.8).

2.3.5 Alkyne-Azide Coupling of PNIPAAm-*co*-HMAAm-*co*-SA (2.5, 5, 7.5, 10, and 12.5 mol %) and Azide Functionalised Double Stranded PCR Products.

Temperature responsive PCR (TR-PCR) bio-conjugates were prepared by mixing azide functionalised ds-PCR product (63 bp) and a large excess of strained alkyne functionalised pNIPAAm-*co*-HMAAm-*co*-SA in a centrifuge tube in a 90:10 acetonitrile/water solution. The centrifuge tube was placed in a PCR machine for 15 h at 60 ^{O}C. The acetonitrile/water solution was evaporated, and the product was redissolved in deionised water. The TR-PCR bio-conjugates were characterised by agarose gels and fluorescence spectroscopy (see Chapter 5, Section 5.8).

2.4 PEG Hydrogel Method

2.4.1 Free Radical Polymerisation of Activated Ester PEG Copolymers (11-56 mol %) p(mPEGA-*co*-AA-NHS)

An example of a typical synthesis for 28 mol % mPEGA-*co*-AA-NHS copolymer termed 22N was as follows: mPEGA (1 g, 2.1 mmol) and AA-NHS (200 mg, 1.1 mmol) were dissolved in 20 mL of dry acetonitrile. AIBN (1.5 mg, 0.01 mmol) was added to the solution, and the flask was fitted with a rubber septum then the solution was purged with nitrogen for 15 min. The mixture was polymerised at 80 ^{O}C for 16 h. After polymerisation, the solution was added to cold diethylether, which resulted in a white emulsion, the solution was decanted into glass centrifuge tubes (50 mL) and then centrifuged for 3 min at 4000 rpm. A yellow oil was observed on the bottom of the tubes, the ether layer was decanted off and then the yellow oil was redissolved in DCM. The yellow oil was then rotary evaporated to dryness to give the final product, with a final AA-NHS ratio of 28 mol % (0.85 g, 70%). The mPEGA-*co*-AA-NHS copolymer was characterised by ^{1}H NMR and ATR-FTIR spectroscopies (see Chapter 6, Section 6.2). This synthesis was repeated for 12, 30, 36, 42 and 46 mol % AA-NHS, hereafter defined as 12N, 30N, 36N, 42N and 46N.

2.4.2 ^{1}H NMR Conversion Method for Activated Ester PEG Copolymers

MPEGA (1 g, 2.1 mmol) and AA-NHS (300 mg, 1.78 mmol) were dissolved in 20 mL of dry acetonitrile. AIBN (1.5 mg, 0.01 mmol) was added to the solution, and the flask was fitted with a rubber septum then the solution was purged with nitrogen for 15 min. The mixture was polymerised at 80 ^{O}C for 22 h. Solution (0.1 mL) was extracted from the vial at 1, 2, 4, 6, 8 and 22 h. Then 50 µL of this solution was added to 0.5 mL $CDCl_3$ in an NMR tube. ^{1}H NMR spectroscopy of the 6 tubes was carried out to measure the conversion of each monomer in the copolymerisation (see Chapter 6, Section 6.2).

2.4.3 Preparation of 11- 56 mol % p(mPEGA-*co*-AA-allylamine)

An example of a typical synthesis involved dissolving 1 g of 14 mol % p(mPEGA-*co*-AA-NHS) in 20 mL of dry THF, in a round bottom flask. The solution was stirred, placed in an ice bath and placed under nitrogen. Allylamine (0.05 g, 0.83 mmol) was added to the flask whilst stirring, the solution turned cloudy after 1 h, the reaction was then stopped after 16 h. The solution was precipitated into 200 mL cold diethyl ether, where a white (NHS) precipitate and white emulsion formed. The solution was filtered to remove the NHS precipitate and the white emulsion was placed into 50 mL centrifuge tubes and centrifuged for 3 min at 4000 rpm. A yellow oil was observed on the bottom of the tubes, the ether layer was decanted off and then the yellow oil was redissolved in DCM. The yellow oil was then rotary evaporated to dryness to give the final product and was characterised by ^{1}H NMR spectroscopy (see Chapter 6, Section 6.3).

2.5 Cross-Linking of PEG Copolymers

2.5.1 Preparation of Polydimethylsiloxane (PDMS) Master

PDMS was made via a hydrosilation reaction where Sylgard A (based) and Sylgard B (curing agent) (Dow Corning ®) were mixed in a 10:1 ratio. The mixture was then deoxygenated and then poured onto a master mould, inside a Teflon mould (a large block of Teflon machined with a 75 mm diameter circle to allow for a silicon wafer to be inserted to a depth of 5 mm). The entire assembly was then cured in an oven for 1 h at 85 °C.

2.5.2 Preparation of 11-56 mol % poly(mPEGA-*co*-AA-allylamine) Cross-linked Thiol-ene Hydrogel.

An example of a typical synthesis of a cross-linked hydrogel disk follows. Pentaerythritol-tetrakis(3-mercaptoacetate) tetrathiol, (432.54 g/mol, 18 µL), diphenyl (2,4,6-trimethylbenzoyl) phosphine oxide (DTPO) (348 g/mol,1 mg, 0.35 mol)) and 200 µL chloroform (CCl_3) was added to 0.3 g of 14 mol% poly(mPEGA-*co*-AA-allylamine). The solution was mixed and deoxygenated in a 1.5 mL centrifuge tube, and then degassed by vacuum and ultra-sonication followed by centrifugation for 1 min. Figure 2.1 shows how the mixture was then poured on to a silicon wafer that had a cured layer of PDMS and a cut out circular mould 5mm in diameter and 1 mm thick. The polymer was then cured for 3 min using a 40-watt UV light at 350 nm. The PDMS layer was peeled off the silicon substrate to reveal the thin film hydrogel disk, the hydrogel disk was subsequently peeled off and used for swelling experiments as is.

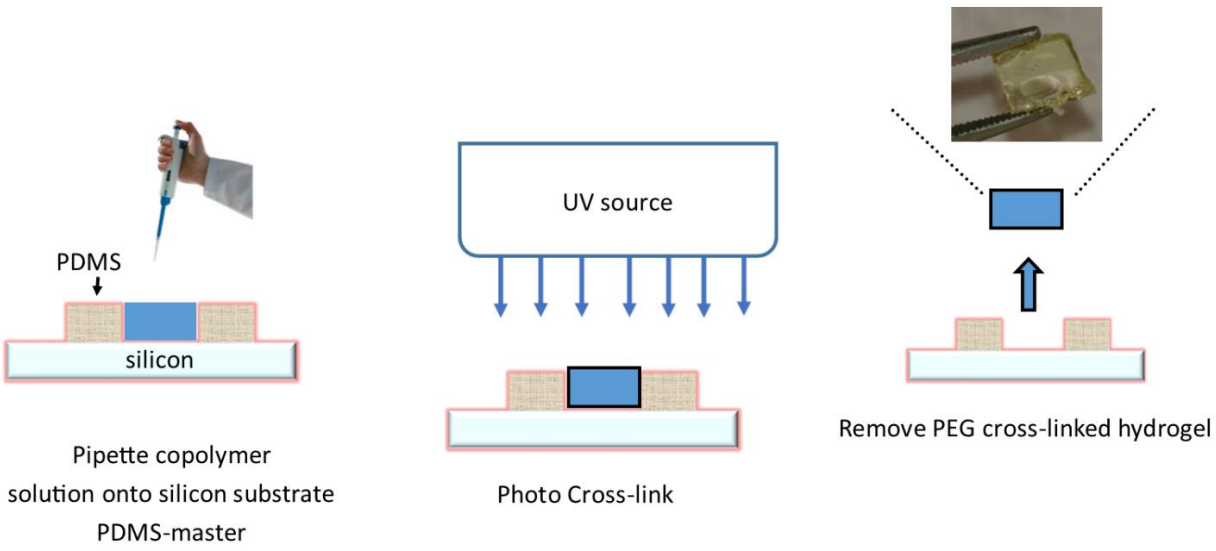

Figure 2.1. Scheme outlining the method used to photo cross-link poly(mPEGA-*co*-AA-allylamine) to form cross-linked hydrogels.

2.5.3 Hydrogel Swelling Method

A series of PEG cross-linked gels, 5 mm in diameter were placed into pre-weighed wire sieve boxes made from stainless steel mesh. These boxes were then placed into Milli-Q water. A box was removed from the water at pre-determined intervals (see Chapter 6, Section 6.6.1) and the excess water was removed by gently blowing the box and sample with nitrogen. The box was then weighed to calculate the weight increase of the sample due to water uptake (see Chapter 6, Section 6.6.2).

2.6 Characterisation Techniques: Grafting-from and Grafting-to Strategy

2.6.1 Nuclear Magnetic Resonance (NMR) Spectroscopy Principles

The molecular structure of organic compounds can be determined by NMR spectroscopy [1]. This is because the nuclear spin properties of certain nuclei in a molecule being investigated can be used to predict chemical structure [2]. Nuclei are normally randomly orientated, the addition of radio frequency (RF) energy when nuclei are placed in a magnetic field causes a flip in spin states [2]. Nuclei that were aligned with the applied field are in the alpha spin state, those that were not aligned are in a higher state (beta spin state) [2]. The energy difference of this transition results in the emission of an NMR signal. Proton solution ^{1}H NMR spectroscopy is the most common method used to elucidate chemical structure due to its abundance in organic molecules [2]. In this study ^{1}H NMR was used to investigate the structure of the organic molecules and the polymers that were synthesised.

2.6.2 Sample Preparation

Solution ^{1}H NMR spectroscopy data of all samples were recorded either on a 400 MHz or 600 MHz Bruker Avance NMR Spectrometer. Samples were dissolved in either $CDCl_3$ or d_6-DMSO and then placed in an NMR tube. Chemical shifts (σ) were recorded in ppm and referenced to the solvent peak (7.26 for $CDCl_3$ and 2.5 for d_6-DMSO). All data were exported as .csv files and then imported into Origin 7.0 for replotting.

2.6.3 Data Acquisition

The NMR data was Fourier transformed, integrated and solvent referenced using the Topspin NMR software (Bruker) or ACD/NMR processor (Academic version). The transformed data was replotted in Origin 7.0.

2.6.4 Attenuated Reflectance-Fourier Transform Infrared (ATR-FTIR) Spectrophotometry

In ATR-FTIR spectrophotometry infrared light travels through an internal reflection element (normally a crystal such as diamond/ZnSe), where the light is bounced through the crystal and meets the surface of the sample [3]. The evanescent wave is absorbed by the sample and the adsorption causes attenuation of the initial infrared beam from which a transmission spectrum can be produced [3].

2.6.5 Sample preparation and data acquisition

ATR-FTIR spectra were obtained using a Perkin Elmer spectrophotometer and a universal ATR sampling accessory. The crystal used was diamond/ZnSe and the spectra obtained were analysed with the Spectrum software version 6.3.4. All Spectra were recorded in the range of 4000-650 cm^{-1} at a resolution of 4 cm^{-1} as an average of four scans. The polymer bio-conjugates produced by the grafting-to method (Chapter 3) were referenced to the starting materials: DNA: 5'NH_2-C6-AGC-TTC-CCA-GTT-TAA-GCT-CTG-AT-3', and HEA.

2.7 Characterisation Techniques: Grafting-from

2.7.1 Matrix Assisted Laser Desorption Time of Flight (MALDI-TOF) Mass Spectrometry Principles

In MALDI-TOF, the sample is solubilised in small organic compounds that form a crystalline matrix when deposited on a conductive sample support [4]. Then irradiation of the crystalline matrix using a nanosecond ultraviolet laser beam is performed [4]. Typically, wavelengths of 266 nm or 377 nm are used [4]. The laser energy decomposes the crystalline matrix and generates a particle cloud and the ions are accelerated by an electric field to a detector [4]. The ion masses are calculated by measuring their time of flight (TOF) [4].

2.7.1.1 Data Acquisition

All MALDI mass spectra were collected by Flinders Analytical. MALDI mass spectra of the DNA: 5'NH_2-C6-AGC-TTC-CCA-GTT-TAA-GCT-CTG-AT-3' calibration standard and the polymer bio-conjugate samples were acquired on a Bruker autoflex III MALDI-TOF mass spectrometer operating in the linear mode. The laser was a Nd:YAG at 355 nm. The MALDI Matrix used was 3-hydroxybenzoic acid (3-HBA) [5].

2.7.2 Electrospray Ionisation Mass Spectrometry (ESI-MS) Principles

When a sample solution is introduced into a reaction chamber, it is charged by applying high voltage [6]. Dispersal of this solution produces ultra-fine droplets and electrical energy aids the transfer of the droplets towards the mass spectrometer [6]. The charged droplets are reduced in size by a temperature or a drying gas and at a critical point, the ions are ejected into the gas phase and accelerated into the mass analyser for mass measurement [6].

2.7.2.1 Data Acquisition

Samples were dissolved in acetonitrile with flow injection analysis at 10 µL/min. All ESI mass spectra were collected by Flinders Analytical. All measurements were performed on a Waters Synapt HDMS spectrometer with the detection of positively charged ions.

2.7.3 Polyacrylamide Gel Electrophoresis (PAGE) Principles

Polyacrylamide gel electrophoresis (PAGE) separates DNA based upon size [7]. The sugar-phosphate backbone of DNA is negatively (-) charged and will migrate in an electric field towards an electrode with the opposite positive (+) charge [7]. Longer lengths (higher molecular weight) of DNA will move slower thorough the gel than smaller lengths (lower molecular weight) [7]. The separation of ss-DNA can be complicated by secondary structures that can form [8]. Denaturing of these secondary structures is achieved by the addition of denaturing agents such as urea and formamide [8]. These denaturing reagents form hydrogen bonds with the DNA bases and prevent the formation of inter-base bonds and therefore, only the length of the DNA will affect mobility [8].

2.7.3.1 Preparation of 20% Acrylamide Gels

An example of the PAGE set-up used for analysis of DNA and DNA polymer bio-conjugates is shown in Figure 2.2. A typical synthesis of acrylamide gels involved adding 6.3 g of urea, 1.5 mL of 10X Tris borate EDTA (TBE) buffer, 2.25 mL of Milli-Q water and 7.5 mL of acrylamide to a beaker which was stirred until the urea was dissolved. The solution was then degassed and the polymerisation was initiated by the addition of 15 µL of 25 % ammonium persulfate (APS) solution and 15 µL of *N,N,N',N'*-Tetramethylethylenediamine (TEMED). The urea/acrylamide solution was then pipetted between two glass plates and a comb was placed between the plates to make the loading wells. The gels were left to cure. When the gels were cured the electrophoresis-cell was assembled. The gels were then placed in the gel box along with the running buffer. The combs were removed, and the wells were flushed with running buffer.

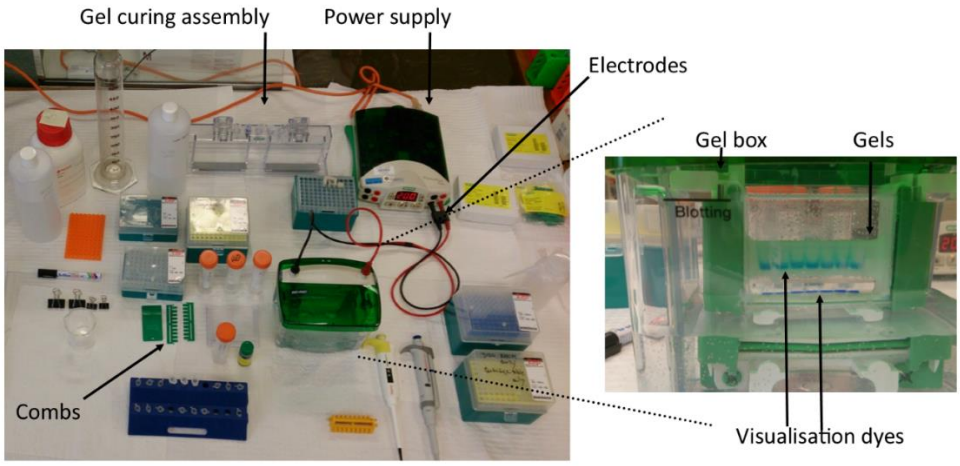

Figure 2.2. PAGE apparatus used to separate DNA.

2.7.3.2 Sample Preparation for PAGE

A typical method for preparing DNA samples and polymer bio-conjugate samples for PAGE is outlined as follows. Samples were mixed with visualisation dyes and prepared at a concentration of between 0.05-0.5 µg/µL. The samples were heated to 96 ^{O}C for 5 min and then cooled on ice for 5 min. The sample solutions were loaded by pipette (typically 10 µL) and a voltage between 100-250 volts was applied. The visualisation dyes were used to monitor the progress of the samples throughout the gel. The separation of samples by electrophoresis and visualisation of the samples by staining (SYBER GREEN (SG) or ethidium bromide (EtBr)) was optimised experimentally.

2.7.3.3 Data Acquisition

All gel electrophoresis was carried out using 20% polyacrylamide denaturing gel using 1× TBE buffer/urea as running buffer. All gels were stained with EtBr or SYBER GREEN for band visualisation and imaged by a BIO-RAD Gel Doc Ez imager software package image lab version 4.0.

2.7.4 Ultra Violet-Visible (UV-Vis) Spectrophotometry Principles

The absorbance of light by a molecule can be measured quantitatively using an Ultraviolet-Visible (UV-Vis) spectrophotometer. Through the application of the beer lambert law, $\mathrm{A} = \epsilon . b . c$ where A is absorbance, ϵ is molar absorptivity, *b* is path length and *c* is concentration; the concentration can be calculated when all other parameters are known.

2.7.4.1 UV-VIS Spectrophotometry of DNA and RAFT Chromophore

The concentration of DNA can be determined by its strong absorbance at 260 nm. RAFT agents possess a thiocarbonyl chromophore that absorbs at around 300-310 nm and therefore their presence can be detected

by UV-Vis spectrophotometry [9]. DNA absorbance and the absorbance of the RAFT chromophore from the RAFT bio-macro agent after polymerisation was measured by pipetting 2 µL of solution onto an optical measurement surface and scanning absorbance from 220-350 nm using a Nano drop 2000 spectrophotometer. The instrument was zeroed with Milli-Q water and DMF. All spectra were exported into Microsoft excel and then imported into Origin 7.0 for replotting.

2.8 Characterisation Techniques Grafting-to Strategy

2.8.1 Size Exclusion Chromatography (SEC) and Gel Permeation Chromatography (GPC)

SEC:GE Healthcare Äkta basic 10. Column: Supderdex 200 10/30, eluted in PBS pH 7.4.GPC: Shimadzu LC-20A GPC, high Resolution column in DMAc 80°C. Shimadzu refractive index detector RID-10A, and 50 µL of a 1mg/mL solution was injected.

All experimental data was performed and collected by Dr Charlotte Williams at the CSIRO manufacturing Flagship division.

2.8.2 Lower Critical Solution Temperature (LCST) of PNIPAAm Principles

The phase separation of pNIPAAm in aqueous solutions is largely driven by the hydrophobic effect [10]. The arrangement of water molecules in solution around the non-polar regions of pNIPAAm results in a decreased entropy (negative ΔS) upon mixing [10]. The exothermic enthalpic (ΔH) forces that drive the hydrogen bond formation between pNIPAAm and water molecules are disrupted at a critical temperature [10]. This leads to entropic forces dominating and the free energy change ($\Delta \mathrm{G}$) becomes positive upon mixing [10]. The observed outcome is the phase separation of pNIPAAm above a lower critical solution temperature (LCST) [10]. This phenomenon turns aqueous solutions containing pNIPAAm cloudy at the LCST and this cloud point can be calculated by the change in transmission of white light [10].

2.8.2.1 Lower Critical Solution Temperature (LCST): PNIPAAm-co-HMAAm (2.5, 5, 7.5, 10, 12.5 mol %) by Transmission of White Light using UV-VIS Spectrophotometry

Six solutions (3 mg/mL) in deionised Milli-Q water of 0H, 2.5H, 5H, 7.5H, 10H and 12.5H samples were prepared. The samples were placed in a Varian Cary G5, UV-Vis spectrophotometer under a nitrogen atmosphere. The UV-Vis spectrophotometer was fitted with a Peltier heater and the Peltier was cooled under a constant flow of water maintained at 25 ^{O}C. The temperature was ramped at 0.5 ^{O}C/min. All spectra performed in triplicate were recorded at 550 nm. The LCST was calculated at the point where transmittance was 50 % for all samples. Transmittance (550 nm light) measurements were recorded at initially 1 ^{O}C intervals and then at 0.5 ^{O}C intervals when approaching the LCST. Transmittance measurements were stopped when three consecutive measurements showed no decrease in the transmittance value. All measurements were performed in triplicate.

2.8.2.2 Lower Critical Solution Temperature (LCST): PNIPAAm-co-HMAAm (2.5, 5, 7.5, 10, 12.5 mol %) and PNIPAAm-co-HMAAm-co-SA (2.5, 5, 7.5, 10, 12.5 %) by Light Scattering using Real-time PCR Machine (Rotogene Q)

The pNIPAAm-*co*-HMAAm copolymers and pNIPAAm-*co*-HMAAm-*co*-SA copolymers (were prepared at 1 mg/mL in Milli-Q water in real time PCR tubes at a volume of 20 µL. The five polymers (pNIPAAm-*co*-HMAAm (2.5-12.5 mol %)) and five polymers pNIPAAm-*co*-HMAAm-*co*-SA (2.5-12.5 mol %) were heated over a temperature ramp that increased at 1 ^{O}C/min starting from 25 ^{O}C to 99 ^{O}C. The light scattering data was collected in triplicate on a real-time PCR machine (Rotogene Q), with software Rotogene Q Software V 2.1.09. The excitation and emission and wavelength was set for 490 nm and 510 nm respectively. All data were exported as .csv files and then imported into Origin 7.0 for replotting.

2.8.3 Dynamic Light Scattering (DLS): Principles

DLS instruments measure the Brownian motion of the particles using a light source. Small particles move faster than large particles [11]. The relationship between the size of a particle and its speed due to Brownian motion can be determined [12]. This is normally calculated from an intensity-intensity time correlation function $G^{(2)}$ (t, q) in the self-beating mode, where G(2) (t, q) is in the following form [13].

$$G^{(2)}(t,q) = A[1 + (\beta(g^{(1)}(t,q))^2]$$

Equation 2.1

Where A is the measured baseline, β a parameter depending on the coherence of detection, t, the delay time and $g^{(1)}(t,q)$, the normalised electric field correlation function which can be related to the line-width distribution *G* (Γ) by [12].

$$g^{(1)}(t,q) = \int G(\Gamma)e^{-\Gamma t}\, d\Gamma$$

Equation 2.2

The line width (Γ) is usually a function of both concentration (C) and theta (Θ) which can be expressed as [12].

$$\frac{\Gamma}{q^2} = D(1 + k_d C)[1 + f(R_g q)^2]$$

Equation 2.3

Where D is the translational diffusion coefficient, k_d is the diffusion second viral coefficient, and f is a

dimensionless constant. At extremely dilute solutions the ratio of $\Gamma/q\text{^}2$ is approximately equal to D. [12] The radius of hydration *r* can be found from using the Stokes-Einstein equation, where kB is the Boltzmann constant, T is the absolute temperature, and ɳ is the shear viscosity of the solvent [13].

$$r = \frac{k_B T}{6\pi\eta D}$$

Equation 2.4

The particles present in the solution scatter light and the correlation function interprets the intensity fluctuations of the scattered light to calculate the size of the particles [11].

2.8.4 DLS Sample Preparation: PNIPAAm-*co*-HMAAm (2.5, 5, 7.5, 10, 12.5 mol %)

Stock solutions (3 mL) of (3, 0.1, 0.05, 0.025, 0.0125 mg/mL) of 2.5H, 5H, 7.5H 10H and 12.5H were filtered through a 0.45 µm nylon filter. Each solution (1 mL) was added to a quartz cuvette.

2.8.4.1 Data Acquisition

The quartz cuvette was heated to the LCST of each polymer (previously determined by UV-Vis spectrophotometry) in a Malvern Instrument Zetasizer Nano series instrument equipped with a 4-mW He–Ne laser operating at l =632.8 nm, an avalanche photodiode detector with high quantum efficiency, and an ALV/LSE-5003 multiple tau digital correlator electronics system. The hydrodynamic radius of the resulting aggregate micelle was measured by cumulant analysis given by this instrument as the Z average size. The Z average size is an intensity mean, and is calculated by the fit of a polynomial to the log of the correlation function and then converted to size using dispersant viscosity and instrumental constants. The width parameter known as the Đ is also calculated from the cumulant mean of the intensity. When Đ below a value of 0.1 are obtained the cumulant analysis method is theorised to be a good representation of the size of the particles.

2.8.5 Critical Micelle Concentration (CMC) Principles

Amphiphilic block polymers, with hydrophilic blocks and hydrophobic blocks form micellular structures in solution [14]. Typically, these micelles have a hydrophobic inner core and hydrophilic outer corona in aqueous solutions [15]. The size of the micelles can be influenced by the length of the hydrophobic or hydrophilic chains. The shape of the micelle can be predicted by the “critical packing” parameter Ns.

$$Ns = \frac{Vc}{a * Lc}$$

Equation 2.5

Where *Ns* is packing parameter, Vc is volume of hydrophobic chain, *a* is cross sectional area of the aggregate expressed per molecule in aggregate and Lc is the length of the hydrophobic chain [16]. The formation of micelles in aqueous solutions is dependent on the concentration of the block copolymer in aqueous solutions [17]. Below a critical concentration the polymers are dissolved in solution [17]. Above the critical micelle concentration (CMC) and at a critical micelle temperature (CMT) the hydrophobic block associates with itself to minimise contact with water molecules, which drives the formation of the core shell micellular structure [17]. The measurement of the CMC and the CMT can be determined by the solubilisation of a probe molecule into the micelle structure [18]. As the molecule is solubilised into the micelle, the change in fluorescence that occurs for the probe molecule can be used to predict the CMC and the CMT [18]. In this thesis, the solubilisation of SYBR GREEN (probe) was used to predict the CMC and the CMT of pNIPAAm-*co*-HMAAm copolymers.

2.8.5.1 Sample Preparation for CMC of PNIPAAm-co-HMAAm (2.5, 5, 7.5, 10, 12.5 %)

A typical method of determining the CMC of pNIPAAm-*co*-HMAAm is described for 2.5H. Firstly, a stock solution (20 µg/µL) in Milli-Q water was prepared. Then 10 µL solutions of 10.0, 9.0, 8.0, 7.0, 6.0, 5.0, 4.0, 3.0, 2.0, 1.0, 0.5, 0.25 and 0.125 µg/µL, were prepared from the stock solutions. 10 µL of SBYR GREEN (1000 X) was added to each solution to give final concentration of 500 X (0.5 mg/mL) [19] for each solution.

2.8.5.2 Data Acquisition

The solutions were analysed using a real-time PCR machine (Rotogene Q), with software Rotogene Q Software V 2.1.09, an excitation wavelength of 497 nm, and an emission wavelength of 520 nm. Using a temperature ramp, the samples were heated from 25 ^{O}C to 99 ^{O}C at a heating rate of 1 ^{O}C/ min. Triplicate runs of each sample were performed. As a control 20 µL of a 500 X SYBR GREEN solution was used as the blank.

2.8.6 Atomic Force Microscopy (AFM) Principles

AFM images are produced by the interaction of an AFM probe (defined as a cantilever with a sharp tip at its end) and a sample [20]. The probe is brought close to the surface and a piezolelectric scanner moves the sample in the X, Y and Z direction [20]. The forces between the probe and surface are maintained through a feedback mechanism [20]. A laser beam is aimed at the back of the cantilever and as the cantilever moves in response to atomic variations on the surface the beam is deflected to a photodiode (Figure 2.3) [20]. The intensity of light measured at the upper and lower half of the diode is used to produce a height image [20].

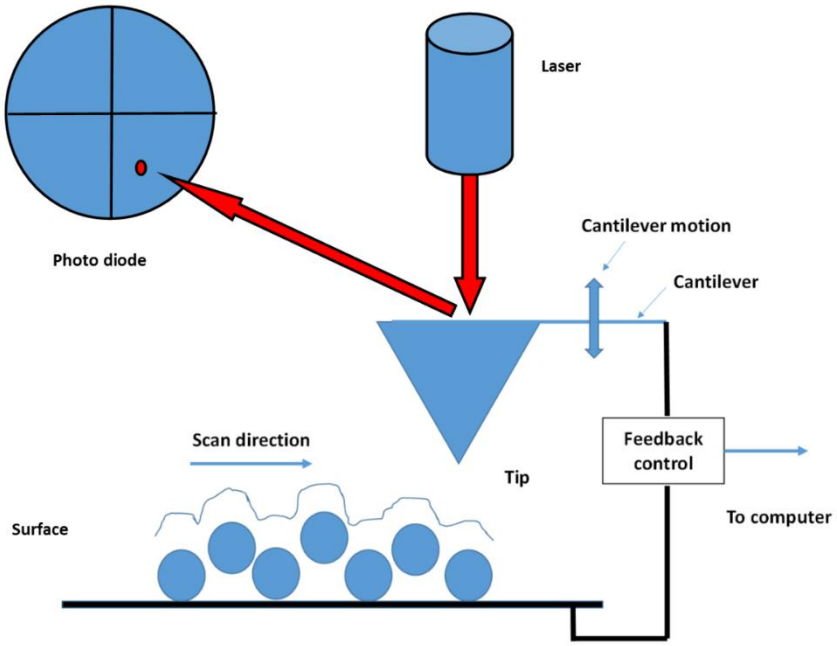

Figure 2.3. Scheme of AFM instrument.

2.8.6.1 Tapping Mode used for Imaging Samples

In this thesis tapping mode was used to image the samples because the lateral resolution of this mode is good for soft samples [20]. Stiff cantilevers are used since the probe is oscillated and the oscillation must be sufficient to pass through the water hydration layer found on most surfaces [20]. During the oscillation, the tip moves into the repulsive regime of the surface and contact with the surface is intermittent [20].

2.8.6.2 AFM Sample Preparation for PNIPAAm-co-HMAAm (2.5, 5, 7.5, 10, 12.5 mol %)

AFM of pNIPAAm-*co*-HMAAm (2.5H, 5H, 10H and 12.5H) on mica was achieved by first cleaving mica with scotch tape to achieve a flat surface. The 2.5H sample was dissolved in a solution of water (Milli-Q) to a final concentration of 20 µg/µL and 0.25 µg/µL. The solutions were then heated to 60 ^{O}C. 0.5 µL of each solution was transferred to the cleaved mica surface. The mica sample was heated for 1 min at 60 ^{O}C to dry the sample. The (5H, 10H, and 12.5 H) were dissolved in Milli-Q water at a concentration of 0.5 µg/µL. The samples were then heated to 60 ^{O}C and 0.5 µL of each solution was transferred to a freshly cleaved mica surface. As a control 0.5 µL of Milli-Q water was added to freshly cleaved mica and it was then heated at 60 ^{O}C for 1 min to dry.

2.8.6.3 Data Acquisition

All samples were imaged in air using a Nanoscope V Multimode 8 microscope and analysed using the Nanoscope software version 8.10 Sr1. The images were obtained in tapping mode in air using the E scanner with ranges between 15 µm in XY and 3 µm in Z, using a silicon nitride cantilever (fundamental resonance

frequency of between (265-400 kHz) with a value line soft tapping mode, force modulation (FMV) tip. Images were obtained using a scan rate of approximately 1 Hz with the parameter set point, amplitude and feedback control optimised for each sample. The images were flattened using the Nanoscope software and the surface coverage of polymeric micelles was measured using the cross-section tool and particle analysis tool.

2.8.7 Agarose Gels

Separation of DNA using agarose occurs due to the phosphate backbone of the DNA (and or RNA) molecule being negatively charged. Therefore, when DNA is loaded into agarose pre-cast wells and an electric field is applied, DNA fragments will migrate to the positively charged anode. Since DNA has a uniform mass/charge ratio, DNA molecules are separated by size within an agarose gel such that the migration distance travelled is inversely proportional to the log of its molecular weight.

2.8.7.1 Agarose (5% and 1.5%) Gel Preparation

Agarose (5 g or 1.5 g) was added to a 250 mL conical flask. TAE buffer (40 mM Tris-acetate,1 mM EDTA pH 8.3) (100 mL) was added to the conical flask and the solution was mixed and dissolved by heating in a microwave. After cooling for 5 min, the gel was poured slowly into the prepared gel tank and the bubbles were removed using a pipette tip. The appropriate gel comb was inserted into the gel and it was cured for 30 min.

2.8.7.2 Agarose Gel Electrophoresis:

PCR product control (5 µL) and TR-PCR bio-conjugate (5 µL) was mixed with DNA loading buffer and electrophoresed through a 5% or 1.5% agarose gel in 1xTAE buffer (40 mM Tris-acetate, 1 mM EDTA, pH 8.3). DNA was stained for 10 min in EtBr (1mg/mL in 18.3 Ω cm water) then photographed with UV illumination using an EZ gel doc system (Promega).

2.8.7.3 TR-PCR Bio-Conjugates Purification

The band observed in the agarose gel representing TR-PCR bio-conjugates was excised and then placed in a centrifuge tube. Tween 20 solution (10 µL) was added and then the sample was shaken (850 rpm) overnight at 40 ^{O}C using an Eppendorf Thermomixer Comfort.

2.8.8 Fluorescence Rotogene Q Principles

The Rotogene Q instrument is a real-time PCR cycler. Each centrifuge tube placed in the instrument is spun in a chamber of moving air (tube-to-tube variation ±0.02 °C). This helps to keep all samples at the same temperature during the rapid thermal cycling required for PCR. When each of the tubes is aligned with the detection optics, the sample is illuminated and a fluorescent signal is captured from a single, short optical pathway [21].

2.8.8.1 Sample Preparation One Pot PCR Click

One pot PCR click reactions (20 µL) contained 0.5 mM of the forward and reverse primers (Table 2.3) 0.01 M tris HCl, 5 mM KCl, 0.5 mM dNTPs, 1 unit of GoTaq DNA polymerase (Promega) and 200 nM of DNA target (Table 2.3) and 2 µL SA copolymer (10S, 10 µg/µL). Reactions were denatured at 95 ^{O}C for 1 min, 50 ^{O}C for 1 min and 72 ^{O}C for 1 min for 37 cycles. The negative control PCR reaction was as above but contained the forward primer without the azide group (Table 2.3). The PCR control PCR reaction was as above but contained no polymer.

2.8.8.2 Sample Preparation for Click in Water

One pot click reactions vials and controls (20 µL) contained 5 µL of SA copolymer (10S, 10 µg/µL), 5 µL of PCR-Az product (30 ng/µL) and 10 µL SG (0.5 mg/mL). The polymer negative control contained 5 µL of pNIPAAm-*co*-HMAAm copolymer (10H, 10 µg/µL), 5 µL of PCR-Az product (30 ng/µL) and 10 µL SG (0.5 mg/mL). The PCR control contained 5 µL of Milli-Q water, 5µL of PCR-Az product (30 ng/µL) and 10 µL SG (0.5 mg/mL). The polymer controls contained 5 µL of Milli-Q water, 5 µL of SA copolymer (10S, 10 µg/µL) or 5 µL of pNIPAAm-*co*-HMAAm copolymer (10H, 10 µg/µL) and 10 µL SG (0.5 mg/mL).

2.8.8.3 Sample preparation for One Pot Click in Buffer

One pot click reactions vials and controls (20 µL) contained 5 µL of SA copolymer (10S, 10 µg/µL), 5 µL of PCR-Az product (30 ng/µL) and 10 µL SG (0.5 mg/mL). The PCR control contained 5 µL of Milli-Q water, 5µL of PCR-Az product (30 ng/µL) and 10 µL SG (0.5 mg/mL).

2.8.8.4 Sample Preparation of Gel Extract from Click Reaction in Acetonitrile

The Tween 20 (10 µL) solution containing the TR-PCR bio-conjugate gel extract was added to a centrifuge tube and then 10 µL of SG solution was added (0.5 mg/mL). The PCR control contained 5 µL of Milli-Q water, 5µL of PCR-Az product (30 ng/µL) and 10 µL SG (0.5 mg/mL).

2.8.8.5 Melt Curve Analysis for One Pot PCR Click, One Pot Click in Water, One Pot Click in Buffer and Analysis of Gel Extract.

The centrifuge tubes were placed in a real-time PCR machine (Rotogene Q). The temperature was ramped from 25 ^{O}C to 100 ^{O}C at 1 ^{O}C /min. The solutions were analysed using a real-time PCR machine, with software Rotogene Q Software V 2.1.09, with an excitation wavelength of 497 nm, and an emission wavelength of 520 nm. All data was exported as .csv files and replotted in Origin 7.0.

2.9 Characterisation Techniques PEG Hydrogel Method

2.9.1 Fluorescence Spectroscopy Principles

In Fluorescence spectroscopy, a beam of light (between 200-800 nm) that passes through a sample solution in a sample cuvette can be absorbed by a molecule [22]. The absorbance of a photon promotes an electron from the ground state to an excited state [22]. Fluorescence occurs when electrons in the excited state return in a very short time frame (pico to nano second) to the ground state and photons of a longer wavelength are emitted [22]. Typically, the detector on a fluorescence spectrometer is set at a 90^{O} angle to the incoming beam of light, so that the fluorescence signal that is measured is not diluted by incoming light [22]. The concentration of the analyte being measured is directly proportional to the intensity of the emission. The intensity is proportional to concentration and quantum yield of the fluorophore. The analyte intensity of a series of standard solutions of known concentration can be used to produce a standard curve by the least squares method. The intensity of the analyte measured by fluorescence can be compared to the standard curve and the concentration of the analyte can be determined from the line of best fit.

2.9.1.1 Standard Curve Preparation for Camptothecin (CPT)

From a 1 mg/mL CPT stock solution (3 mL), standard (1 µg/mL to 20 µg/mL) solutions (3 mL) of CPT were used to prepare a standard curve.

2.9.1.2 Sample Preparation for CPT Release

An example of a typical synthesis of a cross-linked hydrogel disk loaded with CPT is as follows. Pentaerythritol-tetrakis(3-mercaptoacetate) tetrathiol, (432.54 g/mol, 18 µL), diphenyl (2,4,6-trimethylbenzoyl) phosphine oxide (DTPO) (348 g/mol, 1 mg, 0.35 mol)), CPT (20 µg, 57 nmol) and 200 µL chloroform (CCl_3) were added to 0.3 g of 28 mol% poly(mPEGA-*co*-AA-allylamine). The solution was mixed and degassed in a 1.5 mL centrifuge tube, and then degassed by vacuum and ultra-sonication followed by centrifugation for 1 min. Figure 2.1 shows how the mixture was then poured on to a silicon wafer that had a cured layer of PDMS and a cut out circular mould 5mm in diameter and 1 mm thick. The polymer was then cured for 3 min using a 40 watt UV light at 350 nm. The PDMS layer was peeled off the silicon substrate to reveal the thin film hydrogel disk, the hydrogel disk was subsequently peeled off and used for CPT release experiments as is.

2.9.1.3 Data Acquisition

All fluorescence spectra recorded for the standard curve solutions were recorded on a Varian Cary Eclipse Fluorescence spectrometer with Scan software version 1.1 using an excitation wavelength of 254 nm. The emission spectra (standard solutions) were recorded from 420 nm to 600 nm.

The hydrogel disks loaded with CPT were placed in a quartz cuvette. Then, a 0.1 M pH 8 Tris buffer solution

(3 mL) was added to the cuvette and the fluorescence spectra for the hydrogel disk was collected (for 60 min) using the simple reads program (excitation 254 nm, emission 450 nm) to determine the fluorescence intensity (450 nm) due to CPT release from the hydrogel disk. The line of best fit from the calibration curve (standard curve) was then manipulated to calculate the concentration of CPT released from the hydrogel disk.

2.9.2 Stereo Microscope

PEG Hydrogel images were taken using a DP21 digital camera (Olympus), on an Olympus XZS2 stereomicroscope plus with dark field transmission illumination and white fibre optic reflected light source.

2.9.3 Scanning Electron Microscopy (SEM) Principles

The surface structure of a sample can be imaged using a scanning electron microscope (SEM). SEM's operate by focusing an electron beam from an electron source into a beam with a small spot size using an electromagnetic lens. The electrons interact with the surface of a sample and the resulting emitted electrons can be collected on a cathode ray tube to produce an image.

2.9.4 SEM Samples

The PEG hydrogel samples were coated with a thin conducting film (Platinum) and the SEM images taken using an Inspect FEI F50 SEM with an accelerating voltage of 5-10 kV at a working distance of approximately 10 mm.

2.10 References

1. Hooda, S., A. Kumar Goyal, and A.S. Brar, *Stereochemical elucidation of complex α-methyl and β-methylene carbon resonances in poly(2-hydroxy ethyl methacrylate-co-methacrylonitrile) by 2D NMR.* Journal of Applied Polymer Science, 2009. **111**(5): p. 2381-2386.
2. Judd, C.S., et al., *Proton NMR Basics*. 1995, ACS Publications.
3. Mojet, B.L., S.D. Ebbesen, and L. Lefferts, *Light at the interface: the potential of attenuated total reflection infrared spectroscopy for understanding heterogeneous catalysis in water.* Chemical Society Reviews, 2010. **39**(12): p. 4643-4655.
4. Jurinke, C., P. Oeth, and D. van den Boom, *MALDI-TOF mass spectrometry.* Molecular Biotechnology, 2004. **26**(2): p. 147-163.
5. Somogyi, A., et al., *Analysis of All-Aromatic Polyesters by Matrix-Assisted Laser Desorption/Ionization Time-of-Flight Mass Spectrometry.* Macromolecules, 2005. **38**(10): p. 4067-4071.
6. Ho, C.S., et al., *Electrospray Ionisation Mass Spectrometry: Principles and Clinical Applications.* The Clinical Biochemist Reviews, 2003. **24**(1): p. 3-12.
7. Chrambach, A. and D. Rodbard, *Polyacrylamide Gel Electrophoresis.* Science, 1971. **172**(3982): p. 440-451.
8. Albright, L.M. and B.E. Slatko, *Denaturing polyacrylamide gel electrophoresis.* Current Protocols in Nucleic Acid Chemistry, 2001: p. A. 3B. 1-A. 3B. 5.
9. Skrabania, K., et al., *Examining the UV-vis absorption of RAFT chain transfer agents and their use for polymer analysis.* Polymer Chemistry, 2011. **2**(9): p. 2074-2083.
10. Schild, H.G., *Poly(N-isopropylacrylamide): experiment, theory and application.* Progress in Polymer Science, 1992. **17**(2): p. 163-249.
11. Chu, B., *Laser light scattering: basic principles and practice*. 2007: Courier Corporation.
12. Burchard, W., *Static and dynamic light scattering from branched polymers and biopolymers*, in *Light scattering from polymers*. 1983, Springer. p. 1-124.
13. Wu, C. and S. Zhou, *Laser Light Scattering Study of the Phase Transition of Poly(N-isopropylacrylamide) in Water. 1. Single Chain.* Macromolecules, 1995. **28**(24): p. 8381-8387.
14. Kwon, G.S. and K. Kataoka, *Block copolymer micelles as long-circulating drug vehicles.* Advanced Drug Delivery Reviews, 1995. **16**(2): p. 295-309.
15. Rossi, F., G. Perale, and M. Masi, *Device Design: Functional Polymers for Drug Delivery*, in *Controlled Drug Delivery Systems: Towards New Frontiers in Patient Care*. 2016, Springer International Publishing: Cham. p. 61-81.
16. Israelachvili, J.N., D.J. Mitchell, and B.W. Ninham, *Theory of self-assembly of hydrocarbon amphiphiles into micelles and bilayers.* Journal of the Chemical Society, Faraday

Transactions 2: Molecular and Chemical Physics, 1976. **72**(0): p. 1525-1568.

17. Riess, G., *Micellization of block copolymers.* Progress in Polymer Science, 2003. **28**(7): p. 1107-1170.
18. Winnik, F.M. and S.T.A. Regismond, *Fluorescence methods in the study of the interactions of surfactants with polymers.* Colloids and Surfaces A: Physicochemical and Engineering Aspects, 1996. **118**(1): p. 1-39.
19. Zipper, H., et al., *Investigations on DNA intercalation and surface binding by SYBR Green I, its structure determination and methodological implications.* Nucleic Acids Research, 2004. **32**(12): p. e103.
20. Sheiko, S.S., *Imaging of Polymers Using Scanning Force Microscopy: From Superstructures to Individual Molecules*, in *New Developments in Polymer Analytics II*, M. Schmidt, Editor. 2000, Springer Berlin Heidelberg: Berlin, Heidelberg. p. 61-174.
21. Ginzinger, D.G., *Gene quantification using real-time quantitative PCR.* Experimental Hematology, 2002. **30**(6): p. 503-512.
22. Albani, J.R., *Fluorescence spectroscopy principles.* Principles and Applications of Fluorescence Spectroscopy, 2008: p. 88-114.

3 Chapter 3. Polymer Bio-conjugates via the Grafting-from Strategy

Synopsis

In this chapter,carbodiimide coupling was used to prepare a RAFT ester agent, which was then amide coupled to an amine functionalised oligonucleotide by amide coupling. RAFT polymerisation of HEA in solution, using the bio-macro agent was performed to grow p(HEA) from the oligonucleotide. ^{1}H NMR spectroscopy and ESI-MS confirmed the synthesis of the RAFT ester agent. PAGE and MALDI-TOF spectroscopy monitored molecular weight changes of the biomolecule. ATR-FTIR spectroscopy was used to characterise the bio-conjugated products and UV-Vis spectroscopy confirmed the presence of the RAFT agent after polymerisation.

3.1 Chapter 3. Introduction

Biomolecules, can be turned into macro initiators by modifying them to contain functional groups that act as initiators [1]. The grafting from approach, results in polymer growing from the biomolecule and theoretically should lead to higher conjugation efficiencies as well as easier purification strategies [2]. Recently Li *et al.* [3] prepared temperature responsive block copolymers by grafting from a RAFT modified lysozyme. The group showed that the RAFT agent remained stable after polymerisation by chain extending the synthesised protein polymer conjugate to produce a protein block copolymer conjugate [3]. Averick *et al.* [4] have used ATRP in a water based media to grow polymers from bovine serum albumin (BSA). ATRP initiators were attached to BSA and then the oligo ethylene oxide methacrylate monomer was grown from the surface of the protein [4].

Few studies have looked at conjugating polymer to oligonucleotides using macro initiator oligonucleotides, Peng *et al.* [5] recently used RAFT polymerisation to grow poly(monomethoxy-capped oligo(ethylene glycol) methacrylate) from a RAFT functionalised oligonucleotide that was immobilised on a gold substrate. The group hypothesised that the accelerated polymer grafting from the surface that was observed resulted from the presence of DNA [5].

Grafting-from was investigated in this thesis as a method of producing polymer bio-conjugates by growing polymer from an oligonucleotide RAFT agent by polymerising a water-soluble monomer in aqueous solution. Solution based RAFT polymerisation using a RAFT bio-macro agent should be able to achieve greater yields of polymer bio-conjugates than surface attached RAFT bio-macro agents [2]. It was hypothesised that RAFT polymerisation of a RAFT bio-macro agent could produce polymer bio-conjugates and that the purification would be simpler and conjugation efficiency of these polymer bio-conjugates would be greater. In this chapter carbodiimide coupling was used to prepare a RAFT ester agent, which was then amide coupled to an amine functionalised oligonucleotide by amide coupling. Polymer bio-conjugates were then prepared through by RAFT polymerisation of HEA using the RAFT bio-macro agent. The bifunctional RAFT agent was chosen since it could be potentially modified with a temperature responsive block post polymerisation to produce a tri-block temperature responsive copolymer making it useful for drug delivery applications

.

3.2 Synthesis of RAFT Ester Agent

Scheme 3.1 shows the reaction pathway for the formation of the RAFT NHS ester agent (2), termed a RAFT ester agent. The bis (carboxymethyl) trithiocarbonate chain transfer agent (CTA 1) (1) was transformed into an activated ester via NHS/EDC coupling. The experimental details can be found in Chapter 2, Section 2.21. The product was obtained in 25% yield as a yellow powder.

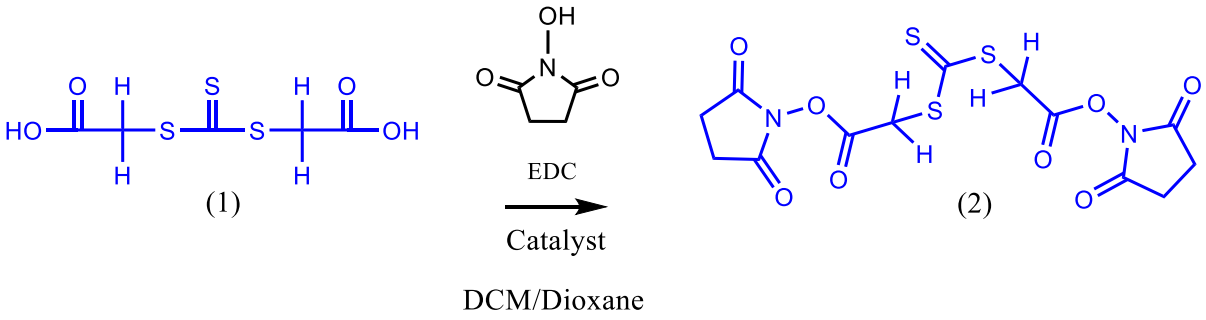

Scheme 3.1. Scheme of RAFT ester agent formation via NHS/EDC coupling.

^{1}H NMR spectroscopy was used to confirm the synthesised RAFT ester product (2). The spectrum (Figure 3.1 a) shows four peaks, two of which are associated with the symmetrical product (2) shown in Scheme 3.1. The singlet (peak a, in Figure 3.1) at 4.8 ppm represents the CH_2 group of (1), CTA 1. The singlet (peak b, in Figure 3.1) at 2.8 ppm represents the CH_2 groups from the activated NHS ester functionality. The peaks at 3.5 ppm and 2.5 ppm in Figure 3.1 represents water and the deuterated solvent DMSO-d6 and the peak at 3.6 ppm represents an impurity from the work up (acetic acid). Integration of the 4.8 ppm peak area and the 2.8 ppm peak area revealed a 1:2 ratio, consistent with expected structure shown in Figure 3.1, compound 2. When this product (2) was compared to the starting material (1) the OH peak from the carboxylic acid group was no longer present (data not shown).

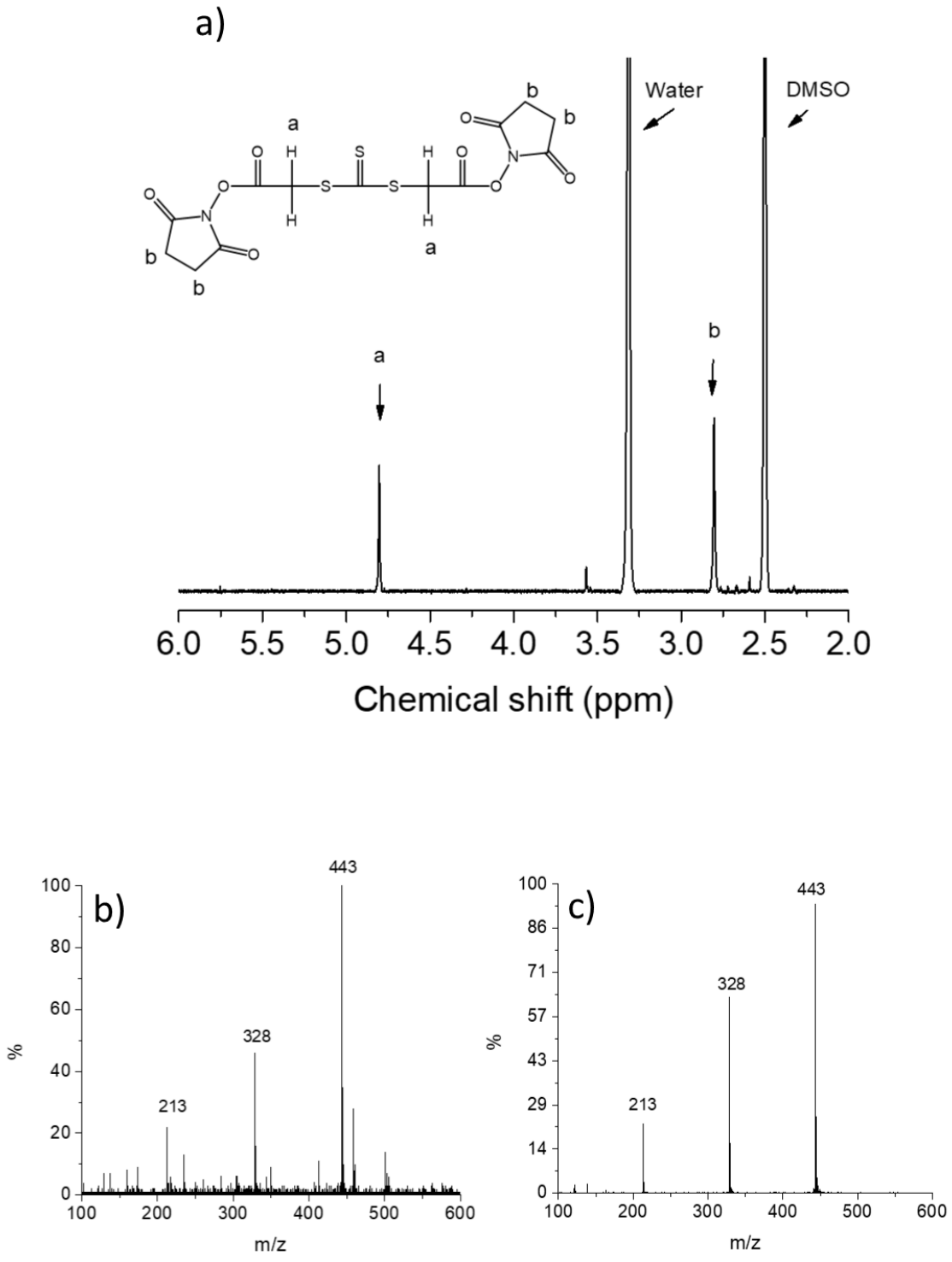

Figure 3.1. a) ^{1}H NMR spectrum of RAFT ester agent in DMSO-d6, 400 MHz, b) Positive ion, ESI mass spectrum of the RAFT ester agent and c) Positive ion, MS/MS of molecular ion peak 443 m/z.

Further confirmation of the successful synthesis of the RAFT ester agent was obtained through ESI mass spectrometry. Figure 3.1 b) shows the mass spectrum of the synthesised RAFT ester agent. The molecular ion peak observed at 443 m/z is attributed to the sodiated RAFT ester product $[C_{13}O_8S_3N_2H_{12}+Na]^+$. An additional peak at 328 m/z represents the RAFT ester product after the loss of one of the NHS groups and the peak at

213 m/z represents the RAFT ester agent after the loss of the second NHS group. Tandem mass spectrometry (MS/MS) of the molecular ion peak at 443 m/z (Figure 3.1 c) shows the fragments at 328 m/z and 213 m/z, which confirms the mass and identity of the RAFT ester agent.

3.3 Synthesis of RAFT Bio-Macro Agent

Scheme 3.2 shows the reaction pathway for the bio-conjugation of the RAFT ester agent (2) to 5'NH_2-C6-AGC-TTC-CCA-GTT-TAA-GCT-CTG-AT-3' (23 mer) (3) an amine terminated single stranded oligonucleotide (ss-DNA) to yield the RAFT bio-macro agent (4). (see Chapter 2, Section 2.2.2 to 2.2.3 for experimental details).

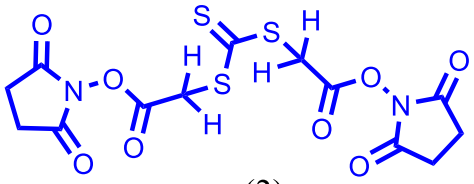

(2)

DMF/PBS buffer

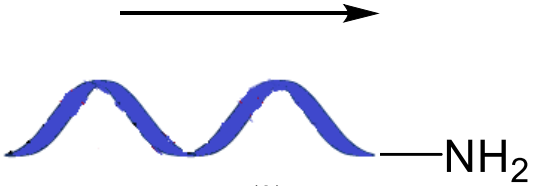

(3)

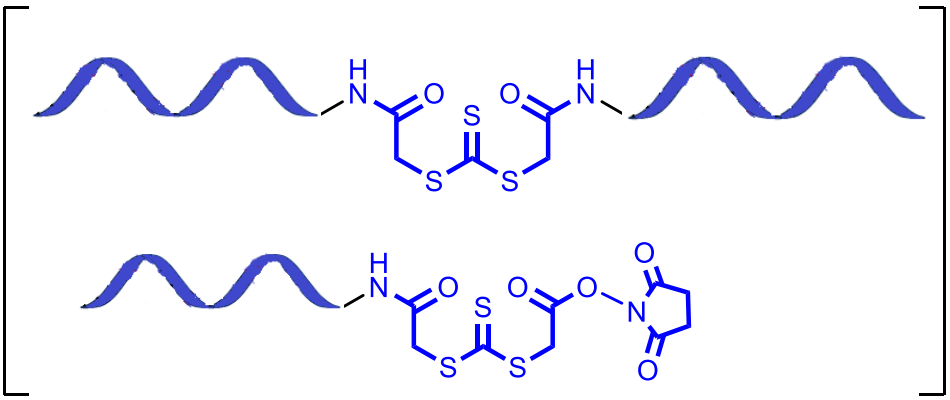

((4), Possible polymer bio-conjugate products)

Scheme 3.2. Scheme of the bio-conjugation reaction pathway using a 5' amine-ss-DNA (23 mer) and the synthesised RAFT ester agent to produce the RAFT bio-macro agent.

MALDI-TOF mass spectrometry was used to examine the possible polymer bio-conjugate products (4). Figure 3.2 is an example of the MALDI-TOF spectrum of the 23 mer ss-DNA (pre-reaction) and the 23 mer ss-DNA bio-conjugated RAFT agent, termed R-ssDNA (post reaction).A sharp peak at 7110 m/z is observed for the ss-

DNA (black, Figure 3.2), which was 58 Daltons less than the expected mass. The mass obtained by MALDI-TOF mass spectrometry may be due to partial loss of the C6-amine end group attached to the 5 'DNA strand. Figure 3.2 also shows a broad peak for R-ssDNA (blue) that ranges form 7110-8100 m/z for the bio-conjugated product. The temperature and the stoichiometry of the ss-DNA:RAFT ester ratios for the bio-conjugation protocol depicted in Figure 3.1, were varied to optimise the conjugation of the RAFT ester agent to ss-DNA. The MALDI-TOF spectra for the bio-conjugated products obtained from varying the bio-conjugation protocol (data not shown) did not vary from the broad peak observed in the R-ss-DNA spectrum shown in Figure 3.2 (blue).

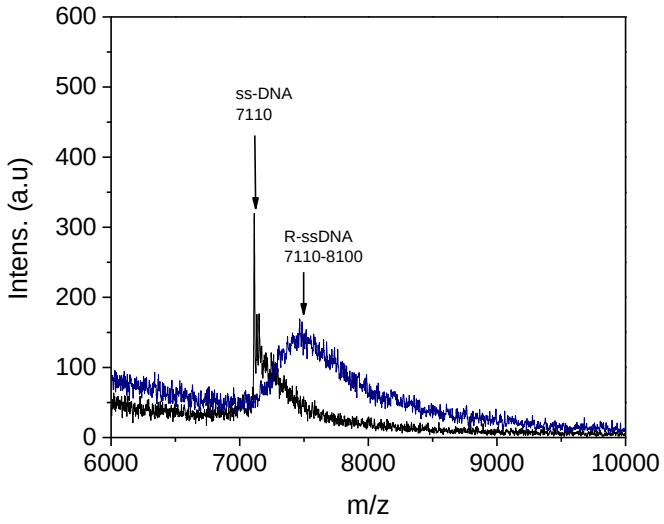

Figure 3.2. MALDI TOF mass spectra from left to right for 23 mer oligo (7110 m/z), R-ssDNA (7110-8100 m/z).

MALDI-TOF mass spectrometry could not determine what effect bio-conjugation reaction conditions had on conjugation efficiency. PAGE can be used to monitor the mass changes in oligonucleotides (oligo's). The oligo's migrate through the gel upon application of an electric field. The negatively charged backbone is attracted to the cathode and oligo's are separated through their electrophoretic mobility based on their length, charge and conformation. In general, shorter oligo's migrate faster than longer oligo's. Denaturing PAGE was used to analysis the bio-conjugation of ss-DNA and the RAFT ester agent.

Figure 3.3 a, b and c shows the d-PAGE gels that were obtained from the bio-conjugation protocol depicted in Figure 3.3 Looking from left right, in lane 1 (labelled DNA, Figure 3.3 a), the migration band of the 23 mer ss-DNA control through the d-PAGE gel is visualised after SG staining and exposure of the gel to UV light. In lane 2 and 3 the migration band of some MW standards (30 bases and 40 bases) are also seen.

Figure 3.3 a, (lane 4, 5 and 6) shows the migration bands of ss-DNA when bio-conjugation to the RAFT agent was performed at 50 ^{O}C and at a 1:1, 1:2 and 2:1 stoichiometric ratio. Figure 3.3. a, (lanes 4-8) showed that migration patterns of the ss-DNA used in the bio-conjugation protocol did not change when compared to the ss-DNA control visualised in lane 1, Figure 3.3 a). The temperature and stoichiometric changes to the bio-conjugation protocol (Figure 3.3 a, lane 4-8) showed no observable difference in the migration pattern of ss-DNA.

The d-PAGE gel depicted in Figure 3.3 b shows the migration band of the 23 mer ss-DNA control in lane 1 and the MW standards migration bands in lane 2 and 3. Lane 4, Figure 3.3 b, shows the migration band of the ss-DNA when the temperature of the bio-conjugation protocol was 60 ^{O}C and the ss-DNA: RAFT ester agent ratio was 2:1. The temperature and stoichiometric changes to the bio-conjugation protocol (Figure 3.3 b, lane 4-7) showed no observable difference in the migration pattern of ss-DNA.

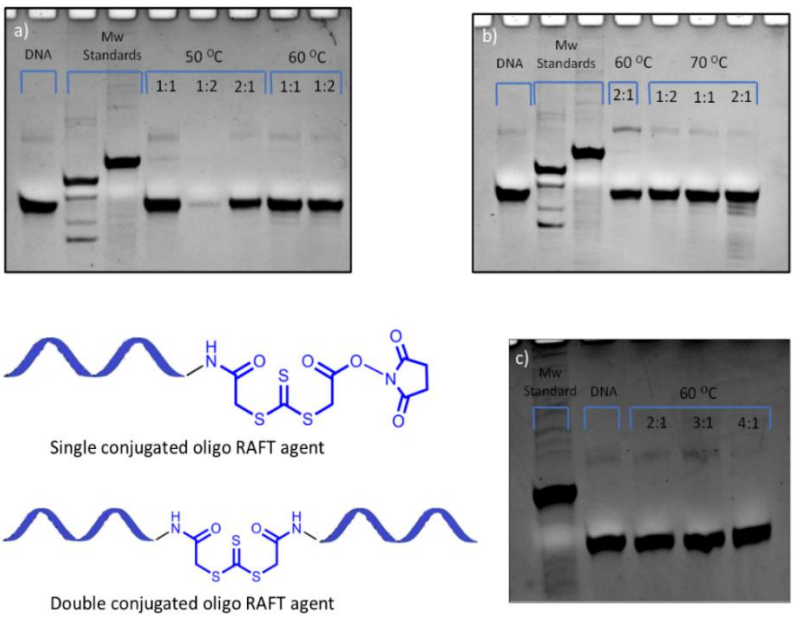

Figure 3.3. a) ss-DNA (23 mer, lane 1), MW standards (lane 2 and 3), 50 ^{O}C protocol, stoichiometric ratios 1:1, 1:2 and 2:1 (lane 4, 5 and 6), 60 ^{O}C protocol, stoichiometric ratios 1:1, and 1:2 (lane 7, and 8), b) ss-DNA (23 mer, lane 1), MW standards (lane 2 and 3), 60 ^{O}C protocol, stoichiometric ratios 2:1 (lane 4), 70 ^{O}C protocol, stoichiometric ratios 1:2, 1:1 and 2:1 (lane 5, 6 and 7),c), MW standards (lane 1), ss-DNA (23 mer, lane2), 60 ^{O}C protocol, stoichiometric ratios 2:1, 3:1 and 4:1 (lane 3, 4 and 5).

Figure 3.3 c, shows the MW standard migration band in lane 1 and the 23 mer ss-DNA control migration bands in lane 2. Lane 3, 4 and 5. Figure 3.3 c, shows the migration band of ss-DNA when the bio-conjugation protocol was 60 ^{O}C and the stoichiometric ratios for ss-DNA: RAFT ester agent were 2:1, 3:1 and 4:1 respectively. Again, there was no observable difference in the migration pattern of the bio-conjugated ss-DNA (lane 3, 4 and 5) and the ss-DNA control (lane 2).

It is clear from the d-PAGE results that there was no change in the migration pattern of ss-DNA after it was bio-conjugated to the RAFT ester agent. The results also suggest that the double conjugated product, depicted in Figure 3.3 a is not a product of the reaction between the 5' amine terminated ss-DNA and the RAFT ester agent. It is hypothesised that the oligo that is attached is inhibiting the second attachment either sterically or through non specific interaction with the incoming oligo, this hypothesis could be potentially explored in future work. The d-PAGE results could not distinguish whether increasing temperature or changing stoichiometry changed the bio-conjugation efficacy. The results from MALDI-TOF mass spectrometry indicated that the molecular weight of the ss-DNA changed from 7100 m/z to a broad distribution of masses that ranged from 7100 m/z to 8100 m/z, the bio-conjugated R-ssDNA was tested for its efficacy as a RAFT bio-macro agent in the RAFT polymerisation of HEA monomer.

3.4 RAFT Polymerisation Using RAFT Bio-Macro Agent

Scheme 3.3 shows the reaction scheme for the RAFT polymerisation of HEA (5) using the RAFT bio-macro agent (R-ssDNA, (4)) to produce p(HEA)-ssDNA bio-conjugates (6). See Chapter 2, Section 2.2.5 for experimental details. The RAFT polymerisation of HEA using the R-ssDNA bio-macro agent was performed at high monomer (HEA) to initiator mol ratios since synthesis of large quantities of the R-ssDNA bio-macro agent was prohibited by cost. It has been shown in the literature that when performing RAFT polymerisation with a bio-macro agent that greater control over the polymerisation can be achieved, if the radical concentration is kept low [5].

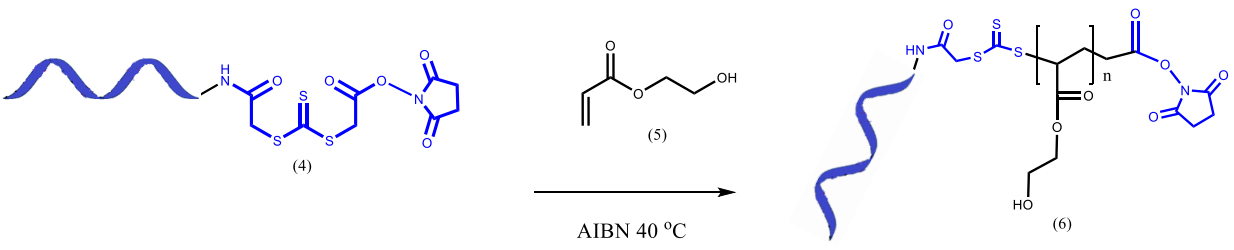

Scheme 3.3. Scheme for RAFT polymerisation of HEA using the RAFT bio-macro agent (R-ssDNA) to produce the p(HEA)-ssDNA bio-conjugate.

The RAFT polymerisation of HEA was performed at a low temperature in a water solvent to control the concentration of radicals generated from the decomposition of AIBN. The half-life of AIBN was calculated to be approximately 10 days when the temperature of polymerisation was maintained at 40 ^{O}C. The RAFT

polymerisation was performed over several days, the p(HEA)-ssDNA bio-conjugate precipitated in a cold 2% sodium perchlorate acetone solution. MALDI-TOF mass spectrometry was used to calculate the molecular weight of the precipitated product. The mass spectrum (Figure 3.4, labelled DNA) showed a sharp molecular ion peak at 7110 m/z for the 23 mer oligo. The broad peak labelled R-ssDNA represents the RAFT bio-macro agent and the peaks labelled P-DNA_2 and P-DNA_3 and P-DNA_7 are the p(HEA)-ssDNA bio-conjugate product recovered after two, three and seven days of polymerisation respectively.

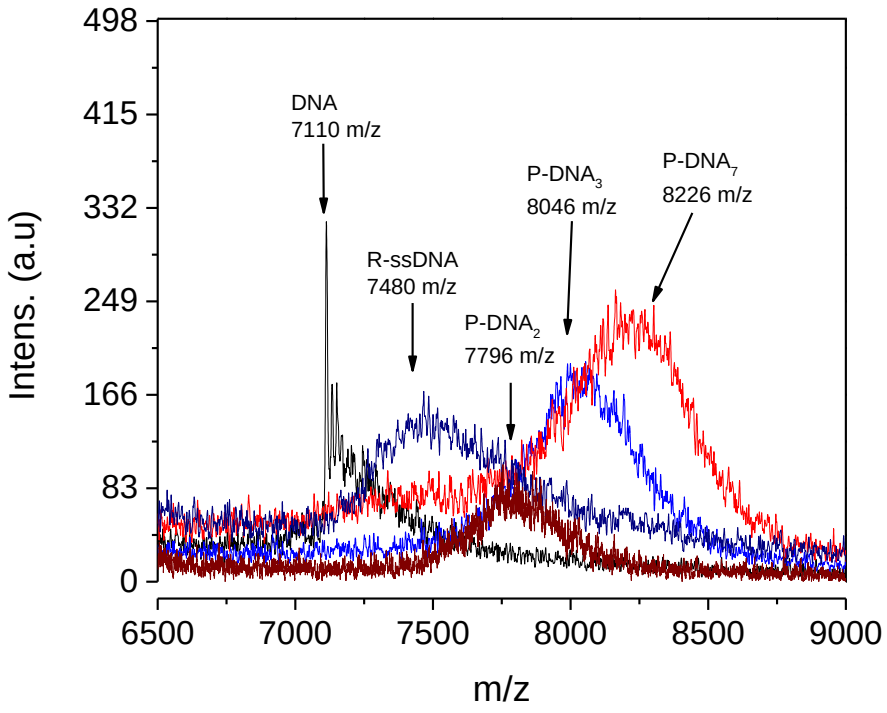

Figure 3.4. MALDI TOF mass spectra from left to right for 23 mer oligo (7110 m/z), R-ssDNA (7480 m/z), P-DNA_2 (7796 m/z), P-DNA_3 (8046 m/z) and P-DNA_7 (8226 m/z).

The R-ssDNA broad peak has a peak max at approximately 7400 m/z (Figure 3.4). After RAFT polymerisation was performed for two days, the recovered product, P-DNA_2, showed a shift to a higher molecular weight, with a peak max at approximately 7796 m/z. After 3 days of polymerisation, the recovered product, P-DNA_3, when analysed by MALDI-TOF mass spectrometry, produced a broad peak with a peak max at 8046 m/z. After 7 days of polymerisation the recovered product, P-DNA_7, when analysed by MALDI-TOF mass spectrometry, produced a much broader peak with a peak max at 8226 m/z. MALDI-TOF mass spectrometry showed that the ss-DNA (23 mer) biomolecule, increased in mass after bio-conjugation and that the subsequent RAFT polymerisation of HEA with the bio-macro agent led to further increases in molecular weight. The results suggested that p(HEA) was grown from the oligonucleotide but growth was limited and slow. The molecular weight of the synthesised bio-macro agent after RAFT polymerisation was also investigated using PAGE. The d-PAGE gel depicted in Figure 3.5 a, shows the migration band of a 10/60 base DNA ladder and the 23 mer ss-DNA control in lane 1 and 2 respectively. The DNA ladder allows for the direct comparison of expected and

actual DNA migration of a known molecular weight. The migration of the ss-DNA control was consistent with the migration of a 23 mer ss-DNA as shown by the DNA reference ladder. Lane 3, (Figure 3.5 a, labelled Day 1), shows the migration of the polymer bio-conjugate (P-DNA_1) after 1 day of polymerisation of HEA using the RAFT bio-macro agent R-ssDNA. The migration of P-DNA_1 was found to have changed relative to the ss-DNA control in Lane 2 and using the DNA ladder as reference, P-DNA_1 was found to migrate through the gel consistent with a 25 mer DNA. The gel results (Figure 3.5 a) indicate that P-DNA_1 had increased in molecular weight. The increase found by d-PAGE analysis was equivalent to 600 Daltons. When the polymerisation of p(HEA) had proceeded for 2 days, d-PAGE analysis (Figure 3.5 a, labelled Day 2) showed that the migration of the polymer bio-conjugate (P-DNA_2) changed relative to the ss-DNA control and P-DNA_1. The reference DNA ladder indicated that the P-DNA_2 migrated through the gel equivalent to a 26 mer DNA, representing an increase of 900 Da when compared to the ss-DNA control.

The polymerisation of HEA using the R-ssDNA agent was continued for seven days and the products recovered on day 3 and day 7 were also analysed using d-PAGE. Figure 3.5 b shows the migration band of a 10/60 base DNA ladder and the 23 mer ss-DNA control in lane 1 and 2, respectively. Lane 3 and 4 (Figure 3.5 b, labelled Day 1 and Day 2) represent the migration of P-DNA_1 and P-DNA_2, respectively. Multiple bands which smeared and spread out in the gel in lane 5 (Figure 3.5 b, labelled day 3) represent the migration of the polymer bio-conjugate P-DNA_3. After 3 days of polymerisation the MW of P-DNA_3 based on the highest visible band was observed to increase relative to the original ss-DNA control; with the DNA reference ladder indicating that the increase was approximately 1200 Da. Multiple bands representing the polymer bio-conjugate (P-DNA_7) recovered after 7 days of polymerisation are observed in lane 6 (Figure 3.5 b, labelled Day 7). Smeared bands are observed and the migration of the highest band increased relative to the ss-DNA control, P-DNA_1, P-DNA_2 and P-DNA_3. The DNA reference ladder indicated that P-DNA_7 had an increase in MW of approximately 1500 Da. The MW of the HEA monomer is 110 Daltons. The gel results indicate that p(HEA) growth from the bio-macro agent progressed from 6 monomer units after 1 day of polymerisation to 15 monomer units after 7 days of polymerisation. The estimated MW for polymer bio-conjugates (P-DNA_1-P-DNA_7) found through d-PAGE analysis are in close agreement with molecular weight results found by MALDI-TOF mass spectrometry. The growth of polymer from the bio-macro agent appeared to slow down as the polymerisation progressed and overall growth of polymer from the biomolecule was limited. The slow growth of the polymer is thought to be due to the availability of radicals over the seven days of polymerisation. Since the growth of polymer is very limited it is also difficult to classify the synthesised product as a “polymer” bio-conjugate

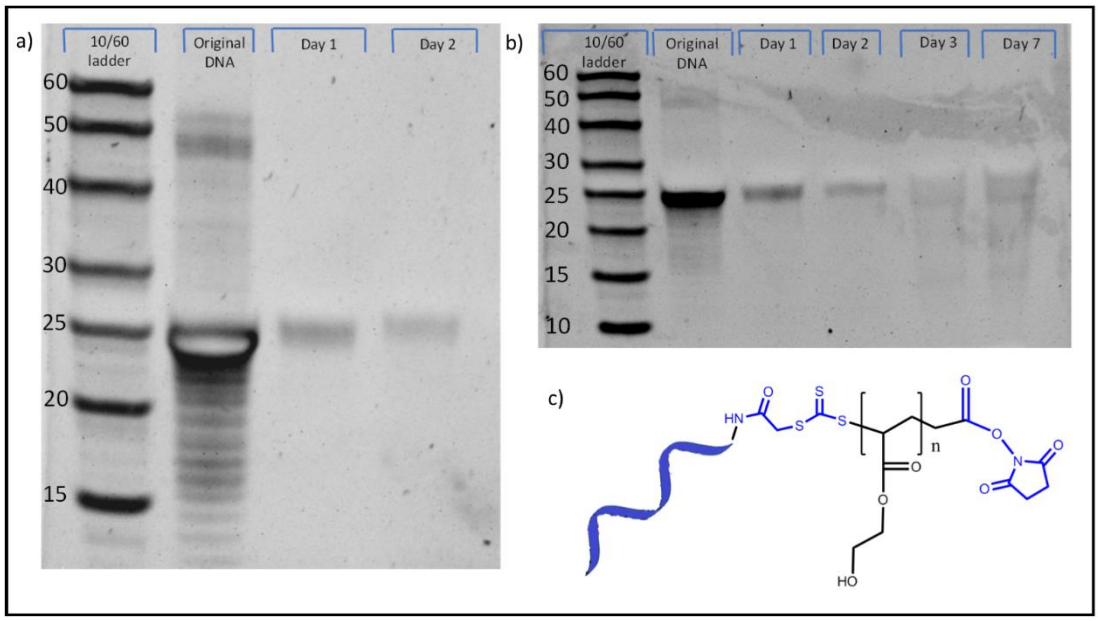

Figure 3.5. Denaturing polyacrylamide gel electrophoresis (d-PAGE) from left to right: a) DNA ladder 10/60 bases (lane 1), original ss-DNA 23 mer (lane 2), p(HEA)-ssDNA bio-conjugate after 1 day (lane 3) and 2 days (lane 4) of polymerisation of HEA using RAFT bio-macro agent, b) DNA ladder 10/60 bases (lane 1), original ss-DNA 23 bases (lane 2) and p(HEA)-ssDNA bio-conjugate after 1 day (lane 3), 2 day (lane 4), 3 day (lane 5) and 7 days (lane 6) of polymerisation of HEA using RAFT bio-macro agent. c) Proposed polymer bio-conjugate structure.

Figure 3.6 a, shows the ATR-FTIR spectrum for the 23 mer ss-DNA, in the high frequency part of the spectrum, peaks associated with amide are observed for the N-H symmetric stretch at around 3374 cm^{-1} and 3173 cm^{-1} [6]. In the low frequency region, the bands around 1643 cm^{-1} and at 1550 cm^{-1} represent the amide I carbonyl and the amide II N-H bend of the amide band [7]. The bands observed between 1500 cm^{-1} and 1250 cm^{-1} represent the base and sugar moieties. The antisymmetric PO_2 stretch is observed at 1213 cm^{-1} and the symmetric PO_2 is observed around 1053 cm^{-1} [7]. The ATR-FTIR spectrum of HEA is shown in Figure 3.6 b, where stretching due to the hydroxyl functional group is observed at 3431 cm^{-1} and from the aliphatic groups (C-H stretching) observed around 2900 cm^{-1}. The carbonyl stretch for HEA is also observed at 1724 cm^{-1}. Figure 3.6 c and d show the ATR-FTIR spectra for the polymer bio-conjugates P-DNA_1, P-DNA_2, P-DNA_3 and P-DNA_7 before (Figure 3.6 c) and after (Figure 3.6 d) freeze drying. The same absorbance for all spectra are observed at 3443 cm^{-1} which is characteristic of the hydroxyl functionality from p(HEA). The N-H symmetric stretch at 3374 cm^{-1} and 3173 cm^{-1} is indicative of the ss-DNA. An absorbance at 3083 cm^{-1} (Figure 3.6 c) is indicative of the aliphatic C-H stretch from HEA. Another peak is also observed at 2353 cm^{-1} due to harmonic overtones from N-H stretches [8]. Figure 3.6 c and d also have bands around 1653 cm^{-1} representing the amide I carbonyl stretch; this band is red shifted relative to the ss-DNA spectrum shown in Figure 9 a. The bands at 1500 cm^{-1} to 1250 cm^{-1} that were seen in Figure 3.6 a representing the base and sugar moieties of the ss-DNA are not observed in Figure 3.6 c and d for the polymer bio-conjugates. The antisymmetric PO_2 stretch for P-DNA_1 to P-DNA_7 is observed at 1254 cm^{-1} (Figure 3.6 c and d) and the symmetric PO_2 is observed around 1047 cm^{-1} (Figure 3.6 c and d) [9].

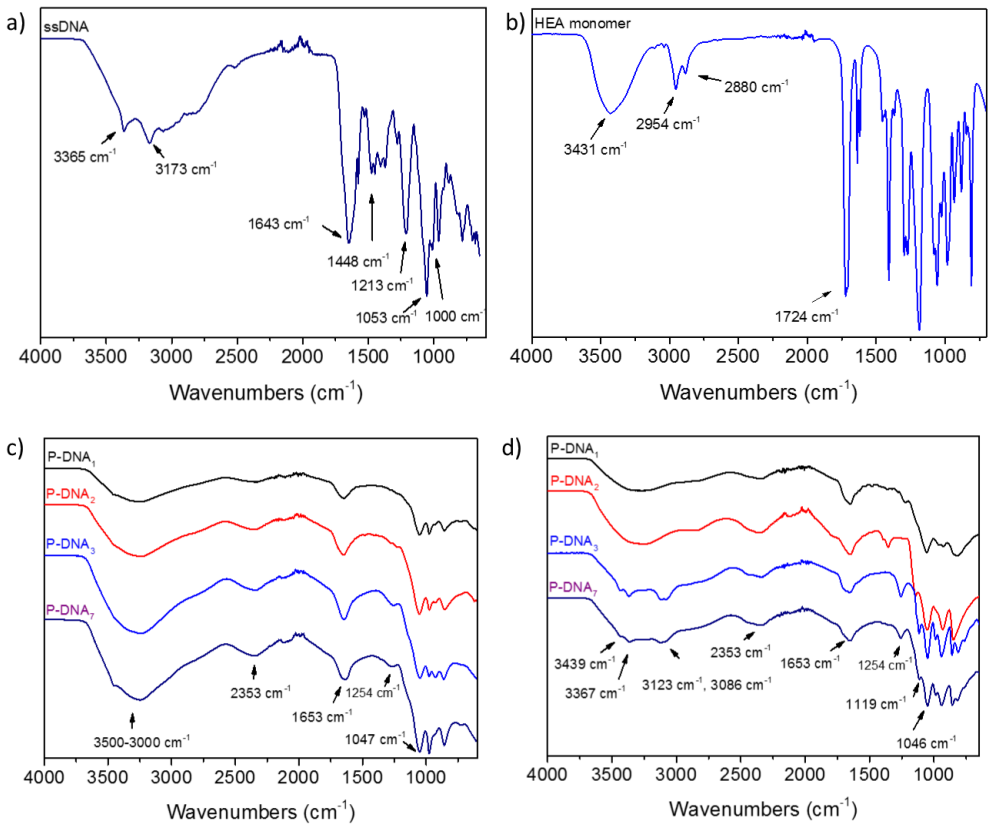

Figure 3.6. a) ATR-FTIR spectra for ss-DNA (23 mer), b) HEA monmer, c) p(HEA)-ssDNA bio-conjugates (P-DNA$_1$-P-DNA$_7$) and d) freeze dried p(HEA)-ssDNA bio-conjugates (P-DNA$_1$-P-DNA$_7$).

The results from ATR-FTIR analysis suggest that the polymerisation of HEA using the RAFT bio-macro agent appears to have influenced the ss-DNA phosphate sugar backbone. Infra-red spectroscopic studies have revealed that the antisymmetric stretch (PO_2) of calf thymus DNA, blue shifts when water is removed and the PO_2 group is then no longer hydrogen bonded to water [8].

The ATR-FTIR spectra for the polymer bio-conjugates (P-DNA$_1$-PDNA$_7$) before (Figure 3.6 c) and after (Figure 3.6 d) freeze drying showed no blue shift. There is however, a blue shift in the antisymmetric PO_2 stretch for the p(HEA)-ss bio-conjugates (P-DNA$_1$-P-DNA$_7$) to 1254 cm^{-1} (Figure 3.6 c and d) from 1213 cm^{-1} the ss-DNA control (Figure 3.6 a). The symmetric PO_2 stretch is also observed to decrease in intensity and blue shift to 1119 cm^{-1} for the p(HEA)-ssDNA bio-conjugates from 1053 cm^{-1} (Figure 3.6 a, ss-DNA control). Carbon disulphide under different synthetic conditions has been used in the literature for the synthesis of phosphorothioates to produce anti-sense DNA [10]. Unwanted side reactions during polymerisation may involve the exchange of oxygen on the phosphate backbone. Although this is a possible explanation for the blue shift in the antisymmetric PO_2 stretch and the symmetric PO_2 stretch, this theory would require further investigation beyond the scope of this thesis [11, 12]. The heterocyclic bases of DNA (Figure 3.7 a, inset) are aromatic and absorb in the ultraviolet region of the electromagnetic spectrum at a wavelength max of approximately 260 nm; using the beer lambert law, the concentration of DNA can be measured by the

absorbance of DNA at 260 nm [13]. RAFT agents comprised of trithiocarbonate groups (Figure 3.7 b, inset) absorb strongly in the near UV range (~ 300 nm) due to an allowed $\pi - \pi^*$ transition, making it essentially a chromophore label, useful for characterising RAFT polymerisation [14]. Figure 3.7 a, shows the absorbance of the 23 mer ss-DNA in the UV region, the absorbance max is observed at approximately 260 nm. Figure 3.7 b shows the absorbance of the synthesised trithiocarbonate RAFT ester agent used in the bio-conjugation experiments, the absorbance max is observed at approximately 300 nm.

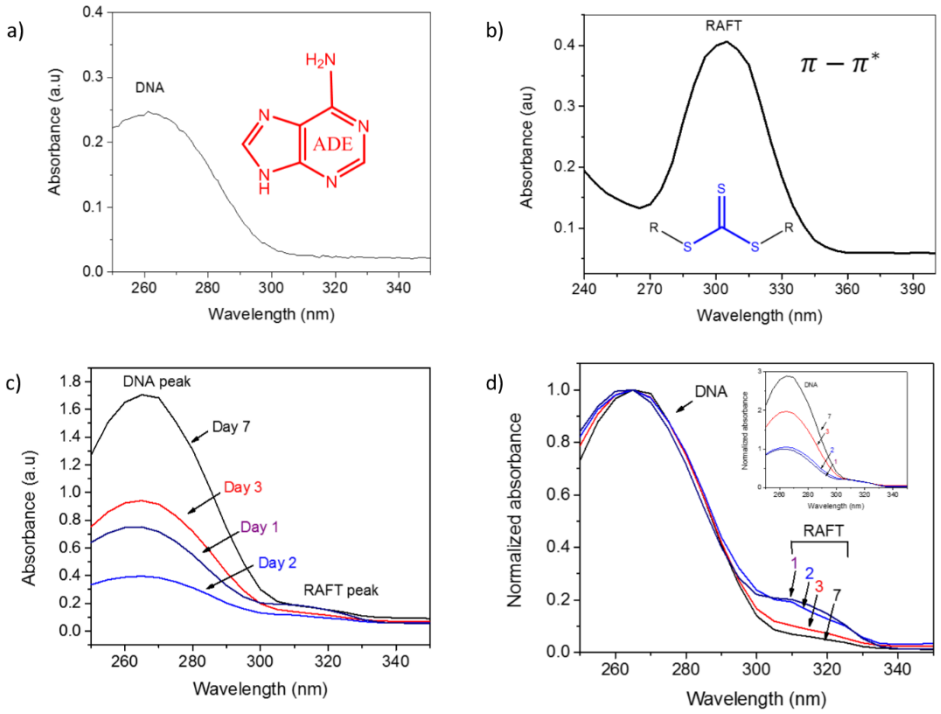

Figure 3.7. a) UV-Vis spectrum of ss-DNA (23 mer) in the near UV range, b) UV-Vis spectrum of RAFT ester agent (near UV range), c) UV-Vis spectra p(HEA)-ssDNA bio-conjugates (P-DNA$_1$-PDNA$_7$), and d) normalised UV-Vis Spectra (near UV range) p(HEA)-ssDNA bio-conjugates (P-DNA$_1$-PDNA$_7$).

The absorbance in the UV range for the isolated polymer bio-conjugated products (P-DNA$_1$-P-DNA$_7$) is shown in Figure 3.7 c. The DNA peak at 260 nm is observed and the absorbance at 260 nm increased with days of polymerisation, except for day 2. The absorbance of ss-DNA measured by UV-Vis before (not shown) and after polymerisation (Figure 3.7 c) varied with respect to the starting concentration. The change in concentration of ss-DNA after polymerisation was first thought to be due to loss of product due to the work-up procedure. The trithiocarbonate peak (~300 nm) is also observed in the normalised absorbance spectra (Figure 3.7 d), the peak is observed to decrease with days of polymerisation. The DNA peak at 260 nm is observed in the normalised spectra (Figure 3.7 d) and the measured absorbance at 260 nm increased with days of polymerisation.

Since the RAFT agent is conjugated to the ss-DNA, it was expected that the absorbance of DNA at 260 nm and the RAFT agent's absorbance at 300 nm should remain the same. It is theorised that the increase in absorbance at 260 nm is due to the growth of p(HEA), but it may also be due to the degradation of DNA. If the change in absorbance was merely due to concentration differences then it would be expected that the d-PAGE gel results shown in Figure 3.5 b) for P-DNA_7 would be a strong intense band, since the highest absorbance at 260 nm was observed for P-DNA_7 (Figure 3.7 c). Instead the observed band for P-DNA_7 is the faintest and DNA bands are observed further down the gel, which could be the degradation products. These degradation products were only observed in gels after 3 days of polymerisation, therefore new experiments were employed to try to increase polymer growth but limit the polymerisation time.

3.5 RAFT Polymerisation Using RAFT Bio-Macro Agent (Lower Concentration of Monomer Method)

The RAFT polymerisation of HEA using the R-ssDNA agent was initially performed at high monomer (HEA) to initiator mol ratios, the results showed slow polymer growth over several days. The low yield and length of time required to grow p(HEA) may be due to the initiator depletion as well as uncontrolled side reactions. Instead of performing the polymerising HEA at high monomer concentrations the RAFT polymerisation of HEA using the bio-macro agent was performed at low monomer concentrations. See Chapter 2, Section 2.2.6 for experimental details. Figure 3.8 shows the MALDI-TOF mass spectra for ss-DNA (black, 7166 m/z), the bio-macro agent R-ssDNA (red, 7315 m/z) and the product of 1 day of polymerisation P-DNA_1 (blue, 7449 m/z). The bio-macro agent product and the polymer bio-conjugate show an increase in MW of approximately 300 and 400 Da respectively. Figure 3.8, low monomer concentration also showed a slow increase in p(HEA) growth when the polymerisation is performed at low monomer concentrations. To increase the growth of p(HEA), additional monomer and HEA were added to the polymerisation as it proceeded.

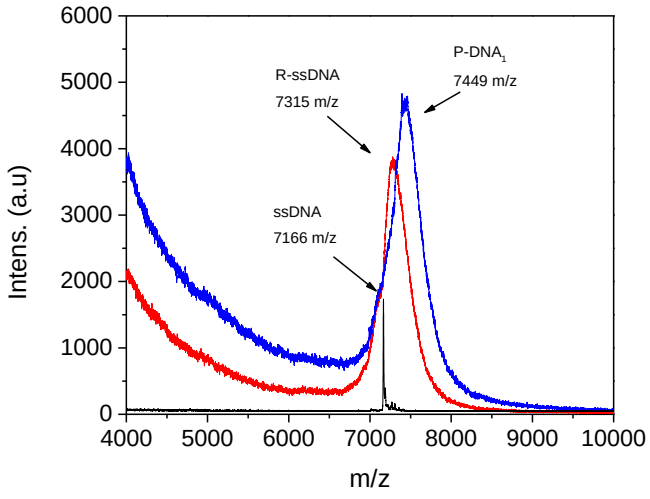

Figure 3.8. MALDI-TOF mass spectra for ss-DNA (7166 m/z), R-ssDNA (7315 m/z) and P-DNA1 (7449 m/z).

3.6 RAFT Polymerisation Using RAFT Bio-Macro Agent (Stepwise Addition method)

The RAFT polymerisation of HEA using the RAFT bio-macro agent was performed at low monomer concentrations and more monomer and initiator were added during the polymerisation. See Chapter 2, Section 2.2.7 for experimental details.

Figure 3.9 a, b shows the MALDI-TOF mass spectra for the RAFT polymerisation of HEA using the RAFT bio-macro agent over 2 days. The peak in black at 7443 m/z (Figure 3.9 a, labelled P-DNA$_1$) is the mass spectrum for the polymer bio-conjugate product isolated after one day of RAFT polymerisation. Monomer and initiator was added to the polymerisation reaction vial after 24 h. The peak in red at 7451 m/z is from the polymer bio-conjugate product (Figure 3.9 a, labelled P-DNA$_2$) isolated after the addition of more monomer and initiator, recovered after 27 h. There appears to be no significant difference in the MW found by MALDI-TOF for the P-DNA$_1$ or P-DNA$_2$. The blue peak at 7732 m/z (Figure 3.9 a, labelled P-DNA$_3$) represents the polymer bio-conjugate isolated after 48 h of RAFT polymerisation. The change in molecular weight for P-DNA$_3$ after the addition of monomer was approximately 300 Da. Interestingly a comparison of the mass spectrum shown in Figure 3.4 for P-DNA$_2$ (high monomer concentration) and for P-DNA$_2$ (Figure 3.9, low monomer concentration) reveals a slower increase in p(HEA) growth when the polymerisation is performed at low monomer concentrations.

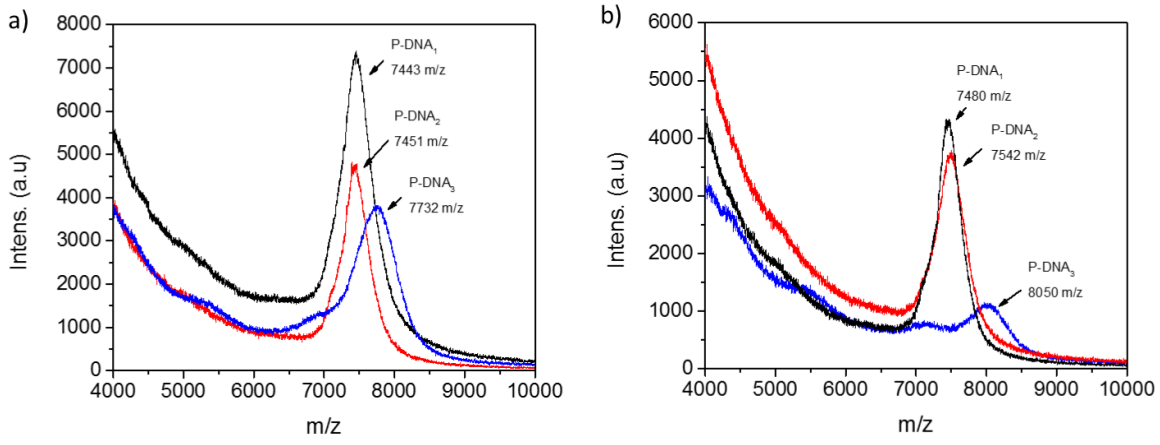

Figure 3.9. a) MALDI-TOF mass spectra for P-DNA$_1$ (24 h), P-DNA$_2$ (27 h) and P-DNA$_3$ (48 h) and b) P-DNA$_1$ (24 h), P-DNA$_2$ (27 h) and P-DNA$_3$ (48 h).

The RAFT polymerisation of HEA was repeated under the same conditions (stepwise addition) and the products are shown in Figure 3.9 b. The MALDI-TOF mass spectra for the polymer bio-conjugates isolated at 24 h (P-DNA$_1$), 27 h (P-DNA$_2$), and 48 h (P-DNA$_3$) showed molecular weights of 7480, m/z, 7542 m/z and 8050 m/z, respectively. The blue peaks (Figure 3.9 a, b, P-DNA$_3$) are significantly broader and have multiple peaks. Which may be due to addition of more monomer and initiator leading to a loss of control over the

polymerisation and degradation of ss-DNA. The results shown in Figure 3.9 b suggest that the RAFT polymerisation of HEA is repeatable using the RAFT bio-macro agent, however the growth of p(HEA) remains slow when the monomer and initiator is added stepwise. The stepwise, low monomer concentration method was not shown to speed up polymer growth of p(HEA) relative to the high monomer concentration method.PAGE was also used to monitor the change in the molecular weight of the stepwise RAFT polymerisation of HEA using the bio-macro agent (Figure 3.10).

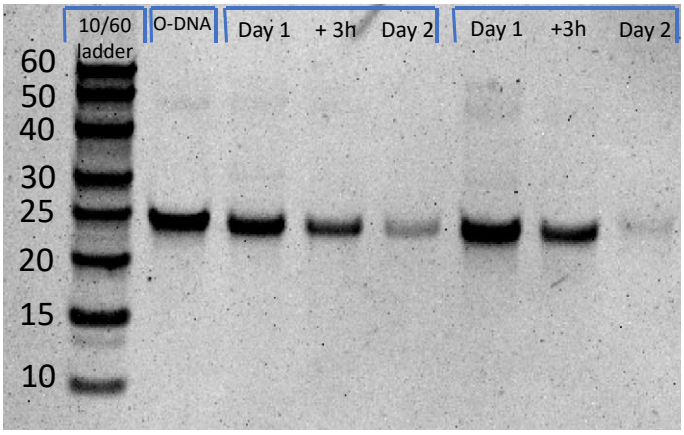

Figure 3.10. Denaturing polyacrylamide gel electrophoresis (d-PAGE) from left to right: DNA ladder 10/60 bases (lane 1), original ss-DNA 23 mer (lane 2), p(HEA)-ssDNA bio-conjugate after 1 day (lane 3), day 1 + 3 h (lane 4), 2 days (lane 5), 1 day (lane 6), 1 day + 3 h (lane 7) and 2 days (lane 8) of polymerisation.

The d-PAGE gel depicted in Figure 3.10 shows the migration band of a 10/60 base DNA ladder and the 23 mer ss-DNA control in lane 1 and 2 respectively. Lane 3 and 6, (Figure 3.10, labelled day 1) represent the migration of the polymer bio-conjugate (P-DNA_1) after 1 day of polymerisation. The migration of P-DNA_1 appears to have migrated faster than the ss-DNA control. Lane 4 and 7 (Figure 3.10, labelled + 3 h) showed no change in the migration for the polymer bio-conjugate (P-DNA_2) compared to P-DNA_1. Lane 5 and 8 (Figure 3.10, labelled day 2) show the migration of the polymer bio-conjugate P-DNA_3. The product (P-DNA_3) does appear to migrate faster through the gel. The gel results suggest that lower molecular weight products are forming during the polymerisation, which may explain the multiple peaks observed in the MALDI-TOF mass spectra for P-DNA_3 (Figure 3.9 a and b). The results indicate that the addition of more monomer and initiator led to a degradation of the ss-DNA, possibly due to an increase in the radical concentration.

3.7 Conclusions

^{1}H NMR spectroscopy and mass spectrometry results confirmed the synthesis of the RAFT ester agent. The bio-conjugation of a RAFT ester agent to an oligonucleotide via amide coupling was confirmed by MALDI-TOF-MS. The mass spectrum of the RAFT bio-macro agent increased after conjugation to the RAFT ester agent. The results from the RAFT polymerisation of HEA using the RAFT bio-macro agent (High concentration monomer method) indicated that p(HEA) growth from the bio-macro agent progressed from 6 monomer units after 1 day of polymerisation to 15 monomer units after 7 days of polymerisation. The estimated MW for polymer bio-conjugates (P-DNA$_1$-P-DNA$_7$) found through d-PAGE analysis were in close agreement with MW results found by MALDI-TOF mass spectrometry. Also, the low radical concentration of radicals due to the long reaction times led to very slow polymer growth which makes it difficult to conclude that these products are “polymer” bio-conjugates. When RAFT polymerisation using the RAFT bio-macro agent was performed at low monomer concentration a slower increase in p(HEA) growth was observed. When radicals were increased via the stepwise addition method, degradation of the DNA was observed. The MALDI-TOF and PAGE results indicated that growth from the RAFT bio-macro agent occurs and therefore bio-conjugates can be prepared by the grafting-from method. However, polymer growth from the RAFT bio-macro agent was slow and the data suggests that DNA may in fact be degraded during RAFT polymerisation. Given these results, an alternative strategy (grafting-to) to produce polymer bio-conjugates was used in the proceeding Chapters.

3.8 References

1. Liu, J., et al., *In situ formation of protein–polymer conjugates through reversible addition fragmentation chain transfer polymerization.* Angewandte Chemie International Edition, 2007. **46**(17): p. 3099-3103.
2. Sumerlin, B.S., *Proteins as Initiators of Controlled Radical Polymerization: Grafting-from via ATRP and RAFT.* ACS Macro Letters, 2011. **1**(1): p. 141-145.
3. Li, H., et al., *Block copolymer conjugates prepared by sequentially grafting from proteinsvia RAFT.* Polymer Chemistry, 2011. **2**(7): p. 1531-1535.
4. Averick, S., et al., *ATRP under Biologically Relevant Conditions: Grafting from a Protein.* ACS Macro Letters, 2012. **1**(1): p. 6-10.
5. He, P. and L. He, *Synthesis of Surface-Anchored DNA−Polymer Bioconjugates Using Reversible Addition−Fragmentation Chain Transfer Polymerization.* Biomacromolecules, 2009. **10**(7): p. 1804-1809.
6. Banyay, M., M. Sarkar, and A. Gräslund, *A library of IR bands of nucleic acids in solution.* Biophysical Chemistry, 2003. **104**(2): p. 477-488.
7. Taillandier, E. and J. Liquier, *[16] Infrared spectroscopy of DNA*, in *Methods in Enzymology*. 1992, Academic Press. p. 307-335.
8. Tsuboi, M., *Application of infrared spectroscopy to structure studies of nucleic acids.* Applied spectroscopy reviews, 1970. **3**(1): p. 45-90.
9. Bonilla, J.V. and G.S. Srivatsa, *Handbook of analysis of oligonucleotides and related products*. 2011: CRC Press.
10. Agrawal, S., et al., *Inhibition of human immunodeficiency virus in early infected and chronically infected cells by antisense oligodeoxynucleotides and their phosphorothioate analogues.* Proceedings of the National Academy of Sciences, 1989. **86**(20): p. 7790-7794.
11. Coates, J., *Interpretation of infrared spectra, a practical approach.* Encyclopedia of analytical chemistry, 2000.
12. Frey, P. and R. Sammons, *Bond order and charge localization in nucleoside phosphorothioates.* Science, 1985. **228**(4699): p. 541-545.
13. Cadet, J., E. Sage, and T. Douki, *Ultraviolet radiation-mediated damage to cellular DNA.* Mutation Research/Fundamental and Molecular Mechanisms of Mutagenesis, 2005. **571**(1–2): p. 3-17.
14. Skrabania, K., et al., *Examining the UV-vis absorption of RAFT chain transfer agents and their use for polymer analysis.* Polymer Chemistry, 2011. **2**(9): p. 2074-2083.

4 Chapter 4. Grafting-to: Synthesis of Temperature Responsive PNIPAAm Copolymers and their Solution Properties

Synopsis

Stimuli responsive polymeric micelles that can potentially deliver drug, or gene, therapy payloads were fabricated by copolymerising a temperature responsive monomer *N*-isopropyl acrylamide (NIPAAm) and an *N*-hydroxyl methyl acrylamide (HMAAm) monomer. the HMAAm content of the synthesised copolymers was varied to tune the temperature response of the resulting copolymers. The LCST, CMC, hydrodynamic size and particle size of polymeric micelles composed of pNIPAAm-*co*-HMAAm copolymers were investigated.

4.1 Chapter 4. Introduction

Delivery of therapeutic drugs for solid tumours remains a challenge; due to a variety of complex problems which include stable circulation, reduced elimination, toxicity for healthy tissue and enhanced targeted uptake of drugs in cancer cells [1-4]. Current research has proposed a wide variety of solutions, most of which include polymers as the drug delivery vehicle [5]. For example, polylactide-*co*-glycolide copolymers have been used to encapsulate therapeutic drugs via oil and water emulsions; where the degradation rate is controlled by molecular weight and copolymer composition [6, 7]. Micro-particles prepared using oil in water emulsions, have in the past suffered from poor encapsulation of water soluble therapeutics and so alternative strategies have been investigated [8]. Polymeric micelles have been heavily investigated as drug carriers due to their size, structure and similarity to natural carriers such as viruses or lipoproteins [9].

Polymers that have regions of hydrophilicity (A block) and regions of hydrophobicity (B block) known as AB di-block copolymers can from micelles in solution. [10]. The first generation of polymeric micelles were typically composed of block copolymers using PEG as the hydrophilic block and a range of hydrophobic blocks such as poly(propylene) glycol, poly(aspartic acid) and poly(ε-caprolactone) [11]. These micelles were shown to be effective at lowering uptake by reticular endothelial systems, preventing protein adsorption and solubilisation of hydrophobic drugs [9]. However, to achieve the controlled release of the drug, attention has also been directed at delivery systems which release their cargo due to specific stimuli. Temperature, pH, light and an electric or magnetic field have all been used to change the conformation of polymer micelles to influence the release profile of a specific drug payload [12-17].

In particular, temperature-responsive micelles have been studied as drug delivery vehicles as they can aggregate in tumours due to the endogenous temperature, or as a result of an external stimulus such as focused ultrasound or hyperthermia treatment [18]. Temperature-responsive polymers such as those based on NIPAAm have been studied extensively due to their sharp phase conformation change at the biologically relevant LCST of 32 ^{O}C. Twaites *et al.* [19] have shown how the temperature-responsive nature of pNIPAAm copolymers can be used as gene delivery vectors. Kotsuchibashi *et al.* [20], through ATRP, used HMAAm to tune the temperature-response of pNIPAAm copolymers and by also making block copolymers they formed micellular structures. RAFT, or ATRP, have been used extensively in the fabrication of new block copolymers that have targeted MWs and low Đ [21-23]. Early ATRP synthesis of block copolymers required the use of a copper catalyst at levels that had potential downstream toxicity consequences, if used in biomedical applications [24-27]. Since RAFT is capable of controlling polymerisation in mild reaction conditions, with a wide range of solvents and monomers, without the need for metal catalysts, it has been heavily investigated for its utility in biomedical applications [28-34]. The smart design through RAFT, and incorporation of smart polymers that are stimuli responsive, is thought to be a necessary strategy in designing novel polymeric drug delivery vehicles [10, 17]. In this Chapter, temperature responsive brush copolymers synthesised by RAFT

polymerisation were investigated. The LCST, CMC and hydrodynamic size of pNIPAAm copolymer micelles are important parameters that influence the formation, uptake and removal of polymeric micelles in drug and gene delivery applications, these parameters were investigated in this thesis.

4.2 Synthesis and Characterisation of PNIPAAm-*co*-HMAAm Copolymers

Thang *et al.* [28, 35] have published comprehensive research in the design of RAFT agents. The RAFT agent is comprised of an R group designated as the leaving group, and a Z group which controls the rate of addition of propagating/fragmenting radicals [35]. The R group is responsible for reinitiating of the polymerisation and the Z group gives control over the polymerisation and needs to be sufficiently stabilising to enhance addition to the carbon disulphide bond [28]. The dithiobenzoate RAFT agent used here, Figure 4.2, (labelled compound 9)), has an alkyl cyano leaving group which is known to be a good leaving R group capable of reinitiating methacrylates and methacrylamide polymerisations [35]. The aromatic Z group of the RAFT agent is frequently used in the literature for the more MAM's class of monomers such as styrene, methyl methacrylate and acrylamide and it is known for its ability to control the Đ of methacrylamide and acrylamide polymerisations [35]. Scheme 4.2 shows the reaction pathway for the synthesis of pNIPAAm-*co*-HMAAm (10). The RAFT polymerisation of NIPAAm (Scheme 4.2, (7)), a temperature responsive acrylamide monomer and HMAAm (Scheme 4.2, (8)), a hydrophilic methacrylamide monomer, was carried out to produce five copolymers with increasing HMAAm content. The mol ratio of HMAAm to NIPAAm was increased from 2.5 mol % to 12.5 mol %, to produce five polymers termed 2.5H, 5H, 7.5H, 10H and 12.5H. The experimental details can be found in Chapter 2, Section 2.3.1.

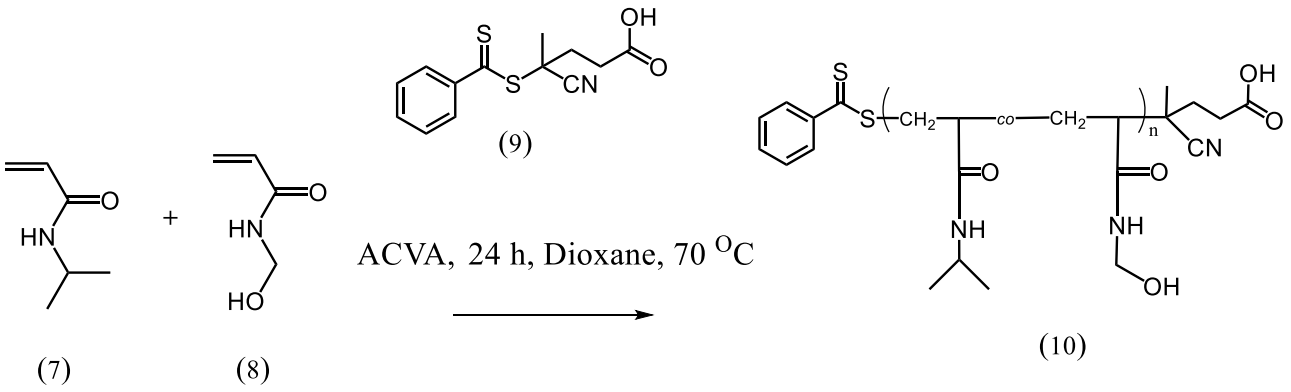

Scheme 4.1. Scheme of polymer synthesis for copolymerisation of pNIPAAm-*co*-HMAAm (2.5, 5, 7.5, 10, and 12.5 mol %).

The effect of increasing HMAAm content of the synthesised copolymer pNIPAAm-*co*-HMAAm was investigated by ^{1}H NMR spectroscopy. Figure 4.1 shows the ^{1}H NMR spectra for pNIPAAm-*co*-HMAAm (0H, 2.5H, 5H, 7.5H, 10H and 12.5H).

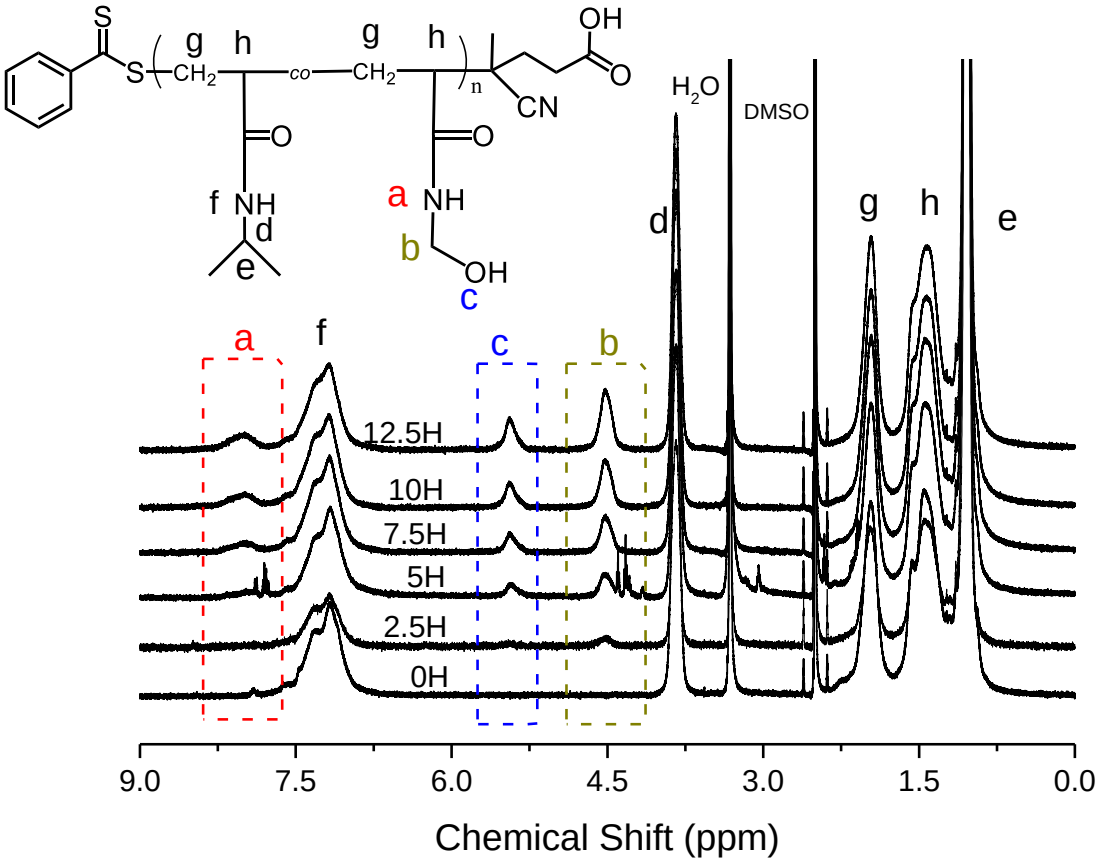

Figure 4.1. ^{1}H NMR spectra in DMSO-d6 of pNIPAAm-*co*-HMAAm copolymers (2.5H, 5H, 7.5H, 10H and 12.5H).

A typical ^{1}H NMR spectrum of a polymer produces broad peaks, the signals observed by ^{1}H NMR spectroscopy relate directly to the structure of the polymer. The spectrum shown in Figure 4.1 has three broad peaks from 1.0-1.4 ppm, which represent the six methyl hydrogens and the C-H/CH_2 polymer back bone from pNIPAAm-*co*-HMAAm. Since the analysis was performed in deuterated DMSO, a solvent peak at 2.5 ppm was observed, as well as a water peak at 3.4 ppm. Two other contributions to the ^{1}H NMR spectra from pNIPAAm occur at 3.8 ppm from the solitary C-H group, with a peak from the amide group at 7.1 ppm. Figure 4.1 shows peaks at 7.9 ppm, 4.5 ppm and 5.4 ppm that can be attributed to the amide group marked in red designated (a) of pHMAAm, the methylene group marked in blue designated (b) of pHMAAm and the hydroxyl group marked in green and designated (c) of pHMAAm respectively. analysis of the peak areas was performed to determine the relevant contributions from each of the copolymers; the analysis was performed to establish whether the synthesis of pNIPAAm-*co*-HMAAm matched the monomer feed ratio. As the feed ratio of HMAAm monomer was increased the subsequent spectra (Figure 4.1) showed a trend where the peak height of the methylene group 4.5 ppm and hydroxyl group 5.4 ppm increased in height relative to the other peaks observed in the spectrum. After integration of all the peaks, the ratio of the methylene group peak (4.5 ppm) and the hydroxyl peak (5.4 ppm) to the C-H group peak at 3.8 ppm from pNIPAAm was used to calculate the pHMAAm content.

A pNIPAAm homopolymer (Figure 4.10, 0H) was also synthesised, as expected its ^{1}H NMR spectrum lacked the peaks at 7.9 ppm, 5.4 ppm and 4.5 ppm associated with pHMAAm. The pNIPAAm homopolymer was not used in further experiments, it was characterised by ^{1}H NMR and GPC as a reference only. ^{1}H NMR spectroscopy showed that the synthetic conditions chosen could deliver a copolymer composition that was governed by the feed ratio of each monomer. The polymer MW and average polymer chain length can be characterised through their separation in solution through a size exclusion column and subsequent detection either by UV-VIS or refractive index detector using a GPC system. The preparation of a standard curve using polymer MW standards (see Chapter 2 Section 2.8.1 for experimental details) then allows for the calculation of MW distributions. Table 1 shows the MW analysis of 2.5H, 5H, 7.5H, 10H and 12.5H copolymers from SEC data using water soluble RAFT pHPMA as the MW standards.

Table 4.1. Sample codes and SEC and GPC data for the copolymerisation of pNIPAAm-*co*-HMAAm (0, 2.5, 5, 7.5, 10 and 12.5 mol %).

Mol %	[NIPAAM]/ [HMAAm][a]	Mn (SEC)[b]	Đ [b]	Mn (GPC)[c]	Đ[c]	Mn (GPC)[d]	Đ[d]
0H	100/0	N/A	N/A	N/A	N/A	N/A	N/A
2.5H	98.5/2.5	34000	1.2	39000	1.2	26000	1.4
5H	95/5	45000	1.2	40000	1.6	43000	1.6
7.5H	92.5/7.5	44000	1.2	40000	1.6	44000	1.6
10H	90/10	46000	1.1	45000	1.6	52000	1.5
12.5H	88.5/12.5	45000	1.1	43000	1.6	43000	1.6

Calculated by [a] ^{1}H NMR.[b] determined by SEC gel filtration in water.[c] determined by Gelfil GPC [d] determined by DMAC GPC

The calculated molecular weights (Mn) were found to be 34000 g/mol, 45000 g/mol, 44000 g/mol, 46000 g/mol and 45000 g/mol, respectively. The Đ measured for all pNIPAAm-*co*-HMAAm copolymers were between 1.1 and 1.2 (Table 4.1). The molecular weight determined by SEC (Table 4 1) for 2.5H was shown by SEC to be lower in molecular weight and have a larger Đ (Table 4 1) than 5H, 7.5H, 10H and 12.5H. As the HMAAm feed ratio increased, the copolymers produced had molecular weights which were approximately equivalent and the Đ improved. The SEC results suggested good control over chain length was achieved and that the molecular weights of the polymers were similar. GPC operates by the same principles as SEC but is named GPC because the solvent used in the mobile phase is an organic solvent instead of water which is used in SEC. Since pNIPAAM is soluble in organic solvents it is commonly used to determine the MWs of pNIPAAm based polymers. The pNIPAAm-*co*-HMAAm copolymers molecular weights were therefore analysed by GPC in an organic solvent with organic soluble standards (Table 4.1). The molecular weights and Đ were recalculated (Table 4.1), the molecular weight for 2.5H was found to be approximately 34,000 g/mol. The molecular weights for 5H-12.5H were found to be approximately 50,000 g/mol. The Đ (Table 4.1), however,

were found to have increased to approximately 1.6, indicating that the copolymers were more polydisperse. Literature has found that molecular weight determination and the living behaviour of pNIPAAm can be difficult to characterise by SEC, or GPC, however the three different measurements obtained by SEC and GPC point to an approximate value of around 30,000 g/mol for 2.5H and approximately 50,000 g/mol for 5H-12.5H [10, 36]. The results agree with the work of Kotsuchibashi *et al.* [20] who established that the copolymerisation of pNIPAAm-*co*-HMAAm achieves greater than 90% conversion from 0-50 mol % with Đ between 1.3-1.6 and a theoretical Mn of approximately 45,000 g/mol; thus kinetic studies to establish control by RAFT polymerisation were not performed. The HMAAm composition of these polymers was further confirmed using ATR-FTIR spectroscopy. Pristine pNIPAAm and pNIPAAM-*co*-HMAAm copolymers with an increasing HMAAm content (0H, 2.5H, 5H, 7.5H, 10H and 12.5H) were investigated by ATR-FTIR spectroscopy. The pNIPAAm and pHMAAm blocks are expected to have a characteristic carbonyl stretch at 1650 cm^{-1} (Figure 4.2) [37].

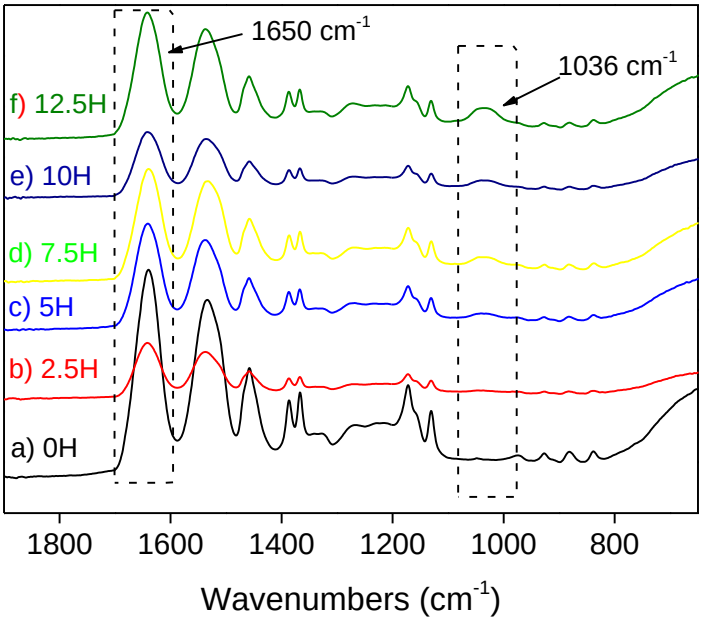

Figure 4.2. ATR-FTIR spectroscopy characterisation pNIPAAm-co-HMAAm copolymers (2.5H, 5H, 7.5H, 10H and 12.5H).

The pHMAAm block was expected to have a C-O stretch at 1036 cm^{-1} [38]. When the spectra of the five copolymers with increasing pHMAAm content were examined (Figure 4.2) it was observed that the peak at 1036 cm^{-1} appeared to be increasing relative to the other peaks as pHMAAm content increased. Integration of the two peak areas (1036 cm^{-1} and 1650 cm^{-1}) was performed to determine if the pHMAAm composition could be determined by ATR-FTIR. A plot of the peak area ratio of the C-O to C=O (amide) stretch at 1036 cm^{-1} and 1650 cm^{-1} respectively as a function of pHMAAm concentration shows a linear trend and a strong correlation of R^2 0.97 (Figure 4.3). The ratio of [NIPAAm]/[HMAAm] calculated using ^{1}H NMR spectroscopy in all, except the 7.5H, pNIPAAm-*co*-HMAAm copolymers (Table 4.2) was in close agreement with the

composition found by linear regression analysis of Figure 4.3 and match the feed ratio of HMAAm for the synthesised copolymers. Discrepancies between the two methods is thought to have arisen due to fitting errors involved in calculating peak areas at 1036 cm^{-1} and 1650 cm^{-1}. While the analysis by ATR-FTIR spectroscopy does not give quantitative confirmation of HMAAm content it does give qualitative evidence of the changing HMAAm composition of the pNIPAAm-*co*-HMAAm copolymers.

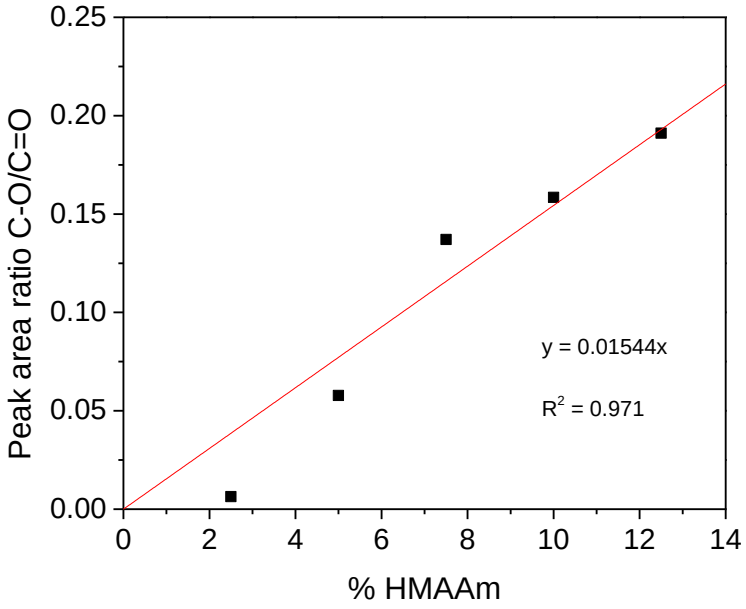

Figure 4.3. Plot of ratio of 1036 cm^{-1}/1650cm^{-1} for pNIPAAm-*co*-HMAAm copolymers (2.5H, 5H, 7.5H, 10H and 12.5H).

Table 4.2. Comparison of NIPAAm to HMAAm ratio of pNIPAAm-*co*-HMAAm copolymers using ^{1}H NMR spectroscopy and ATR-FTIR spectroscopy.

Mol %	[NIPAAM]/[HMAAm][a]	[% HMAAm][b]
0H	100/0	N/A
2.5H	98.5/2.5	2.1
5H	95/5	4.9
7.5H	92.5/7.5	9.3
10H	90/10	10.5
12.5H	88.5/12.5	12.3

Calculated by [a] ^{1}H NMR and [b] determined by linear regression calibration curve (ATR-FTIR).

4.3 Lower Critical Solution Temperature of PNIPAAm-*co*-HMAAm Copolymers by UV-Vis Spectrophotometry

The motivation for controlling HMAAm content of the pNIPAAm-*co*-HMAAm copolymers was to control the LCST and therefore the temperature at which micelles form. Temperature responsive polymers such as

pNIPAAm undergo a coil to globule transition above their LCST and this can lead to the formation of micelles [39]. The formation of these micelles for pNIPAAm block copolymers (pNIPAAm-*co*-HPMAm-lactate)-*b*-PEG) has been found in literature to occur at the critical micelle temperature (CMT) [40, 41]. The change in the LCSTs of the synthesised copolymers that occurs due to different HMAAm composition was monitored using UV-Vis spectrophotometry. Since the LCST can be equivalent to the CMT for polymers containing pNIPAAm, it was important to establish the LCST of the pNIPAAm-*co*-HMAAm copolymers. When pNIPAAm homopolymer (0H) and pNIPAAm-*co*-HMAAm copolymers (2.5H, 5H, 7.5H, 10H and 12.5H) were dissolved in aqueous solutions such as water, the solution remained clear (Figure 4.4, left). At temperatures around the LCST (approximately 40 ^{O}C) the pNIPAAm solution initially turned cloudy and then opaque (Figure 4.4, right) (See Chapter 2 Section 2.8.2 for experimental details).

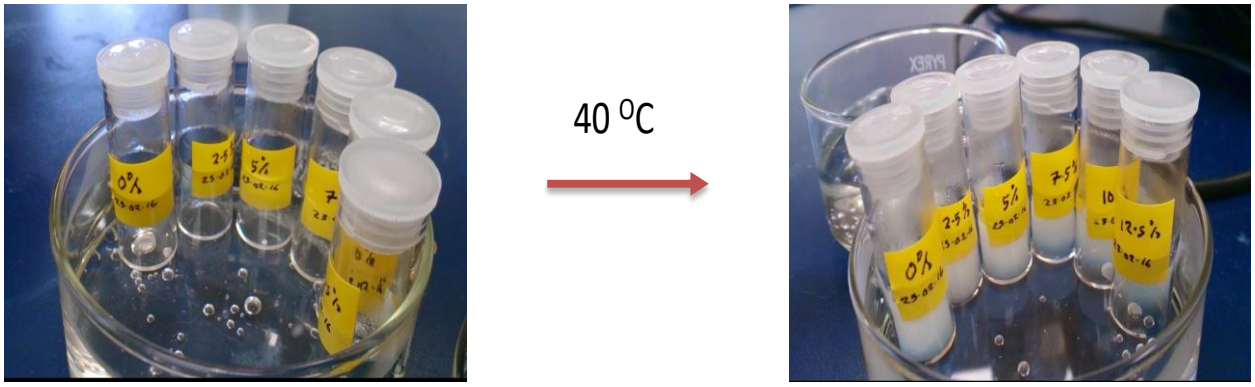

Figure 4.4. LCST phase transition image of pNIPAAm-co-HMAAm copolymers (2.5H, 5H, 7.5H, 10H and 12.5H) at 40 ^{O}C.

Figure 4.5 shows the UV-Vis transmittance at 550 nm for pNIPAAm (0H) and pNIPAAm-*co*-HMAAm copolymers (2.5H, 5H, 7.5H, 10H and 12.5H) (see Chapter 2 Section 2.8.2.1 for experimental details). As shown, the transmittance for all the polymers (Figure 4.5) dropped from T = 100% to almost T= 0 % for all the polymers upon increasing the temperature. The temperature at which each polymer showed a significant sharp reduction in transmittance varied from 28.5 ^{O}C for 0H to 37.5 ^{O}C for 12.5H. The decrease in transmittance at 550 nm for the polymer solutions (Figure 4.5) shows the temperature at which the polymer transitions from a relaxed solvated state to a collapsed contracted state. The calculated LCSTs at approximately 50 % transmittance for pNIPAAm (0H) and pNIPAAm-*co*-HMAAm copolymers (2.5H, 5H, 7.5H, 10H and 12.5H) were 28.5 ^{O}C, 30 ^{O}C, 30.5 ^{O}C, 32 ^{O}C, 34 ^{O}C and 37.5 ^{O}C, respectively.

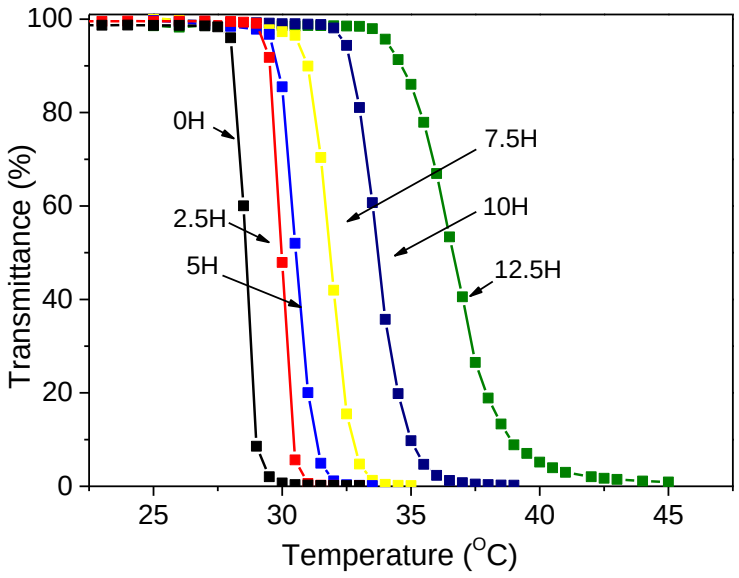

Figure 4.5. Plot of UV transmission at 550 nm versus temperature in water for pNIPAAm-*co*-HMAAm copolymers (0H, 2.5H, 5H, 7.5H, 10H and 12.5H).

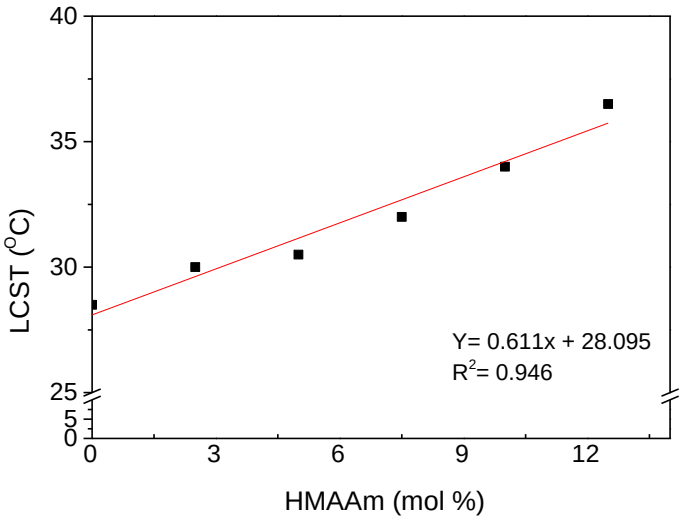

Figure 4.6. Plot of LCSTs pNIPAAm-*co*-HMAAm copolymers (0H, 2.5H, 5H, 7.5H, 10H and 12.5H) versus HMAAm mol %.

When the LCSTs of pNIPAAm (0H) and pNIPAAm-*co*-HMAAm copolymers (2.5H, 5H, 7.5H, 10H and 12.5H) were plotted against HMAAm content the plot showed a linear increase in their LCSTs in response to the increasing HMAAm content consistent with literature (Figure 4.6) [33, 41]. The plot has a strong correlation factor (R^2 of 0.946) and clearly shows that the LCST of pNIPAAm-*co*-HMAAm copolymers can be controlled by the changing the ratio of HMAAm monomer in the pNIPAAm-*co*-HMAAm copolymer. Knowing the LCST for these copolymers allowed the subsequent determination of the CMC at the CMT [41, 42].

4.4 Determination of Critical Micelle Concentration (CMC) for PNIPAAm-*co*-HMAAm Copolymers using Fluorescence Spectroscopy

The size, shape and composition of polymeric micelles can play a vital role in the solubilisation of hydrophobic drugs, or the delivery of gene vectors [43, 44]. The formation of polymeric micelles is governed by their concentration in aqueous media and this can be monitored through measurement of the CMC [45]. The CMC and critical aggregation concentration has been widely studied using hydrophobic probes and can be obtained from the measurements of the changes in the emission band intensity [46]. Hydrophobic probes, pyrene, *N*-phenyl-1-naphthylamine (PNA), 8-anilino-1-naphthalenesulfonicacid (ANS) can detect the formation of hydrophobic nano-domains through their change in fluorescence in aqueous solutions of surfactants and amphiphilic copolymers [47]. In particular, the change in pyrene's emission band intensities is thought to be solvent dependant [46].

SYBR Green (SG) is routinely used to quantify double stranded DNA as it intercalates in the base pairing of DNA and absorbs light at 497 nm and then fluoresces at 520 nm [48]. In an aqueous environment SG will emit a weak signal at 520 nm, however, a sharp increase greater than 1000-fold is observed in a hydrophobic environment [49]. Real-time PCR using SG allows for continuous fluorescence observation of the amplification of DNA that is both rapid and quantifiable [50].

Recently, Chovelon *et al.* [51] have highlighted the capability of the unique short fluorescence lifetime of SG in aqueous solutions to produce intercalator displacement assays and label free biosensors. These assays can utilise DNA structures (duplex, hairpin, G-quadraplex and single-stranded) and ligands such as ions, or small organic molecules through a ligand-induced change of the SG fluorescent signal [51]. The structure of SG is reported to be a monomeric unsymmetrical cyanine dye comprising an *N*-alkylated benzothiazolium or benzoxazolium ring system, which is linked by a monomethine bridge to a pyridinium or quinolinium ring system that carries a substituent with a heteroatom (see Figure 4.8, inset) [52].

The incorporation and length of *N*-alky chains in cyanine dyes has been shown to increase its incorporation into hydrophobic domains such as peptide bi-layers [53]. SG is primarily used as an intercalator whereby evidence suggests that the intercalation via the SG propyl arm like structure allows it to intercalate into the minor groove of DNA [48, 49]. When SG intercalates into the minor groove of DNA, electrostatic interactions from the thiazole group also help to stabilise the complex [48].

Figure 4.7 shows the energy level diagram for a typical polymethine dye. Light can promote an electron from the $S0 \rightarrow S1, Sn$ singlet excited state. Then relaxation $(Sn \rightarrow S1)$ can occur via internal conversion (ic), intersystem crossing (K_{isc}), $(S1 \rightarrow T1)$, internal conversion (K_{ic}) $(S1 \rightarrow S0)$ and photo isomerisation (K_{rot}) $(S1 \rightarrow S0)$ to form the cis cyanine. The subsequent increase in fluorescence after intercalation is largely thought to occur due to the change in the viscosity of the complex leading to a restriction of trans-cis

isomerisation of the dye molecule [48, 49, 54].

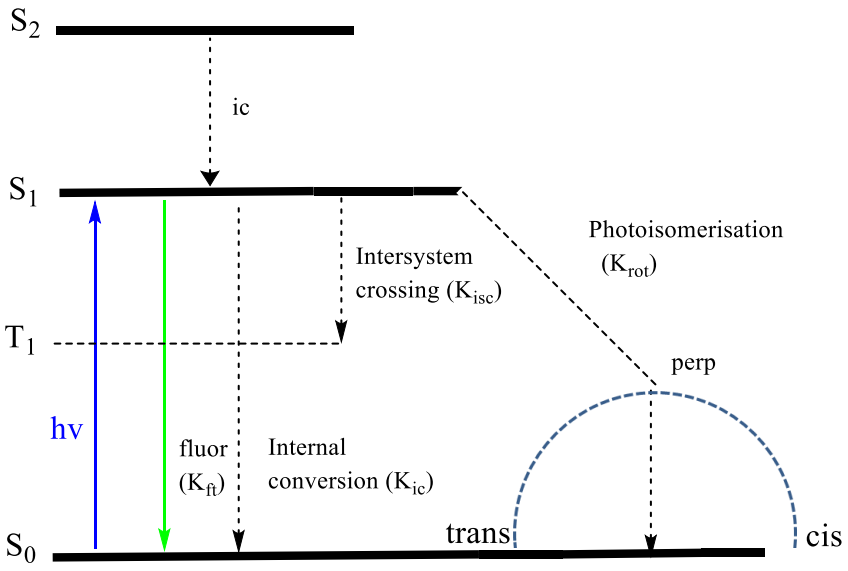

Figure 4.7. Singlet excited state energy level diagram of a typical polymethine dye and the relaxation processes that follow. Adapted from [23].

In this work SG is used as an intercalator into pNIPAAm. It is proposed that the hydrophobic domain from pNIPAAm would be favourable to SG intercalation. In this work, the CMC of the pNIPAAm-*co*-HMAAm copolymers were investigated using the change in fluorescence of SG in solution at the LCST of the polymers. It was proposed in this thesis that the pNIPAAm-*co*-HMAAm copolymers forms micelles into which the SG will migrate due to hydrophobic interaction with the *N*-alkylated functionality of the SG molecule.

Figure 4.8 is a Scheme of the proposed worm-like micelles pNIPAAm-*co*-HMAAm copolymers that may form at the CMC. This is based on the theory regarding molecular curvature that dictates what shape these assemblies will take. It is possible to control the shape by controlling the parameter *Ns* according to Equation 4.1 [55]. Where *Ns* is packing parameter, *Vc* is volume of hydrophobic chain, *a* is cross sectional area of the aggregate expressed per molecule in aggregate and *Lc* is the length of the hydrophobic chain [56]. Normally spherical micelles form where: $Ns \leq 1/3$, cylindrical micelles when $1/3 \leq Ns \leq 1/2$ and enclosed membrane structures (vesicles) where $\frac{1}{2} \leq N_s \leq 1$ and if p > 1, the volume is an inverted truncated cone [57-59].

$$Ns = \frac{Vc}{a * Lc}$$

Equation 4.1

It is expected based on the packing parameter equation that the micelles will form inverted truncated rod like structures. As the pNIPAAm-*co*-HMAAm copolymers collapses as the LCST (*Lc*) decreases, the area of the

polar OH group (*a*) should remain constant; the volume of the hydrophobic component (*Vc*) will increase and exceed the volume of the hydrophilic head group (*a*). *Ns* will increase as a result and should be greater than 1.

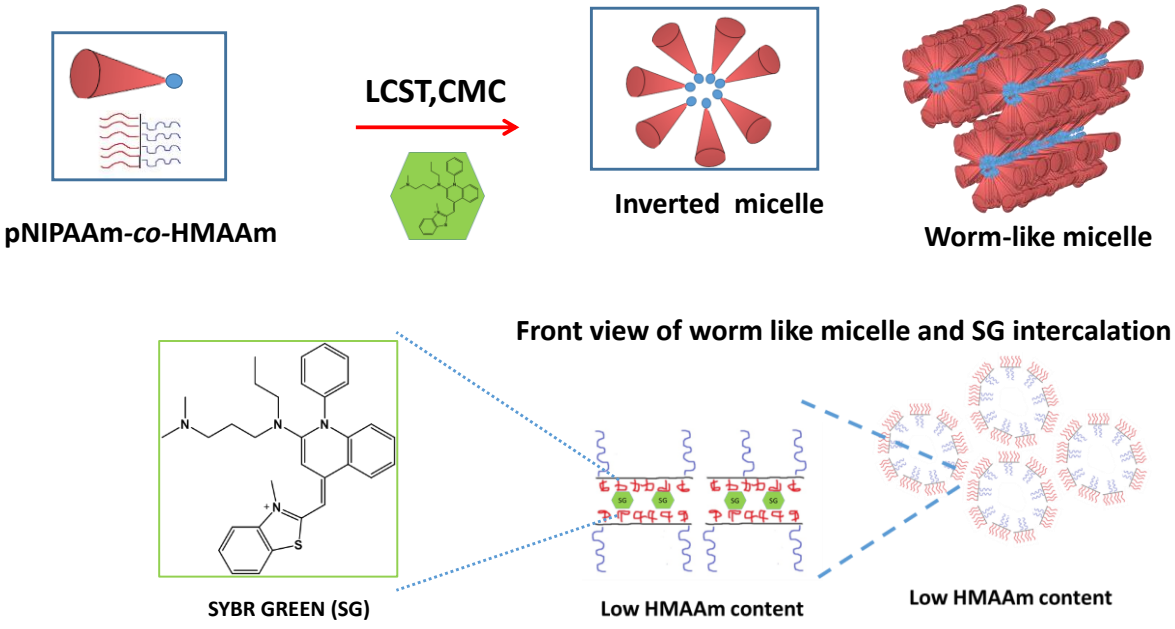

Figure 4.8. Proposed Scheme diagram of the worm-like pNIPAAm-*co*-HMAAm copolymer and its intercalation with SYBR Green at the CMC.

To investigate the intercalation of SG into pNIPAAm-*co*-HMAAm copolymers worm-like structures fluorescence of SG at the CMC was investigated. Figure 4.9 shows the change in fluorescence intensity of SG for the five pNIPAAm-*co*-HMAAm copolymers (2.5H, 5H, 7.5H, 10H and 12.5H) at a concentration of 5 mg.mL^{-1} as the temperature was increased from 25 ^{O}C to 99 ^{O}C (see Chapter 2, Section 2.8.5.1 for experimental details). The initial increase in fluorescence intensity for the five pNIPAAm-*co*-HMAAm copolymers (2.5H, 5H, 7.5H, 10H and 12.5H) occurred at close to the calculated LCSTs of the copolymers (Table 4.3). When the temperature was raised above the LCST a decrease in fluorescence intensity was observed (Figure 4.9). This is thought to be occurring due to the collapsing of the micellular structure. As pNIPAAm is known to shrink at increased temperatures this would lead to a more closed structure [60]. This may result in SG being pushed out of the micelle structure leading to a decrease in fluorescence, as was observed. Heating of the dye does not affect the fluorescence as is seen by the control (blank) in Figure 4.9. The results show that fluorescence intensity is greater for 2.5H at 5 mg.mL^{-1} when compared with 5H, 7.5H, 10H and 12.5H pNIPAAm-*co*-HMAAm copolymers at the same concentration (Figure 4.9). Furthermore, Figure 4.9 shows that pNIPAAm-*co*-HMAAm (12.5H) had a greater fluorescence than 10H at the same concentration.

An investigation of the CMC was performed by maintaining the dye concentration constant and decreasing the concentration of the pNIPAAm-*co*-HMAAm polymer solutions (Figure 4.10 (a-i)). As the 2.5H

concentration was reduced a fluorescent signal could still be observed at 0.025 mg.mL^{-1}, below this concentration, no fluorescent signal could be resolved when compared to the background (Figure 4.10 (a) and (b)). Figure 4.10 (c) and (d) show the change in fluorescence intensity for 5H. The fluorescence intensity also decreased with the concentration of the 5H copolymer down to 0.025 mg.mL^{-1} (Figure 4.10 (d)). Below this concentration the fluorescent signal was not distinguishable from the blank signal (Figure 4.10). Figure 4.10 (e) shows the fluorescence intensity for the 7.5H copolymer at a concentration of 5 mg.mL^{-1}, a significant drop in fluorescence intensity when compared with the 2.5H copolymer (Figure 4.10 (a)) was observed at the same concentration of 5 mg.mL^{-1}.

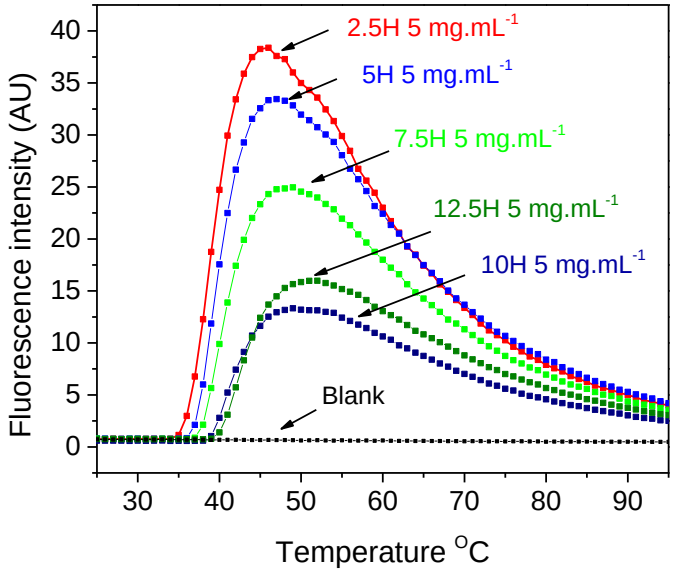

Figure 4.9. Change in fluorescence intensity of SG for pNIPAAm-*co*-HMAAm copolymers (2.5H, 5H, 7.5H, 10H and 12.5H) at 5 mg.mL^{-1} as the temperature was increased from 25 ^{O}C to 99 ^{O}C.

The fluorescence intensity followed the previous trend of decreasing intensity with concentration of the copolymer until it reached a concentration of 0.1 mg.mL^{-1} (Figure 4.10 (f)). Below 0.1 mg.mL^{-1} no fluorescence was observed, which suggested that the onset of aggregates that facilitated fluorescence of SG for the 7.5H copolymer occurred at a higher polymer concentration than the 2.5H and 5H copolymers. Fluorescence intensity (Figure 4.10 (g)) also decreased for the 10H copolymer at a concentration of 5 mg.mL^{-1} relative to 2.5H, 5H, and 7.5H copolymers. Below 0.5 mg.mL^{-1} (Figure 4.10 (h)) it was difficult to observe a fluorescence signal, indicating that the aggregation of the 10H copolymer was occurring at a higher concentration than the 2.5H, 5H, and 7.5H copolymers. Figure 4.10 (i) shows the fluorescence for the 12.5H copolymer, here the fluorescence signal for the copolymer at a concentration of 5 mg.mL^{-1} actually increased relative to the 10H copolymer at the same concentration.

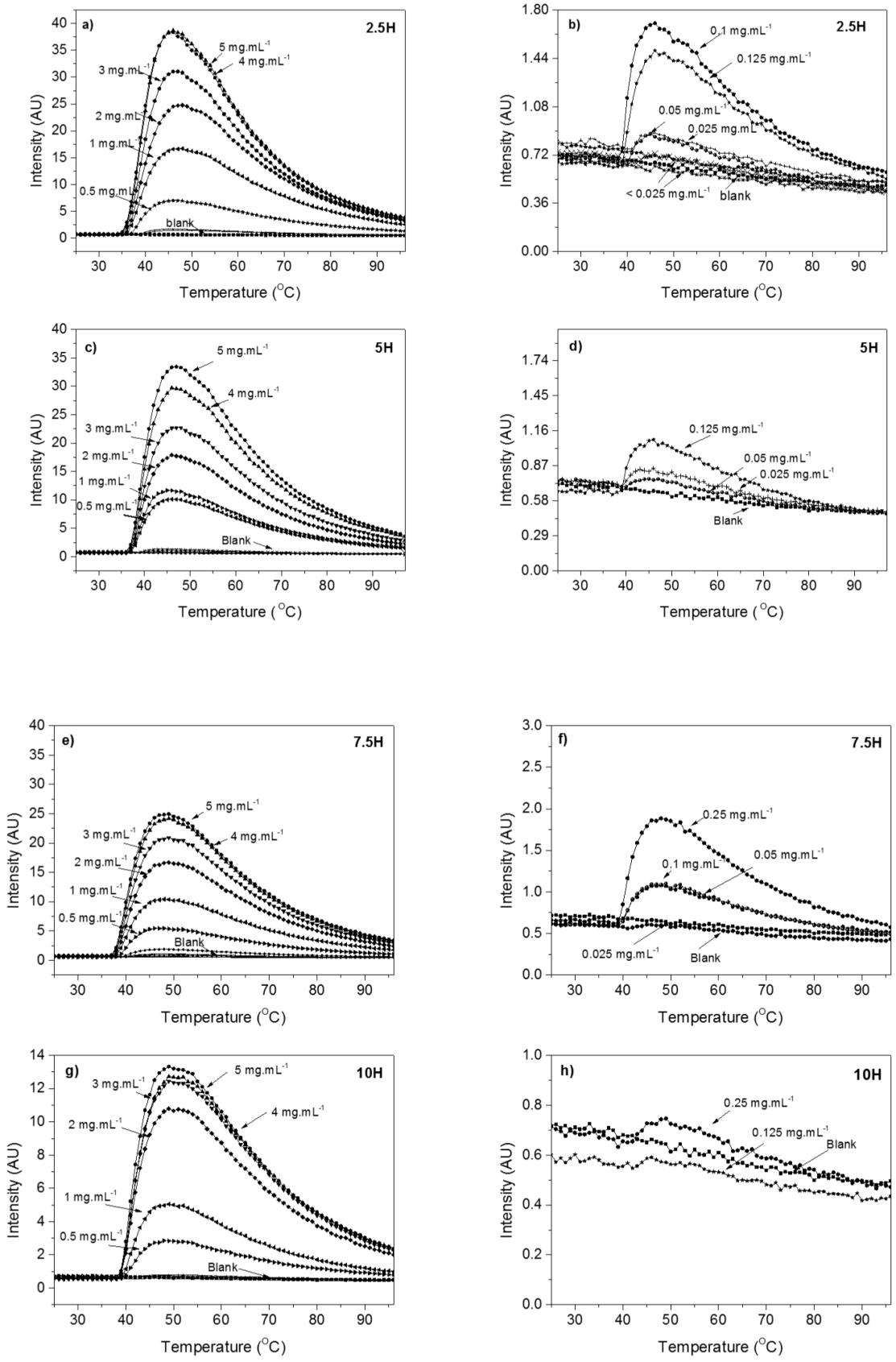

Figure 4.10. SYBR Green fluorescence of (a) 2.5H, (5 mg.mL^{-1} to 0.5 mg.mL^{-1}), (b) 2.5H, (0.125 mg.mL^{-1} to 0.025 mg.mL^{-1}), (c) 5H, (5 mg.mL^{-1} to 0.5 mg.mL^{-1}), (d) 5H, (0.125 mg.mL^{-1} to 0.025 mg.mL^{-1}), (e) 7.5H, (5 mg.mL^{-1} to 0.5 mg.mL^{-1}), (f) 7.5H, (0.25 mg.mL^{-1} to 0.05 mg.mL^{-1}), (g) 10H, (5 mg.mL^{-1} to 0.5 mg.mL^{-1}), (h) 10H, (0.25 mg.mL^{-1} to 0.125 mg.mL^{-1}).

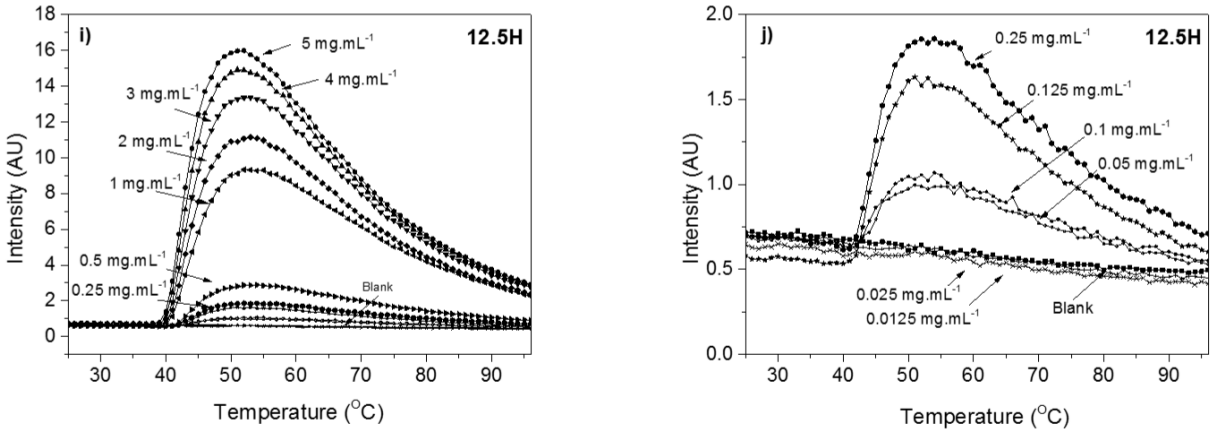

Figure 4.11 continued. SYBR Green fluorescence of (i) 12.5H, (5 mg.mL^{-1} to 0.25 mg.mL^{-1}) and (j) 12.5H, (0.25 mg.mL^{-1} to 0.0125 mg.mL^{-1}).

The fluorescence intensity for the 12.5H, was however, still lower than the other 2.5H, 5H, and 7.5H copolymers at the same concentration of 5 mg.mL^{-1}. The minimum concentration that a fluorescence signal (Figure 4.10 (j)) could be observed for the 12.5H copolymers was 0.1 mg.mL^{-1}. This concentration was lower than the 10H copolymer and equivalent to the 7.5H copolymer. This fluorescence occurred at an increased LCST suggesting a double temperature-responsive micelle structure. As pNIPAAm forms micelles at the LCST, it is expected that the SG dye in an aqueous environment will migrate due to hydrophobic interaction with the *N*-alkylated functionality of the SG molecule. The change in the dipole moment, viscosity and prevention of trans–cis isomerisation of the dye as it enters a more hydrophobic environment are factors that cause SG to fluoresce [49, 61].

Since SG's fluorescence largely results from intercalation effects, and this leads to the subsequent restriction of trans to cis isomerisation. It is therefore proposed that the pNIPAAm-*co*-HMAAm brushes combine to form a domain that is favourable for SG intercalation. The domains vary in their ability to restrict trans to cis isomerisation based upon the HMAAm content. It was theorised that as the NIPAAm content decreased, the number of hydrophobic domains would decrease leading to a reduction in fluorescence. It was proposed that at 12.5% feed ratio the change in fluorescence at low concentrations could be due to the copolymer having a more block like composition where there are larger regions of hydrophilicity. This could potentially lead to micellular structures forming at different temperatures.

Figure 4.11 shows a plot of average fluorescence intensity versus molar concentration for pNIPAAm-*co*-HMAAm copolymers 2.5H, 5H, 7.5H, 10H and 12.5H. Two lines are seen to intersect in Figure 4.11 (a), (b), (c), (d) and (e) which represent the average fluorescence intensity found for each copolymer below the concentration where no fluorescence was resolved above the background; and above the concentration where fluorescence was detected. Extrapolation of each of the lines yields a crossover point which can be

taken as the CMC for the pNIPAAm-*co*-HMAAm copolymers 2.5H, 5H, 7.5H, 10H and 12.5H (Figure 4.11 (a), (b), (c), (d) and (e).

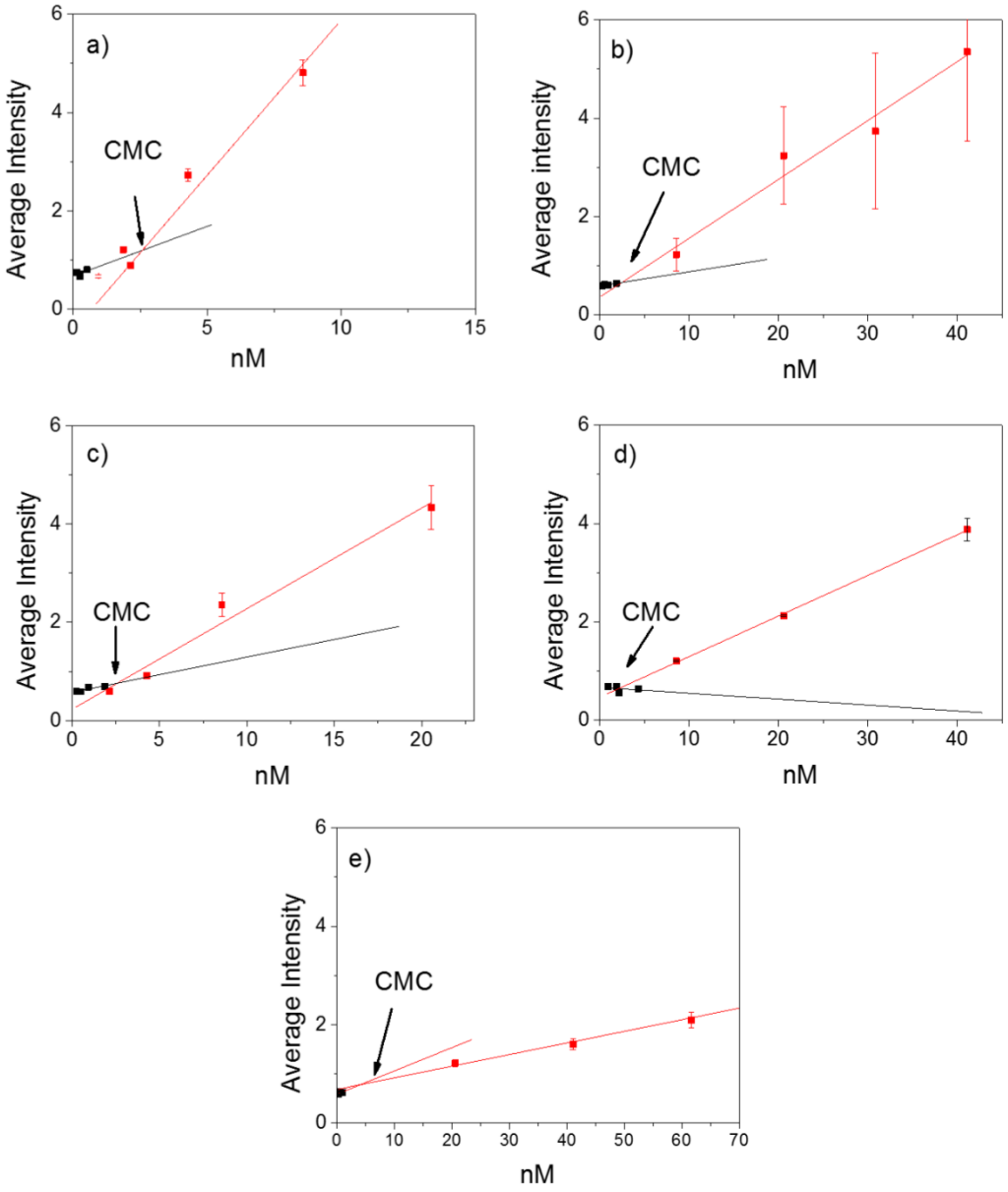

Figure 4.12. CMC crossover point for (a) 2.5H (b) 5H, (c) 7.5H, (d) 10H and (e) 12.5H.

A quantitative method (Eq. 2) of calculating the CMC for pNIPAAm-*co*-HMAAm copolymers 2.5H, 5H, 7.5H 10H and 12.5H was performed by using the line of best fit $Y = mx + c$ (above the CMC) and then using the average of fluorescence values obtained below the CMC.

$$CMC = \frac{(Av\ intensity\ below\ CMC + 10 \times STD + Intercept)}{Slope}$$

Equation 4.2

Table 4.3 shows the calculated molar concentration of the pNIPAAm-*co*-HMAAm copolymers 2.5H, 5H, 7.5H, 10H and 12.5H. The 2.5H copolymer had the lowest CMC concentration at 2.17 nM, which suggests that it starts to form aggregates at much lower copolymer concentrations than the other tested copolymers. The 5H and 7.5H were calculated to have similar CMC concentrations of 4.74 nM and 4.56 nM, respectively (Table 4.3). These values were greater than the CMC concentration of the 2.5H copolymer. The 10H and 12.5H copolymers (Table 4.3, 9.51 nM and 9.98 nM respectively) also showed an increase in the CMC concentration relative to all other copolymers tested. A plot of CMC's concentration versus the HMAAm content yielded a straight line, with a correlation R^2 value of 0.97. The correlation value indicates the CMC's of the synthesised pNIPAAm-*co*-HMAAm copolymers were controlled by the feed ratio of the HMAAm monomer (Figure 4.12). The data suggests that as the NIPAAm content is reduced the CMC increases (Table 4.3). These results found in this study are consistent with what has been found previously in literature [40].

DLS was then used to determine the hydrodynamic radius of the micelles at high and low concentrations of polymer and to investigate any effects on micellular structure that occurred due to increasing HMAAm in the copolymer.

Table 4.3. Sample codes, formula designation for LCSTs, CMC's and hydrodynamic radius of the pNIPAAm-*co*-HMAAm copolymers.

Run	[NIPAAM]/[HMAAm][a]	LCST[b] (^{O}C)	CMC[c] (nM)	D_H[d] (nm)	Đ[d]
2.5H	98.5/2.5	30	2.17	96	0.11
5H	95/5	30.5	4.74	82	0.07
7.5H	92.5/7.5	32	4.56	119	0.03
10H	90/10	34	9.51	124	0.03
12.5H	88.5/12.5	36.5	9.98	117	0.01

[a]Calculated by ^{1}H NMR. [b]determined by UV spectroscopy. [c]determined by fluorescence spectroscopy. [d]determined by DLS

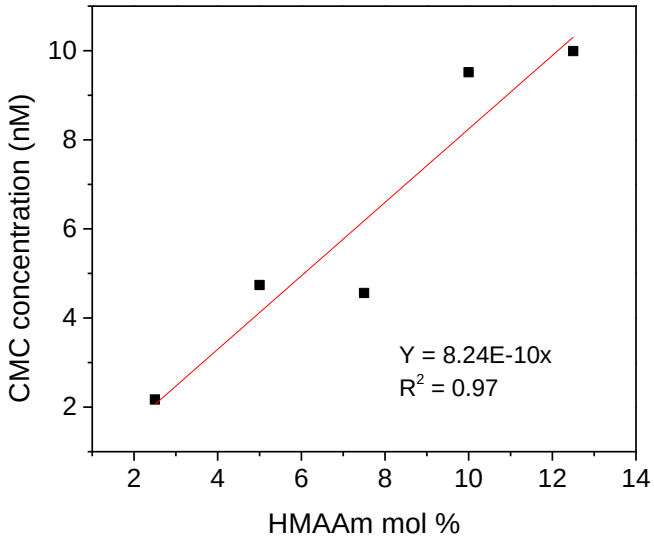

Figure 4.13. Plot of CMC's versus HMAAm mol %.

4.5 Hydrodynamic Size Measurement of Aggregates of PNIPAAm-*co*-HMAAm Copolymers using Dynamic Light Scattering (DLS)

The phase transition of pNIPAAm block copolymers, and the resulting aggregate size, has been extensively studied using dynamic light scattering. Schilli *et al.* [62] have reported that block copolymers of pNIPAAm and polyacrylic acid (pNIPAAm-*b*-PAA) can form star like micelles depending on the pH and temperature; at lower temperatures larger aggregates and micelles were found to coexist. Studies by Hennick *et al.* [63] have shown that the concentration of block copolymers of pNIPAAm-*co*-*N*-(2-hydroxypropyl) methacrylamide-dilactate can play a role in the size of the aggregates that form. The contour length of an approximately 50,000 g/mol polymer such as the synthesised (10H, Table 4.3) pNIPAAm-*co*-HMAAm copolymer is expected to be around 111 nm. The end to end distances (*r*) increases as a function of $N^{1/2}$ to give $r \sim 10$ nm where *N* is the chain length [64]. The theoretical value is true if it is assumed that water is a theta (θ) solvent but it would increase to $r \sim 16$ nm if it was considered to be a good solvent [29, 64].

The theoretical radius of gyration R_g for the linear chain is smaller than the end to end distance by a factor of $\sqrt{6}$ to give a theoretical R_g of ~ 4 nm for (θ) solvent and $R_g \sim 6$ nm for a good solvent [65]. As the copolymer solutions approaches their LCSTs, if water then becomes a poor solvent; r then increases as a function *of* $N^{1/3}$ leading to an end to end distance ~ 5 nm and an $R_g \sim 2$ nm [65]. D_H is a measure of the radius of an effective sphere that has Brownian motion whereas R_g measures the mean root square distance between the ends of the polymer chain [66]. The two methods of measurement are related by $R_g = 1.5 D_H$ for a coil conformation and $R_g = (3/5)^{1/2} D_H$ for globule conformations [64, 67].

The five pNIPAAm-*co*-HMAAm copolymers (2.5 to 12.5 mol %) were investigated by DLS above their LCSTs

and at different concentrations. DLS analysis of the copolymers in solution above their LCSTs for the 2.5H, 5H, 7.5H, 10H and 12.5H copolymers (see Chapter 2, Section 2.8.4.1 for experimental details) was first performed at 3 mg.mL^{-1}; which is above the CMC values calculated by fluorescence. The hydrodynamic diameter (D_H) of 2.5H, 5H, 7.5H, 10H and 12.5H was found to be 231 ±71 (nm), 188 ± 42 (nm), 164 ± 41 (nm), 144 ± 31 (nm), and 115 ± 43 (nm), respectively (Figure 15). The Đ, a measure of particle distribution, remained low (0.01-0.10) which suggests that particle size was uniform (Table 4.3). It was observed that aggregates formed (Figure 4.13) and that the diameter of the aggregated particles decreased with increasing concentration of HMAAm. The change in concentration of the copolymers in solution and the relationship with aggregation size was investigated. The concentration of the 2.5 to 12.5 mol % copolymer solution was reduced to around the CMC as determined by fluorescence.

The hydrodynamic diameter (D_H) of 2.5H, 5H, 7.5H, 10H and 12.5H at the lowest resolved concentration was found to be 96 ± 37 (nm), 82 ± 24 (nm), 119 ± 29 (nm), 124 ± 30 (nm), and 117 ± 27 (nm) respectively (Table 4.3). DLS was able to resolve particles up to 0.0125 mg.mL^{-1} when there was a lower concentration of HMAAm (2.5H (Figure 4.14 a)), 5H (Figure 4.14 b) and 7.5H (Figure 4.14 c)). As the concentration of HMAAm (10H (Figure 4.14 d) and 12.5H (Figure 4.15 e)) increased, the concentration at which particles were resolved increased to 0.025 mg.mL^{-1}.

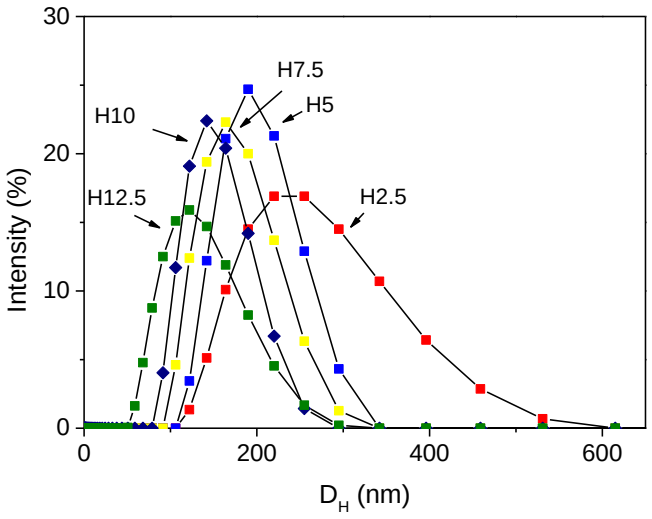

Figure 4.14. Plot of changing hydrodynamic radius size pNIPAAm-*co*-HMAAm copolymers (2.5H, 5H, 7.5H, 10H and 12.5H) at the same concentration of 3 mg.mL^{-1}.

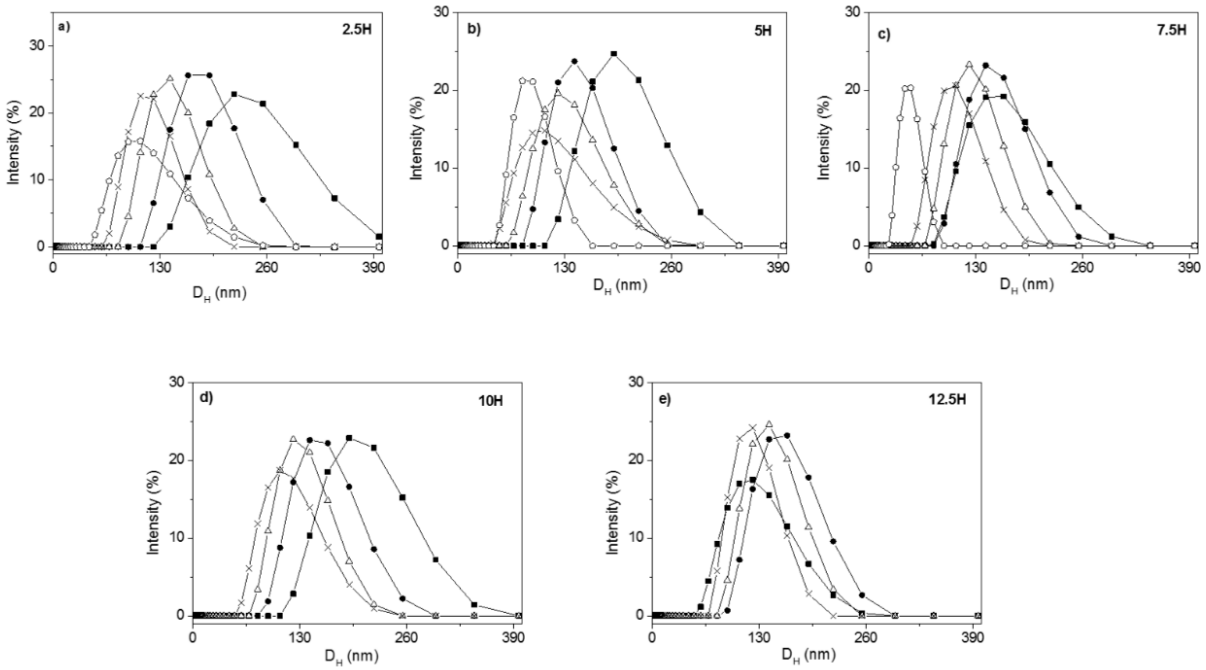

Figure 4.15. Plot of changing hydrodynamic radius of a) 2.5H at a concentration of 3 mg.mL^{-1} (-■-), 0.1 mg.mL^{-1} (-●-), 0.05 mg.mL^{-1} (-Δ-), 0.025 mg.mL^{-1}) (-×-) and 0.0125 mg.mL^{-1} (-⌂-), b) 5H at a concentration of 3 mg.mL^{-1} (-■-), 0.1 mg.mL^{-1} (-●-), 0.05 mg.mL^{-1} (-Δ-), 0.025 mg.mL^{-1}) (-×-) and 0.0125 mg.mL^{-1} (-⌂-), c) 7.5H at a concentration of 3 mg.mL^{-1} (-■-), 0.1 mg.mL^{-1} (-●-), 0.05 mg.mL^{-1} (-Δ-), 0.025 mg.mL^{-1}) (-×-) and 0.0125 mg.mL^{-1} (-⌂-), d) 10H at a concentration of 3 mg.mL^{-1} (-■-), 0.1 mg.mL^{-1} (-●-), 0.05 mg.mL^{-1} (-Δ-) and 0.025 mg.mL^{-1}) (-×-) and e) 12.5H at a concentration of 3 mg.mL^{-1} (-■-), 0.1 mg.mL-1 (-●-), 0.05 mg.mL^{-1} (-Δ-) and 0.025 mg.mL^{-1}) (-×-).

The relationship between the concentration of the copolymers, HMAAm content and D_H by DLS corroborates the calculation of the CMC by fluorescence spectroscopy. DLS could characterise the diameters of these aggregates at different concentrations but the concentration at which particles could be resolved varied with increasing hydrophilicity (HMAAm content). The fact that DLS could resolve particles at lower concentrations with lower HMAAm content indicates that the CMC is lower when there is a higher concentration of the hydrophobic block (pNIPAAm). The results indicate that aggregation is dependent on concentration and HMAAm content. As the copolymer concentration is increased, interaction with nearest neighbours lead to larger aggregates forming. The theoretical D_H of the copolymer solutions at the LCST and above the estimated CMC and (Table 4.3) if no aggregation was occurring should represent the globule conformation and would be ~ 4 nm for a single chain.Since the measured value for all pNIPAAm-*co*-HMAAm copolymers (Figure 4.13) for D_H is much larger than the theoretical value, aggregation of the polymer chains in solution is occurring. It is thought that aggregation of particles is occurring more readily where there is an increased NIPAAm character as would be expected as it is the temperature responsive component of the copolymer and should therefore have the greatest influence upon aggregation [67]. DLS also showed that the copolymers at concentrations above the CMC with more NIPAAm character tended to form larger aggregates. An investigation using AFM was undertaken to see if individual micelles were forming at the LCSTs of the pNIPAAm-*co*-HMAAm copolymers 2.5H, 5H, 7.5H, 10H and 12.5H.

4.6 Atomic Force Microscopy Analysis of PNIPAAm-*co*-HMAAm Copolymers Assembled on a Mica Surface

Diblock copolymers thin film microstructure on a mica surface through selective solvent and rapid solvent extraction has previously been verified through AFM [68, 69]. Studies by Meiners *et al.* [68] have shown that adsorption of entire micelles on to the mica surface can be achieved [68]. In the past, the combination of DLS and AFM have been used to elucidate the CMC of a diblock copolymer poly(styrene-*b*-2-vinylpyridine) [68]. It was thought that micelles should be adsorbed on the surface a mica substrate, through rapid solvent evaporation of the pNIPAAm-*co*-HMAAm copolymer solution, above the CMC and the LCST. Here we investigated the synthesised pNIPAAm-*co*-HMAAm copolymers adsorbed onto a mica surface. The different widths, heights and aspect ratios for each of the copolymers adsorbed onto the mica surface were examined by AFM (see Chapter 2, Section 2.8.6 for experimental details).

Adsorption of the micelles was confirmed by AFM and the heights, width and aspect ratio were compared to the particle size data determined by DLS. Many particles on the mica surface for 2.5H, 5H, 10H and 12.5H (Figure 4.15) were observed by AFM. The analysis of the particles height and width using the Nanoscope software can be performed by the cross-sectional analysis tool where each individual particle is examined or through using the particle analysis tool which can detect all the particles by adjusting the parameters in the software. Initially, particle analysis was performed to establish the mean height and mean diameter of the particles. Figure 4.15 (a) shows a 5 by 5-micron image of the 2.5H sample. Particle analysis for the 2.5H sample (Figure 4.15 a) revealed a particle count of 184 and a mean height of 33 ± 9 (nm) and a mean diameter of 156 ± 72 (nm). To establish the accuracy of the particle analysis software, the cross-sectional analysis tool was used to examine the same 5 by 5-micron image (Figure 4.15 a) cropped into four 2.5 by 2.5-micron images. Two of these images which represents half the area analysed by particle analysis were then analysed by cross section analysis. The total count of particles was 191, the mean height was determined to be 35 ± 7 (nm) and the mean diameter was 115 ± 22 (nm). The particle count calculated by cross- sectional analysis was greater than that found by the particle analysis software, which only had a particle count of 184. The standard deviation for the mean diameter using particle analysis was also much greater than the standard deviation for the mean diameter found through the cross-sectional tool.

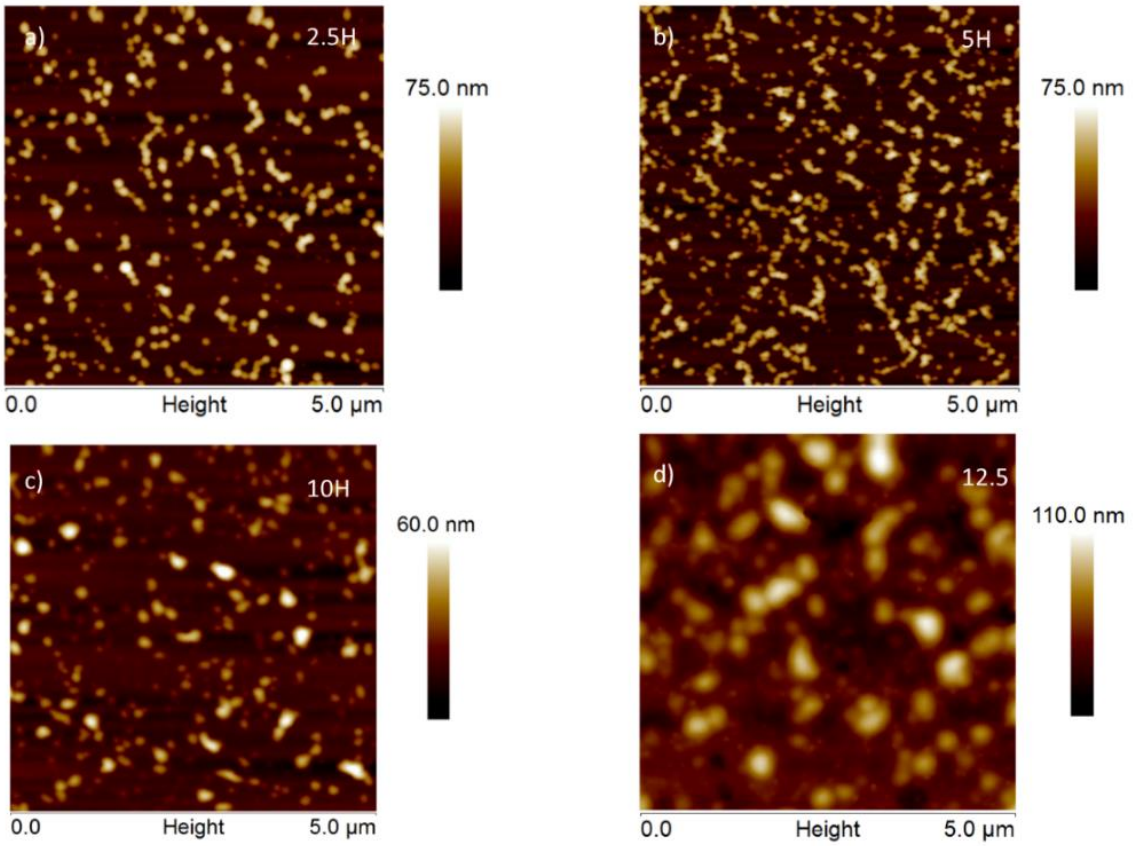

Figure 4.16 Tapping mode AFM Height images, a) 5 by 5-micron image 2.5H, b) 5 by 5-micron image 5H, c) 5 by 5-micron image 10H and d) 5 by 5-micron image 12.5H.

Clearly, the particle analysis software had difficulty in resolving individual particles, as shown by the large error in the mean diameter and the smaller particle count. The mean height 33 ± 9 (nm) established by particle analysis considering the standard deviation was the same as the mean height established by cross section analysis (35 ± 7 (nm)). Thus, the mean height value by particle analysis is a useful fast indicator of changing height across the sample range. AFM of a 5 by 5-micron image (Figure 4.15 (b), (c) and (d)) of the 5H, 10H and 12.5H samples were examined by particle analysis and cross-sectional analysis. The mean heights by particle analysis for the 5H, 10H and 12.5H samples were calculated to be 34 ± 8 (nm), 21 ± 8 (nm) and 40 ± 18 (nm) respectively. A sample size of 90 particles from the same 5 by 5-micron images (Figure 4.15 (b), (c) and (d)) examined by particle analysis for the 5H, 10H and 12.5H samples were then examined by cross section analysis; this resulted in mean heights of 34 ± 8 (nm), 19 ± 8 (nm) and 41 ± 13 (nm), respectively (Table 4.4).

Table 4.4. AFM cross sectional analysis of pNIPAAm-*co*-HMAAm copolymers (2.5H, 5H, 10H and 12.5H).

Run	Width[a]	Height[a]	Aspect ratio[a]
2.5H	115 ± 22	35 ± 7	3.2:1
5H	90 ± 15	34 ± 8	2.6:1
10H	145 ± 35	19 ± 8	7.6:1
12.5H	328 ± 64	41 ± 13	7.8:1

[a]Calculated by AFM cross section tool

Although a smaller sample size was used, the standard deviation indicates the mean height value was the same as that found by particle analysis. The mean diameters of 5H, 10H and 12.5H samples were determined to be 90 ± 15 (nm), 145 ± 35 (nm) and 328 ± 64 (nm), respectively (Table 4.4). The mean diameter data only corresponds to cross section analysis of the 90 particles for each copolymer sample (5H, 10H and 12.5H) as it was established previously that particle analysis is not accurate at determining the mean diameter of the particles. A change in the mean height and diameters of the particles from the 2.5H, 5H, 10H and 12.5H was observed by AFM.

Having established the height and diameter of the 2.5H, 5H, 10H and 12.5H copolymer particles by cross sectional analysis, the aspect ratio of the particles on the surface of the mica were then calculated. The 2.5H, 5H, 10H and 12.5H samples had an aspect ratio of 3.2:1, 2.6:1, 7.6:1 and 7.8:1, respectively (Table 4.4). The aspect ratio of the particles reduced with respect to HMAAm content from the 2.5 mol % to the 5 mol % and then the aspect ratio increased for the 10 mol % and 12.5 mol %. DLS showed that the hydrodynamic diameter (D_H) of 2.5H, 5H, 7.5H, 10H and 12.5H at the lowest resolved concentration was found to be 96 ± 37 (nm), 82 ± 24 (nm), 119 ± 29 (nm), 124 ± 30 (nm), and 117 ± 27 (nm), respectively (Table 4.3). The mean width of the particles found by AFM (Table 4.4), considering the standard deviation of each measurement; falls within the range found by DLS for the 2.5H, 5H and 10H copolymers. The mean width for the 12.5H copolymer (Table 4.4) does fall outside the standard deviation found by DLS. Questions remain as to whether the particles grow on the surface or are deposited as unique aggregates. The diameter and height changes difference observed by AFM may occur due to the interaction of the polar mica surface and the polar head group of the HMAAm copolymer. The copolymers with the least HMAAm content (2.5H and 5H) appear to grow on the surface like islands, resembling a Volmer–Weber growth process [70, 71]. This could be due to the preference of the particles to interact with themselves and not the surface. As the HMAAm content is increased (10H and 12.5H) the copolymers would have some preference for the surface due to the polar head groups and this could lead to layers plus islands (Stranski-Krastanov) like growth [70, 71]. The results suggest that the copolymers with the increased HMAAm content wet the surface more readily. This is thought to be due to a greater amount of hydrophilic character as the HMAAm content is increased. It is theorised that the interaction between the polar head groups of the HMAAm copolymer will wet the surface of the mica more

readily leading to greater spreading of the particle. When imaging soft materials using AFM, it is possible that the deformation of the particle could occur due to the tip interacting with the sample [72]. To establish if AFM analysis of the particles could be influenced by the tapping force, the same area of the 2.5H sample was imaged with a 10% decrease in the set point. Particle analysis showed that the mean height and diameter for both images (data not shown) did not change as result of an increase in force; this shows that any particle height variation between samples is not the result of particle deformation due to changes in the set point.

Directly comparing the hydrodynamic size found by DLS and AFM is problematic given the different interactions of the copolymers with the surface of the mica. Although particles could be observed by AFM, further investigation by AFM is still required to more adequately explain and understand the hydrophobic core hydrophilic shell-like nature of these particles as they assemble on a mica surface.

4.7 Conclusions

Temperature responsive copolymers of pNIPAAm and HMAAm were synthesised by RAFT polymerisation. These copolymers provided the polymer framework used in Chapter 5 to graft DNA via SPAAC chemistry to the backbone of the temperature responsive copolymers

^{1}H NMR spectroscopy was used to calculate the pHMAAm content, after integration of all the peaks, the ratio of the methylene group peak (4.5 ppm) and the hydroxyl peak (5.4 ppm) to the C-H group peak at 3.8 ppm from pNIPAAm confirmed that the feed ratio of the monomer in the copolymerisation was retained in the final polymer composition. The three different measurements obtained by SEC and GPC point to an approximate value of around 30,000 g/mol for 2.5H and approximately 50,000 g/mol for 5H-12.5H, with Đ between 1.3-1.6, The results indicate that good control over molecular weight and Đ was achieved by RAFT polymerisation.

A plot of the peak area ratio of the C-O to C=O (amide) stretch at 1036 cm^{-1} and 1650 cm^{-1} respectively as a function of pHMAAm concentration shows a linear trend and a strong correlation of $R^2 = 0.95$ (Figure 4). The results indicate that the composition of the copolymer matched the feed ratio of each monomer in the copolymerisation.

When the LCSTs of pNIPAAm (0H) and pNIPAAm-*co*-HMAAm copolymers (2.5H, 5H, 7.5H, 10H and 12.5H) were plotted against HMAAm content the plot showed a linear increase in their LCSTs in response to the increasing HMAAm content consistent with literature (Figure 4.6) [33, 41]. The plot has a strong correlation factor ($R^2 = 0.946$) and clearly shows that the LCST of pNIPAAm-*co*-HMAAm copolymers can be controlled by the changing the ratio of HMAAm monomer in the pNIPAAm-*co*-HMAAm copolymer.

The SG fluorescence intensity for all synthesised pNIPAAm-*co*-HMAAm copolymers increased with polymer concentration (Figure 4.10 (a- j)). The initial increase in SG fluorescence intensity for the five pNIPAAm-*co*-HMAAm copolymers (2.5H, 5H, 7.5H, 10H and 12.5H) occurred at close to the calculated LCSTs of the copolymers (Table 4.3). It is proposed that the pNIPAAm-*co*-HMAAm brushes combine to form a domain that is favourable for SG intercalation. The calculated CMC concentration of the pNIPAAm-*co*-HMAAm copolymers 2.5H, 5H, 7.5H, 10H and 12.5H were 2.17 nM, 4.74 nM and 4.56 nM, 9.51 nM and 9.98 nM respectively. A plot of CMC's concentration versus the HMAAm content yielded a straight line, with a correlation R^2 value of 0.97. The correlation value indicates the CMC's of the synthesised pNIPAAm-*co*-HMAAm copolymers were controlled by the feed ratio of the HMAAm monomer (Figure 4.12). The data suggests that as the NIPAAm content is reduced the CMC increases (Table 4.3).

DLS showed that the hydrodynamic diameter (D_H) of 2.5H, 5H, 7.5H, 10H and 12.5H at the lowest resolved concentration was found to be 96 ± 37 (nm), 82 ± 24 (nm), 119 ± 29 (nm), 124 ± 30 (nm), and 117 ± 27 (nm),

respectively (Table 4.3). DLS could characterise the diameters of copolymer aggregates at different concentrations but the concentration at which copolymer aggregates could be resolved varied with increasing hydrophilicity (HMAAm content). The fact that DLS could resolve copolymer aggregates at lower concentrations with lower HMAAm content indicates that the CMC is lower when there is a higher concentration of the hydrophobic block (pNIPAAm). The results indicate that aggregation is dependent on concentration and HMAAm content. The mean width of the particles for 2.5H, 5H, 10H and 12.5H found by AFM, were 115 ± 22, 90 ± 15, 145 ± 35, 328 ± 64 respectively. The mean height of the particles for 2.5H, 5H, 10H and 12.5H 35 ± 7, 34 ± 8, 19 ± 8 and 41 ± 13, respectively. Considering the standard deviation of each measurement the values found fall within the range found by DLS for the 2.5H, 5H and 10H copolymers. The mean width for the 12.5H copolymer (Table 4.4) does fall outside the standard deviation found by DLS. The results suggest that the copolymers with the increased HMAAm content wet the surface more readily. This is thought to be due to a greater amount of hydrophilic character as the HMAAm content is increased. It is theorised that the interaction between the polar head groups of the HMAAm copolymer will wet the surface of the mica more readily leading to greater spreading of the particle.

4.8 References

1. Akimoto, J., M. Nakayama, and T. Okano, *Temperature-responsive polymeric micelles for optimizing drug targeting to solid tumors.* Journal of Controlled Release, 2014. **193**: p. 2-8.
2. Matsumura, Y. and H. Maeda, *A New Concept for Macromolecular Therapeutics in Cancer Chemotherapy: Mechanism of Tumoritropic Accumulation of Proteins and the Antitumor Agent Smancs.* Cancer Research, 1986. **46**(12 Part 1): p. 6387-6392.
3. Liu, F., et al., *Temperature-Sensitive Polymersomes for Controlled Delivery of Anticancer Drugs.* Chemistry of Materials, 2015. **27**(23): p. 7945-7956.
4. Srivastava, A., et al., *Polymers in Drug Delivery.* Journal of Biosciences and Medicines, 2016. **4**(01): p. 69.
5. Rossi, F., G. Perale, and M. Masi, *Device Design: Functional Polymers for Drug Delivery*, in *Controlled Drug Delivery Systems: Towards New Frontiers in Patient Care*. 2016, Springer International Publishing: Cham. p. 61-81.
6. Jeffery, H., S.S. Davis, and D.T. O'Hagan, *The preparation and characterisation of poly(lactide-co-glycolide) microparticles. I: Oil-in-water emulsion solvent evaporation.* International Journal of Pharmaceutics, 1991. **77**(2): p. 169-175.
7. Blanco Prieto, M.J., et al., *Characterization of V3 BRU peptide-loaded small PLGA microspheres prepared by a (w1/o)w2 emulsion solvent evaporation method.* International Journal of Pharmaceutics, 1994. **111**(2): p. 137-145.
8. Davis, S.S., L. Illum, and S. Stolnik, *Polymers in drug delivery.* Current Opinion in Colloid & Interface Science, 1996. **1**(5): p. 660-666.
9. Harada, A. and K. Kataoka, *Supramolecular assemblies of block copolymers in aqueous media as nanocontainers relevant to biological applications.* Progress in Polymer Science, 2006. **31**(11): p. 949-982.
10. Stenzel, M.H., *RAFT polymerization: an avenue to functional polymeric micelles for drug delivery.* Chemical Communications, 2008(30): p. 3486-3503.
11. Pratten, M.K., et al., *Micelle-forming block copolymers: Pinocytosis by macrophages and interaction with model membranes.* Die Makromolekulare Chemie, 1985. **186**(4): p. 725-733.
12. Smith, A.E., X. Xu, and C.L. McCormick, *Stimuli-responsive amphiphilic (co)polymers via RAFT polymerization.* Progress in Polymer Science, 2010. **35**(1–2): p. 45-93.
13. Bae, Y., et al., *Design of Environment-Sensitive Supramolecular Assemblies for Intracellular Drug Delivery: Polymeric Micelles that are Responsive to Intracellular pH Change.* Angewandte Chemie, 2003. **115**(38): p. 4788-4791.
14. Jiang, J., X. Tong, and Y. Zhao, *A New Design for Light-Breakable Polymer Micelles.* Journal of the American Chemical Society, 2005. **127**(23): p. 8290-8291.
15. Kim, H., S.-M. Jeong, and J.-W. Park, *Electrical Switching between Vesicles and Micelles via Redox-Responsive Self-Assembly of Amphiphilic Rod−Coils.* Journal of the American

Chemical Society, 2011. **133**(14): p. 5206-5209.

16. Satarkar, N.S. and J.Z. Hilt, *Magnetic hydrogel nanocomposites for remote controlled pulsatile drug release.* Journal of Controlled Release, 2008. **130**(3): p. 246-251.
17. Mura, S., J. Nicolas, and P. Couvreur, *Stimuli-responsive nanocarriers for drug delivery.* Nature Materials, 2013. **12**(11): p. 991-1003.
18. Schmaljohann, D., *Thermo- and pH-responsive polymers in drug delivery.* Advanced Drug Delivery Reviews, 2006. **58**(15): p. 1655-1670.
19. Twaites, B.R., et al., *Thermo and pH responsive polymers as gene delivery vectors: effect of polymer architecture on DNA complexation in vitro.* Journal of Controlled Release, 2004. **97**(3): p. 551-566.
20. Kotsuchibashi, Y., et al., *Synthesis and characterization of double thermo-responsive block copolymer consisting N-isopropylacrylamide by atom transfer radical polymerization.* Journal of Polymer Science Part A: Polymer Chemistry, 2008. **46**(18): p. 6142-6150.
21. Klok, H.A., *Biological-synthetic hybrid block copolymers: Combining the best from two worlds.* Journal of Polymer Science Part a-Polymer Chemistry, 2005. **43**(1): p. 1-17.
22. Boyer, C., et al., *Well-Defined Protein−Polymer Conjugates via in Situ RAFT Polymerization.* Journal of the American Chemical Society, 2007. **129**(22): p. 7145-7154.
23. Gao, H. and K. Matyjaszewski, *Synthesis of functional polymers with controlled architecture by CRP of monomers in the presence of cross-linkers: From stars to gels.* Progress in Polymer Science, 2009. **34**(4): p. 317-350.
24. Boyer, C., et al., *Bioapplications of RAFT Polymerization.* Chemical Reviews, 2009. **109**(11): p. 5402-5436.
25. Wang, J.-S. and K. Matyjaszewski, *Controlled/"living" radical polymerization. atom transfer radical polymerization in the presence of transition-metal complexes.* Journal of the American Chemical Society, 1995. **117**(20): p. 5614-5615.
26. Matyjaszewski, K. and J. Xia, *Atom Transfer Radical Polymerization.* Chemical Reviews, 2001. **101**(9): p. 2921-2990.
27. Boyer, C., et al., *Copper-Mediated Living Radical Polymerization (Atom Transfer Radical Polymerization and Copper(0) Mediated Polymerization): From Fundamentals to Bioapplications.* Chemical Reviews, 2016. **116**(4): p. 1803-1949.
28. Moad, G., et al., *Advances in RAFT polymerization: the synthesis of polymers with defined end-groups.* Polymer, 2005. **46**(19): p. 8458-8468.
29. Lowe, A.B., M. Torres, and R. Wang, *A doubly responsive AB diblock copolymer: RAFT synthesis and aqueous solution properties of poly (N-isopropylacrylamide-block-4-vinylbenzoic acid).* Journal of Polymer Science Part A: Polymer Chemistry, 2007. **45**(24): p. 5864-5871.
30. Legge, T.M., A.T. Slark, and S. Perrier, *Novel Difunctional Reversible Addition Fragmentation*

Chain Transfer (RAFT) Agent for the Synthesis of Telechelic and ABA Triblock Methacrylate and Acrylate Copolymers. Macromolecules, 2007. **40**(7): p. 2318-2326.

31. Chua, G.B.H., et al., *Synthesis and Thermoresponsive Solution Properties of Poly[oligo(ethylene glycol) (meth)acrylamide]s: Biocompatible PEG Analogues.* Macromolecules, 2012. **45**(3): p. 1362-1374.
32. Gregory, A. and M.H. Stenzel, *Complex polymer architectures via RAFT polymerization: From fundamental process to extending the scope using click chemistry and nature's building blocks.* Progress in Polymer Science, 2012. **37**(1): p. 38-105.
33. Kotsuchibashi, Y., et al., *A 'smart'approach towards the formation of multifunctional nano-assemblies by simple mixing of block copolymers having a common temperature sensitive segment.* Polymer Chemistry, 2012. **3**(5): p. 1150-1157.
34. McCormick, C.L. and A.B. Lowe, *Aqueous RAFT Polymerization: Recent Developments in Synthesis of Functional Water-Soluble (Co)polymers with Controlled Structures.* Accounts of Chemical Research, 2004. **37**(5): p. 312-325.
35. Keddie, D.J., et al., *RAFT Agent Design and Synthesis.* Macromolecules, 2012. **45**(13): p. 5321-5342.
36. Schild, H.G., *Poly(N-isopropylacrylamide): experiment, theory and application.* Progress in Polymer Science, 1992. **17**(2): p. 163-249.
37. Jadhav, S.A., et al., *Synthesis of poly(N-isopropylacrylamide) by distillation precipitation polymerization and quantitative grafting on mesoporous silica.* Journal of Applied Polymer Science, 2016. **133**(44): p. n/a-n/a.
38. Young, A.M., S.A. Rafeeka, and J.A. Howlett, *FTIR investigation of monomer polymerisation and polyacid neutralisation kinetics and mechanisms in various aesthetic dental restorative materials.* Biomaterials, 2004. **25**(5): p. 823-833.
39. Rapoport, N., *Physical stimuli-responsive polymeric micelles for anti-cancer drug delivery.* Progress in Polymer Science, 2007. **32**(8–9): p. 962-990.
40. Convertine, A.J., et al., *Direct Synthesis of Thermally Responsive DMA/NIPAM Diblock and DMA/NIPAM/DMA Triblock Copolymers via Aqueous, Room Temperature RAFT Polymerization.* Macromolecules, 2006. **39**(5): p. 1724-1730.
41. Neradovic, D., C.F. van Nostrum, and W.E. Hennink, *Thermoresponsive Polymeric Micelles with Controlled Instability Based on Hydrolytically Sensitive N-Isopropylacrylamide Copolymers.* Macromolecules, 2001. **34**(22): p. 7589-7591.
42. Rijcken, C.J.F., et al., *Novel Fast Degradable Thermosensitive Polymeric Micelles Based on PEG-block-poly(N-(2-hydroxyethyl)methacrylamide-oligolactates).* Biomacromolecules, 2005. **6**(4): p. 2343-2351.
43. Xu, W., P. Ling, and T. Zhang, *Polymeric Micelles, a Promising Drug Delivery System to Enhance Bioavailability of Poorly Water-Soluble Drugs.* Journal of Drug Delivery, 2013. **2013**: p. 15.

44. Yaşayan, G., et al., *Multi-modal switching in responsive DNA block co-polymer conjugates.* Physical Chemistry Chemical Physics, 2013. **15**(38): p. 16263-16274.
45. Li, Y., B.S. Lokitz, and C.L. McCormick, *Thermally Responsive Vesicles and Their Structural "Locking" through Polyelectrolyte Complex Formation.* Angewandte Chemie International Edition, 2006. **45**(35): p. 5792-5795.
46. Winnik, F.M. and S.T.A. Regismond, *Fluorescence methods in the study of the interactions of surfactants with polymers.* Colloids and Surfaces A: Physicochemical and Engineering Aspects, 1996. **118**(1): p. 1-39.
47. Kujawa, P., F. Tanaka, and F.M. Winnik, *Temperature-Dependent Properties of Telechelic Hydrophobically Modified Poly(N-isopropylacrylamides) in Water: Evidence from Light Scattering and Fluorescence Spectroscopy for the Formation of Stable Mesoglobules at Elevated Temperatures.* Macromolecules, 2006. **39**(8): p. 3048-3055.
48. Zipper, H., et al., *Investigations on DNA intercalation and surface binding by SYBR Green I, its structure determination and methodological implications.* Nucleic Acids Research, 2004. **32**(12): p. e103.
49. Dragan, A.I., et al., *SYBR Green I: Fluorescence Properties and Interaction with DNA.* Journal of Fluorescence, 2012. **22**(4): p. 1189-1199.
50. Morrison, T.B., J.J. Weis, and C.T. Wittwer, *Quantification of lowcopy transcripts by continuous SYBR® green I monitoring during amplification.* BioTechniques, 1998. **24**(6): p. 954-962.
51. Chovelon, B., et al., *A lifetime-sensitive fluorescence anisotropy probe for DNA-based bioassays: The case of SYBR Green.* Biosensors and Bioelectronics, 2017. **90**: p. 140-145.
52. Vitzthum, F. and J. Bernhagen, *SYBR Green I: an ultrasensitive fluorescent dye for double-standed DNA quantification in solution and other applications.* Recent Research Developments in Analytical Biochemistry, 2002. **2**: p. 65-93.
53. Krieg, M., M.B. Srichai, and R.W. Redmond, *Photophysical properties of 3,3'-dialkylthiacarbocyanine dyes in organized media: unilamellar liposomes and thin polymer films.* Biochimica et Biophysica Acta (BBA) - Biomembranes, 1993. **1151**(2): p. 168-174.
54. Martini, I. and G.V. Hartland, *Relaxation dynamics in the first excited singlet state of a cyanine dye: HITC.* Chemical Physics Letters, 1996. **258**(1): p. 180-186.
55. Feng, Y., Z. Chu, and C.A. Dreiss, *Smart wormlike micelles: design, characteristics and applications*. 2015: Springer.
56. Shaul, B. and W. Gelbart, *Theory of chain packing in amphiphilic aggregates.* Annual Review of Physical Chemistry, 1985. **36**(1): p. 179-211.
57. Blanazs, A., S.P. Armes, and A.J. Ryan, *Self-assembled block copolymer aggregates: from micelles to vesicles and their biological applications.* Macromolecular rapid communications, 2009. **30**(4-5): p. 267-277.

58. Song, S., A. Song, and J. Hao, *Self-assembled structures of amphiphiles regulated via implanting external stimuli.* RSC Advances, 2014. **4**(79): p. 41864-41875.
59. Nagarajan, R., *Molecular Packing Parameter and Surfactant Self-Assembly: The Neglected Role of the Surfactant Tail.* Langmuir, 2002. **18**(1): p. 31-38.
60. Liu, R., M. Fraylich, and B.R. Saunders, *Thermoresponsive copolymers: from fundamental studies to applications.* Colloid and Polymer Science, 2009. **287**(6): p. 627-643.
61. Lee, H., et al., *Fluorescence lifetime properties of near-infrared cyanine dyes in relation to their structures.* Journal of Photochemistry and Photobiology A: Chemistry, 2008. **200**(2–3): p. 438-444.
62. Schilli, C.M., et al., *A New Double-Responsive Block Copolymer Synthesized via RAFT Polymerization: Poly(N-isopropylacrylamide)-block-poly(acrylic acid).* Macromolecules, 2004. **37**(21): p. 7861-7866.
63. Neradovic, D., et al., *The effect of the processing and formulation parameters on the size of nanoparticles based on block copolymers of poly(ethylene glycol) and poly(N-isopropylacrylamide) with and without hydrolytically sensitive groups.* Biomaterials, 2004. **25**(12): p. 2409-2418.
64. De Gennes, P.-G., *Scaling concepts in polymer physics*. 1979: Cornell university press.
65. DesCloizeaux, J. and G. Jannink, *Polymers in solution*. 1990: Clarendon Press Oxford.
66. Linegar, K.L., et al., *Hydrodynamic radius of polyethylene glycol in solution obtained by dynamic light scattering.* Colloid Journal, 2010. **72**(2): p. 279-281.
67. Mukherji, D., et al., *Relating side chain organization of PNIPAm with its conformation in aqueous methanol.* Soft Matter, 2016. **12**(38): p. 7995-8003.
68. Meiners, J.C., et al., *Adsorption of Block-Copolymer Micelles from a Selective Solvent.* Macromolecules, 1997. **30**(17): p. 4945-4951.
69. Meiners, J.C., et al., *Two-dimensional micelle formation of polystyrene-poly(vinylpyridine) diblock copolymers on mice surfaces.* Applied Physics A, 1995. **61**(5): p. 519-524.
70. Fu, C., et al., *Unravelling the Self-Assembly of Hydrogen Bonded NDI Semiconductors in 2D and 3D.* Chemistry of Materials, 2016. **28**(3): p. 951-961.
71. *Chapter 1 Surfaces for Supramolecular Systems*, in *Supramolecular Chemistry at Surfaces*. 2016, The Royal Society of Chemistry. p. 1-54.
72. Wiedemair, J., et al., *In-Situ AFM Studies of the Phase-Transition Behavior of Single Thermoresponsive Hydrogel Particles.* Langmuir, 2007. **23**(1): p. 130-137.

5 Chapter 5. Grafting-to: Conjugation of DNA to PNIPAAm Copolymers

Synopsis

Temperature responsive pNIPAAm-*co*-HMAAm copolymers (see Chapter 4, Section 4.2 for experimental details) were functionalised with acid modified DBCO by Steglich esterification using the hydroxyl functionality of the HMAAm polymer to produce pNIPAAm-*co*-HMAAm strained alkyne (SA) copolymers. The pNIPAAm-*co*-HMAAm-*co*-SA functionalised copolymers were then used to graft an azide terminated PCR product at the 5' end via an azide-alkyne click reaction to yield a temperature responsive PCR (TR-PCR) bio-conjugate. The LCST of the resulting TR-PCR bio-conjugates were investigated using a light scattering method that utilised a real-time PCR machine. Agarose gels were used to confirm the grafting of the azide termin ated PCR product to the SA functionalised pNIPAAm-*co*-HMAAm-*co*-SA copolymers. The release profile of SG from the prepared TR-PCR bio-conjugates was also investigated using fluorescence spectroscopy.

5.1 Chapter 5. Introduction

The preparation of “smart” polymer conjugates for various applications in medicine and biotechnology involves the attachment of biomolecules such as peptide, protein, antibodies and DNA to polymers that respond to stimuli such as temperature, light, and pH [1, 2].

The coupling of smart polymers with biomolecules has been achieved through amine, thiols or cycloaddition based modifications [3-6]. Recently, a thiol modified peptide met-enkephalin (tyrosine-glycine-glycine-phenylalanine-methionine), which has anti-tumour activity against a diverse range of cancers, was conjugated to a temperature responsive polymer poly(di(ethylene glycol) monomethyl ether methacrylate)-ran-(oligo(ethylene glycol) monomethyl ether methacrylate) [7]. Under controlled heating conditions, and in the presence of sodium dodecyl sulphate (SDS), the bio-conjugate chains self-assembled to form mesoglobules of controlled sizes. Degradation of the particles occurred in the presence of glutathione, which demonstrated the utility for these nano carriers as controlled release vehicles of anti-cancer peptides [7].

Temperature responsive micellar worms and temperature responsive thiol conjugated protein-polymer conjugates comprising of pNIPAAm-*b*-pStyrene and pNIPAAm-*b*-Vitronectin (VN) have been used to disassociate and propagate human embryonic stem cells (hESCs) via a temperature switch [8]. This resulted in a greater than 30-fold increase in cell number, without the need for cell membrane disrupting enzymes. Perrier *et al.* [9] have used a surfactant free approach via RAFT emulsion polymerisation to prepare uniform 11 nm sized polystyrene latex particles, using preformed HOOC-polyacrylamide-block-polystyrene (HOOC-PAAm-*b*-PS) copolymer micelles as latex particle precursors. The results showed how a model microRNA could be released through the reduction of a disulphide linker using the biological relevant reducing agent glutathione [9]. Polymer-protein and DNA conjugates can lead to conjugates with significant biological activity that imparts molecular recognition properties to the conjugate [10-12]. The recognition properties of these polymers have been combined with temperature responsive polymers such as pNIPAAm for use in diagnostics assays [2, 13]. Hoffman *et al.* [2] conjugated pNIPAAm to the lysine residue of anti-prostate specific antigen (PSA) Immunoglobulin G (IgG) using carbodiimide chemistry via the polymer end-carboxylate. The antibody-pNIPAAm conjugates were enriched through repeated injection of the solution into a micro-reactor followed by thermal precipitation of the conjugates and then removal of the solvent so that the conjugates are enriched [2]. The smart polymer−protein conjugates microfluidic immunoassays showed antigen specific signals which were detectable at a clinically significant range [2].

Smart polymer bio-conjugates have also been investigated for their utility in drug delivery applications. Using a combination of 1-ethyl-3-(3-dimethylaminopropyl)carbodiimide (EDC) and thiol-ene chemistry to attach oligonucleotides to alginate; Brundo *et al.* [14] used the molecular recognition properties of oligonucleotides and a cross-linked alginate gel to generate blood based refilling of intra-tumour drug depots. The

oligonucleotides facilitated targeted delivery of drugs by using the recognition properties of the oligonucleotide [14]. Bioorthogonal reactions are selective chemical reactions inert to biological moieties, examples of which include the copper catalysed azide-alkyne cycloaddition (CuAAC), and strain-promoted azide-alkyne cycloaddition (SPAAC) [15-17]. Biorthogonal chemistries have found great use in functionalising fluorophores to biomolecules [18]. Recently, difluorinated cyclooctyne (DIFO) has been shown to react with azides on intact-proteins [19]. The reaction proceeded at a rate comparable to that of CuAAC chemistry but without the need for toxic metal catalysts. It was then used for dynamic imaging of cell-surface glycans in live cells [19]. Polymeric multifunctional dendrimers which can be used for synthesising controlled architectures suitable for drug delivery have also been investigated for their utility in SPAAC chemistry.

The functionalisation of poly(amido)-based dendrons by Ornelas *et al.* [20] using a number of variations of CuAAC chemistry resulted in dendrons that had significant levels of copper contamination. When Ornelas *et al.* [20] instead used a copper-free SPAAC strategy the functionalised poly(amido)-based dendrons were produced in high yield and with no toxic metal contamination. The SPAAC strategy has also been used to conjugate PEG to biomolecules, recently Debets *et al.* [21] PEGylated an azide containing *Candida antartica* lipase B (AHA-CalB) through mixing with an aza-dibenzocyclooctyne moiety that had been amine conjugated to methoxy-polyethyleneglycol (DIBAC-mPEG2000). The results indicate that aza-DIBAC is a fast and efficient reagent capable of conjugating polymers to biomolecules [21]. Recently, Ta *et al.* [22] demonstrated DOX release from polymer modified liposomes, DOX is an anthracycline antibiotic used in chemotherapy. The copolymer of NIPAAm and propylacrylic acid (PAA) (pNIPAAm-*co*-pPAA) imparted temperature and pH responsive properties that destabilised the liposomes due to a temperature, or pH, switch [22]. The results showed that the temperature induced release of doxorubicin (DOX) occurred at temperatures below the threshold where tissue damage could occur and that the pH sensitive release of DOX would be ideal in acidic environments commonly found in tumour sites [22]. Zhang *et al.* [23] used gold nanorods conjugated to C-quadraplex DNA, intercalated with DOX. pH and near infrared light were shown to be effective stimuli, for the release of the anti-cancer drug DOX, from the C-quadraplex DNA [23]. To our knowledge very few studies have looked at using polymer-polymerase chain reaction conjugates to facilitate the organisation, or cross-linking, of micelle structures. This in term may be a useful method to generate novel polymeric vesicles capable of delivering a drug payload. This project aimed to develop temperature responsive bio-conjugates that could be used in the delivery of drugs, used in cancer therapy. Here, we used RAFT polymerisation to design; tuneable temperature-responsive copolymers that have a site-specific moiety and a strained alkyne, useful for conjugation to DNA probes. RAFT polymerisation was used to prepare pNIPAAm-*co*-HMAAm copolymers (see Chapter 4, Section 2.3.1). The pNIPAAm-*co*-HMAAm copolymers were functionalised with a DBCO moiety due its bioorthogonal properties that make it chemo specific in that it reacts with azides spontaneously. The specificity and simplicity of the strained “click” reaction has the added benefit of eliminating the need for metal catalysts; normally required for traditional cycloaddition chemistry [4]. The 1,

3-dipolar cycloaddition reaction with azides results in the formation of a five-membered ring that leads to multiple covalent bonds and a stable product. The newly formed bonds are resistant to pH changes making them stable in solution. After functionalisation of the polymer with a strained alkyne, the hydrophilic (blocks) of DNA were attached via a strained azide-alkyne reaction (mechanism discussed in Chapter 1, Section 1.2.5). It is proposed, that the newly synthesised TR-PCR bio-conjugates, can be loaded with an intercalator and then by controlling the temperature that intercalator can be released from the TR-PCR bio-conjugates. As a proof of concept, the synthesised TR-PCR bio-conjugates, were combined with SG, a known DNA intercalator, and then monitored by fluorescence spectrometry.

5.2 Synthesis and Characterisation of PNIPAAm-*co*-HMAAm-*co*-SA Copolymers

Scheme 5.1 shows the synthetic path to produce SA functionalised pNIPAAm-*co*-HMAAm-*co*-polymers. EDC and 4-pyrrolidinepyridine was used in a Steglich esterification using the hydroxyl functionality of the pNIPAAm-*co*-HMAAm (2.5-12.5H mol %) (11) and the carboxylic acid of DBCO (12). This yielded a SA functionalised (2.5-12.5 mol %) pNIPAAm-*co*-HMAAm-*co*-SA copolymer (denoted 2.5-12.5S) (13). The experimental details can be found in Chapter 2 Section 2.3.2.

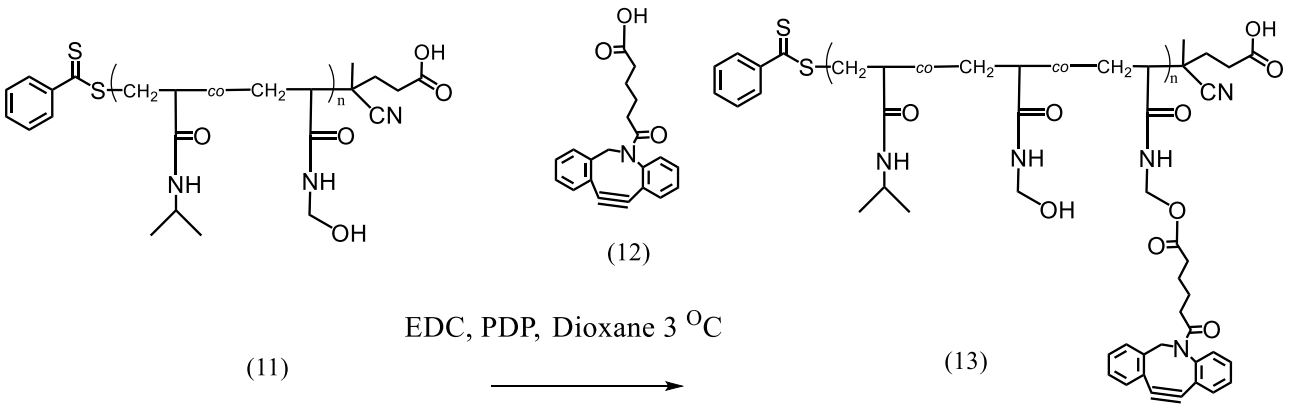

Scheme 5.1. Steglich esterification of pNIPAAm-*co*-HMAAm and dibenzylcyclooctyne-acid to yield the new strained alkyne functionalised (2.5-12.5 mol %) pNIPAAm-*co*-HMAAm-*co*-SA copolymer.

The ^{1}H NMR spectrum shown in Figure 5.1 has three pNIPAAm-*co*-HMAAm copolymer back bone peaks (1.0-1.4 ppm, C-H/CH_2), and solvent peaks at 2.5 ppm 3.4 ppm (DMSO-d6, H_2O). Other contributions from pNIPAAm occur at 3.8 ppm (C-H group), and a peak from the amide group at 7.1 ppm. Figure 5.1 shows peaks at 7.9 ppm, 4.5 ppm and 5.4 ppm that can be attributed to the amide group, methylene group and the hydroxyl group of pHMAAm, respectively. The peaks observed in Figure 5.1 at between 7-8 ppm, labelled region i, and at 5 ppm, labelled region j represent the DBCO moiety attached to the polymer backbone after esterification.

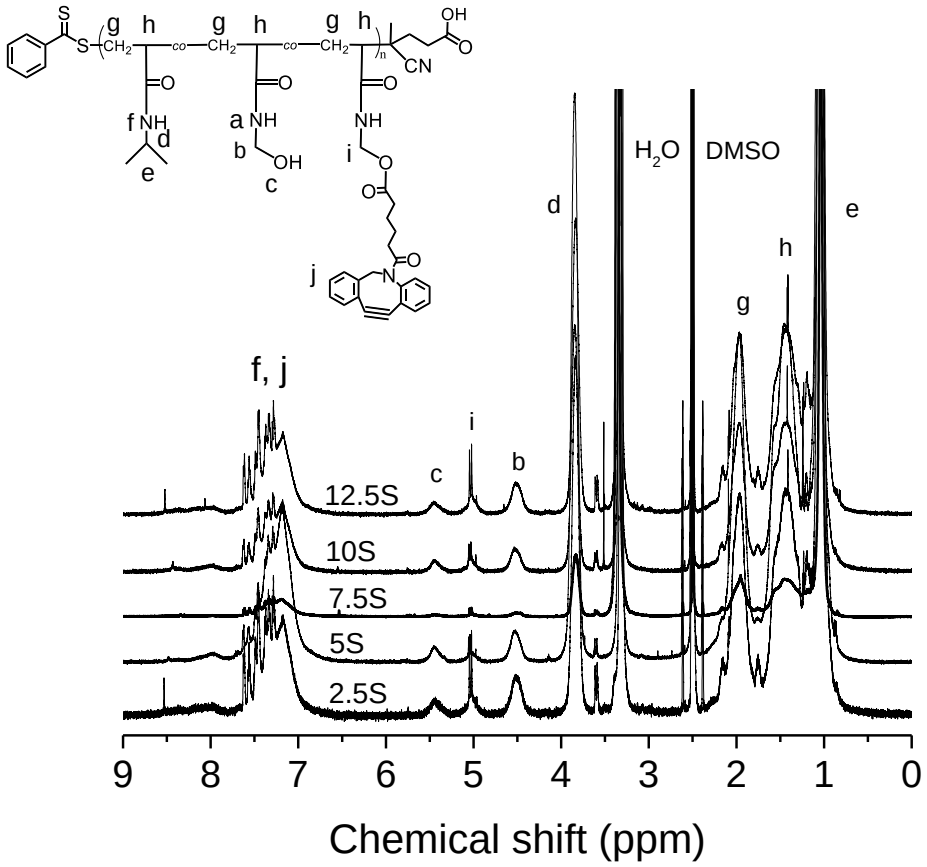

Figure 5.1. ^{1}H NMR spectra in DMSO-d6 of pNIPAAm-*co*-HMAAm-*co*-SA copolymers (2.5S, 5S, 7.5S, 10S and 12.5S).

Figure 5.2 shows the comparison of the ^{1}H NMR spectrum for pNIPAAm-*co*-HMAAm copolymer (10H, bottom, blue) and the SA copolymer (10S, top, black). The new multiplet peaks observed for (10S, black) is due to the aromatic groups of DBCO (labelled S, 7-8 ppm) and the doublet peak at 5 ppm for the (CH_2 group, labelled S). Previous analysis of pNIPAAm-*co*-HMAAm (2.5H-12.5H) copolymers performed in Chapter 4, Section 4.2 showed that the ratio of the methylene group peak (4.5 ppm) and the hydroxyl peak (5.4 ppm) to the C-H group peak at 3.8 ppm from pNIPAAm can be used to calculate the pHMAAm content (shown in Table 5.1). ^{1}H NMR integration of peaks (3.8 ppm, 4.5 ppm and 5.4 ppm) for pNIPAAm-*co*-HMAAm-*co*-SA (2.5S-12.5S) copolymers was performed to determine the HMAAm and DBCO content.

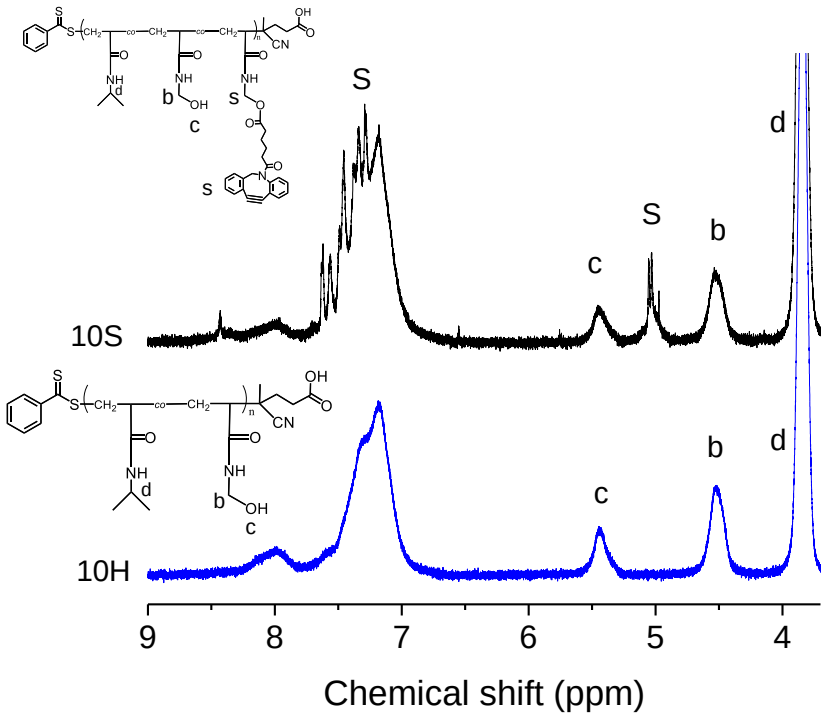

Figure 5.2. Comparison of ^{1}H NMR spectrum of pNIPAAm-*co*-HMAAm copolymer (10H) before Steglich esterification and after esterification to yield pNIPAAm-*co*-HMAAm-*co*-SA copolymers (10S).

Table 5.1 shows the ^{1}H NMR estimated HMAAm content and DBCO content of 2.5S-12.5S copolymers, since there appears to be unreacted DBCO present in each spectrum. All the SA copolymers (2.5S-12.5S) showed a change in HMAAm content by ^{1}H NMR analyses, which indicates that the esterification reaction was successful and DBCO was therefore attached to all the pNIPAAm-*co*-HMAAm (2.5H-12.5H) copolymers. However, none of the SA copolymers analysed by ^{1}H NMR showed a complete loss of the hydroxyl group peak at 5.44 ppm, which suggest that the conversion was incomplete. The DBCO content shown by ^{1}H NMR analyses for all the SA copolymers was found to be 4%, 1%, 3.5%, 3% and 1.5% for the 2.5S, 5S, 7.5S,10S and 12.5S copolymers respectively. The 2.5S copolymer appears to increase its HMAAm content by ^{1}H NMR analysis, the reason for this result is unknown

Table 5.1. Sample codes and ^{1}H NMR analysis of SA copolymers.

Sample Code	[NIPAAM]/[HMAAm][a]	Sample code	[NIPAAM]/[HMAAm/SA][a]
2.5H	98.5/2.5	2.5S	88.5/8/4
5H	95/5	5S	95/4/1
7.5H	92.5/7.5	7.5S	92.5/4/3.5
10H	90/10	10S	90/7/3
12.5H	88.5/12.5	12.5S	88.5/11/1.5

Calculated by [a] ^{1}H NMR.

ATR-FTIR spectroscopy was also used to investigate the change in the HMAAm content of the SA copolymers. Previous analysis of the pNIPAAm-*co*-HMAAm copolymers using ATR-FTIR spectroscopy (see Chapter 2, Section 4.2) established that the C-O stretch at 1036 cm^{-1} increased with increasing pHMAAm composition. A plot of the peak area ratio of the C-O to C=O (amide) stretch at 1036 cm^{-1} and 1650 cm^{-1}, respectively, as a function of pHMAAm composition showed a linear trend and a correlation of R^2 of 0.95 (see Chapter 4, Section 4.2). Since the hydroxyl group from pHMAAm would be transformed in the esterification shown in Scheme 5.1, it was theorised that a change in ATR-FTIR spectra would occur.

A change in the ATR-FTIR spectra (not shown) of the pNIPAAm-*co*-HMAAm copolymers after esterification was observed. The normalised spectra of pNIPAAm-*co*-HMAAm (2.5H-12.5H) copolymers (Figure 5.3 a) was compared to the normalised spectra of SA copolymers 2.5S-12.5S (Figure 5.3 b). The 5S, 7.5S, 10S, and 12.5S copolymers all showed a reduction in the C-O stretch at 1036 cm^{-1} which was thought to be due to the successful esterification and attachment of the DBCO moiety. The 2.5S copolymer did show an increase in this stretch which was inconsistent with the other results.

Since the previous analysis of peak ratio of the C-O/C=O of the synthesised pNIPAAm-*co*-HMAAm copolymers revealed the HMAAm composition, the peak area ratio of the C-O/C=O peaks for the SA coupled SA copolymers were also investigated to see if it could determine the SA composition. Figure 5.4 a) shows the comparison of the C-O/C=O peak area ratio before SA coupling and after SA coupling (Figure 5.4 b)). The peak area ratio for C-O/C=O decreased after SA coupling for the 5S, 7.5S, 10S, and 12.5S copolymers when compared to the peak area ratios before SA coupling. The trend in the peak area ratio observed was not uniform, the 2.5S increased, which was again inconsistent with all the other SA copolymers. The 5S ratio decreased and the 7.5S showed a significant drop in peak area ratio. The 12.5S also had a significant drop in peak area ratio and the 10S also decreased in peak area ratio relative to the 10H copolymer.

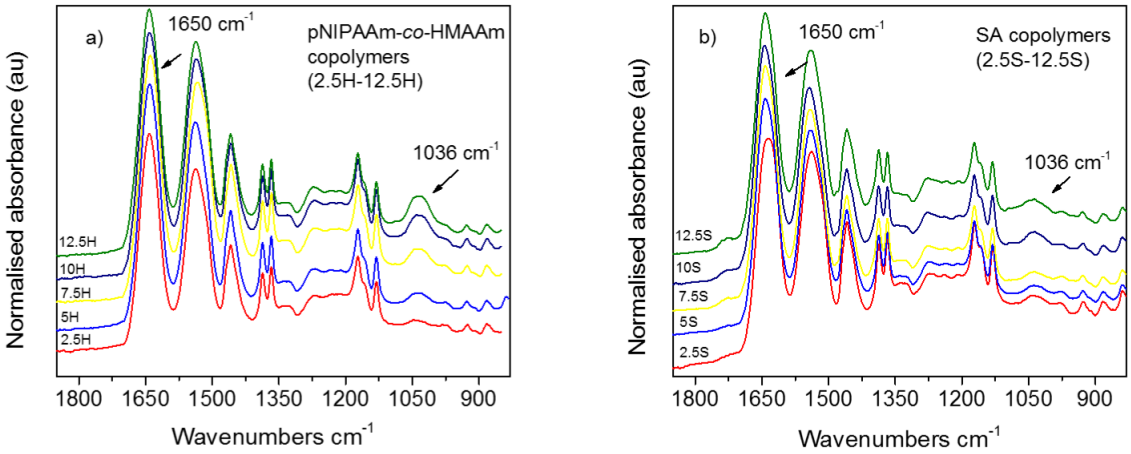

Figure 5.3. Normalised ATR-FTIR spectra before SA coupling a) 2.5H-12.5H and after SA coupling b) 2.5S to 12.5S.

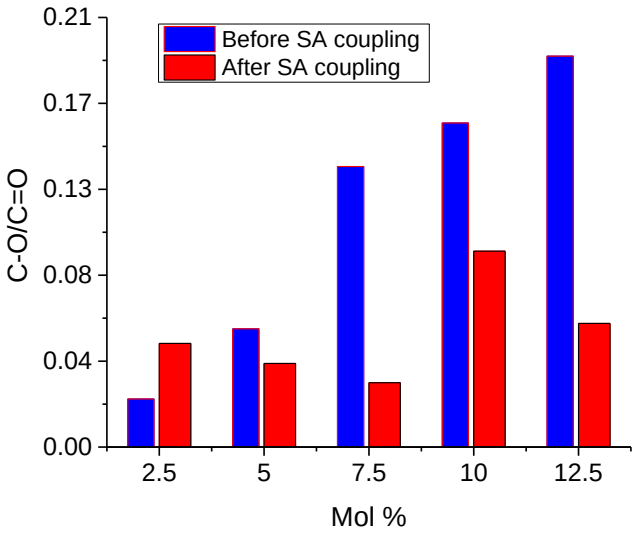

Figure 5.4. The peak area ratio of C-O/C=O before SA coupling a) 2.5H-12.5H and after SA coupling b) 2.5S to 12.5S.

Although the trend in DBCO functionalisation was not consistent for all the copolymers, ATR-FTIR analysis suggested that esterification of the hydroxyl group had occurred, however the exact DBCO composition of the synthesised copolymers was not able to be calculated by ATR-FTIR. Further evidence that may support DBCO functionalisation of the pNIPAAm-co-HMAAm copolymers was the presence of faint peak at 2329 cm^{-1} which might be indicative of the strained alkyne stretch (data not shown). Since ATR-FTIR analysis showed that the hydroxyl functionality of the HMAAm and the carboxylic acid of the DBCO was transformed by Steglich esterification using catalysed EDC coupling; the subsequent SA copolymers (2.5S-12.5S) were investigated for any subsequent changes in their solution properties.

5.3 Lower Critical Solution Temperature (LCST) Analysis of pNIPAAm-*co*-HMAAm-*co*-SA via Light Scattering

As this project aimed to develop temperature responsive DNA polymer bio-conjugates, a constant limitation is the concentration of DNA available for conjugation. It follows then that it would be useful to have a method of analysing the solution properties of these temperature responsive DNA polymer conjugates as their efficacy as drug delivery agents will be heavily influenced by their solution properties. Nobuo *et al.* [24] recently reported the interaction of pNIPAAm with sodium dodecyl sulphate when investigating the critical aggregate concentration. Their investigation also found that fluorescent measurements of pNIPAAm with an incident light of 392 nm produced a spectral band at 563 nm [24]. The presence of this spectral band was thought to occur because no band pass filter was mounted on the fluorometer [24]. The spectral band at 563 nm was determined to be due to an anti-stoke line of Raman scattering and the intensity of this band was proportional to pNIPAAm concentration [24]. Light Scattering has been used extensively to study the aggregation properties of pNIPAAm. It can also be used to determine the LCST of pNIPAAm, since the refractive index of the pNIPAAm in solution changes at the LCST, which results in an increase in light intensity at the detector [25].

LCSTs of polymers are generally measured by UV-Vis spectrometry, but this technique can require a lot of sample (milligrams). Since the DNA bio-conjugates produced in this thesis only required milligrams of SA polymer, another method was needed to measure the LCSTs of the SA copolymers. A low volume, light scattering method is reported in this thesis for the first time. The light scattering method of measuring LCSTs only requires micrograms since the volume being measured is very small (microliters). Real-time PCR machines are routinely used for monitoring PCR reactions via the measurement of fluorescent signal [26]. Here, a real-time PCR machine was used for the first time as a method of measuring the LCSTs of temperature responsive copolymers and temperature responsive polymer bio-conjugates. Often the characterisation of these polymer bioconjugates can be difficult with respect to their solution properties, and so the light scattering that occurs for aggregates at the LCST was investigated by monitoring the change in the light intensity of the pNIPAAm-*co*-HMAAm copolymers before and after esterification with DBCO. The five synthesised polymers (pNIPAAm-*co*-HMAAm (2.5-12.5 mol %)) previously analysed by UV-Vis spectroscopy (see Chapter 4, Section 4.3) were shown to have distinct sharp LCSTs that increased with increasing HMAAm content. The same polymers were examined using a real-time PCR machine. The excitation and emission wavelength was set for 490 nm and 510 nm respectively (see Chapter 2, Section 5.3 for experimental details).

The pNIPAAm-*co*-HMAAm copolymers were prepared at 1 $mg.mL^{-1}$ in Milli-Q water in real time PCR tubes at a volume of 20 µL. The five polymers (pNIPAAm-*co*-HMAAm (2.5-12.5 mol %)) were heated over a temperature ramp that increased at 1 $^{O}C.min^{-1}$ starting from 25 ^{O}C and continued past the LCST temperature. Figure 5.5 shows the change in light intensity that occurred as the temperature was increased. The copolymer

2.5H synthesised, with the lowest HMAAm content, showed an increase in light intensity (Table 5.2) at 33 ^{O}C. The 5H, 7.5H, 10H and 12.5H all showed an increase in light intensity at 35.7 ^{O}C, 36.7 ^{O}C, 38.3 ^{O}C and 40.3 ^{O}C respectively (Table 5.2). The temperature where light scattering began, increased as the HMAAm content of the synthesised copolymers increased. The temperature that this occurred changed with increasing HMAAm content. Table 5.2 shows the difference in the LCSTs of pNIPAAm-*co*-HMAAm copolymers calculated by UV-Vis and by light scattering spectroscopies.

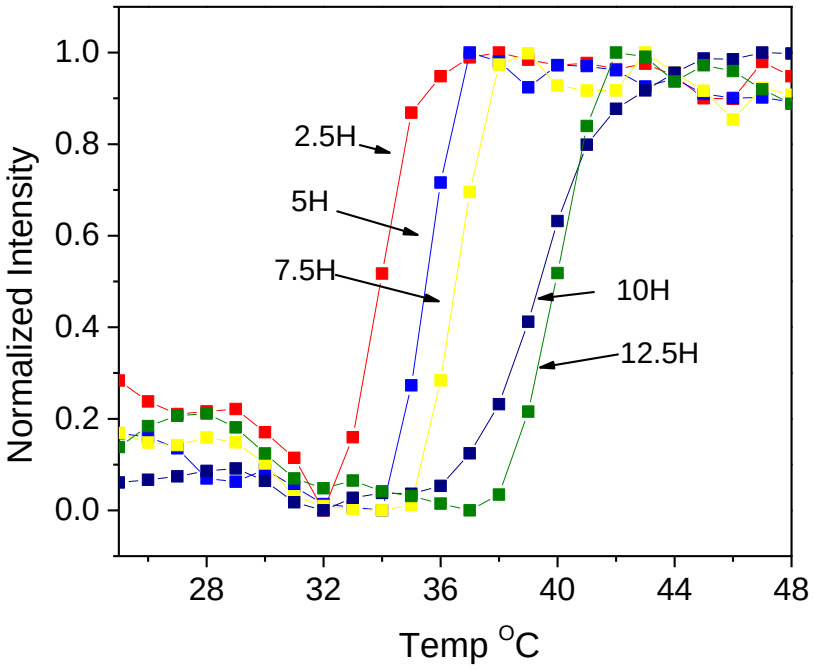

Figure 5.5. Light intensity versus temperature of pNIPAAm-*co*-HMAAm (2.5-12.5 mol %) by a Rotogene Q fluorescence detector (510 nm) (real-time PCR machine).

The LCST''s calculated by either UV-Vis, or light scattering spectroscopy were performed in triplicate to establish the accuracy of the method. The LCSTs were calculated by plotting the temperature versus the rate of change which produced a maximum value and this value was taken to be the LCST. Triplicate measurements of the LCSTs by UV-Vis returned the same value for the LCST, with no error found in the standard deviation. Triplicate analysis of the LCSTs by light scattering found that there was a ± 0.6 ^{O}C standard deviation in the LCST value found for 2.5H, 5H, 7.5H, 10H and 12.5H

Table 5.2. LCSTs pNIPAAm-*co*-HMAAm, by UV-Vis and light scattering spectroscopies. SA copolymers LCSTs by Light scattering.

pNIPAAm-*co*-HMAAm	LCST [a] (^{O}C)	LCST [b] (^{O}C)	SA	LCST [b] (^{O}C)
2.5H	30.0	33.3 ± 0.1	2.5S	36.1 ± 0.1
5H	30.5	35.7 ± 0.6	5S	35.3 ± 0.6
7.5H	32.0	36.7 ± 0.6	7.5S	34.0 ± 0.0
10H	34.0	38.3 ± 0.6	10S	39.3 ± 0.6
12.5H	36.5	40.3 ± 0.6	12.5S	39.0 ± 1.0

[a] Determined by UV-Vis spectroscopy. [b]Determined by light scattering (Rotogene Q).

As the light scattering events can potentially lead to variances in the light intensities, the data was then processed via a five-point Savitzky Golay smoothing function to see if a more precise value for the LCSTs could be obtained (data not shown). The smooth function had no effect on the value or error in the LCSTs calculated by light scattering. A plot of the LCST versus HMAAm content showed a linear relationship between the LCST and HMAAm, where Y = 0.6667x + 31.38 with an R^2 value of 0.9874. The R^2 improved from the UV-Vis method of analysis previously performed where an R^2 of 0.946 was reported. The LCSTs determined by UV-Vis spectroscopies were found to be lower in value, beginning at 30 ^{O}C for 2.5H and increased proportional to HMAAm content up to an LCST of 36.5 ^{O}C for 12.5H. The LCSTs calculated by light scattering started at 33.3 ^{O}C for 2.5H and then increased proportional to HMAAm content to reach 40.7 ^{O}C for 12.5H.

The observed change in light intensities at the LCSTs found for pNIPAAm-*co*-HMAAm (2.5-12.5 mol %) did not vary significantly (Figure 5.5). It was observed that light intensity increased at around the previously determined LCSTs found by UV-Vis (Table 6). This increase in light intensity is thought to occur due to scattering effects of the aggregates that form at the LCST of the copolymers. The results by light scattering were consistent with the trend observed by UV-Vis analysis where a drop-in transmittance due to the change in transparency at a specific temperature changed with increasing HMAAm content. Although the LCSTs differed by UV-Vis analysis and light scattering, the trend that was observed was the same. It is proposed that the LCSTs found by light scattering were more accurate than those found by UV-Vis spectrometry based on the R^2 value from the linear fit of the data and the low errors associated with heating the tubes when using the real-time PCR instrument (see Chapter 2, Section 2.8.8). Having established the real-time PCR machine as a method capable of calculating the LCST of pNIPAAm-*co*-HMAAm copolymers, the change in the LCSTs of the copolymers after esterification with the DBCO-acid was calculated. Figure 5.6 shows the raw data for light intensity versus temperature for pNIPAAm-*co*-HMAAm (2.5H, 5H, 7.5H, 10H and 12.5H) and pNIPAAm-*co*-HMAAm-*co*-SA (2.5S, 5S, 7.5S, 10S and 12.5S). Table 5.2 shows the change in the LCSTs observed

by light scattering after esterification. The 2.5H increased its LCST by approximately 2.8 ^{O}C ± 0.1, 5H decreased by 0.4 ^{O}C ± 0.6, 7.5H decreased by 2.7 ^{O}C ± 0.0, 10H increased by 1.0 ^{O}C ± 0.6 and 12.5H decreased by 1.3 ^{O}C ± 1.0. There are errors in calculating the LCSTs by the light scattering method but the change in light intensity and the change in the temperature at which that occurs suggests that a change in the solution properties does occur when the DBCO is attached to the copolymers. When comparing the relative intensity of 2.5H and 2.5S (Figure 5.6 a) it is observed that the 1/10-fold change in intensity for 2.5H was smaller at the LCST compared with an increase of approximately 1/5-fold for 2.5S. 2.5S also has a higher initial intensity under the same conditions. This trend continued with 5H and 5S (Figure 5.6 b) where the change in intensity for 5H was approximately 1/5-fold compared with 4/5-fold for 5S. Indeed 7.5H, 10H and 12.5H (Figure 5.6 c-e) all showed an increase in intensity at the LCST of approximately 1/5-fold. However, 7.5S, 10S and 12.5S (Figure 5.6 c-e) increased in intensity approximately 1-fold. It can clearly be seen from close inspection of the 5H and 5S fluorescent data (Figure 5.6 f) that the intensity transition is greater at the LCST and it also broadens for 5S when compared with 5H.

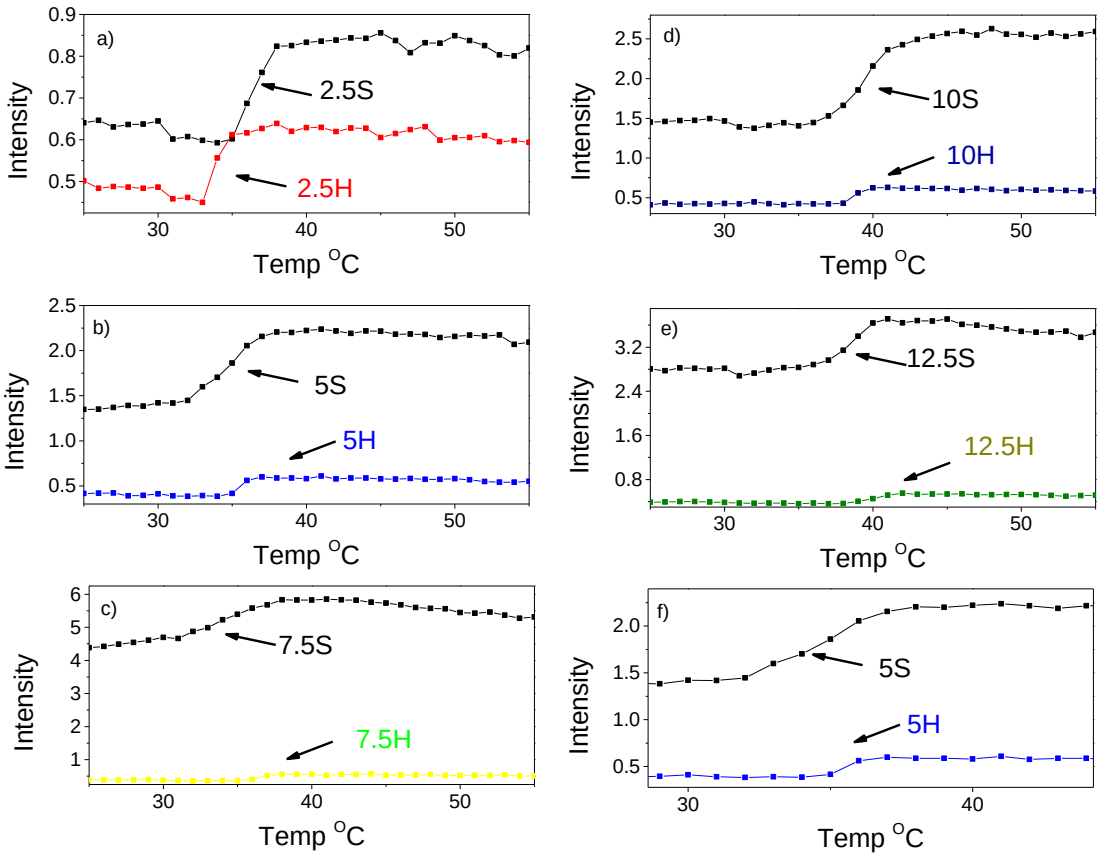

Figure 5.6. Light scattering intensity for a) pNIPAAm-*co*-HMAAm (2.5H) and pNIPAAm-*co*-HMAAm-*co*-SA (2.5S), b) pNIPAAm-*co*-HMAAm (5H) and pNIPAAm-*co*-HMAAm-*co*-SA (5S), c) pNIPAAm-*co*-HMAAm (7.5H) and pNIPAAm-*co*-HMAAm-*co*-SA (7.5S), d) pNIPAAm-*co*-HMAAm (10H) and pNIPAAm-*co*-HMAAm-*co*-SA (10S), e) pNIPAAm-*co*-HMAAm (12.5H) and pNIPAAm-*co*-HMAAm-*co*-SA (12.5S), and f) pNIPAAm-*co*-HMAAm (5H) and pNIPAAm-*co*-HMAAm-*co*-SA (5S).

All the SA copolymers were found to have a broader transition at the LCST which makes a precise LCST value for this transition more difficult to calculate. Figure 5.7 shows the normalised light intensity versus temperature data for SA copolymers (2.5S, 5S, 7.5S, 10S, and 12.5S).

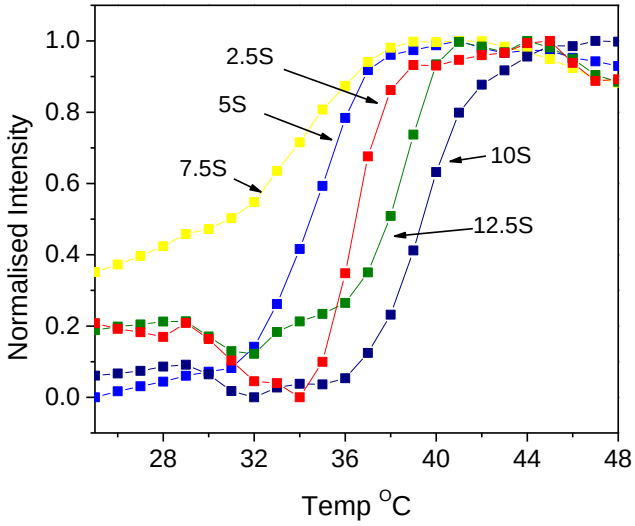

Figure 5.7. Light intensity versus temperature after DBCO coupling by Rotogene Q fluorescence detector (510 nm).

The light scattering results shown by Figure 5.6 (a-f) and Figure 5.7 showed that some of the SA copolymer samples had a significant decrease in their LCST (7.5H and 12.5H). The 2.5H sample had an increase in LCST, which was consistent with ATR-FTIR results and ^{1}H NMR results. Considering the error in calculating the LCSTs for the 10H and 5H samples appeared to have the same LCST. However, Figure 5.6 does show that their LCSTs broaden after SA coupling. The variation in light scattering of all SA copolymers is theorised to occur due to the successful esterification reaction of HMAAm with DBCO-acid. The pNIPAAm-*co*-HMAAm (2.5H-12.5H) copolymers reaction with DBCO produced SA (2.5S-12.5S) copolymers as shown by NMR and ATR-FTIR analysis and through their change in their subsequent LCSTs. There appears to be many advantages of using the real time PCR machine as method of analysing the LCSTs of temperature responsive polymer bioconjugates. The volume required for analysis of a DNA polymer bio-conjugate is small (20 µL). Thus being able to measure the LCST of the polymer bio-conjugates when there is a limited supply of the sample is a useful advantage. Also as the real-time PCR machine is designed for controlling temperature, it is a very simple process to run a temperature ramp for measuring the LCSTs. Another advantage of this method, is the fact that multiple samples can be analysed making it a very fast method of analysis.

5.4 Synthesis of TR-PCR Bio-conjugates in a One Pot PCR "Click" Reaction

A SA copolymer (10S) was used to produce TR-PCR bio-conjugates. Initial conjugation experiments involved performing the PCR reaction and the SPAAC reaction of an azide end functionalised PCR product with the SA copolymer (10S) in one pot. 5'Azide PCR primers were used in a PCR reaction to produce an azide functionalised ds-DNA, termed PCR-Az (see Chapter 2, Section 2.8.8.1 for experimental details). Scheme 5.2 shows the different reaction pathways that may occur to produce TR-PCR bio-conjugates in a one pot reaction. The path 1 (red box, left, Scheme 5.2) is where the PCR reaction (labelled PCR, middle) proceeds first to produce the PCR product and then this is followed by the "click" reaction with the SA copolymer. Path 2 (purple rectangle, right, Scheme 5.2) could involve the forward primers "click" reaction with the SA functionalised copolymer (labelled P, Scheme 5.2) and then this reaction could be followed by a PCR reaction. Agarose gels and melt curve analysis using SG were used to characterise the TR-PCR bio-conjugates.

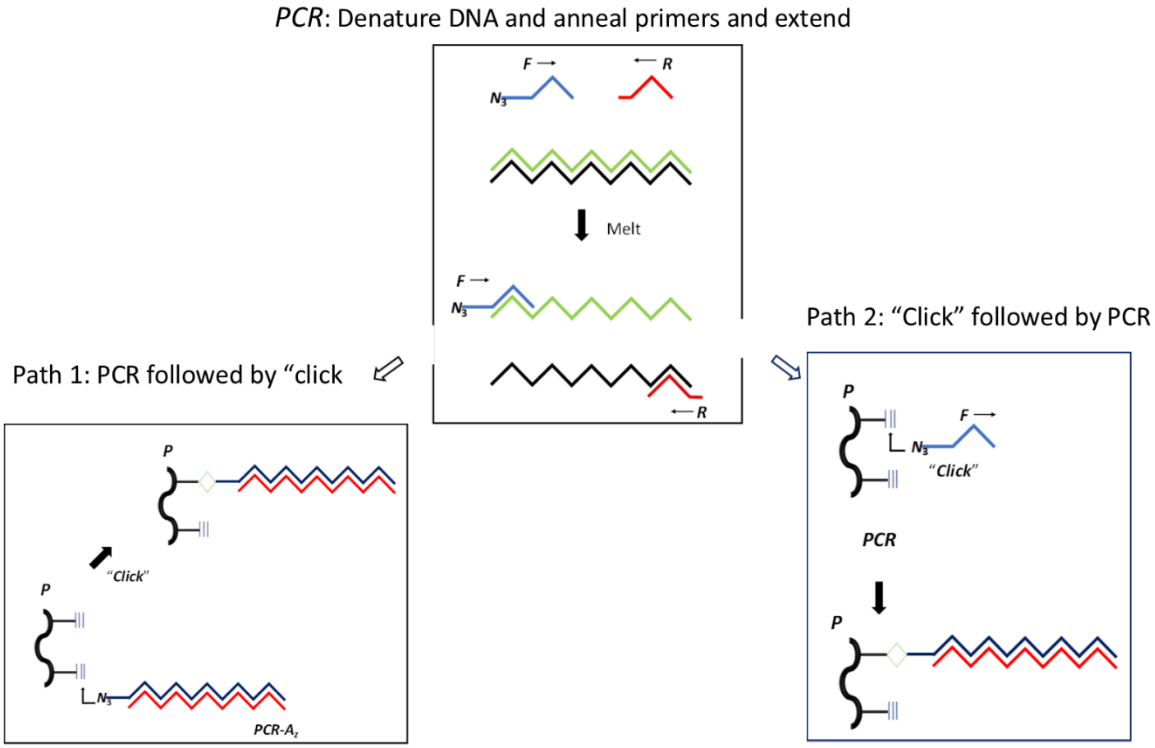

Scheme 5.2. Scheme for one pot PCR "Click" reaction.

The TR-PCR bio-conjugates produced from the reaction scheme, depicted in Scheme 5.2 were run down an agarose gel along with the relevant controls. The gel was stained, using ethidium bromide and visualised using a gel doc instrument (See Chapter 2 Section 2.8.7 for experimental details). Figure 5.8, shows the agarose gel results, from the conjugation experiment, with a SA copolymer (10S). In lane 1, a 50 bp ladder,

serves as a molecular weight marker for the migration of the 63 bp PCR-Az product; the band that is seen the furthest down the gel, represents DNA that is 50 bp long. Lane 2, shows the control PCR-Az product without polymer. The migration of the control PCR-Az is slower than the 50 bp DNA in lane 1. The control reaction using a PCR primer not end functionalised with an azide and the SA copolymer was isolated from a one pot PCR reaction. The control product was then run in lane 3. The band that is visible in the agarose gel shows an equivalent migration to that of the PCR-Az product (control) in lane 2. The result indicates that PCR was successful in the one pot reaction and that the polymer did not interfere with PCR in this experiment.

The reaction product isolated from the one pot PCR click reaction between SA copolymer and the PCR-Az product is shown in lane 4. The observed difference in the migration bands of the PCR-Az product control in lane 2 and the potential conjugate product (TR-PCR bio-conjugate) in lane 4 was small. The gel shows that the band is further down the gel.

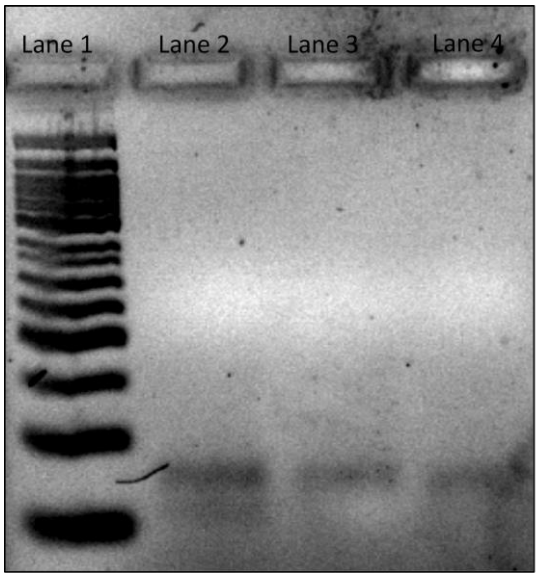

Figure 5.8. Agarose gel, lane 1, 50 bp ladder, lane 2 PCR-Az product, lane 3 PCR + SA (control), and lane 4 TR-PCR bio-conjugate.

To confirm that the product in lane 4 was a TR-PCR bio-conjugate product, the melt curve of this product was investigated using a real-time PCR instrument (see Chapter 2, Section 2.8.8.5 for experimental details). When DNA and SG are mixed in aqueous solution, the intercalation of SG into DNA results in a fluorescence signal that can be measured by a real-time PCR machine. When DNA reaches a critical temperature, the DNA melts or denatures as the hydrogen bonds between the bases are disrupted. The denaturing of DNA leads to a reduction in the observed fluorescence signal as the SG molecule moves from a constrained hydrophobic environment (inside DNA) to one that is unconstrained and hydrophilic (outside DNA). This causes the fluorescence of SG to decrease (quench) and this decrease can be measured by the real-time PCR instrument. The melt curves of one pot PCR click reaction products were analysed by mixing the reaction products with SG in a centrifuge tube and then measuring the fluorescence intensity of SG using a real-time PCR machine

(see Chapter 2, Section 2.8.8.5 for experimental details). Figure 5.9 a) shows the melt curve of the PCR-Az product (black curve), the potential TR-PCR bio-conjugate SG, labelled PCR-Az-SA (red curve) and the control labelled PCR + SA (blue curve). The fluorescence intensity for the PCR-Az product remained constant from 25 ^{O}C to 40 ^{O}C but began to steadily decrease after 40 ^{O}C to almost zero intensity at 100 ^{O}C. Both the PCR-SA product and the control (PCR + SA) product (Figure 5.9 a) showed a lower initial fluorescence intensity when compared to the PCR-Az control. The fluorescence intensity for the PCR-SA product also remained constant from 25 ^{O}C to around 50 ^{O}C and then the intensity began to decrease gradually to reach a much lower intensity (less than 90 % of initial intensity) at 100 ^{O}C. The PCR + SA control (blue curve, Figure 5.9 a) melt curve appeared to match the melt curve of PCR-SA (red curve, Figure 5.9 a).

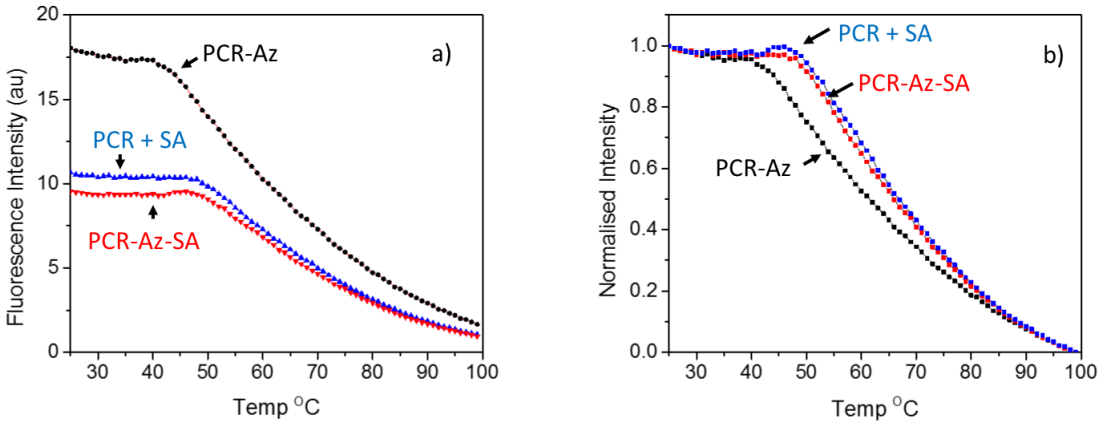

Figure 5.9. Melt curves of one pot PCR click reaction products for, a) PCR-Az (black line), PCR + SA (blue line) and PCR-Az-SA (red line) and b) Normalised melt curves of one pot PCR click reaction products for PCR-Az (black line), PCR + SA (blue line) and PCR-Az-SA (red line).

When each of the melt curves PCR-Az product (black curve), PCR-Az-SA (red curve) and the control labelled PCR + SA (blue curve) shown in Figure 5.9 a were normalised, some differences in the initial melt temperatures were observed. The PCR-Az is shown to melt at 40 ^{O}C, whereas the PCR-SA and PCR + SA melt closer to 50 ^{O}C (Figure 5.9 b). Also, the PCR + SA control appears to increase in intensity at approximately 40 ^{O}C whereas the PCR-Az-SA products intensity remains constant.

It was proposed that the increase in intensity observed for the PCR + SA control is due to the SA polymer intercalating SG as it reaches its LCST. The PCR-Az-SA remains constant because it is a TR-PCR bio-conjugate product and this has resulted in a change in the melt temperature of the initial PCR-Az as well as a change to LCST of the initial SA copolymer. Further experiments were conducted to confirm this hypothesis. These experiments involved performing PCR to produce PCR products and then attempting the click reaction in different solvent conditions.

5.5 TR-PCR Bio-conjugates via Click Reaction in Aqueous Solution.

Scheme 5.3 shows, the general synthetic pathway to produce TR-PCR bio-conjugates. In step one, 5'Azide PCR primers were used in a PCR reaction to produce an azide functionalised ds-DNA, termed PCR-Az. In step two, the PCR-Az product was conjugated to SA polymer (10S). The SA polymer and the PCR-Az were mixed together in a centrifuge tube along with SG. The centrifuge was heated from 25 ^{O}C to 99 ^{O}C using a temperature ramp (8 cycles). The reaction was monitored by measuring the SG intensity over time (see Chapter 2, Section 2.3.5 and 2.8.8.5 for experimental conditions).

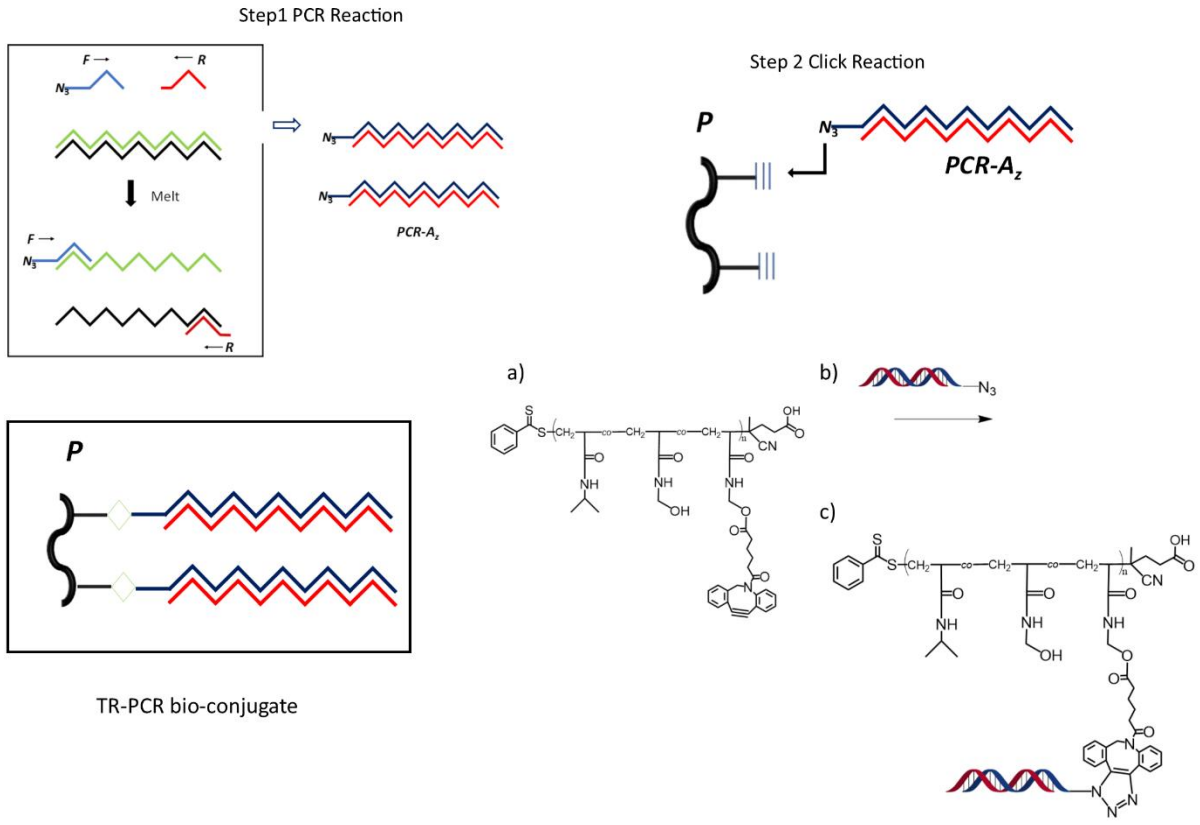

Scheme 5.3. Step 1) PCR reaction to produce PCR-Az product. Step 2) Click reaction where a) pNIPAAm-*co*-HMAAm-*co*-SA copolymers react with b) azide functionalised double stranded DNA (ds-DNA) to generate c) pNIPAAm-*co*-HMAAm-*co*-SA-*co*-ds-DNA functionalised polymer (TR-PCR bio-conjugate).

Figure 5.10 a show the melt curve for the PCR-Az product. Initially, the measured SG fluorescence intensity for the PCR-Az product was high, but the intensity began to decrease when the temperature reached approximately 48 ^{O}C. The temperature point where intensity begins to decrease is thought to represent the start of the melt curve. The SG intensity for the PCR-Az product continued to gradually decrease as the temperature was ramped to 100 ^{O}C. When the TR-PCR bio-conjugate (Figure 5.10 b) melt curve was measured by the real-time PCR machine, its melt curve did not match that which was observed for the PCR-Az control. Firstly, the fluorescence intensity of the TR-PCR bio-conjugate was reduced when compared to the PCR-Az control.

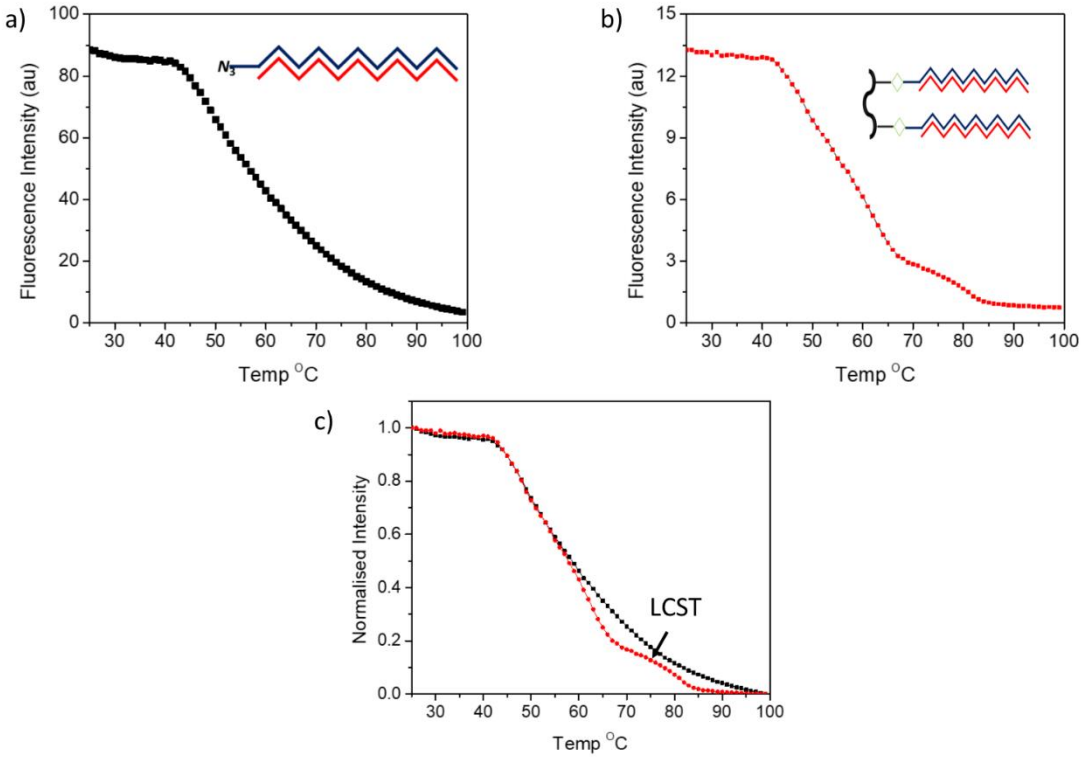

Figure 5.10. a) Melt curve for the PCR-Az product (black line), b) melt curve for TR-PCR bio-conjugate (red line) and c) normalised melt curves of PCR-Az product and TR-PCR bio-conjugate.

The measured intensity for the TR-PCR bio-conjugate also decreased as the temperature increased. However, the TR-PCR bio-conjugate product melt curve gradient appeared much faster. Finally, at approximately 70 ^{O}C the fluorescence intensity of SG was observed to increase. It is theorised that this intensity increases for the TR-PCR bio-conjugate product may be due to a change in the LCST of the TR-PCR bio-conjugate product. Figure 5.10 c shows the normalised intensity of PCR-Az control and the TR-PCR bio-conjugate. The intensity gradient of the TR-PCR bio-conjugate melt curve decreases at a faster rate than the PCR Az melt curve. Also, a significant increase in fluorescence intensity at approximately 70 ^{O}C is observed for the TR-PCR bio-conjugate. The PCR-Az product control (Figure 5.10 c) showed no such increase in fluorescence intensity at this temperature. The results of the one pot PCR click reaction indicate that the click reaction between PCR-Az and SA copolymer produced TR-PCR bio-conjugates.

The melt curve for the copolymer control reaction product (pNIPAAm-*co*-HMAAm (10H) + PCR-Az) (Figure 5.11 a) was different to the PCR-Az control (Figure 5.10 a) and the TR-PCR bio-conjugate (Figure 5.10 b). SG fluorescence intensity is observed to increase as temperature is increased from 25 ^{O}C to 40 ^{O}C, and then at 40 ^{O}C, a jump in intensity is observed followed by a steady decrease in intensity after 50 ^{O}C. The reason for the increase in SG intensity (at 40 ^{O}C) can be explained by the results shown in Figure 5.11 b. The SA copolymer (10S) and the 10H copolymer were added to an aqueous solution along with SG and then they were subjected to the same melt curve analysis conditions in the real-time PCR machine. Figure 5.11 b shows

that both the 10S copolymer (green curve) and 10H copolymer (blue curve) intercalate SG, since fluorescence intensity increases as the polymers approach their LCSTs. This result was expected as this has been shown to occur previously (see Chapter 4, Section 4.4).

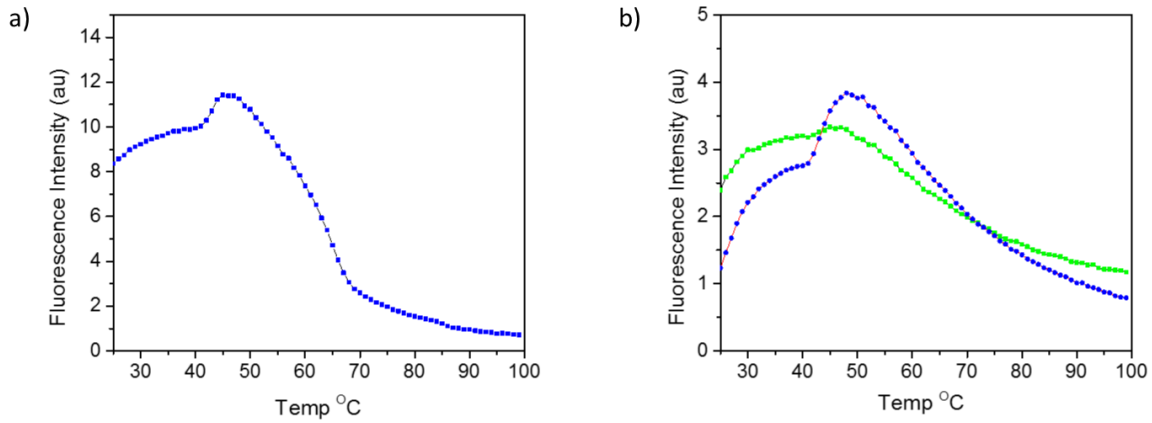

Figure 5.11. a) Melt curve for the copolymer control reaction product (pNIPAAm-co-HMAAm (10H) + PCR-Az) (blue line) and b) melt curve for SA copolymer (10S) (green line) and the 10H copolymer (blue line).

These results confirm that the 10H copolymer did not react with the PCR-Az product. These results also suggest that the melt curve shown in Figure 5.10 b is due to the successful conjugation of SA copolymer to PCR-Az product. To understand any solvent effects and to establish how fast the SA copolymer reacted with the PCR-Az product, an experiment was devised to test the speed of the reaction in a buffer solution

5.6 Synthesis of TR-PCR Bio-conjugates Click in Buffer

The impact the buffer had on the conjugation was investigated by a click experiment in buffer. A pre-prepared PCR-Az product was reacted with the SA copolymer by heating in a real-time PCR machine using a temperature ramp. SG was also added so that the progress of the reaction could be monitored in real time (see Chapter 2, Section 2.3.5 and 2.8.8.5 for experimental conditions). Figure 5.12 a) shows the fluorescence intensity of SG as the temperature was increased. Initially the fluorescence intensity is seen to be stable from 25 ^{O}C to around 40 ^{O}C, then, there is an increase in fluorescence intensity at 40 ^{O}C, followed by a gradual decrease in fluorescence as the temperature is increased to 100 ^{O}C. After the temperature reached 100 ^{O}C, the solution was cooled back down to 25 ^{O}C and then the reaction mixture was heated again using the same temperature ramp. Figure 5.12 b shows the fluorescence intensity of the second run. The fluorescence intensity appears to have dropped from its previous level and the increase at 40 ^{O}C is also not as significant.

The melt curve also appears to have inflection points at around 50 ^{O}C which suggests that the LCST of the SA copolymer may have shifted to a higher temperature when it was conjugated to the PCR-Az product. After cooling the reaction back to 25 ^{O}C, the click reaction was heated for a third time using the same temperature

ramp. Figure 5.12 c shows that the fluorescence intensity has decreased again when compared to the previous runs. Also, there is a decrease in intensity at 40 ^{O}C instead of an increase as was seen previously. The melt curve also shows some inflection points at 45 ^{O}C and 50 ^{O}C, which may be due to the shift in the LCST of the SA copolymer as PCR-Az is being attached to the SA copolymer backbone. The melt curve data shown in Figure 5.12 (a-c) suggested that the click reaction between the SA polymer and the PCR-Az product occurs rapidly.

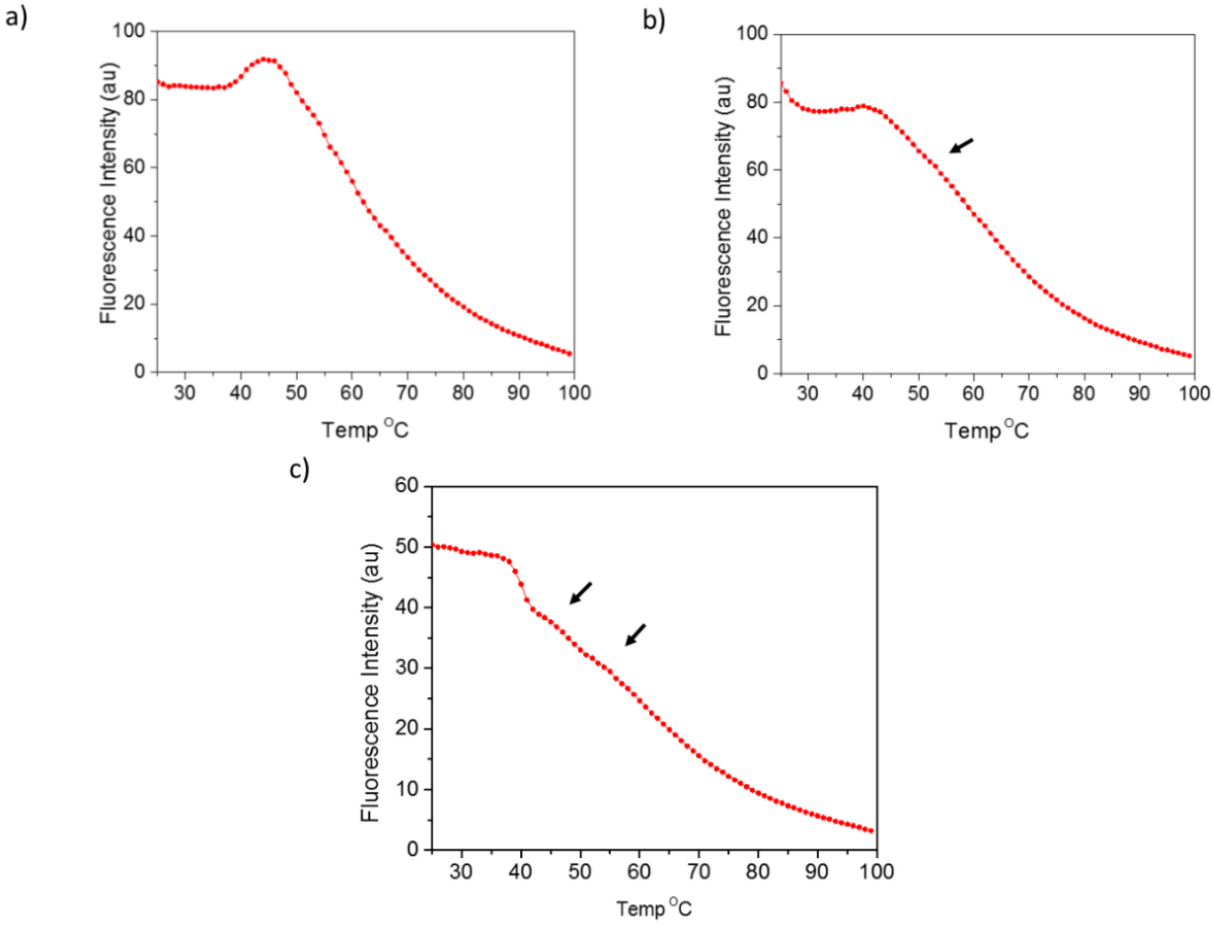

Figure 5.12. Melt curves for reaction between PCR-Az and PCR-Az in buffer, a) run 1, b) run 2 and c) run 3.

The successful conjugation appears to affect the intercalation of SG into DNA and the LCST of the SA copolymer. It is also likely, given the rapid nature of the click reaction, that the azide primer used in the previous one pot PCR click experiment (Chapter 5, Section 5.5) could react with the SA copolymer during the PCR reaction. The reaction product of the click experiments after only one heating cycle was run down an agarose gel to confirm the conjugation product. Figure 5.13 shows the agarose gel results from the one pot click experiment, with a SA copolymer (10S) and the PCR-Az product. In lane 1, Figure 5.13, is the 50 bp ladder, in Lane 2 the band observed represents the PCR Az control. Lane 3 shows another band that has a similar migration to the PCR-Az control in lane 2. This band is also a control, this band represents the reaction

product of a 63 bp PCR product (not end functionalised with an azide) and SA polymer (10S). The band in lane 3 does not appear to have a different migration through the gel when compared to the PCR-Az control in lane 2.

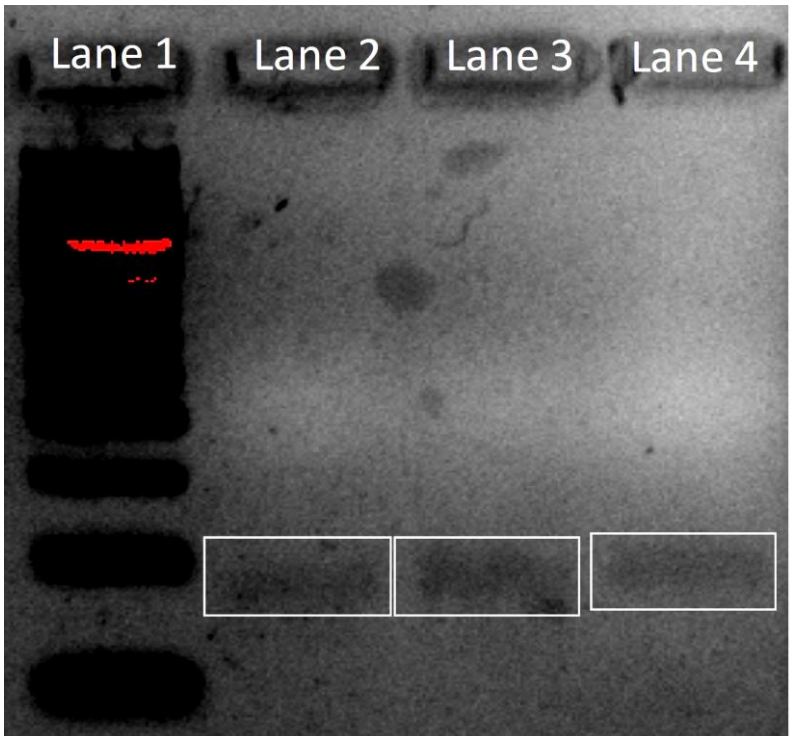

Figure 5.13. Agarose gel, lane 1, 50 bp ladder, lane 2 PCR-Az product (control), lane 3 PCR product (control), and lane 4 TR-PCR bio-conjugate.

The band observed in lane 4, Figure 5.13 represents the reaction product of the click reaction (one heating cycle) between the PCR-Az product and the SA copolymer. The band for the conjugation product (lane 4, Figure 5.13) is faint and has slower mobility through the agarose gel, however, these results were not conclusive in showing the conjugation product. It was theorised that conjugation efficiency could be improved by suppressing the LCST of the SA copolymer. Therefore, another click experiment was conducted in organic solvent.

5.7 Synthesis of TR-PCR Bio-conjugates in a Click Reaction in Acetonitrile.

The SA (10S) copolymers were conjugated to PCR products in acetonitrile. First, 5' azide and 3' alkyne PCR primers, were used in a PCR reaction to produce an azide and alkyne functionalised ds-DNA which was 63 bp long, termed PCR-AzA (see Chapter 2, Section 2.3.5 and 2.8.8.5 for experimental details). The 5' azide PCR product was then conjugated to the SA copolymers, to give new TR-PCR bio-conjugates. The TR-PCR bio-conjugates products were characterised by agarose gel electrophoresis. (see Chapter 2, Section 2.8.7 for experimental details). The TR-PCR bio-conjugates produced from the click reaction were run down an agarose

gel along with the relevant controls. The gel was stained, using ethidium bromide and visualised using a gel doc instrument. Figure 5.14 a, shows the agarose gel results, from the conjugation experiment, with a SA copolymer (10S). In lane 1, a 50 bp ladder, serves as a molecular weight marker for the migration of the 63 bp PCR-AzA product; the band that is seen the furthest down the gel, represents DNA that is 50 bp long. Lane 2, shows the control PCR-AzA product as produced by the PCR reaction (Figure 5.14 a); its migration through the gel is higher than the 50 bp band. The PCR-Aza 63 bp migration through the gel, is consistent with the expected migration when compared to the DNA molecular weight markers, shown in lane 1, Figure 5.14 a.

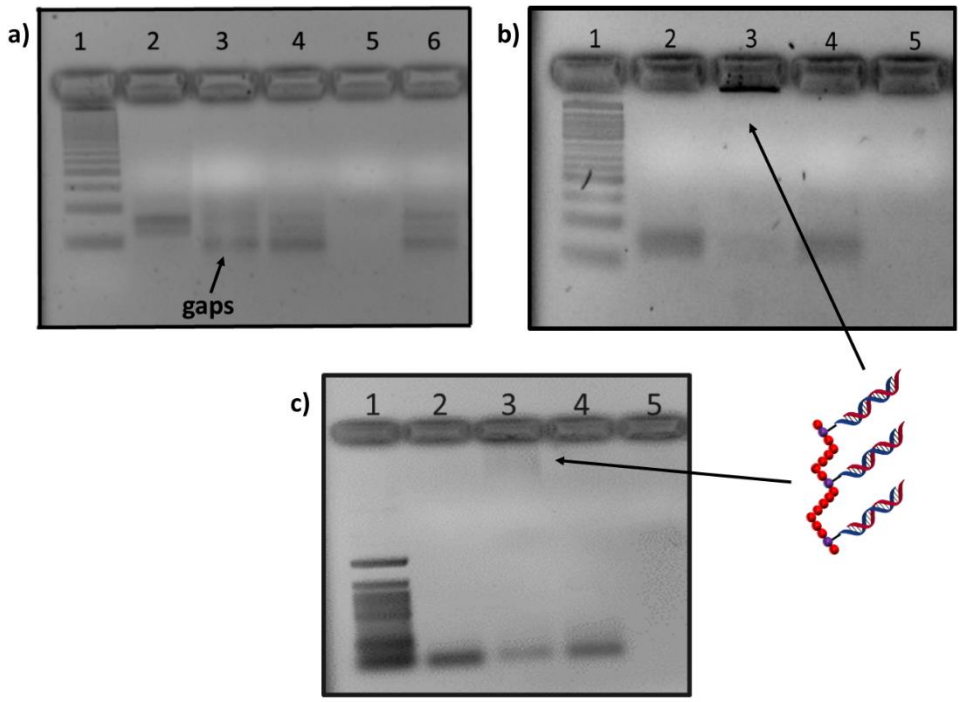

Figure 5.14. a) Gel electrophoresis (5% agarose) of 50-1350 bp DNA ladder (lane1), control 63 bp PCR-AzA (lane 2), 63 bp PCR-AzA + SA copolymer (10S) (lane 3), control 63 bp PCR-AzA (lane 4), control SA copolymer (10S) (lane 5), and control pNIPAAm-*co*-HMAAm (10H) + 63 bp PCR-AzA (lane 6) b) Gel electrophoresis (5% agarose) of 50-1350 bp DNA ladder (lane1), control 63 bp PCR-Az (lane 2), 63 bp PCR-Az + SA copolymer (10S) in acetonitrile (lane 3),) and 63 bp PCR-Az in acetonitrile (lane 4) and control SA copolymer (10S) (lane 5) and d) Gel electrophoresis (1.5% agarose) of 50-1350 bp DNA ladder (lane1), control 63 bp PCR-Az (lane 2), 63 bp PCR-Az + SA copolymer (10S) in acetonitrile (lane 3), 63 bp PCR-Az in acetonitrile (lane 4) and control SA copolymer (10S) (lane 5).

The reaction between the SA copolymer (10S) and PCR-AzA, is shown in lane 3, Figure 5.14 a. A change in the PCR-AzA migration pattern, lane 3 (Figure 5.14 a), is observed relative to lane 2; three bands were observed and some gaps in those bands were also observed. In Lane 4, a PCR-AzA negative control sample, was exposed to the same experimental conditions used in the conjugation experiment. The negative PCR-AzA control also showed a change in the migration of PCR-AzA, relative to lane 2, with three clear bands observed, but this time, no gaps in those bands were observed. The SA copolymer (10S) (lane 5), was used as a negative control; no band was observed for the SA copolymer (10S). The pNIPAAm-*co*-HMAAm copolymer (10H), without the SA alkyne functionality (lane 6, Figure 5.14 a), was also used as a negative control. The negative pNIPAAm-

co-HMAAm copolymer (10H) control, showed three bands, which resembled the migration of PCR-AzA, observed in lane 4. The results obtained from the agarose gel, (Figure 5.14 a) indicate that PCR-AzA, may have reacted with the SA copolymer (10S), due to the gaps in the bands, observed in lane 3. The results from the negative PCR-AzA controls, that were run in water (lane 2) and in acetonitrile (lane 4), suggested that there may have been solvent effects or some other side reactions occurring with the alkyne functionalised PCR strand of the ds-PCR product.

The copolymer without the SA functionality, (lane 6) did not appear to react with the PCR-AzA product. It was theorised that the gaps in the bands observed in Figure 5.14 a, lane 3 were due to the PCR-AzA products reaction with the SA copolymer. A successful reaction could result in a lower concentration of DNA being observed in the gel. It was also theorised based on previous results that the intercalation of SG into DNA will be affected by its conjugation to SA copolymers. This may result in no bands being observed when running gels because the DNA bio-conjugate will have a reduced capacity to intercalate SG.

To test if the alkyne functionality of the PCR-AzA product was reacting, to give side reactions, under experimental conditions; a newly prepared PCR product that was 63 bp long, containing only the 5'azide functional group termed PCR-Az was used in the conjugation of a PCR product to a SA copolymer (10S). The PCR-Az and SA copolymer (10S) (lane 3, Figure 5.14 b)), were run onto a 5% agarose gel to determine if the "click" reaction between the SA copolymer and the PCR-Az product had been successful. The migration of PCR-Az through the agarose gel, lane 3, (Figure 5.14 b) for the PCR-Az + SA copolymer (10S), differed significantly when compared to the migration into the gel of the control PCR-Az (lane 2) and the negative control (lane 4, PCR-Az). There was no change in the migration of the negative control PCR-Az (lane 4) with acetonitrile. The strong band visualised in the top of the well, lane 3, Figure 5.14 b is thought to be a high molecular weight TR-PCR bio-conjugate. Results from Figure 5.14 b also suggest that the alkyne functionality of the PCR-AzA product (Figure 5.14 a), had reacted under the previous experimental conditions to give side products. Again, no band was observed for the negative control SA copolymer (10S) (lane 5, Figure 5.14 b). It was expected that the TR-PCR bio-conjugate should migrate into an agarose gel which had been prepared with a lower percentage of agarose. Further analysis of the synthesised TR-PCR bio-conjugate was performed using a 1.5% agarose gel. Lane 1, Figure 5.14 c, shows the increased mobility of the 50 bp molecular weight standards through the gel, due to reduced resistance from the lower percentage agarose gel. The 1.5% gel of the PCR-Az + SA copolymer (10S) in lane 3, Figure 5.14 c, showed a faint smeared band migrating into the gel and another band which matched the original control PCR-Az product (lane 2, Figure 5.14 c). There was no change in the migration of the PCR-Az control (lane 4, Figure 5.14 c) with acetonitrile and no band was observed for the negative control SA copolymer (10S) (lane 5, Figure 5.14 c). The agarose gel results (Figure 5.14 c), suggest that conjugation between the PCR-Az and the SA copolymer had occurred, but that the conjugation efficiency may not have reached 100 % conversion; as evidenced by the presence of the

secondary band in lane 2, Figure 5.14 c. The high molecular weight TR-PCR bio-conjugate visualised as the strong band in lane 3, at the top of the well (Figure 5.14 b) was cut out of the gel (Figure 5.15) and then the TR-PCR bio-conjugate was extracted and purified in water (see Chapter 2 Section 2.8.4 for experimental details). The TR-PCR bio-conjugate and a PCR-AZ control were placed in centrifuge tubes along with SG and the change in SG fluorescence was measured using a real-time PCR machine (see Chapter 2, Section 2.8.5 for experimental details).

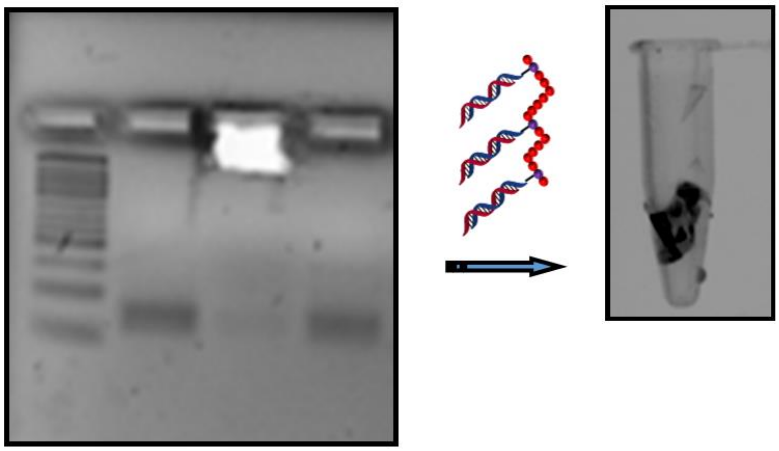

Figure 5.15 TR-PCR bioconjugate gel extraction for gel electrophoresis (5% agarose) of 50-1350 bp DNA ladder (lane1), control 63 bp PCR-Az (lane 2), 63 bp PCR-Az + SA copolymer (10S) in acetonitrile (lane 3),) and 63 bp PCR-Az in acetonitrile (lane 4).

The SG fluorescence intensity decreases steeply (approximately 50%) for the TR-PCR bio-conjugate between 25 ^{O}C to 40 ^{O}C (Figure 5.16 a). After 40 ^{O}C, the decrease in SG fluorescence intensity for the TR-PCR bio-conjugate flattens out and even increases at around 50 ^{O}C. The SG fluorescence intensity also decreases for the control PCR-Az (Figure 5.16 b) but the decrease is more prominent after 50 ^{O}C, however there is no observed increase in SG intensity after 50 ^{O}C. Figure 5.16 c shows the normalised fluorescence intensity of the TR-PCR bio-conjugate compared with the PCR-Az product. The change in the melt profile of the TR-PCR bio-conjugate compared to the PCR-Az control appears to be significant, suggesting that the conjugation of the temperature responsive polymer (pNIPAAm-*co*-HMAAm-*co*-SA, 10S) to the PCR-Az product has influenced the melt temperature of the PCR-Az product.

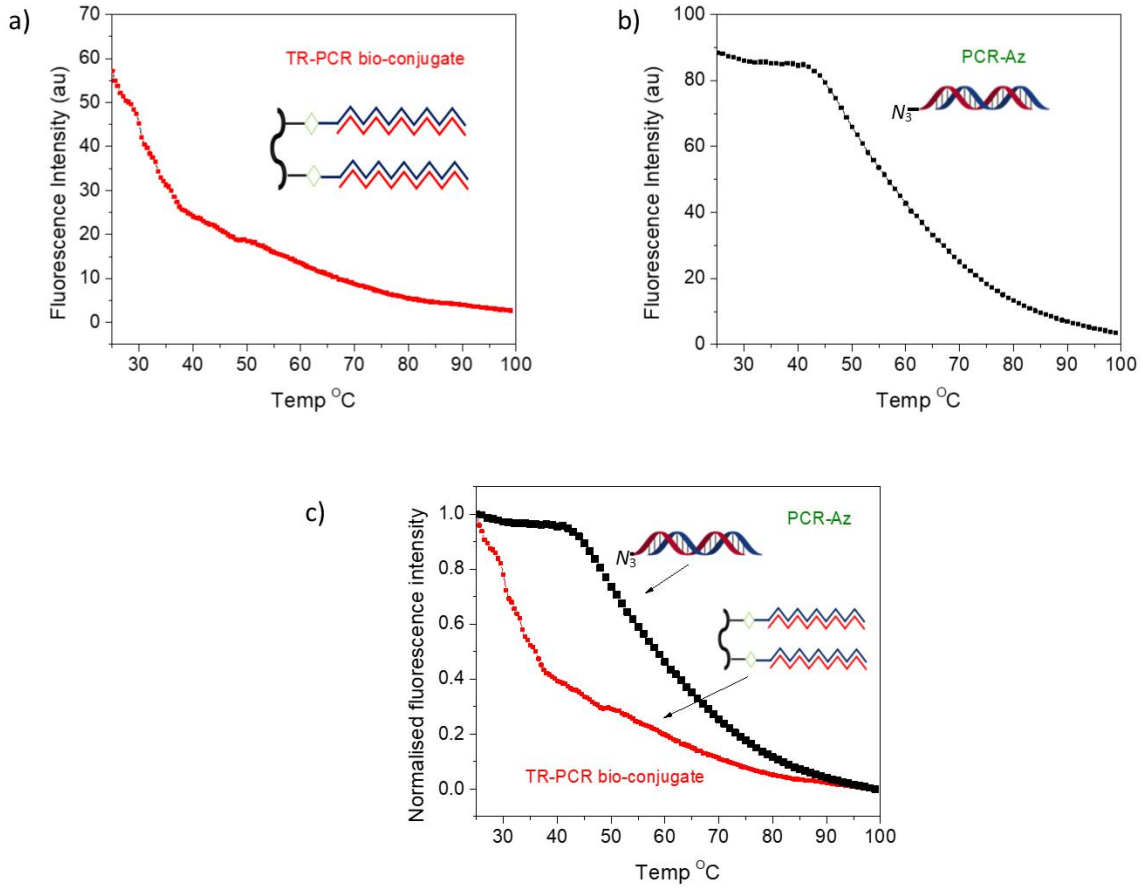

Figure 5.16.a), Melt curve for TR-PCR bio-conjugate b), melt curve for PCR-Az and c) normalised melt curve for TR-PCR bio-conjugate and PCR-Az

The pNIPAAm-*co*-HMAAm (10H) copolymer has been shown previously to uptake SG, as it forms aggregates at its LCST (see Chapter 4, Section 4.3). It was expected that the conjugation of a temperature responsive polymer to amphiphilic DNA should impact the LCST of the polymer. Figure 5.16 c shows an inflection point at 50 ^{O}C indicating that SG is being incorporated back into a hydrophobic environment. These results suggest that the SA copolymers (10S) LCST has shifted to a higher temperature when it was conjugated to the PCR-Az product. Under previous conjugation conditions in both the one pot PCR click reaction and the click reaction in buffer, melt curve analysis did not show as large a difference between the PCR-Az control and the TR-PCR bio-conjugate product. The significant difference between the melt curve of the PCR-AZ product and the melt curve of the TR-PCR bio-conjugate (Figure 5.16 c) suggests that the conjugation to the polymer was greater when the reaction was performed in acetonitrile.

5.8 Conclusions

The grafting-to strategy employed in this thesis produced TR-PCR bioconjugates that displayed tuneable solution properties. The pNIPAAm-*co*-HMAAm (2.5H-12.5H) copolymers synthesised in Chapter 4 were reacted via an esterification reaction with DBCO to produce SA (2.5S-12.5S) copolymers as shown by ^{1}H NMR spectroscopy and ATR-FTIR spectroscopy. However, the conversion was found to be low. A newly developed light scattering method for the determination of LCSTs showed that after esterification, some of the SA copolymer samples had a decrease in their LCST (5S, 7.5S and 12.5S) whereas (2.5S and 10S) had an increase in their LCST. The variation of the SA copolymers LCSTs as shown by the light scattering method was theorised to result from the different conversions that occurred during the esterification of pNIPAAm-*co*-HMAAm with DBCO-acid.

It was reported here, how the temperature responsive SA functionalised pNIPAAm copolymers, that had been conjugated to dsDNA; displayed different mobility through an agarose gel. The conjugation and melt profile of PCR products conjugated to the SA copolymer (10S) was greater when the reaction was performed in acetonitrile, when compared to the one pot PCR click reaction and the click reactions in buffer and H_2O. It is also reported here that the LCST of the conjugated polymer is affected by its conjugation to DNA as evidenced by the melt curve analysis. When the temperature responsive polymer is conjugated to DNA it appears to also affect the DNA's capacity to intercalate SG. This phenomenon could be potentially exploited for drug delivery applications.

5.9 References

1. Cobo, I., et al., *Smart hybrid materials by conjugation of responsive polymers to biomacromolecules.* Nature Materials, 2015. **14**(2): p. 143-159.
2. Ebara, M., et al., *Smart Bioconjugates*, in *Smart Biomaterials*. 2014, Springer Japan. p. 237-284.
3. Heredia, K.L. and H.D. Maynard, *Synthesis of protein-polymer conjugates.* Organic & Biomolecular Chemistry, 2007. **5**(1): p. 45-53.
4. Li, H., et al., *Protein conjugation of thermoresponsive amine-reactive polymers prepared by RAFT.* Polymer Chemistry, 2011. **2**(2): p. 323-327.
5. Heredia, K.L., et al., *In Situ Preparation of Protein−"Smart" Polymer Conjugates with Retention of Bioactivity.* Journal of the American Chemical Society, 2005. **127**(48): p. 16955-16960.
6. Dehn, S., et al., *Altering Peptide Fibrillization by Polymer Conjugation.* Biomacromolecules, 2012. **13**(9): p. 2739-2747.
7. Szweda, R., et al., *Smart Polymeric Nanocarriers of Met-enkephalin.* Biomacromolecules, 2016. **17**(8): p. 2691-2700.
8. Chen, X., et al., *Thermoresponsive Worms for Expansion and Release of Human Embryonic Stem Cells.* Biomacromolecules, 2014. **15**(3): p. 844-855.
9. Poon, C.K., et al., *Preparation of Inert Polystyrene Latex Particles as MicroRNA Delivery Vectors by Surfactant-Free RAFT Emulsion Polymerization.* Biomacromolecules, 2016. **17**(3): p. 965-973.
10. Stenzel, M.H., *RAFT polymerization: an avenue to functional polymeric micelles for drug delivery.* Chemical Communications, 2008(30): p. 3486-3503.
11. Boyer, C., V. Bulmus, and T.P. Davis, *Efficient Usage of Thiocarbonates for Both the Production and the Biofunctionalization of Polymers.* Macromolecular Rapid Communications, 2009. **30**(7): p. 493-497.
12. Dehn, S., et al., *Synthetic Strategies for the Design of Peptide/Polymer Conjugates.* Polymer Reviews, 2011. **51**(2): p. 214-234.
13. Yin, X., A.S. Hoffman, and P.S. Stayton, *Poly(N-isopropylacrylamide-co-propylacrylic acid) Copolymers That Respond Sharply to Temperature and pH.* Biomacromolecules, 2006. **7**(5): p. 1381-1385.
14. Brudno, Y., et al., *Refilling drug delivery depots through the blood.* Proceedings of the National Academy of Sciences, 2014. **111**(35): p. 12722-12727.
15. Sletten, E.M. and C.R. Bertozzi, *From Mechanism to Mouse: A Tale of Two Bioorthogonal Reactions.* Accounts of Chemical Research, 2011. **44**(9): p. 666-676.
16. Wittig, G. and A. Krebs, *Zur Existenz niedergliedriger Cycloalkine, I.* Chemische Berichte, 1961. **94**(12): p. 3260-3275.

17. Rostovtsev, V.V., et al., *A stepwise huisgen cycloaddition process: copper (I)-catalyzed regioselective "ligation" of azides and terminal alkynes.* Angewandte Chemie, 2002. **114**(14): p. 2708-2711.
18. Codelli, J.A., et al., *Second-Generation Difluorinated Cyclooctynes for Copper-Free Click Chemistry.* Journal of the American Chemical Society, 2008. **130**(34): p. 11486-11493.
19. Baskin, J.M., et al., *Copper-free click chemistry for dynamic in vivo imaging.* Proceedings of the National Academy of Sciences, 2007. **104**(43): p. 16793-16797.
20. Ornelas, C., J. Broichhagen, and M. Weck, *Strain-Promoted Alkyne Azide Cycloaddition for the Functionalization of Poly(amide)-Based Dendrons and Dendrimers.* Journal of the American Chemical Society, 2010. **132**(11): p. 3923-3931.
21. Debets, M.F., et al., *Aza-dibenzocyclooctynes for fast and efficient enzyme PEGylation via copper-free (3+2) cycloaddition.* Chemical Communications, 2010. **46**(1): p. 97-99.
22. Ta, T., et al., *Thermosensitive Liposomes Modified with Poly(N-isopropylacrylamide-co-propylacrylic acid) Copolymers for Triggered Release of Doxorubicin.* Biomacromolecules, 2010. **11**(8): p. 1915-1920.
23. Zhang, W., et al., *pH and near-infrared light dual-stimuli responsive drug delivery using DNA-conjugated gold nanorods for effective treatment of multidrug resistant cancer cells.* Journal of Controlled Release, 2016. **232**: p. 9-19.
24. Uehara, N. and M. Ogawa, *Interaction of Poly(N-isopropylacrylamide) with Sodium Dodecyl Sulfate below the Critical Aggregation Concentration.* Langmuir, 2014. **30**(22): p. 6367-6372.
25. Virtanen, J., et al., *Aggregation in Aqueous Poly(N-isopropylacrylamide)-block-poly(ethylene oxide) Solutions Studied by Fluorescence Spectroscopy and Light Scattering.* Macromolecules, 2002. **35**(12): p. 4763-4769.
26. Gentilini, F. and M.E. Turba, *Optimization of the Divergent method for genotyping single nucleotide variations using SYBR Green-based single-tube real-time PCR.* Mutation Research/Fundamental and Molecular Mechanisms of Mutagenesis, 2014. **766–767**: p. 14-18.

6 Chapter 6. PEG copolymers and Cross-linked Peg Hydrogels

Synopsis

This chapter describes work towards the development of a PEG platform to be used as part of a grafting-to strategy designed to make temperature responsive bio-conjugated bio-compatible polymers. The synthesis of NHS functionalised PEG copolymers prepared by FRP and post functionalisation of NHS-PEG copolymers to alkene functionalised PEG copolymers is discussed. This chapter also describes thiol-ene photo cross-linking of, alkene functionalised PEG copolymers that resulted in cross-linked hydrogels. The cross-link density of these cross-linked hydrogels is investigated in this chapter by swelling and drug release experiments.

6.1 Introduction

Polymeric hydrogels comprised from natural, synthetic or hybrid materials have been used in a wide range of bio medical applications [1]. In hydrogels the chemical, covalent or physical cross-link of a polymeric material results in a three-dimensional network that swells in a solvent (generally water) [2]. The balance between the cross-linking and the water sorption (via capillary, osmotic and hydration forces) imparts unique mechanical properties and diffusion characteristics to the hydrogel network [3]. Since these hydrated hydrogels possess similar properties to biological tissues, they are, in general, biocompatible. Polymer hydrogels have been used as the primary material in contact lenses, tissue engineering and controlled drug delivery applications [4-7]. Common synthetic hydrogels include poly pHEMA, PVA and PEG [8-10]. In the 1960's and 1970's, PEG hydrogels were heavily investigated due to their excellent biocompatibility and resistance to protein adsorption [11]. Early methods of producing PEG hydrogels involved cross-linking PEG with gamma or electron beam radiation, as well as reactions between PEG functionalised with isocyanates and alcohols [3, 12].

To overcome inhomogeneity and to improve mechanical properties, other methods of cross-linking PEG have been investigated [13]. Chemical cross-linking via condensation reactions, click chemistry and enzymatic reactions have all been used to cross-link PEG [13]. A recent attempt to utilise PEG hydrogels in tissue engineering applications was reported by Sakai *et al.* [14], who developed a tetra PEG hydrogel by the condensation of macro monomers of PEG. The synthesised tetrahedron-like PEG macro monomers were combined with propyl amine or succinamidyl glutarate and when mixed together led to a gel within several minutes [14]. The tetra-PEG gel possessed a maximum breaking stress of 9.6 MPa which is comparable to native articular cartilage [14]. Malkoch *et al.* [15] have recently used tetra azide functionalised PEG and di-acetylene PEG to produce a network hydrogel with improved mechanical properties and the potential to incorporate additives through the click functionality. Erhbar *et al.* [16] have combined, through Michael addition like reactions an 8 arm PEG polymer and peptides to produce a hydrogel loaded with vascular endothelial growth factors.

In vitro analysis of these hydrogels showed them to be responsive to protease degradation, making these gels a potential synthetic substitute to fibrin in tissue engineering applications as well as novel drug delivery vehicles [16]. The stability of PEG core star block copolymers containing ester linkages and amide linkages has been investigated by Buwalda *et al.* [17]. The group showed that block copolymers of poly(ethylene glycol)-*co*-poly(L-lactide)(PEG-PLA) degraded at the ester linkage preferentially when an ester bond was used to link the two blocks [17]. When amide linkages were used to link the two blocks, degradation occurred via hydrolysis of the poly(L-lactide) block [17]. The slower degradation of the amide linked PEG-PLA block copolymer could be potentially useful for drug delivery applications [17]. Bottle brush-like PEG copolymers with NHS ester groups have been used by Ameringer *et al.* [18] to produce antifouling polymer coatings that

can be functionalised with biological molecules making them useful for cell culturing and tissue engineering applications. The delivery of therapeutic proteins, peptides and oligonucleotides in the 1990's led to the need for a suitable delivery vehicle. In response, West *et al.* [19] developed a PEG hydrogel through photo polymerisation of a PEG precursor that had a reactive acrylate group. A photo initiator and UV light were used to cross-link the PEG precursor [19]. The advantage of this method was that the hydrogels could be formed *in situ* which helped to localise the release of any therapeutic drugs [19]. Recent developments in producing PEG hydrogels include the use of click chemistry via thiol-ene addition reactions. Aimetti *et al.* [20] employed peptide cross-links formed by thiol-ene photo polymerisation to release model proteins. Further, the group showed that the bioactivity of lysozyme exposed to thiol-ene photo polymerisation conditions remained greater than 90% [20]. In this chapter, linear comb pPEGA-*co*-Acrylic acid NHS copolymers p(mPEGA-*co*-AA-NHS) copolymers were synthesised through free radical polymerisation of mPEGA and acrylic acid-NHS (AA-NHS) monomers. The monomer ratios were varied from 12 mol % AA-NHS to 46 mol % AA-NHS. This yielded six copolymers with increasing mol ratios of AA-NHS. Allyl amine was then used to transform the NHS functionality of the p(mPEGA-*co*-AA-NHS) copolymers to produce six p(mPEGA-*co*-AA-Allyl) copolymers.

The six p(mPEGA-*co*-AA-Allyl) copolymers were then combined with a tetrathiol cross-linker and were then crosslinked via thiol-ene click chemistry by exposure to UV light to form circular disk hydrogels. The different swelling ratios of the photo polymerised hydrogels in water were investigated. Fluorescence spectroscopy was used to monitor the release of a model anti-cancer drug camptothecin which was encapsulated into the hydrogel disk during the photo polymerisation cross-link step.

6.2 Synthesis P(mPEGA-*co*-AA-NHS) Copolymer

Scheme 6.1 shows the reaction pathway for the synthesis of p(mPEGA-*co*-AA-NHS) copolymer (16). The free radical polymerisation of an AA-NHS monomer (14) and a water soluble mPEGA monomer (15) and was carried out to produce six copolymers with increasing AA-NHS content. The feed mol ratio of AA-NHS to mPEGA was increased from 12 mol % to 46 mol %. The experimental details can be found in Chapter 2, Section 2.4.1.

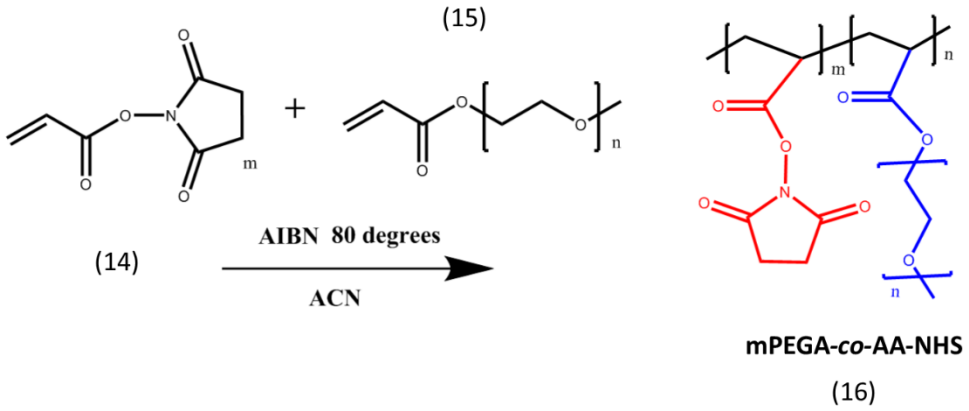

Scheme 6.1. Scheme of polymer synthesis for copolymerisation of p(mPEGA-*co*-AA-NHS) copolymer (12, 22, 30, 36, 42 and 46 mol %).

The increasing AA-NHS content of the synthesised copolymer of p(mPEGA-*co*-AA-NHS) was investigated by ^{1}H NMR spectroscopy. Figure 6.1 shows the ^{1}H NMR spectra for the 12, 22, 30, 36, 42 and 46 mol % p(mPEGA-*co*-AA-NHS) copolymers termed 12N, 22N, 30N, 36N, 42N and 46N respectively. The spectra show a broad polymer peak (labelled e, in Figure 6.1) between 4.3-4.1 ppm which represents the O-CH_2 group of the mPEGA backbone, another peak (e, in Figure 6.1) between 3.5-3.7 ppm is indicative of the PEG functionality (O-CH_2-CH_2)$_n$. Another contribution to the ^{1}H NMR spectrum is observed at 3.3 ppm (labelled d, in Figure 6.1) which represents the methoxy group from the PEG functionality. The NHS symmetrical CH_2 groups (labelled c, in Figure 6.1) from the p(mPEGA-*co*-AA-NHS) copolymer are also observed in the ^{1}H NMR spectra at 2.8 ppm The CH and CH_2 of the polymer backbone is observed at 2.4-1.5 ppm (labelled a, b, in Figure 6.1). Figure 6.1 shows a trend where the NHS peak (labelled c, in Figure 6.1) increases relative to other peaks observed in the spectra as the mol ratio of AA-NHS is increased in the feed ratio of the p(mPEGA-*co*-AA-NHS) copolymers.

The two peaks at 2.8 ppm (AA-NHS, CH_2 group) and 3.3 ppm (mPEGA, CH_3 group) were integrated to calculate peak areas and the ratio of the 2.8/3.3 ppm was used to determine the composition of the copolymer. Integration of the peaks and calculation of mol ratios found that 12N had an 11 NHS mol % ratio and 22N, 30N, 36N, 42N and 46N had 28, 42, 51, 58 and 56 NHS mol % ratios, respectively. The results showed that the feed ratio of AA-NHS differed from the mol ratio of AA-NHS calculated by ^{1}H NMR spectroscopy but that the AA-NHS mol % did increase with increasing feed of AA-NHS monomer. The yield calculated for each copolymer (Table 6.1) was based on the yield of polymer collected by weight to the starting amount of monomer, a greater than 70 % yield was observed for all copolymerisations.

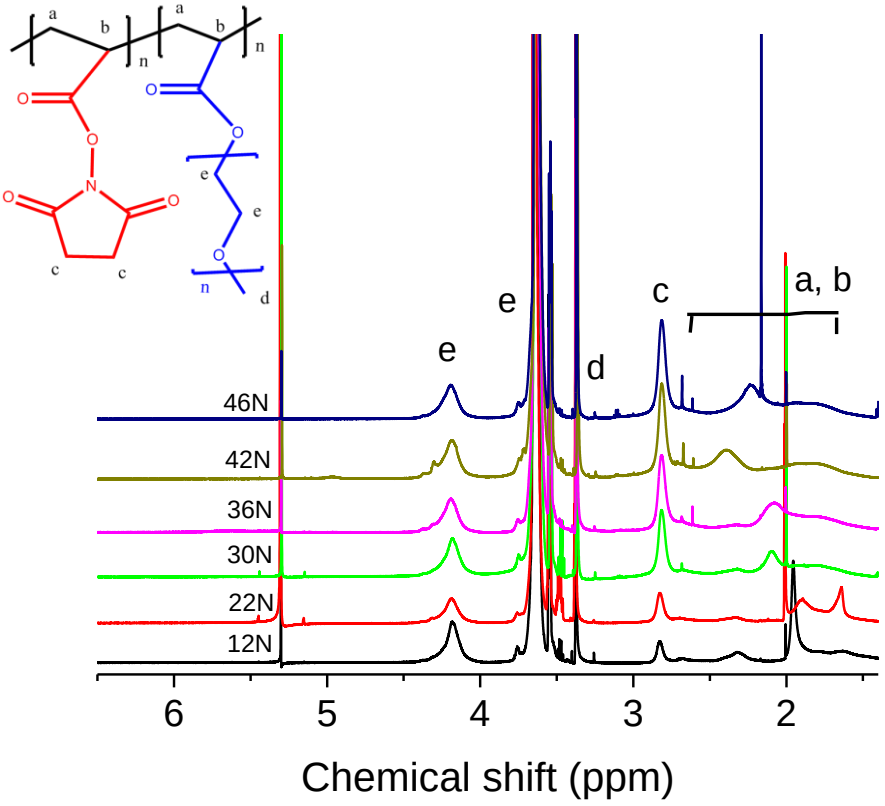

Figure 6.1. ^{1}H NMR spectra in $CDCl_3$ of p(mPEGA-*co*-AA-NHS) copolymer (22N, 30N, 36N, 42N and 46N).

Table 6.1. Sample codes and AA-NHS composition and polymer conversion for p(mPEGA-*co*-AA-NHS) copolymers.

Mol % (In feed ratio)	mol % [AA-NHS][a]	Yield[b] (%)
12N	11	75
22N	28	73
30N	42	75
36N	51	73
42N	58	86
46N	56	92

Calculated by [a] ^{1}H NMR. [b]Yield calculated by amount of recovered polymer by weight compared to starting material

Since the copolymers that were synthesised with a higher feed ratio of AA-NHS monomer differed from the feed ratio calculated by ^{1}H NMR spectroscopy; the 46N copolymer was chosen, for further study by ^{1}H NMR spectroscopy to measure the conversion of AA-NHS monomer and the mPEGA monomer to polymer over time. Figure 6.2 shows the ^{1}H NMR spectrum and the change in peak intensities for the 46N copolymer over time. The alkene chemical shifts of each monomer were first determined by ^{1}H NMR spectroscopy (data not

shown), then the change in intensity over time for the alkene peak from each monomer was used to monitor the conversion of each monomer to polymer. Figure 6.2 shows that the alkene of the mPEGA monomer has three peaks due to the three hydrogens attached at a chemical shift of (doublet, 6.38-6.35 ppm, multiplet, 6.12-6.08 and doublet, 5.8-5.79). Also observed in the spectrum (Figure 6.2) are the hydrogens attached to the alkene for AA-NHS monomer at a chemical shift of (doublet, 6.66-6.64 ppm, multiplet, 6.31-6.26 ppm and doublet 6.15-6.14 ppm). It can be observed in Figure 6.2 that over time the peaks associated with the AA-NHS monomer (doublet, 6.66-6.64 ppm, multiplet, 6.31-6.26 ppm and doublet 6.15-6.14 ppm) are reducing in height and by 6 hours into the polymerisation the peaks have disappeared from the ^{1}H NMR spectrum. The peaks associated with the mPEGA monomer (doublet, 6.66-6.64 ppm, multiplet, 6.31-6.26 ppm and doublet 6.15-6.14 ppm) also reduce in height but remain after 6 h and 8 h of polymerisation. At 22 h of polymerisation there are no peaks observed that are associated with the alkene hydrogens from mPEGA.

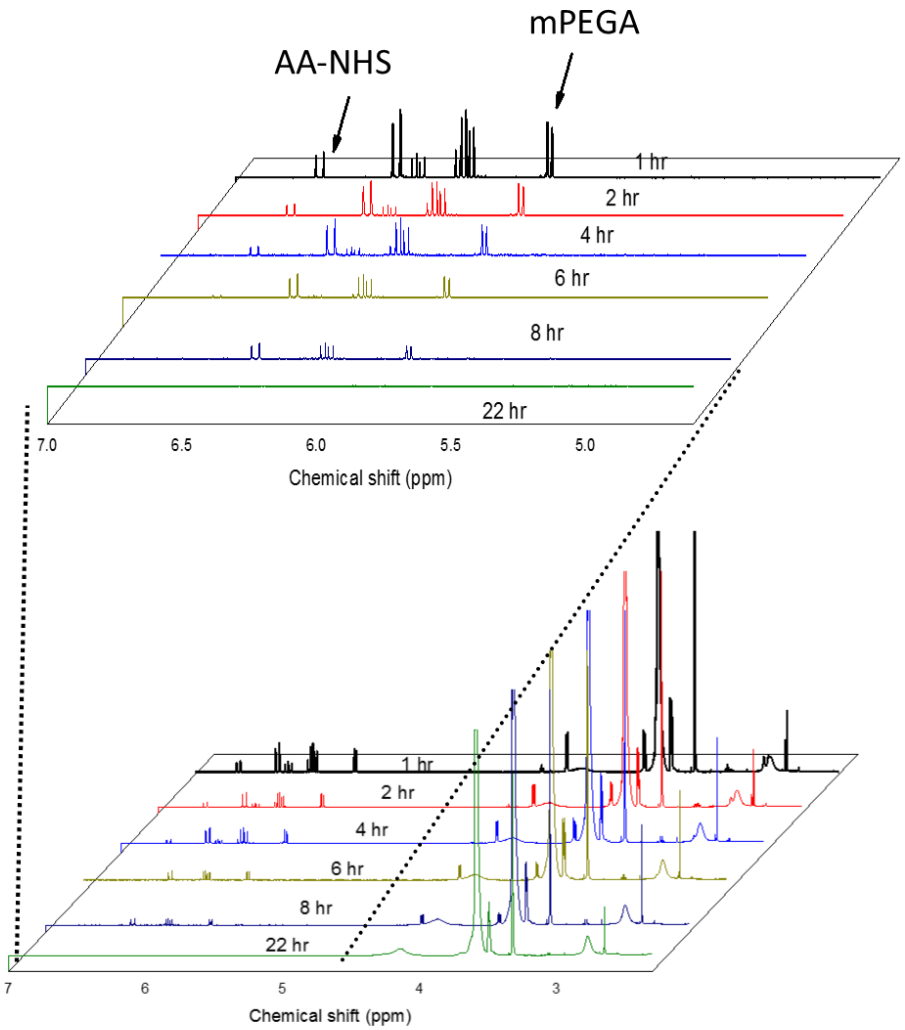

Figure 6.2. ^{1}H NMR in $CDCl_3$ spectra of polymerisation to measure the conversion of AA-NHS monomer and the mPEGA monomer to p(mPEGA-*co*-AA-NHS) copolymer (46N) over time (0-22 h).

The results from ^{1}H NMR analysis suggested that AA-NHS monomer was being incorporated into the copolymer in the early stages of the polymerisation. It is proposed based on ^{1}H NMR analysis that the copolymerisation of AA-NHS and mPEGA resulted in a blocky type copolymer, with a blocky p(AA-NHS) polymer forming early in the polymerisation and then a blocky p(mPEGA) forming after the AA-NHS monomer has been consumed in the polymerisation. Figure 6.3 shows a proposed schematic of the polymerisation. ^{1}H NMR analysis also suggests that the AA-NHS block is present in greater amounts than the feed ratio, which could mean that some compositional drift was occurring due to different reactivity ratios [21].

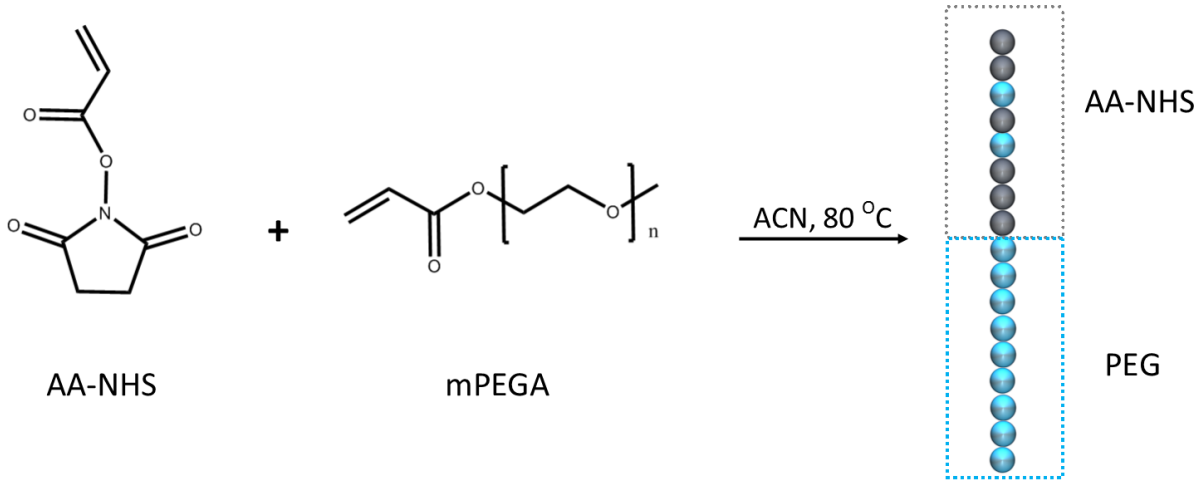

Figure 6.3. Proposed blocky structure of p(mPEGA-*co*-AA-NHS) copolymers.

It is likely that the FRP used here to produce NHS-PEG copolymers had some compositional drift. Future work could involve controlling compositional drift during the copolymerization by limiting monomer conversion [22]. It is also possible to control compositional drift by adding the more reactive monomer slowly using a semi-batch process [23]. For the purposes of this study, it was thought that these copolymers could still be used to produce a PEG platform for temperature responsive bio-conjugated cross-linked micelles. In this chapter, the use of thiol-ene click chemistry was investigated as a strategy for the attachment of pre-prepared temperature responsive polymer bio-conjugates. Therefore, the NHS functionalised copolymer were transformed to alkene functionalised PEG copolymers using allyl amine.

6.3 Synthesis of P(mPEGA-*co*-AA-Allyl) Copolymer

Scheme 6.2 shows the reaction between p(mPEGA-*co*-AA-NHS) (16) copolymer(12N-46N) and allyl amine (17) to yield six p(mPEGA-*co*-AA-Allyl) copolymers (18) with increasing allyl content now termed 12A-46A. The experimental details can be found in Chapter 2, Section 2.5.2.

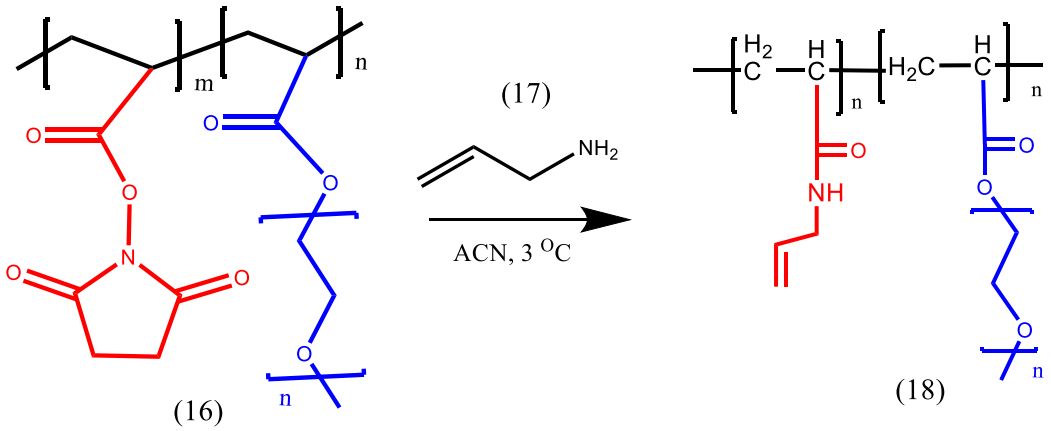

Scheme 6.2. Scheme of ally amine reaction with p(mPEGA-*co*-AA-NHS) copolymer (22N, 30N, 36N, 42N and 46N) to produce p(mPEGA-*co*-AA-Allyl) copolymers.

^{1}H NMR spectroscopy was used to investigate the transformation of p(mPEGA-*co*-AA-NHS) copolymer to (mPEGA-*co*-AA-Allyl) copolymer through nucleophilic substitution of the NHS group by allyl amine. Figure 6.4 a and b shows the ^{1}H NMR spectra for 12N-46N and 12A-46A respectively. Figure 6.4 b shows a broad polymer peak (labelled e in Figure 6.4) between 4.3-4.1 ppm which represents the O-CH_2 group of the PEG backbone. The NHS symmetrical CH_2 groups that was previously observed in the p(mPEGA-*co*-AA-NHS,^{1}HNMR spectra (Figure 6.1) copolymer is not observed in the ^{1}H NMR spectra at 2.8 ppm, in Figure 6.4 b. There are also peaks between 5.8 ppm and 5.3 ppm (Figure 6.4 c). The peaks between 5.8 ppm and 5.3 ppm are thought to correspond to the newly attached alkene functionality of the allyl amine moiety.

The disappearance of the broad NHS peak (Figure 6.4 d, 2.8 ppm) and its replacement with a sharp peak at 2.7 ppm (Figure 6.4 d) is theorised to be the free NHS group cleaved during the synthesis. The ^{1}H NMR peak analysis and integration results suggest that the newly transformed PEG allyl copolymers (12A-46A, Figure 6.4) now have an equivalent allyl composition to what was found previously for the NHS composition of the NHS-PEG copolymers (12N-46N) (Table 6.1). The 22N ally copolymer did show a slight peak at 2.8 ppm and so to confirm the composition of the synthesised 22N p(mPEGA-*co*-AA-NHS) copolymer and the allyl amine transformed 22N p(mPEGA-*co*-AA-Allyl) copolymer; further evidence was sought using ATR-FTIR spectroscopy.

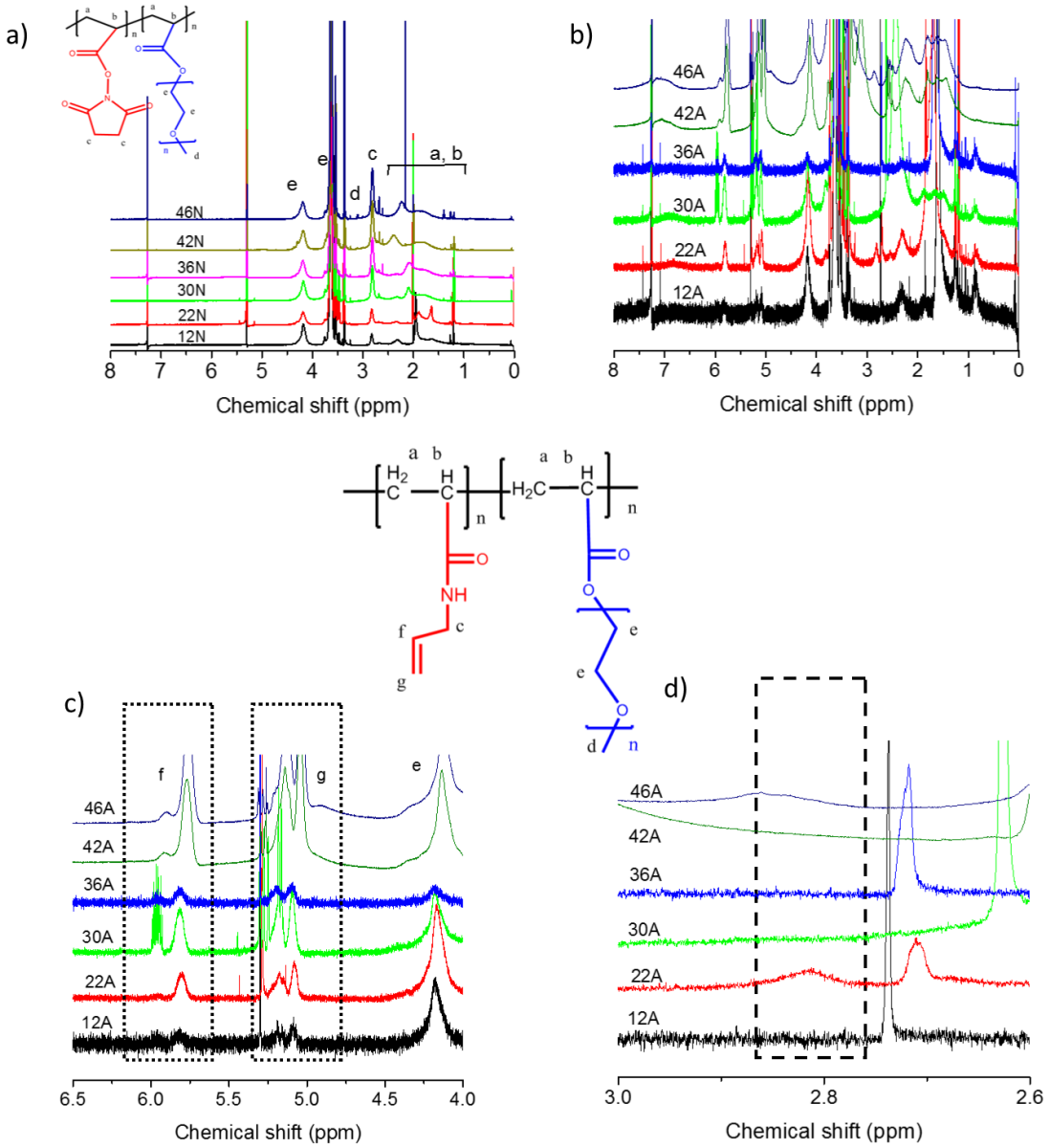

Figure 6.4. a) ^{1}H NMR spectra in $CDCl_3$ of p(mPEGA-*co*-AA-NHS) copolymer (22N, 30N, 36N, 42N and 46N), b) ^{1}H NMR spectra in $CDCl_3$ of p(mPEGA-*co*-AA-allyl) copolymer (12A, 30A, 36A, 42A and 46A), c) inset of ^{1}H NMR spectra in $CDCl_3$ of p(mPEGA-*co*-AA-allyl) copolymer (12A, 30A, 36A, 42A and 46A) between 6.5 ppm and 4.0ppm and d) inset of ^{1}H NMR spectra in $CDCl_3$ of p(mPEGA-*co*-AA-allyl) copolymer (12A, 30A, 36A, 42A and 46A) between 2.6 ppm and 3.0 ppm.

The ATR-FTIR spectra (Figure 6.5) shows the transmittance intensities for mPEGA monomer, p(mPEGA-*co*-AA-NHS) copolymer (22N) and p(mPEGA-*co*-AA-Allyl) copolymer (22A). In the high frequency region of the spectrum for the mPEGA monomer (Figure 6.5 a, black), the CH_2 of the methylene group is observed between 2950-2830 cm^{-1} due to the PEG backbone (O-CH_2-CH_2). This CH_2 stretch is also observed in the p(mPEGA-*co*-AA-NHS) copolymer (Figure 6.5 a, blue) and p(mPEGA-*co*-AA-allyl) copolymer (Figure 6.5 a, red) at the same frequency. Also in Figure 6.5 a, red another peak is observed at 3344 cm^{-1} which is attributed to an N-H stretch in the p(mPEGA-*co*-AA-Allyl) copolymer. In the low frequency region of the spectrum for the mPEGA monomer (Figure 6.5 b, black), the carbonyl group stretch is observed at 1720 cm^{-1}.

The carbonyl stretches of the p(mPEGA-*co*-AA-NHS) copolymer (Figure 6.5 b, blue) and p(mPEGA-*co*-AA-Allyl) copolymer (Figure 6.5 b, red) was blue-shifted to 1736 cm^{-1} and at 1730 cm^{-1} respectively. Figure 6.5 b, red also shows two peaks (1780 cm^{-1} and 1809 cm^{-1}) attributed to carbonyl groups of the NHS moiety in the p(mPEGA-*co*-AA-NHS) copolymer spectrum. Figure 6.5 b, red) shows peaks in the p(mPEGA-*co*-AA-Allyl) copolymer spectrum attributed to the alkene group from allyl amine at 1670 cm^{-1} (C=C) and the amide bond at 1640 cm^{-1} (amide I) and at 1532 cm^{-1} (amide II).

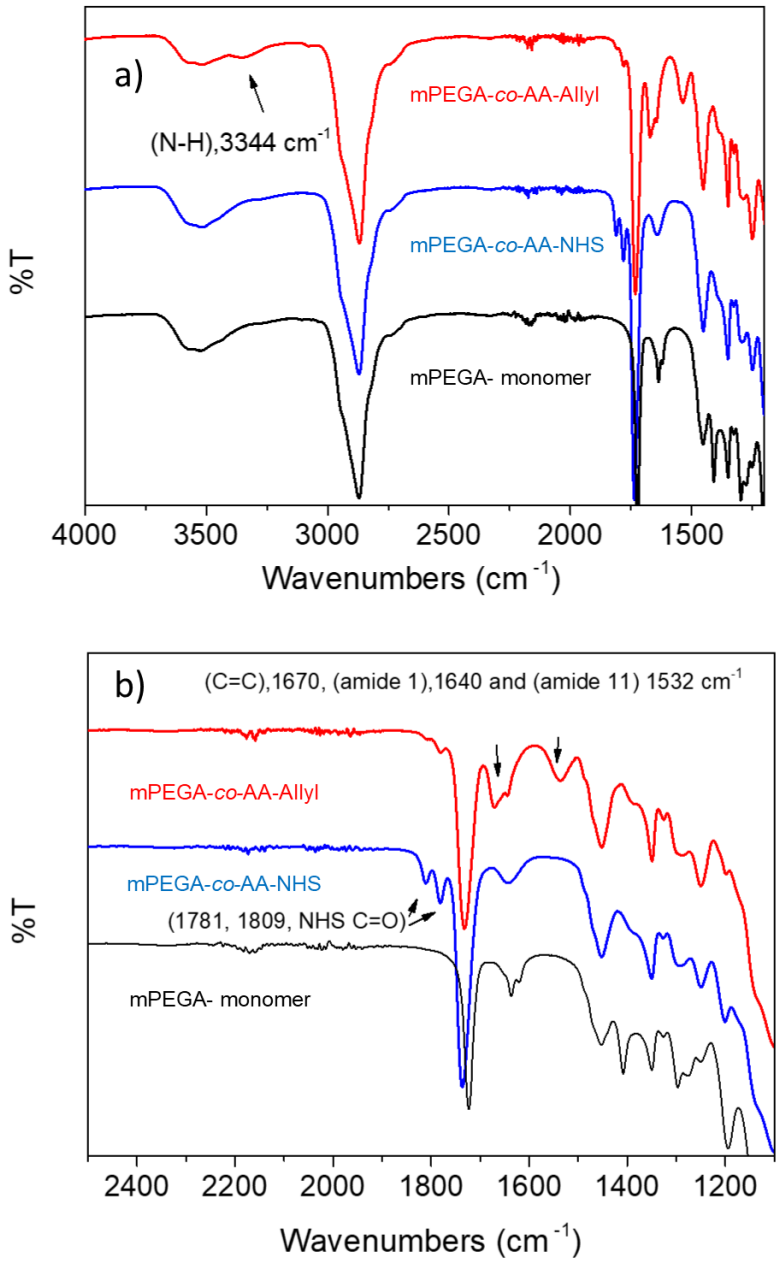

Figure 6.5. ATR-FTIR spectroscopy characterisation a) high to low frequency spectrum of mPEGA monomer, p(mPEGA-*co*-AA-NHS) copolymer (22N) and p(mPEGA-*co*-AA-allyl) copolymer (22A), b) low frequency spectrum of mPEGA monomer, p(mPEGA-*co*-AA-NHS) copolymer (22N) and p(mPEGA-*co*-AA-allyl) copolymer (22A).

The results from ATR-FTIR analysis show with the appearance of the carbonyl stretch (1780 cm^{-1} and 1809

cm^{-1}) in the p(mPEGA-*co*-AA-NHS) copolymer spectrum that the successful copolymerisation of AA-NHS and mPEGA monomers was achieved. The results for the p(mPEGA-*co*-AA-Allyl) copolymer (Figure 6.5 b, red), also show nucleophilic substitution by allyl amine to remove the NHS group from p(mPEGA-*co*-AA-NHS) copolymer due to the appearance of the alkene group in the spectrum at 1670 cm^{-1}, amide bond at 1640 cm^{-1}, 1532 cm^{-1} (amide I, amide II) and coupled with the disappearance of the NHS carbonyl stretch at 1780 cm^{-1} and 1809 cm^{-1}. ^{1}H NMR spectroscopy and ATR-FTIR spectroscopy confirmed the copolymerisation of mPEGA and AA-NHS, with ^{1}H NMR spectroscopy giving an estimate of the composition of the six copolymers. The goal of this chapter was to produce temperature responsive bio-conjugated cross-linked hydrogels; however, first, model cross-link experiments were trialled here. A multi armed organic thiol molecule was used to confirm that the synthesised p(mPEGA-*co*-AA-Allyl) copolymers could be cross-linked via thiol-ene click chemistry.

6.4 Photo Cross-Linked PEG (CLP) Hydrogels via Thiol-ene Click Chemistry

Figure 6.6 shows the process used to produce cross-linked p(mPEGA-AA), termed CLP hydrogels from the p(mPEGA-*co*-AA-Allyl) copolymers (12A-46A). The CLP hydrogel was prepared by mixing the copolymer in a centrifuge tube with a tetra thiol cross-linker, a UV initiator and solvent ($CHCl_3$), followed by deoxygenation by purging with N_2. The copolymer solution was then centrifuged and then pipetted onto a silicon substrate which had a thin 1 mm thick poly dimethyl siloxane (PDMS) layer with circular or square sections removed at a specified diameter. The copolymer solution was then cross linked via thiol-ene click chemistry by exposure to 365 nm light for a period of 3 min. The experimental details can be found in Chapter 2, Section 2.5.2.

Control experiments were performed to ascertain the mechanism for cross linking, the same process was used as is shown in Figure 6.6 however the tetrathiol cross linker was not included in the preparation of hydrogels. The subsequent solutions when exposed to UV-light failed to cross-link, indicating that thiol-ene click was responsible for cross-linking of the CLP hydrogels. Using the process shown in Figure 6.6, the (12A-46A) (mPEGA-*co*-AA-allyl) copolymers were cross-linked to produce CLP hydrogel disks termed CLP (12H-46H). It was expected that the CLP hydrogel disks would have different amounts of cross-linking based on the amount of cross-link groups available.

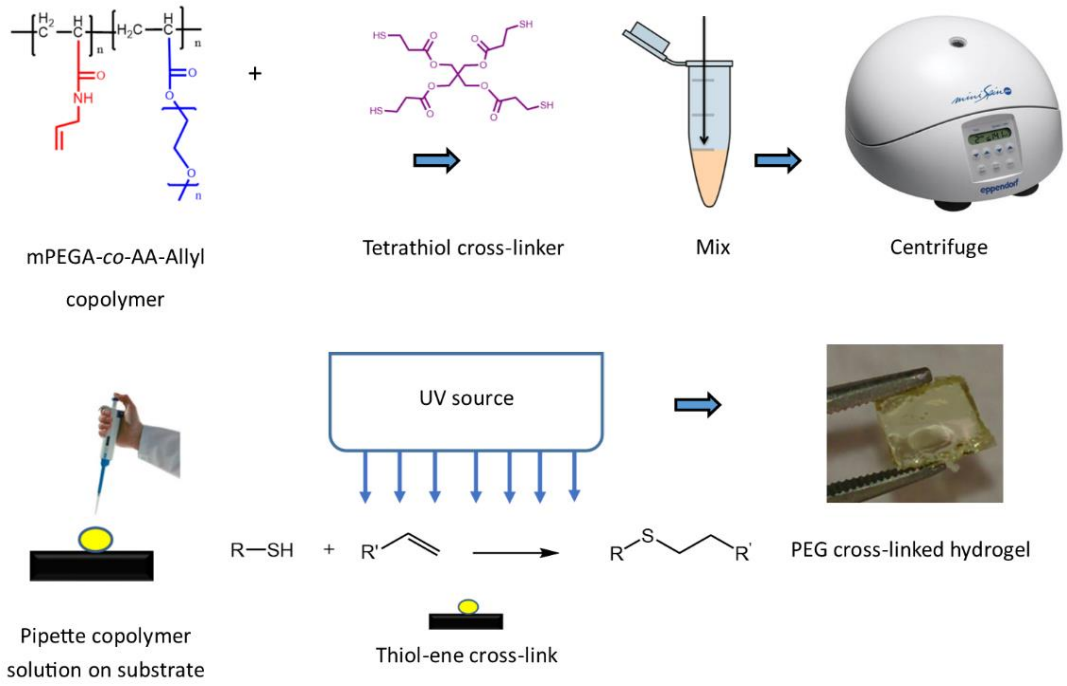

Figure 6.6. Scheme of method used to prepare cross-linked PEG (CLP) hydrogels (12H-46H) from p(mPEGA-co-AA-Allyl) copolymers (12A-46A).

The variation in cross-link density is likely to result from variability in the mol ratios of monomers when the initial copolymers were prepared. To test this hypothesis the CLP hydrogels were examined for their swelling capacity through their uptake of water.

6.4.1 Cross-Linked PEG (CLP) Hydrogel Swelling

Circular CLP (12H-46H) hydrogel disks were prepared by the method shown in Figure 6.6, the eight circular CLP hydrogel disks shown in Figure 6.7, were weighed and then placed in a small wire basket followed by immersion in water. Each of the wire baskets containing one circular CLP hydrogel disk was removed from the water at a specific time interval, excess water was removed by careful blowing of the disk with nitrogen, and then the disk was reweighed to measure the water uptake of the CLP hydrogel disk. The experimental details can be found in Chapter 2, Section 2.5.3.

Figure 6.7 a, from left to right, shows the change in swelling for the 12H CLP hydrogel disks after they were removed from the water at the allotted time intervals of 1, 2, 3, 4, 5, 10, 20 and 30 min. The 12H CLP hydrogel disks, when placed in water, underwent rapid swelling. The initial diameter of the prepared 12H CLP hydrogel disks was measured at 4.00 mm, after 30 min the final measured diameter of the 12H CLP hydrogel disk was found to be 5.58 mm, an increase of 1.58 mm or 40%. The thickness of the 12H CLP hydrogel disk also increased 33 % from 1.00 mm to 1.33 mm. This is a total increase in volume of 173% for the 12H CLP hydrogel

disk, after immersion in water for 30 min. Figure 6.7 b shows the change in swelling that occurred for each of the 22H CLP hydrogel disks over 30 min. Swelling occurred rapidly when the disks were placed in water, the initial diameter before swelling and the final measured diameter after swelling for 22H were 4.00 mm and 5.58 mm respectively.

Table 6.2. Change in diameter, thickness and volume % for CLP hydrogels (12H-46H).

CLP	Initial diameter (mm)	Final diameter (mm)	Initial Thickness (mm)	Final Thickness (mm)	Volume increase (%)
12H	4	5.58	1	1.33	173
22H	4	5.58	1	1.10	131
30H	4	N/A	1	N/A	N/A
36H	4	N/A	1	N/A	N/A
42H	4	4.10	1	1.00	N/A
46H	4	4.10	1	1.00	N/A

Diameters were measured using digital Calipers

The initial diameter before swelling for 30H hydrogel disk was also 4.00 mm, however the gel fractured, meaning the measurement of the final diameter was not possible. However, Figure 6.7 c clearly shows that the change in diameter due to swelling for 30H hydrogel disk is reduced when compared to the 12H and 22H hydrogel disks over the same measured time.

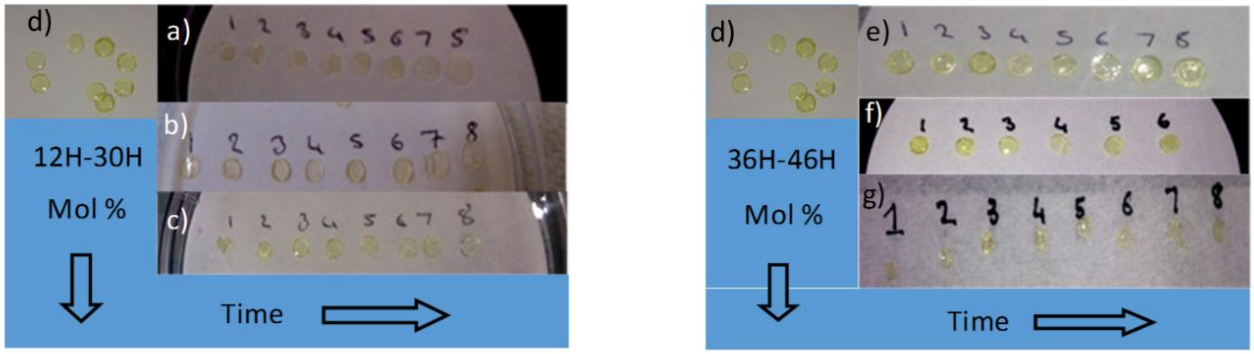

Figure 6.7. a) left to right, swelling for 12H CLP hydrogel disks after removal from water at intervals of 1, 2, 3, 4, 5, 10, 20 and 30 min, b) left to right, swelling for 22H CLP hydrogel disks after removal from water at intervals of 1, 2, 3, 4, 5, 10, 20 and 30 min, c) left to right, swelling for 30H CLP hydrogel disks after removal from water at intervals of 1, 2, 3, 4, 5, 10, 20 and 30 min, d) optical image of hydrogel disks when dry, e) left to right, swelling for 36H hydrogel disks after removal from water at intervals of 1, 2, 3, 4, 5, 10, 20 and 30 min, f) left to right, swelling for 42H CLP hydrogel disks after removal from water at intervals of 1, 2, 3, 4, 5, 10, 20 and 30 min and g) left to right, swelling for 46H CLP hydrogel disks after removal from water at intervals of 1, 2, 3, 4, 5, 10, 20 and 30 min.

The thickness of the 22H CLP hydrogel changed from 1.00 mm (before swelling) to 1.10 mm (after swelling). The total increase in volume was 131%. Figure 6.7 c shows the swelling change for each hydrogel disk over time for the 30H CLP hydrogel disk.

Figure 6.7 e-g, shows the change in swelling over time for 36H-46H hydrogel disks, the diameter and thickness of the 36H hydrogel disk was not measured after swelling due to the disks fragile nature. The 42H and 46H hydrogel disks showed only a 0.10 mm increase in diameter after swelling and no change in thickness, the disks remained glassy after swelling but did change from flat disks to disks that had some curvature. The results obtained from measuring the diameter, thickness and fragility of the CLP hydrogel disks indicated that swelling occurred for all samples (12H-46H), however, the volume change of the disks appeared to be greater for the CLP hydrogel disks (12H-30H) with a lower amount of cross-link sites available.

To measure the water uptake of the prepared CLP hydrogel disks(12H-46H), the disks were weighed before swelling (W_d) and after swelling (W_s) and using Equation 6.1 the change in swell ratios over time was calculated.

$$\frac{W_s - W_d}{W_d}$$

Equation 6.1

Figure 6.8 a shows the swell ratio with time for the CLP hydrogel disks, namely 12H (blue), 22H (red) and 30H (black). The trend lines shown in the plot are used for visualisation of the data set only. Figure 6.8 a, blue shows that the 12H CLP hydrogel disks had a maximum swell ratio of approximately 300%, the swell ratio reduced for the 22H (red) hydrogel disks to an approximate maximum of 250% and 200% for the 30H (black) hydrogel disk. Figure 6.8 b shows the swell ratios for 36H (black), 42H (red) and 46H (blue) hydrogel disks, the maximum swell ratio for 36H hydrogel disk is found to be approximately 300%, followed by 200% for 42H hydrogel disk and finally a maximum swell ratio of 90% was found for 46H. It appears from the data that as the cross-link density increases for the CLP hydrogel disks, the swell ratio decreases.

Often in the literature, models are used to describe the uptake of water by hydrogel polymers, these models, developed by Alfrey *et al.* [17], consider the rate of uptake, or diffusion of water into the hydrogel and the rate of relaxation of the polymer network. If diffusion occurs at a slower rate than polymer chain relaxation, then Fickian diffusion is expected to occur [24]. Where diffusion occurs at a faster rate than the relaxation rate of the polymer chain, non-Fickian diffusion occurs [24]. If the diffusion and relaxation rates are between Fickian and non-Fickian diffusion, then the diffusion is said to be anomalous [24].

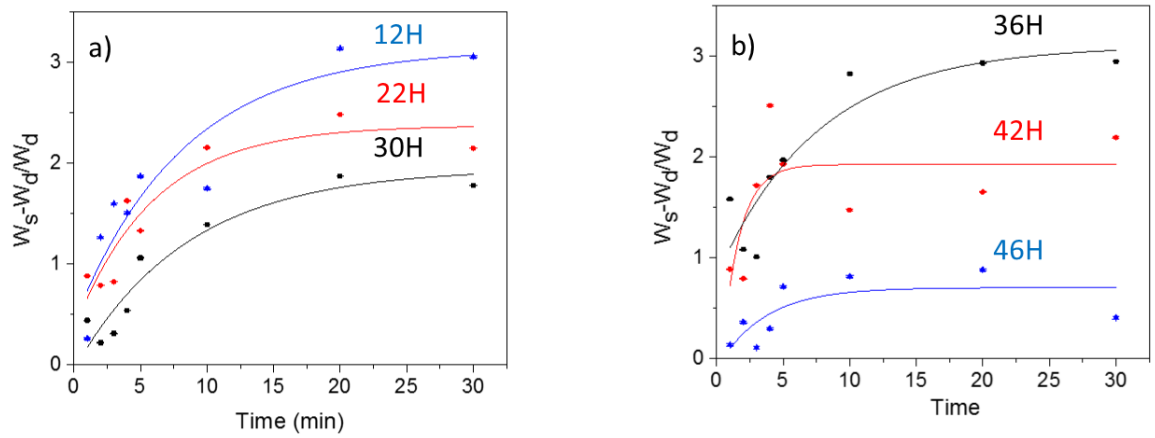

Figure 6.8. a) Swell ratios of CLP hydrogel disks (12H-30H), b) swell ratios of CLP hydrogel disks (36H-46H).

Gravimetric measurements are widely used to determine the transport mechanism in hydrogels where the data found through the use of Equation 6.1 can be modified so that that $W_s - W_d/W_d$ at time t becomes S_t and S_e are the equilibrium value found from the data set [25]. Normalisation of the mass data set yields Equation 6.2 which can be equated to the Ritger and Peppas model where M_t is equal to the mass absorbed by the polymer at time t and M_∞ is the equilibrium hydration level [26].

$$\frac{S_t}{S_e} = \frac{M_t}{M_\infty} = kt^n$$

Equation 6.2

Theory dictates that for diffusion to be purely Fickian the exponent n in Equation 6.2 would be 0.5 in a thin film and 0.45 in a cylindrical sample, therefore a plot of S_t/S_e *vs* $t^{1/2}$ should indicate whether the diffusion is Fickian [26]. The exponent n can be calculated by plotting ln S_t/S_e versus ln t, if the exponent n is found to be equal to 0.5 (for thin film) then the diffusion is Fickian [26]. Figure 6.9 a and b show the plot of S_t/S_e *vs* $t^{1/2}$ for the 12H-46H samples; the trend lines shown in the plots are for visualisation only. Taking the logarithm of Equation 6.2 results in Equation 6.3.

$$ln\frac{S_t}{S_e} = \ln k + n \ln t$$

Equation 6.3

A plot of ln S_t/S_e versus ln t gives a straight line with the value of n from the slope of the linear regression and the value of k from the intercept. The diffusion coefficient (D) can then be calculated using Equation 6.4, where r is equal to the radius of the disk and the constants n and k_d can be obtained from the fit of Equation 6 3 to the data set [25].

$$D = \pi r^2 \left(\frac{k_d}{4}\right)^{\frac{1}{n}}$$

Equation 6.4

When the CLP hydrogel disks (12H-46H) were initially immersed in water they underwent rapid swelling, potentially leading to errors in the first data point. When the disks were left in water for a long time the gels fractured, leading to further errors in the data set. Thus, the removal of the first and last data points improved the linear fit and subsequent R^2 value for each data set (Table 6.3). The diffusion coefficients for the CLP hydrogel disks (12H-46H) were calculated from inputting the corresponding n and k_d values found from the line of best for each data set Figure 6.9 c and d. Table 6.3 shows the constants n and k_d and the calculated diffusion coefficients D_o for each of the CLP hydrogel disks. The calculated n of 0.33 for 12H indicates that diffusion is non-Fickian, the subsequent diffusion coefficient D_o = 7.9 x 10^{-3} cm^2 s^{-1} (Table 6.2) for 12H hydrogel disk is not consistent with Fickian diffusion when compared to literature values which can range from 1 x 10^{-8} cm^2 s^{-1} to 1 x 10^{-6} cm^2 s^{-1} for systems that are governed by Fickian diffusion [3, 27]. The R^2 value of 0.90 observed for the 12H hydrogel disk sample suggests the data is reasonably accurate and since experimental evidence indicates rapid swelling is occurring, it is reasonable to conclude that Fickian diffusion is not occurring for the 12H hydrogel disks. The 22H and 36H hydrogel disks had n values of 0.53 and 0.96 and R^2 values of 0.95 and 0.94 respectively, which are also not consistent with Fickian diffusion (Table 6.3).

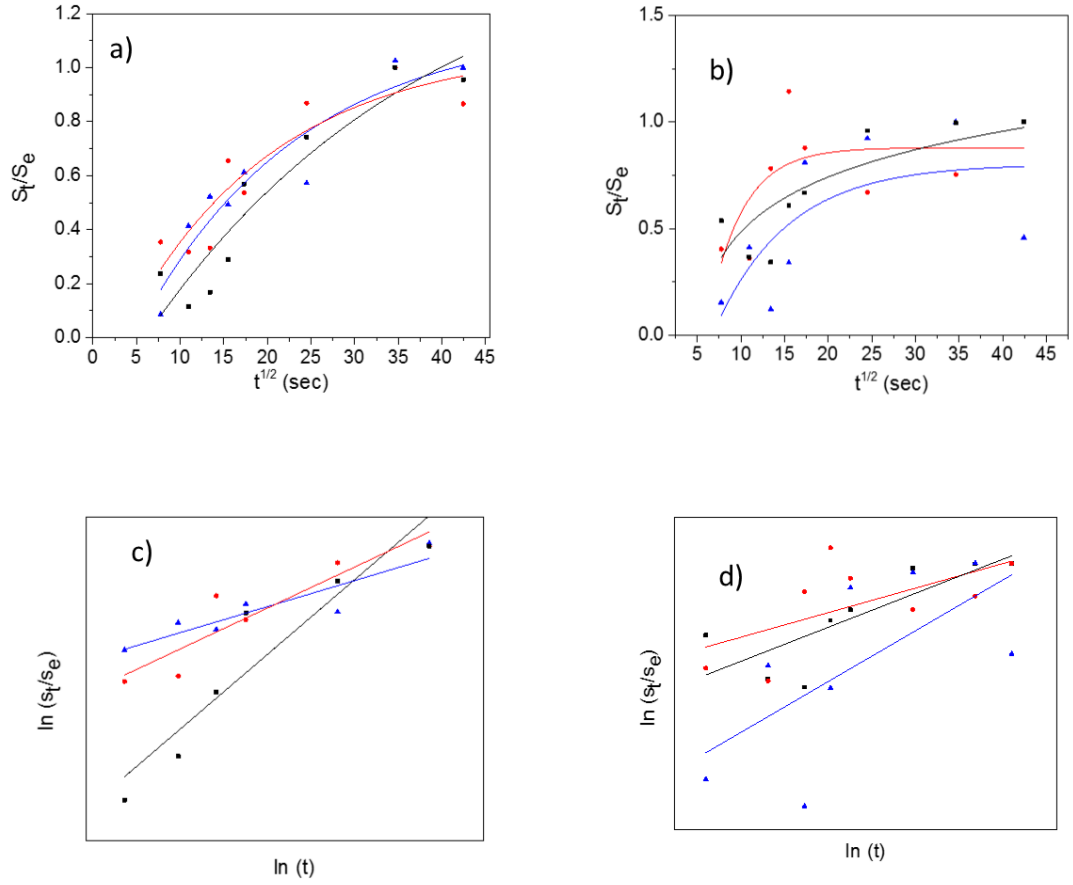

Figure 6.9. a) plot of S_t/S_e *vs* $t^{1/2}$ for CLP hydrogel disks (12H-30H), b) plot of S_t/S_e *vs* $t^{1/2}$ CLP hydrogel disks (36H-46H), c) A plot of ln S_t/S_e versus ln *t* for CLP hydrogel disks (12H-30H) and d) A plot of ln S_t/S_e versus ln *t* for CLP hydrogel disks (36H-46H).

Table 6.3. Sample codes for cross-linked hydrogels and their calculated values (*n, k_d, and D_0*) from swelling analysis.

(Sample codes)	[a]*n*	[a]k_d	[b]D_0 x 10^{-3} cm^2 s^{-1}	[a]R^2
12H	0.33	0.087	7.9	0.90
22H	0.53	0.027	1.6	0.92
30H	0.96	0.001	0.04	0.94
36H	0.49	0.034	2.2	0.91
42H	0.21	0.032	48	0.30
46H	0.67	0.009	0.46	0.70

Calculated by [a] Equation 6 3 and [b] Equation 6.4

Again, the calculated D_o of 0.04 x 10^{-3} cm^2 s^{-1} and 2.2 x 10^{-3} cm^2 s^{-1} for 22H and 36H respectively, differed with literature values for Fickian diffusion. The 36H sample also had non-Fickian diffusion as shown by the n value (0.49, Table 6.3) however D_o (48 x 10^{-3} cm^2 s^{-1}, (Table 6.3) appeared to increase, which was consistent with swelling observations shown by Figure 6.8 d. The low R^2 values for 42H and 46H hydrogel disks shown in Table 6.3 suggests the n, k_d and $D_o$values obtained are not well represented by the Ritger Peppas model used.

Overall the data shows an initial fast capillary like uptake of water followed by an anomalous diffusion uptake for the 12H-36H hydrogels disks. The 42H and 46H hydrogel disks also undergo rapid swelling followed by anomalous diffusion, observed as a small change in diameter over time (Figure 6.7 e and f). Further modelling would need to be performed to better understand the rapid water uptake and release from the synthesised CLP hydrogels disks, which is beyond the scope of this thesis. However, the data does provide a baseline for future cross-link experiments.

6.4.2 Cross-linked PEG (CLP) Hydrogel Disk Microstructure

Microscopy analysis of a hydrogel disk was undertaken to establish if the structure of the cross-linked PEG hydrogel contributed to the observed swelling properties. When the 22H CLP hydrogel disk was examined by SEM (Figure 6.10 a and b), the gel appeared quite compact. There did not appear to be any pores and the fine cracks that are observed on the surface (Figure 6.10 a) may be due to the freeze-drying process. SEM analysis showed that diffusion of solutes into the hydrogel disk did not occur due to some sort of porous structure. It has been reported in the literature that hydrogels made from PEG have a degree of crystallinity and these ordered regions are able to form trihydrated complexes with water [3]. The crystallites of anhydrous PEG can be detected under cross polarisers on an optical microscope [3]. Stereo microscopy was also used to examine the structural morphology of the 22H freeze-dried hydrogel disk.

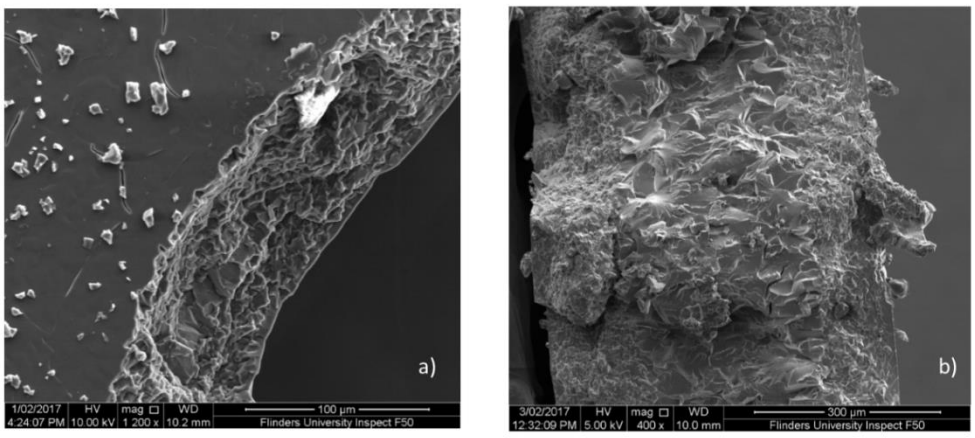

Figure 6.10. SEM images of 22H hydrogel disk after swelling and freeze-drying, a) top view and b) side view.

Figure 6.11 a shows an optical image of a 22H CLP hydrogel disk, and the disk after swelling in water and freeze drying (Figure 6.10 b). The change in the hydrogel width (Figure 6.11 a and b) is due to the swelling that occurred. After freeze-drying the 22H hydrogel disk also changed from transparent to slightly opaque and rings were also visible to the naked eye. The 22H hydrogel disk was visualised using a Stereo microscope (64 X magnification, bright field), (Figure 6.11 d), where concentric dendritic like rings approximately 100 microns apart were observed. Dark field microscopy indicated that the sample was crystalline with some fine structure revealed between the rings (Figure 6.11 e). These may be fracture points, probably due to the freeze-drying process.

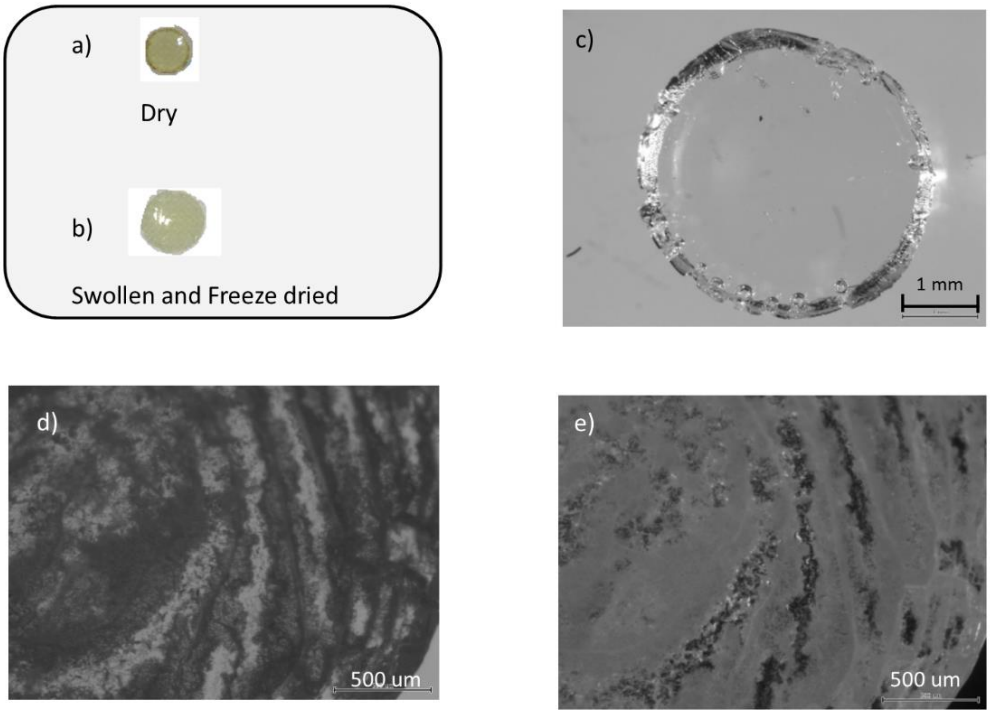

Figure 6.11. a) Optical image of 22H hydrogel disk before swelling, b) optical image 22H hydrogel disk after swelling and freeze-drying, c) bright field image of 22H hydrogel disk before swelling d) bright field image after swelling and e) dark field image of 22H hydrogel disk after swelling and freeze-drying.

6.4.3 CLP Hydrogel Disk Drug Release Studies

A study was performed on the low cross linked 22H CLP hydrogel disk and the more cross-linked 36H CLP hydrogel disk to evaluate the release of a model anti-cancer drug, Camptothecin (CPT) encapsulated in the hydrogel during the UV cross-link stage. The same protocol depicted in Figure was 6.2 was used to encapsulate CPT into the 22H and 36H CLP hydrogel disk. CPT was mixed with a p(mPEGA-AA-Allyl) solution, a tetrathiol cross-linker, an UV initiator and deoxygenated by purging with nitrogen. The mixture was then centrifuged followed by pipetting onto a silicon substrate and exposed to UV light to produce a cross-linked hydrogel. The experimental details can be found in Chapter 2, Section 2.9.1.2. Since CPT is known to fluoresce (λ_{em} = 430 nm – 600 nm) nm) upon excitation with UV light (λ_{ex} = 370 nm), fluorescence spectroscopy was

chosen as a method of monitoring the release of CPT from the 22H and 36H CLP hydrogel disk when immersed in water. The 22H and 36H CLP hydrogel disks were immersed in Tris buffer (0.1 M, pH 8) solution and then at specified time intervals the emission spectrum from 370 nm excitation wavelength was monitored to obtain an emission spectrum for CPT from 430 nm to 600 nm. The experimental details can be found in Chapter 2, Section 2.9.1.1.

Standards of CPT were used to prepare a standard curve (Figure 6.12 b). The line of best fit from the calibration curve was then manipulated to calculate the concentration of CPT released from the 22H CLP hydrogel disk over time. The experimental details can be found in Chapter 2, Section 2.9.1.1. Figure 6.12 a show the CPT fluorescence emission spectra acquired from monitoring the 22H CLP hydrogel disk in Tris buffer solution over the release period of 0-60 minutes. The λ_{max} (450 nm) at each time interval was used as the y value in the $y = mx + c$ equation generated from the calibration curve (Figure 6.12 b, R^2 = 0.99). The equation was then manipulated to calculate the concentration of CPT at each time interval M_t and the amount of CPT released was calculated from equation 5. Where M_o is equal to the amount of drug loaded into the CLP hydrogel disk during the UV cross-link step.

$$Ratio\ of\ drug\ released = \frac{M_t}{M_o}$$

Equation 6.5

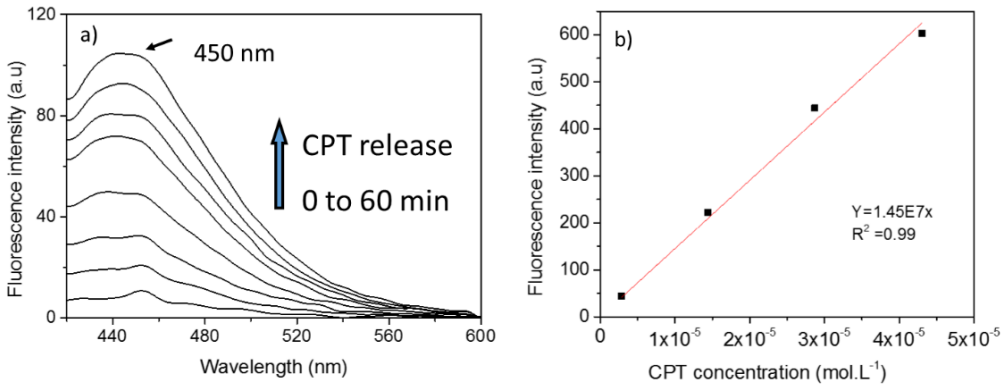

Figure 6.12. a) Fluorescence emission spectra from 430 nm to 600 nm for CPT released from 22H CLP hydrogel disk over 60 min and b) CPT calibration curve, developed from known concentrations of CPT.

Figure 6.13 a shows a plot of the sustained CPT release over time for 22H CLP hydrogel disk. After 60 min in water, the amount of CPT released was found to be 10% of the initial amount loaded. The transport mechanism of the drug out of the 22H CLP hydrogel disk was also investigated using the Ritger peppas model (Equation 6.2) by plotting M_t/M_e vs $t^{1/2}$ where M_e is the equilibrium concentration.

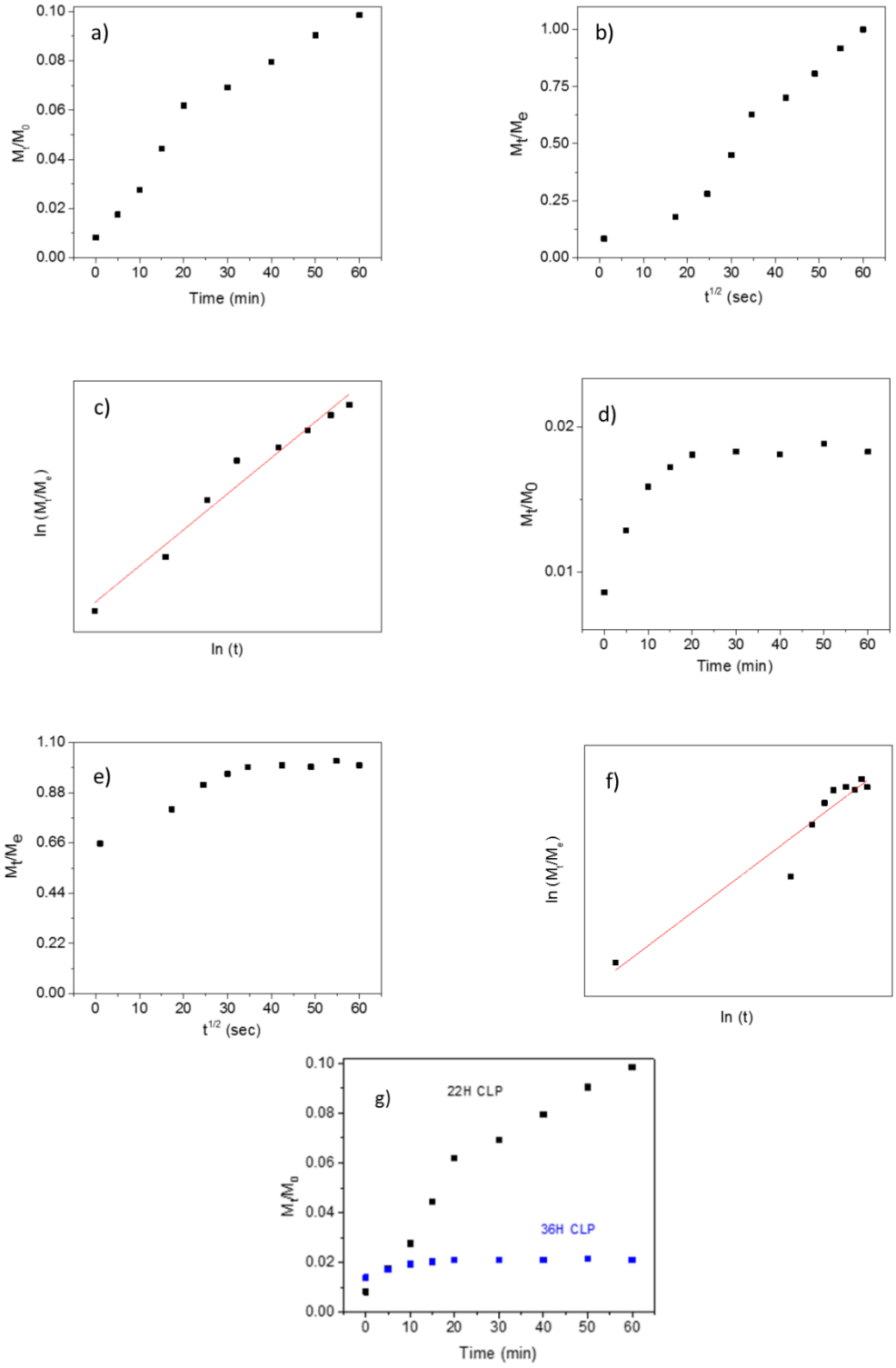

Figure 6.13. a) plot of M_t/M_0 *vs t* for 22H CLP hydrogel disk, b) plot of M_t/M_e *vs* $t^{1/2}$ for 22H CLP hydrogel disks, c) plot of ln M_t/M_e versus ln *t* for 22H CLP hydrogel, d) plot of M_t/M_0 *vs t* for 36H CLP hydrogel disk, e) plot of M_t/M_e *vs* $t^{1/2}$ for 36H CLP hydrogel disks, f) plot of ln M_t/M_e versus ln *t* for 36H CLP hydrogel and g) plot of M_t/M_0 *vs t* for 22H and 36H CLP hydrogel disks.

Figure 6.13 b shows that the data set does not follow a typical trend associated with Fickian diffusion. Figure 6.13 c shows the plot of ln M_t/M_e vs ln (t), the linear regression of this plot was used to determine the exponent n of Equation 6.3 and k_d. These values were then used in Equation 6.4 to determine the diffusion coefficient D_o for CPT release from the 22H CLP hydrogel disk. The constant n, found by regression analysis of Figure 6.13 c was found to be 0.70 and the subsequent D_o, was calculated to be 1.63 X 10^{-4} cm^2 s^{-1}.

Figure 6.13 d shows the CPT release profile for the 36H CLP hydrogel disk. Initially a fast release of CPT is observed from 0-10 min, after this time the release of CPT plateaued. The constant *n*, found by regression analysis of Figure 6.13 f was found to be 0.055. The diffusion coefficient for 36H CLP hydrogel disk was calculated using equation 4 and was found to be 3.69 x 10^{-1} cm^2 s^{-1}. Over the 60-min time interval, less than 2% of the CPT drug (calculated from the calibration curve, Figure 6.12 b) had been released from 36H CLP hydrogel disk compared with 10% for the 22H CLP hydrogel disk (Figure 6.14 g). The more cross-linked 36H CLP hydrogel disk had an initial burst release of CPT as water rapidly entered the cross-link system, this quickly reached an equilibrium and the release of CPT stopped over the measured time. The drug release experiment results indicate that the transport mechanism of CPT for the low cross-linked hydrogel (22H) and high cross-linked hydrogel (36H) is via non-Fickian diffusion. The D_0 values measured for both hydrogel disks differed from the literature values obtained for small molecule diffusion from a thin film hydrogel [27]. It is thought that the fast swelling that occurs for the 22H and 36H hydrogel disks is due to a transport mechanism that may result from an interconnected crystalline polymer network (ICPN).

6.5 Conclusion

A PEG platform designed to make temperature responsive bio-conjugated bio-compatible micelles as part of a grafting-to strategy was produced. The NHS-PEG copolymers were synthesised by FRP with different degrees of NHS functionality. These NHS-PEG copolymers were reacted with amine groups to introduce double bond functionality which transformed them into alkene-PEG copolymers. When a thiol cross-linker molecule was reacted with the double bonds of the alkene-PEG copolymers via thiol-ene click photo-polymerisation, cross-linked hydrogels were produced. Results showed that increasing cross-link density of the hydrogel decreased the swelling profile of the hydrogel disk in water. Diffusion into the hydrogel in aqueous solutions was found to be rapid and non-Fickian. The microstructure of the CLP hydrogel disks was investigated using stereo microscopy and SEM to establish how the morphology of the disks may drive the solute transport mechanism. Stereo microscope analysis showed that the cross-linked hydrogel was made up of a crystalline network and this may be the reason for the fast swelling and diffusion properties that were observed. The diffusion of a model drug (CPT) out of the cross-linked hydrogel was also examined and this was also found to be non-Fickian. At low cross-link density, a sustained release of the model drug was observed. When the cross-link density was increased the release, profile changed to burst release.

6.6 References

1. Buwalda, S.J., et al., *Hydrogels in a historical perspective: From simple networks to smart materials.* Journal of Controlled Release, 2014. **190**: p. 254-273.
2. Peppas, N.A. and A.R. Khare, *Preparation, structure and diffusional behavior of hydrogels in controlled release.* Advanced Drug Delivery Reviews, 1993. **11**(1-2): p. 1-35.
3. Graham, N.B. and M.E. McNeill, *Hydrogels for controlled drug delivery.* Biomaterials, 1984. **5**(1): p. 27-36.
4. Kubinová, Š., et al., *The use of superporous Ac-CGGASIKVAVS-OH-modified PHEMA scaffolds to promote cell adhesion and the differentiation of human fetal neural precursors.* Biomaterials, 2010. **31**(23): p. 5966-5975.
5. Davis, S.S., L. Illum, and S. Stolnik, *Polymers in drug delivery.* Current Opinion in Colloid & Interface Science, 1996. **1**(5): p. 660-666.
6. Sanson, N. and J. Rieger, *Synthesis of nanogels/microgels by conventional and controlled radical crosslinking copolymerization.* Polymer Chemistry, 2010. **1**(7): p. 965-977.
7. Hoffman, A.S., *Hydrogels for biomedical applications.* Advanced drug delivery reviews, 2012. **64**: p. 18-23.
8. Kostina, N.Y., et al., *Non-fouling Hydrogels of 2-Hydroxyethyl Methacrylate and Zwitterionic Carboxybetaine (Meth)acrylamides.* Biomacromolecules, 2012. **13**(12): p. 4164-4170.
9. Zalipsky, S. and J.M. Harris, *Introduction to Chemistry and Biological Applications of Poly(ethylene glycol)*, in *Poly(ethylene glycol)*. 1997, American Chemical Society. p. 1-13.
10. Rosiak, J.M. and P. Ulański, *Synthesis of hydrogels by irradiation of polymers in aqueous solution.* Radiation Physics and Chemistry, 1999. **55**(2): p. 139-151.
11. Lutz, J.-F. and A. Hoth, *Preparation of Ideal PEG Analogues with a Tunable Thermosensitivity by Controlled Radical Copolymerization of 2-(2-Methoxyethoxy)ethyl Methacrylate and Oligo(ethylene glycol) Methacrylate.* Macromolecules, 2005. **39**(2): p. 893-896.
12. King, P.A. and J.A. Ward, *Radiation chemistry of aqueous poly(ethylene oxide) solutions. I.* Journal of Polymer Science Part A-1: Polymer Chemistry, 1970. **8**(1): p. 253-262.
13. Hennink, W. and C.F. Van Nostrum, *Novel crosslinking methods to design hydrogels.* Advanced drug delivery reviews, 2012. **64**: p. 223-236.
14. Sakai, T., et al., *Design and Fabrication of a High-Strength Hydrogel with Ideally Homogeneous Network Structure from Tetrahedron-like Macromonomers.* Macromolecules, 2008. **41**(14): p. 5379-5384.
15. Malkoch, M., et al., *Synthesis of well-defined hydrogel networks using Click chemistry.* Chemical Communications, 2006(26): p. 2774-2776.
16. Ehrbar, M., et al., *Enzymatic formation of modular cell-instructive fibrin analogs for tissue engineering.* Biomaterials, 2007. **28**(26): p. 3856-3866.

17. Buwalda, S.J., et al., *Influence of Amide versus Ester Linkages on the Properties of Eight-Armed PEG-PLA Star Block Copolymer Hydrogels.* Biomacromolecules, 2010. **11**(1): p. 224-232.
18. Ameringer, T., et al., *Polymer coatings that display specific biological signals while preventing nonspecific interactions.* Journal of Biomedical Materials Research Part A, 2012. **100A**(2): p. 370-379.
19. West, J.L. and J.A. Hubbell, *Photopolymerized hydrogel materials for drug delivery applications.* Reactive Polymers, 1995. **25**(2): p. 139-147.
20. Aimetti, A.A., A.J. Machen, and K.S. Anseth, *Poly(ethylene glycol) hydrogels formed by thiol-ene photopolymerization for enzyme-responsive protein delivery.* Biomaterials, 2009. **30**(30): p. 6048-6054.
21. Dubey, A., N.A.D. Burke, and H.D.H. Stöver, *Preparation and characterization of narrow compositional distribution polyampholytes as potential biomaterials: Copolymers of N-(3-aminopropyl)methacrylamide hydrochloride (APM) and methacrylic acid (MAA).* Journal of Polymer Science Part A: Polymer Chemistry, 2015. **53**(2): p. 353-365.
22. Peiffer, D. and R. Lundberg, *Synthesis and viscometric properties of low charge density ampholytic ionomers.* Polymer, 1985. **26**(7): p. 1058-1068.
23. Ehrlich, G. and P. Doty, *Macro-ions. III. The Solution Behavior of a Polymeric Ampholyte1.* Journal of the American Chemical Society, 1954. **76**(14): p. 3764-3777.
24. Alfrey, T., E. Gurnee, and W. Lloyd. *Diffusion in glassy polymers*. in *Journal of Polymer Science Part C: Polymer Symposia*. 1966. Wiley Online Library.
25. George, K.A., et al., *Investigation into the Diffusion of Water into HEMA-co-MOEP Hydrogels.* Biomacromolecules, 2004. **5**(4): p. 1194-1199.
26. Ritger, P.L. and N.A. Peppas, *A simple equation for description of solute release I. Fickian and non-Fickian release from non-swellable devices in the form of slabs, spheres, cylinders or discs.* Journal of controlled release, 1987. **5**(1): p. 23-36.
27. Davis, B.K., *Diffusion in Polymer Gel Implants.* Proceedings of the National Academy of Sciences, 1974. **71**(8): p. 3120-3123.

7 Chapter 7. Conclusions and Future Work

7.1 Conclusions

The aim of this thesis was to develop temperature responsive, bio-compatible bio-conjugated polymers that could be adapted for drug delivery, tissue engineering and affinity applications. Polymer/DNA bio-conjugates were prepared by the grafting-from and the grafting-to strategy. Chapter 3 showed that pHEA polymer bio-conjugates could be made by the grafting-from strategy. A RAFT (bis(carboxymethyl)trithioester) bio-macro initiator, was produced when amine functionalised oligonucleotides were amide coupled to a RAFT ester agent using NHS/EDC chemistry. The RAFT bio-macro agent was used in the RAFT polymerisation of HEA monomer, where pHEA polymer was observed to grow from the RAFT bio-macro agent. This thesis concluded that the purification of the polymer bio-conjugates was facile, however, polymer growth from the RAFT bio-macro agent was slow. The grafting-from method used in this thesis resulted in limited growth of polymer from the RAFT bio-macro agent. MALDI-TOF mass spectrometry analysis and PAGE analysis suggested that RAFT polymerisation using the RAFT bio-macro agent may have led to the degradation of the DNA that was attached. Polymer bio-conjugates were also prepared via the grafting-to strategy. This strategy involved the independent preparation of polymers, followed by their conjugation to DNA.

Chapter 4 investigated the synthesis of temperature responsive (pNIPAAm-*co*-polymers), biocompatible (PEG copolymers) polymer bio-conjugates via the grafting-to strategy. In Chapter 4, pNIPAAm-*co*-HMAAm copolymers (low HMAAm content to high HMAAm content) were prepared by RAFT polymerisation. It was confirmed that the feed ratio of the monomer in the copolymerisation was retained in the final polymer composition. It was shown that the temperature response of the pNIPAAm-*co*-HMAAm copolymers could be tuned by changing the ratio of HMAAm monomer in the pNIPAAm-*co*-HMAAm copolymer. When the copolymers composition of HMAAm was increased, the LCSTs (measured by UV-Vis) of the copolymers increased linearly with HMAAm content from 28.5 ^{O}C (low HMAAm content) to 37.5 ^{O}C (high HMAAm content).

It was also shown that the pNIPAAm-*co*-HMAAm copolymers form micelles at their LCSTs and that these micelles intercalate SG. As the SG molecule was incorporated into the micelles of the pNIPAAm-*co*-HMAAm copolymers at their LCSTs, SG fluorescence was observed. The CMC of the pNIPAAm-*co*-HMAAm copolymers were calculated using SG as a hydrophobic probe molecule. The CMC of the pNIPAAm-*co*-HMAAm copolymers was found to increase as the HMAAm composition increased. The hydrodynamic diameter of the micelles formed by pNIPAAm-*co*-HMAAm copolymers was also measured. DLS results confirmed that the micelles hydrodynamic size depended on temperature and concentration. Micelles were only observed above the LCST of the pNIPAAm-*co*-HMAAm copolymers. When the concentration of each of the copolymers

measured by DLS was reduced to below the CMC (as measured by the SG probe method), no micelles were detected by DLS. These results confirm the CMC values found by the SG probe method.

Finally, AFM was used to measure the height and width of the polymeric micelle particles (pNIPAAm-*co*-HMAAm copolymers) adsorbed onto a mica surface. Cross section analysis and particle analysis showed that aspect ratio of particles increased as the HMAAm content increased. This is thought to be due to a greater amount of hydrophilic character as the HMAAm content is increased. It is theorised that the interaction between the polar head groups of the HMAAm copolymer will wet the surface of the mica more readily leading to greater spreading of the particle.

In Chapter 5 the synthesised pNIPAAm-*co*-HMAAm copolymers were post functionalised using DBCO to yield strained alkyne (SA) functionalised copolymers (pNIPAAm-*co*-HMAAm-*co*-SA). The LCSTs of the SA copolymers were successfully measured using a low volume, light scattering method, which to the best of our knowledge has not been reported before. The light scattering method of measuring LCSTs only required micrograms of sample since the volume being measured is very small (microliters) and because the measurement was performed in a real-time PCR machine, multiple samples can be measured very quickly.

Chapter 5, also showed that PCR products that were end functionalised with azides (PCR-Az) could be coupled via SPAAC chemistry to SA copolymers to produce TR-PCR bio-conjugates. DNA melt curves showed that conjugation of PCR-Az products is possible through a one pot PCR click reaction. However, it was unclear whether azide-PCR primers or PCR-Az products were conjugated to the SA copolymer. Agarose gel analysis of the one pot PCR reaction did not show conclusively that the click reaction produced TR-PCR bio-conjugates, but the gels did show that the SA copolymer did not interfere with PCR. However, it is also theorised that the conjugation of PCR-Az products or azide-PCR primers to SA copolymers may alter DNA's capacity to intercalate SG and this may make visualisation of TR-PCR bio-conjugates in gels more difficult. DNA melt curve analysis suggested that conjugation of PCR-Az products to SA copolymers in buffer and aqueous solutions is possible and that the reaction between the SA copolymer and the PCR-Az product is fast. Conjugation efficiency appeared to be improved when PCR-Az products were conjugated to SA copolymers in an organic solvent as evidenced by the high molecular weight product visualised in agarose gels.

The melt temperature of DNA was found to be impacted by its conjugation to the SA copolymers, which has potential implications for drug delivery applications. Results also suggest that the LCST of the polymer that was conjugated to DNA, changes upon conjugation and that this LCST can be determined by the uptake of SG as the SA copolymer forms micelles.

Finally, in Chapter 6, NHS-PEG copolymers were synthesised by FRP with different degrees of NHS functionality. Results showed that NHS-PEG copolymers reacted with allylamine to produce alkene-PEG

copolymers. Thiol cross-linker molecules were reacted with the alkene-PEG copolymers via thiol-ene click photo-polymerisation and cross-linked hydrogels were produced. Results showed that increasing cross-link density of the hydrogel decreased the swelling profile of the hydrogel disk in water. Diffusion into the hydrogel in aqueous solutions was found to be rapid and non-Fickian. SEM and stereo microscope analysis showed that the cross-linked hydrogel was made up of a crystalline network and this may be the reason for the fast swelling and diffusion properties that were observed. The diffusion of a model drug out of the cross-linked hydrogel was also examined and this was also found to be non-Fickian. At low cross-link density, a sustained release of the model drug was observed. When the cross-link density was increased the release, profile changed to burst release.

7.2 Future Work

Polymer bio-conjugates in this thesis were synthesised to develop a platform of temperature responsive, bio-compatible polymers bio-conjugates. Although the polymer growth from the RAFT bio-macro agent used in Chapter 3 was slow and the data suggests that DNA may in fact be degraded during RAFT polymerisation, questions remain about why the oligo that is attached to the RAFT agent is only attached on one side. It is hypothesised that the oligo that is attached is inhibiting the second attachment either sterically or through non-specific interaction with the incoming oligo, this hypothesis could be potentially explored in future work. Further investigation of the PEG hydrogels is also required to determine the soluble fraction of the cross-linked gels, this may help explain the large errors and anomalous diffusion that was observed. Also, better control over the PEG gels architecture could be achieved by manipulating the feed ratio of the two monomers and monitoring conversion to produce functionalised polymers that are better defined. It may also be better to trial RAFT polymerisation of the copolymer system to better control the MW of the polymers produced. Future work could also involve measuring the reversibility of the LCSTs of the synthesised pNIPAAm copolymers to determine the stability of the micellular system. Temperature responsive bio-conjugates were produced in this thesis, but their conjugation to the PEG platform was not achieved. The synthesised temperature responsive bio-conjugates could be attached to the PEG platform to produce bio-conjugated cross-linked micelles. Bio-conjugated cross-linked micelles are being investigated as drug delivery vehicles. Future work could involve converting the RAFT end group of the TR-PCR bio-conjugate to a thiol group so that it could be attached to the PEG platform via a thiol-ene click reaction. Instead of cross-linking the PEG platform using a thiol-ene cross-linker, an alternative, reversible cross-linked system is proposed. DNA, via base pair hybridisation could be used to prepare reversible cross-linked hydrogels. This thesis has demonstrated that the melt temperature of DNA can be controlled by its attachment to the temperature responsive pNIPAAm therefore, the DNA cross-linked system could be reversibly cross-linked through manipulation of the melt temperature of DNA using a temperature switch. This PEG-TR-DNA platform could allow for the stimuli release of an encapsulated drug, making it potentially useful for drug delivery

applications. This platform could also have potential use in the enrichment and detection of DNA biomarkers. The PEG-TR-DNA platform could be immobilised on a microfluidic chip. This could be achieved by first preparing an amine derivatised glass slide. Immobilisation of DNA on the surface could be achieved by the reaction of NHS-PEG-TR-DNA with the amine derivatised glass slide. The DNA, once immobilised could act as a capture probe and the melt temperature of DNA could be controlled by pNIPAAm. This platform could be potentially used for the release and enrichment of dilute DNA biomarkers.